Digital CDMA Multi-Carrier Demodulator

by

William Ming Wan

A thesis submitted to the Department of Electrical & Computer Engineering

in conformity with the requirements for the degree of Master of Science (Eng.)

Queen's University

Kingston, Ontario, Canada

June 1996

The author has granted a non-exclusive licence allowing the National Library of Canada to reproduce, loan, distribute or sell copies of this thesis in microform, paper or electronic formats.

The author retains ownership of the copyright in this thesis. Neither the thesis nor substantial extracts from it may be printed or otherwise reproduced without the author's permission.

L'auteur a accordé une licence non exclusive permettant à la Bibliothèque nationale du Canada de reproduire, prêter, distribuer ou vendre des copies de cette thèse sous la forme de microfiche/film, de reproduction sur papier ou sur format électronique.

L'auteur conserve la propriété du droit d'auteur qui protège cette thèse. Ni la thèse ni des extraits substantiels de celle-ci ne doivent être imprimés ou autrement reproduits sans son autorisation.

0-612-28260-0

Canadä

ABSTRACT

In a conventional base station receiver, the received signal is digitized at base band. In cellular and personal communication systems (PCS), in which a large number of carriers are frequency multiplexed in a frequency band, this arrangement puts a lot of stress on the base station real estate and power consumption since by digitizing at base band, each carrier needs an independent radio and intermediate frequency (IF) receiver unit. With the advance of digital signal processing(DSP) technology, processing cost and speed have improved dramatically. Thus it is now feasible to digitize signals and process these signals by DSP at a higher frequency. In this thesis a multi-carrier demodulator is developed for direct sequence code division multiple access (DS-CDMA) for PCS at 1.9 GHz with the assumption that all the carriers occupying the same PCS spectrum are DS-CDMA. Two approaches are considered in which the signal is digitized at IF. Thus all the carriers in the spectrum share the same radio front end. The first approach is to select and down shift individual signal carriers by a numerically controlled oscillator (NCO). Although digitized at IF band the signal is decimated to the lowest possible rate by a decimation filter. A carrier select finite impulse response (FIR) filter and interpolation filter are used for carrier shaping and sampling rate adjustment according to the IS-95+ standard. In the second approach a transmultiplexer is used for multi-carrier demodulation. A transmultiplexer includes a polyphase filter bank and Fast Fourier Transform (FFT) processor. In a conventional transmultiplexer the output sampling frequency of the FFT equals the carrier spacing. Due to the spectral characteristic of the IS-95+ CDMA carrier, the transmultiplexer is required to provide a higher sampling frequency at the FFT output. In this thesis, time-domain analysis of a transmultiplexer for this special case is developed. Due to the mismatch of the sampling rate of the FFT output and the base band CDMA demodulator, a rate conversion system is necessary. A rate conversion

system is designed and realized. The complexities of systems realized by both approaches are examined. The transmultiplexer approach has a five-to-one complexity advantage over the per-carrier approach provided that the spectrum is fully utilized. For a system with low spectrum occupancy, the transmultiplexer approach suffers the disadvantage of high start up costs. The performance of the transmultiplexer is compared against requirements derived from the IS-95+ standard.

Acknowledgment

I would like to sincerely thank my supervisors Dr. Peter J. McLane and Dr. Leo Strawczynski for their guidance and support. True appreciation is expressed for their advice and recommendation throughout the course of this work. The Telecommunications Research Institute of Ontario (TRIO) and Nortel are gratefully acknowledged for providing financial support, space and computing facility for my studies through the Research Partnership Program. Various personnel in Nortel Wireless Networks are thanked for their valuable advice.

I am deeply in debt to John McNicol, David Choi, Brad Morris, Greg Carlton, Peter Deane and Hong Zhao of Nortel Wireless Networks for their assistance on this project. It was a lot of fun to work with them, and I wish them luck with their own careers.

The staff of TRIO office are thanked for their help with contracts and other administrative details. Finally, to my parents and friends, thank you for your love and support.

Table of Contents

LIST OF FIGURES

-

LIST OF TABLES

SUMMARY OF NOTATION

Abbreviations

ADC   - analog-to-digital converter

CDMA   - code division multiple access

CIC   - cascaded-integrator-comb

CIRF   - cochannel interference reduction factor

dB   - decibel

dBm   - decibel milliwatt

DDS   - direct digital synthesizer

DFT   - discrete fourier transform

DS-CDMA   - direct spreading code division multiple access

DSP   - digital signal processor/digital signal processing

FDM   - frequency division multiplex

FER   - frame error rate

FFT   - fast fourier transform

FIR   - finite impulse response

GHz   - giga hertz

GSM   - global system for communications

HDF   - high decimation filter

Hz   - hertz

I   - in phase

IF   - intermediate frequency

IFFT	- inverse fast fourier transform
ISI	- intersymbol interference
kcps	- kilo chips per second
kHz	- kilohertz
Mcps	- million chips per second
MIPS	- million instructions per second
MHz	- megahertz
NCO	-numerically controlled oscillator
NF	- noise figure
PCM	- pulse code modulation
PCS	- personal communication system
PN	- pseudo noise
Q	- quadrature phase
QPSK	- quadrature phase shift keying
RF	- radio frequency
ROM	- read only memory
SAR	- signal-to-aliasing ratio
SCR	- signal-to-crosstalk ratio
SAW	- surface acoustic wave
SDR	- signal-to-distortion ratio
SFDR	- spurious free dynamic range
SNR	- signal-to-noise ratio
TDM	- time division multiplex

TDMA	- time division multiple access
TIA	- Telecommunications Industry Association
TMUX	- transmultiplexer

Symbols, variables, and functions

ΔF	- carrier spacing of each QPSK-CDMA signal multiplexed in the frequency
$\Delta\phi$	- phase increment of NCO/DDS per cycle
$\uparrow i$	- up-sampler by a factor of i
$\downarrow d$	- down-sampler by a factor of d
β	- excess bandwidth of raise cosine pulse
$\sigma_{Thermal\ Noise}^{2}$	- thermal noise power
$\sigma_{Quantization}^{2}$	- quantization noise power
$b[n]$	- sampling point of 10 MHz signal
B_{max}	- maximum register width for HDF
B_{n}	- noise bandwidth
$BHFC(e^{jw})$	- frequency response of cascade of baseband filter and quantized channelizer DSP
$c[m]$	- output of 2nd order approximation

$CIC(e^{jw})$	- frequency response of CIC interpolator (N=3, R=4, M=1)
$CICq(e^{jw})$	- frequency response of quantized CIC interpolator (N=3, R=4, M=1)
Ds	- minimum separation between two cochannel cell
$D[n]$	- data sequence input to the IS-95+ transmitter
$D_{8fc}(e^{jw})$	- frequency response of $d_{8fc}'[m]$
$D_{10}(e^{jw})$	- frequency response of $d_{10}'[n]$
$d_k[n]$	- estimated kth carrier's data from the receiver
$D_{qk}(e^{jw})$	- quantized estimated kth carrier's data from the receiver
$d_{8fc}[m]$	- output of the 2nd order approximation sampled at $8xf_{chip}$
$d_{10}[n]$	- input to the 2nd order approximation sampled at 10 Mhz
E_b	- energy per bit
$e[n,k]$	- the complex error by rounding off the product $x[n]W_N^{kn}$ in FFT
f_{chip}	- chip rate = 1.2288 MHz
f_{ck}	- clock frequency of NCO/DDS
f_k	- centre frequency of the kth carrier
f_{IF}	- center frequency of immediate frequency
f_{out}	- per-carrier output sampling frequency of the transmultiplexer
f_s	- ADC sampling frequency
$FFT(e^{jw})$	- per carrier FFT output (transmultiplexer)
$FIR(e^{jw})$	- frequency mask for carrier select filter in per-carrier approach ..
G_p	- processing gain
$g[m]$	- interpolation filter
$g_m[n]$	- system impulse response of rate conversion system

$h[n]$	- carrier select FIR filter
$h_k[m]$	- subfilter at the N-1-k th polyphase filter branch
$h_{HT}[n]$	- Hilbert transformer
$h_{LP}[n]$	- half band low pass filter in the Hilbert transformer
$H_1(e^{jw})$	- frequency response of HDF N=8, M=1,R=24
$H_2(e^{jw})$	- frequency response of HDF N=8, M=2, R=24
$H_b(e^{jw})$	- frequency response of the baseband filter specified by IS-95+
$H_c(z)$	- z-domain system function of a comb filter
$H_I(z)$	- z-domain system function of a integrator
$HDF(e^{jw})$	- frequency response of HDF (N=8, R=24, M=1)
$HDFq(e^{jw})$	- frequency response of quantized HDF (N=8, R=24, M=1)
$HF(e^{jw})$	- frequency response of cascade of HDF and carrier select filter at 2xfchip
$HFC(e^{jw})$	- frequency response at the output of the CIC interpolator (in the channelizer DSP)
$i_k[n]$	- real part of the kth QPSK signal
I	- interpolation factor required by 2nd order interpolation
IFIR1	- first stage interpolation filter of the rate change mechanism
IFIR2	- second stage interpolation filter of the rate change mechanism
$I[n]$	- output of IS-95+ baseband filter at in-phase rail
$I_k[n]$	- in-phase input to the IS-95+ base band filter at the transmitter model
$I_o[x]$	- the modified zeroth-order Bessel function
M	- differential delay of CIC filter
N	- number of CDMA carrier in Block A,B or C frequency spectrum or

number of stage of CIC filter

N_{IF} - Noise power at IF

N_o - noise density

$P(f)$ - power response of HDF

$q_k[n]$ - imaginary part of the kth QPSK signal

$Q[n]$ - output of IS-95+ base band filter at quadrature-phase rail

$Q_k[n]$ - quadrature-phase input to the IS-95+ transmitter model

$Q(e^{jw})$ - frequency response of quantized carrier select filter in per-carrier approach

$Q_k[n]$ - QPSK signal modulated by the kth carrier

$\hat{Q}_k[m]$ - quadrature-phase output of the kth rate change mechanism

R - rate conversion factor of CIC filter

$R(e^{jw})$ - frequency response of Rx[n] with improved stop band attenuation\

$R_{15}(e^{jw})$ - receiver filter prototype sampled at 15 MHz used in the transmultiplexer

$Rp(e^{jw})$ - frequency response of polyphase carrier select filter with adaptation to

           transmultiplexer components

R_c - cell radius

$R_{rrc}(e^{jw})$ - frequency response of the root raise cosine pulse

$R_{rc}(e^{jw})$ - frequency response of raise cosine pulse

$R_x(e^{jw})$ - frequency response of receiver impulse response

$r_{rrc}[n]$ - impulse response of root raise cosine pulse

$r_{rc}[n]$ - impulse response of raise cosine pulse

$r_x[n]$ - receiver impulse response

$S(f)$	- frequency response of the base band filter specified by IS-95+
$S(e^{jw})$	- frequency response of input to the transmultiplexer front end
$S_A(e^{jw})$	- frequency response of the output of the transmultiplexer front end
$s[l]$	- output of the IS-95+ transmitter model
$s_k(t)$	- the kth carrier modulated CDMA signal
t_{8fc}	- $1/(8 \times f_{chip})$
t_{10}	- 1/10 MHz
$THFC(e^{jw})$	- frequency response of cascade of transmitter and per-carrier channelizer
$TR_I[n]$	- in-phase system function of the transmultiplexer
$TR_Q[n]$	- quadrature-phase system function of the transmultiplexer
$t_x[n]$	- transmitter impulse response
$T_x(e^{jw})$	- frequency response of transmitter impulse response
$v[k]$	- intermediate variable of rational rate conversion system
$w[k]$	- intermediate variable of rational rate conversion system
$w[m]$	- output of up-sampler
W_N^k	- $e^{-j(2\pi k/N)}$
$W(e^{jw})$	- frequency response of output of up-sampler
$w'[n]$	- output of decimation filter
$W'(e^{jw})$	- frequency response of output of decimation filter
$x[n]$	- input to rate conversion system
$x_k[m]$	- the kth transmultiplexer per-carrier complex output
$X(e^{jw})$	- frequency response of input to rate conversion system
$y[n]$	- complex input to transmultiplexer

$y_I[n]$	- imaginary part of $y[n]$
$y_{IF}[n]$	- input to the transmultiplexer at IF
$y_{Ik}[n]$	- imaginary part of $y[n]$ at the kth subfilter branch
$y_{mI}[n]$	- $y_{IF}[n]$ multiplied by sine mixer
$y_{mR}[n]$	- $y_{IF}[n]$ multiplied by cosine mixer
$y_R[n]$	- real part of $y[n]$
$y_{Rk}[n]$	- real part of $y[n]$ at the kth subfilter branch
$y[m]$	- output of interpolator
$Y(e^{jw})$	- frequency response of output of rate conversion system

Chapter One

Introduction

1.1 Motivation

Code division multiple access (CDMA), one of the newest members in the family of cellular interface protocols, is designed to provide high capacity cellular communications. Operating in the 850 MHz frequency range, trial systems have been deployed in areas such as Vancouver and Hong Kong. As one of the winners of the recent personal communication system (PCS) spectrum auctions in the U.S. has declared their intention to use CDMA, it is expected that CDMA will be widely deployed. PCS spectrum allocation in the U.S. specifies that a cellular operator can use spectrum in blocks of 15 MHz or 5 MHz. Each frequency block is shared by multiple PCS carriers. As a result there is a need to develop a wideband receiver/multi-carrier demodulator for CDMA PCS base station systems.

Traditionally, a single carrier in the radio frequency (RF) signal in a cellular radio system is band selected and down-converted through dedicated analog devices to baseband. At baseband the signal is digitized and then processed by a digital signal processor (DSP). However, with the availability of cheaper and faster digital hardware, such as analog-to-digital converters (ADCs) and DSPs, the trend is to move the digitization of the signal closer to the radio antenna [18]. The ultimate goal is to implement all the receiver functions through digital hardware and software. The advantage of digitizing cellular radio signals at a higher frequency is flexibility [17]. By changing the software in the

1

DSPs, the DSPs are able to switch channels, change modulation schemes or receive different types of signals. In cellular systems at 850 MHz and PCS at 1.9 GHz, a base station is expected to handle a large number of radio carriers simultaneously. If a single carrier of the radio signal is digitized at baseband, as is typically done today, a large number of dedicated analog radio receivers are required. This puts a strain on base station cost and power consumption. By digitizing over a wider bandwidth, a single radio front end can be shared among different carriers. In addition, when digitizing a signal at a higher rate, copies of the spectrum of the analog signal that are present in the spectrum of the sampled signal become increasingly separated as the sampling rate is increased beyond the Nyquist sampling rate. This simplifies the analog anti-aliasing filters in the receiver radio as the distortion caused by spectrum overlap is reduced [18].

The objective of this thesis is to develop DSP algorithms for the implementation of a digital CDMA multi-carrier demodulator. The multi-carrier demodulator is also called a wideband channelizer, since its function is to demultiplex and recover carrier signals which have been frequency multiplexed in a frequency spectrum. In this thesis the multi-carrier CDMA signal refers to specifications documented in the IS-95+ CDMA Standard - Personal Station- Base Station Compatibility Requirements for 1.8 to 2.0 GHz Code Division Multiple Access (CDMA) Personal Communications Systems [5] as adopted by Telecommunications Industry Association (TIA). According to the IS-95+ standard [5], a CDMA carrier channel has a bandwidth of 1.25 MHz. The frequency allocation plan specified by the IS-95+ standard [5] is illustrated in Fig 1.1. On the forward link, from base station to cellular hand set, a Block A, B or C wireless operator can frequency multiplex up to eleven 1.25 MHz

CDMA carriers within a 15 MHz spectrum and transmit it over the air. On the reverse link, the radio

signals with an aggregate bandwidth up to 15 MHz from mobile users are received by the base station

transceiver and down-shifted to baseband. The frequency allocation plan for a Block A, B or C is

shown in Fig.1.2. The guard band shown in Fig. 1.2 is the frequency space where there is no carrier

signal; its purpose is to decrease interference from and to the signals in an adjacent band. It should be

noted that although this thesis puts an emphasis on cellular signals in Block A,B and C, signals in

other blocks, i.e. Block D and E (5 MHz PCS Spectrum Block), can also use the same DSP design

with a minor adjustment in terms of bandwidth and the number of carrier signals.
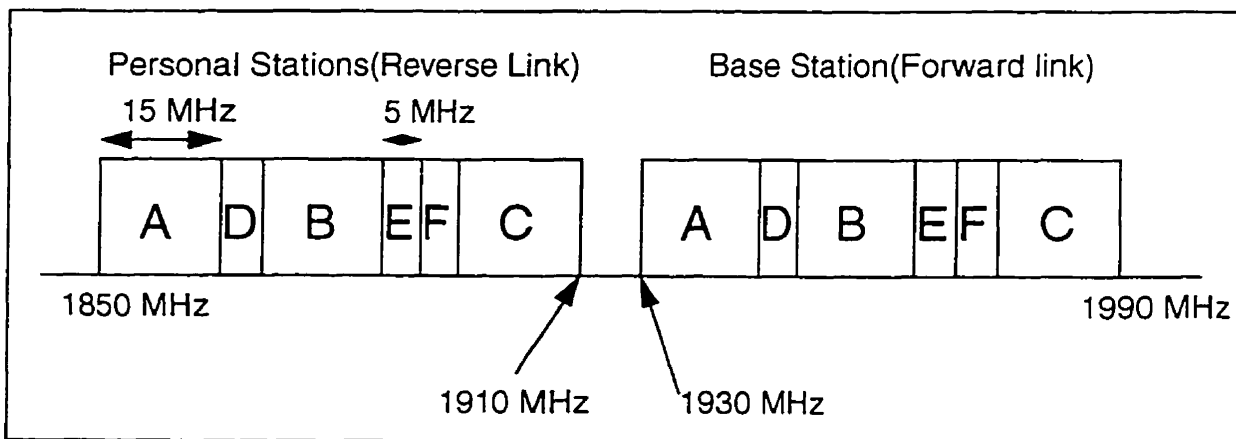
Fig. 1.1 PCS at 1.9 GHz frequency allocation plan
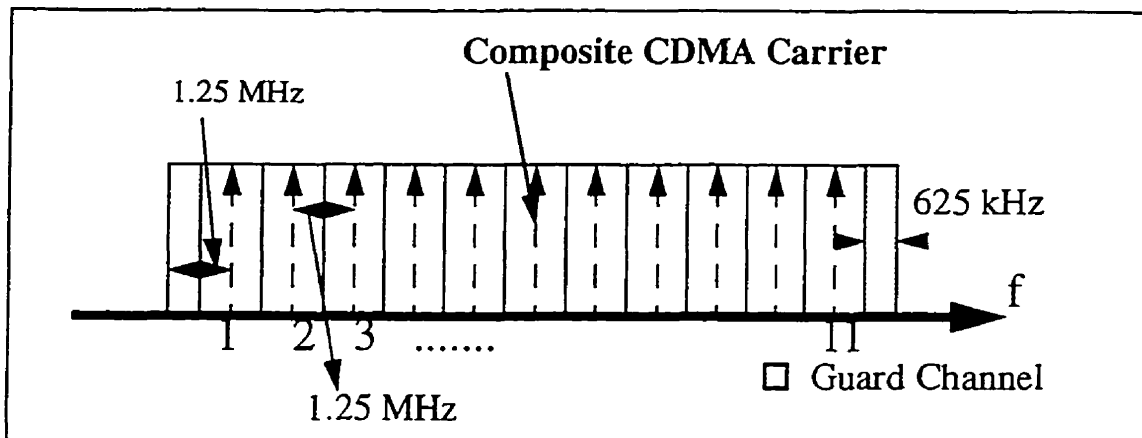
Fig.1.2 Frequency allocation plan of the IS-95+ standard [5] for Block A, B or C

In this thesis it is assumed that the 15 MHz spectrum received at the base station is digitized at an intermediate frequency (IF). Carrier channels from remote terminals contained in the spectrum are demultiplexed through a multi-carrier demodulation DSP and fed into a baseband CDMA demodulator operating on a per-carrier basis, as shown in Fig. 1.3. The RF stage receiver shown in Fig. 1.3 includes an antenna subsystem, high frequency bandpass filters, amplifiers and frequency down-shifters. The wideband CDMA spectrum of 15 MHz or 5 MHz is bandpass filtered, amplified and block down-converted to the IF frequency by the RF stage receiver. The signals outside the selected block are attenuated. At the IF frequency further bandpass filtering, usually by surface acoustic wave (SAW) filter, is conducted by the IF stage receiver. In this manner the out of spectrum signals are further attenuated. The IF stage signals are digitized by an ADC with sampling rate at least twice the maximum frequency component of the signals at the IF frequency. Undersampling of the IF signals is possible but it is not considered in this thesis. At this point it should be noted that all the components before the ADC in the wideband receiver chain are analog. Digitization

starts at the ADC. The 11 individual carriers of bandwidth 1.25 MHz that have been multiplexed in
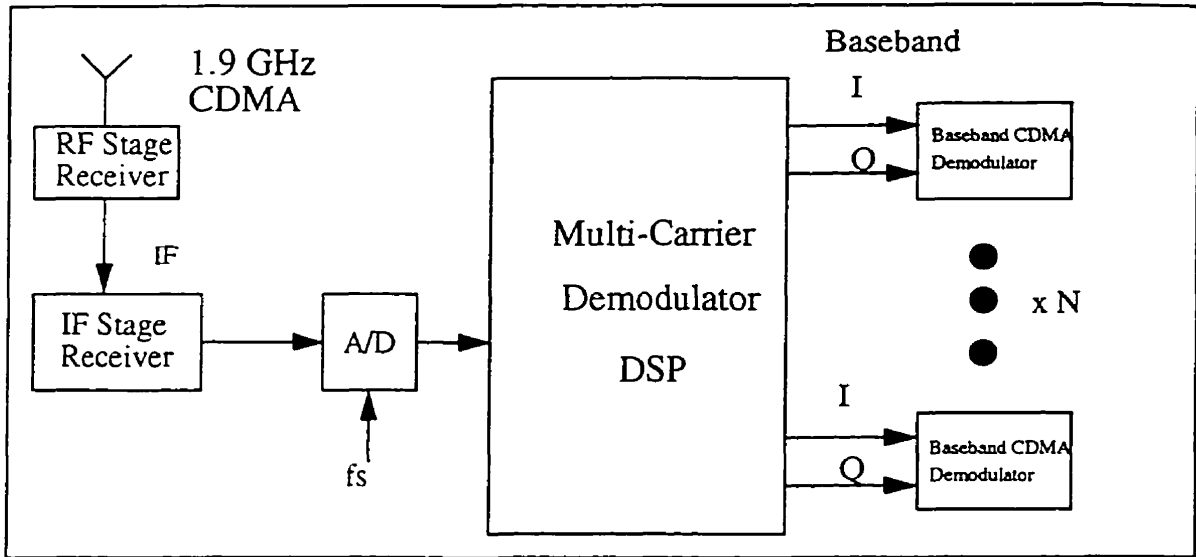
Fig. 1.3 Simplified Structure of a CDMA Base Station wideband receiver chain

the digitized spectrum are selected, demultiplexed and down-shifted to baseband by the multi-carrier demodulator DSP. Since each CDMA carrier is modulated by the quadrature phase shift keying (QPSK) modulation format, each carrier has two output branches at the demodulator DSP: denoted as the I - in phase and Q - quadrature phase signals. The baseband I and Q signals of each carrier are then input to the baseband CDMA demodulator. Throughout this thesis, it is assumed that the baseband CDMA demodulator accepts baseband signals at a sampling rate of $8f_{chip}$, where $f_{chip} = 1.2288$ MHz is the chip rate of the CDMA signal. A further assumption is that the input signal to the baseband demodulator is quantized to 4-bit accuracy. The main function of the baseband CDMA demodulator is to decorrelate or despread the composite CDMA baseband signals. The output of the baseband demodulator is an estimate of the transmitted information sequence.

The design criteria of the multi-carrier demodulation DSP system is to minimize the complexity and distortion added to the CDMA signals by the demodulator system itself. In addition, the DSP system has to process the CDMA signal so that it complies with the requirements set by the IS-95+ standard [5]. By the Nyquist sampling theorem, the sampling rate must be equal to at least twice the signal bandwidth in order to maintain the integrity of the signal. Therefore, due to the large bandwidth of the CDMA signal, a high sampling rate is needed. DSP complexity is a function of number of operations performed per second which is in turn a function of signal sampling rate. In the case of digital filters such as finite impulse response (FIR) filters, a major type of digital filter used in this thesis, the system complexity is a function of the data rate and the number of filter coefficients. In order to make the digital filters used in the DSPs realizable, the length of the digital filters has to be kept to a minimum.

Two options for designing the multi-carrier DSP will be considered: 1) down-shifting the desired signals to baseband on a per-carrier basis; and 2) multi-carrier frequency demultiplexing through a polyphase-FFT (Fast Fourier Transform) transmultiplexer [6]. These two options are discussed in detail in Chapters Three and Four respectively.

1.2 CDMA Overview

Direct sequence code division multiple access (DS-CDMA), hereafter referred to as CDMA, is an air interface protocol utilizing spread spectrum techniques. The communications path

from base station to handset is called the forward link. The communications path from handset to base station is called the reverse link. This thesis focuses on finding methods for multi-carrier demodulation for the reverse link. The following sections present an introduction to CDMA theory, and the structure of the forward link and the reverse link specified by the IS-95+ standard [5].

1.2.1 Introduction to DS-CDMA Theory

In DS-CDMA, as specified in the IS-95+ standard [5], data from different users is modulated by a pseudo random binary sequence of different time offsets and share the same frequency spectrum during transmission. When one looks at a composite CDMA signal, signals from different users appear to be superimposed. The method by which data-modulated carrier from an individual user is spread by direct modulation of a wideband spreading signal is called direct sequence spread spectrum. There are other types of spread spectrum systems in which the spreading code is used to control the frequency of transmission of the data-modulated carrier, such as frequency hopping spread spectrum. DS- CDMA is the spreading scheme specified by the IS-95+ standard [5] and therefore the CDMA system discussed in this thesis refers to the DS-CDMA system. At the receiver of the CDMA system, after proper down-shifting and filtering operations, the overlapped CDMA signals from different users are separated by correlating or despreading with the same binary sequence that the reference user employed at the transmitter. By correlating a composite CDMA signal with a reference pseudo random binary sequence, the interfering CDMA signals effectively appear as white noise. Thus the reference CDMA signal, which has been generated by modulation of the data

sequence with the reference pseudo random binary sequence is extracted from the composite CDMA signals.

Power control is used extensively in most CDMA systems. It is used to ensure that the signal power of each user/handset sharing the same frequency spectrum has the same power arriving at the base station [27]. Assume a single cell site with perfect power control and N users. The base station receives a composite CDMA signal containing the desired signal from one user of power S and signals from the other N-1 users of power S each. The interference power relative to the desired signal is (N-1)S. The signal-to-noise ratio (SNR) for the desired signal at the base station is, ignoring thermal and other noise [27],

$$SNR = \frac{S}{(N-1)\,S} = \frac{1}{(N-1)} \qquad (1.1)$$

Assuming that the information rate of a user is R and the bandwidth of the CDMA signal is W, the energy-per-bit-to-noise-density ratio, E_b/N_o, is [27]:

$$\frac{E_b}{N_o} = \frac{\frac{S}{R}}{\frac{(N-1)\,S}{W}} = \frac{\frac{W}{R}}{N-1} \qquad (1.2)$$

where E_b is the energy per bit and N_o is the effective noise power density which is the interference power per unit bandwidth. By comparing (1.1) and (1.2), one finds that the E_b/N_o is W/R times greater than the SNR. The W/R ratio is the processing gain [27]. Ignoring background noise and interference from other cells and assuming that the E_b/N_o required to obtain an acceptable error rate is 6 dB, W = 1.2288 MHz and R = 9600 bits per second, up to 32 users can simultaneously use this

8

,

channel [29]. The low E_b/N_o ratio used is due to the high redundancy error correction coding techniques employed in the CDMA system.

The main attraction of the CDMA system relative to the analog and other digital systems is its gain in capacity. As suggested in [28], the cochannel interference reduction factor (CIRF) is:

$$CIRF = \frac{D_s}{R_c} \qquad (1.3)$$

where D_s is the minimum separation between two cochannel cells and R_c is the cell radius. For CDMA, unlike other air interface protocols, CIRF = 2 which means that the same radio channel can be reused in all neighboring cells. Together with the low E_b/N_o, voice duty cycle monitoring and sectoring, CDMA has the potential for high capacity systems.

1.2.2 IS-95+ standard CDMA Forward Link Transmitter

In the forward link, a handset user can occupy one "channel". Each "channel" is modulated by an assigned Walsh function which is selected from a set of 64 Walsh functions. There are 64 Walsh chips in each Walsh function or Walsh symbol. The 64 Walsh functions form a Hadamard matrix [34]. A Walsh function is a row from the matrix. Each Walsh function is orthogonal to the other 63 Walsh functions. Suppose that the Walsh function consists of 1's and -1's. The convolution of any two non-identical Walsh function is zero while the convolution of any two identical Walsh functions is 64. The Walsh modulation in the forward link is conducted such that each error correction encoded data bit is multiplied by 64 Walsh chips from the assigned Walsh function. Thus each

data bit is spread to 64 chips. The Walsh spreading is done at 1.2288 MHz. The data before spreading is at a rate of 19.2 kbit/s or less.

The Walsh modulated data at 1.2288 MHz is split into two branches: the I and Q signals branches of the CDMA signals. The Walsh chips at the I signal branch are further modulated by an I -channel pseudo noise (PN) code and the Walsh chips at the Q signal branch are further modulated by a Q-channel PN code. Both I,Q-channel PN codes have the same period of 32,768 symbols but they are generated by different polynomials. At the I and Q signal branches the PN spread sequence is pulse shaped by a baseband filter and then quadrature modulated to the corresponding carrier frequency. For an input data rate of 9600 Hz, the Walsh and PN code spread the data by a factor of 128. This is equivalent to a 21 dB processing gain.

One of the important characteristics of the forward link is the use of a pilot channel. The pilot channel is a "channel" with no data. It is modulated by the 0th Walsh function. The purpose of the pilot channel is to allow coherent demodulation at the handset. The pilot channel only exists in the forward link since it would be power inefficient for each handset to transmit a pilot channel signal [27]. In addition, insertion of a pilot channel in the reverse link (handset to base station) would increase the co-channel interference. This would, in turn, decrease capacity. Thus, there is no coherent demodulation in the reverse link. Besides the pilot channel, the 32nd Walsh function is reserved for a "sync channel" [5]. All the other "channels" can be used for traffic or paging. As specified by the IS-95+ standard [5], a traffic channel is the path between handset and base station
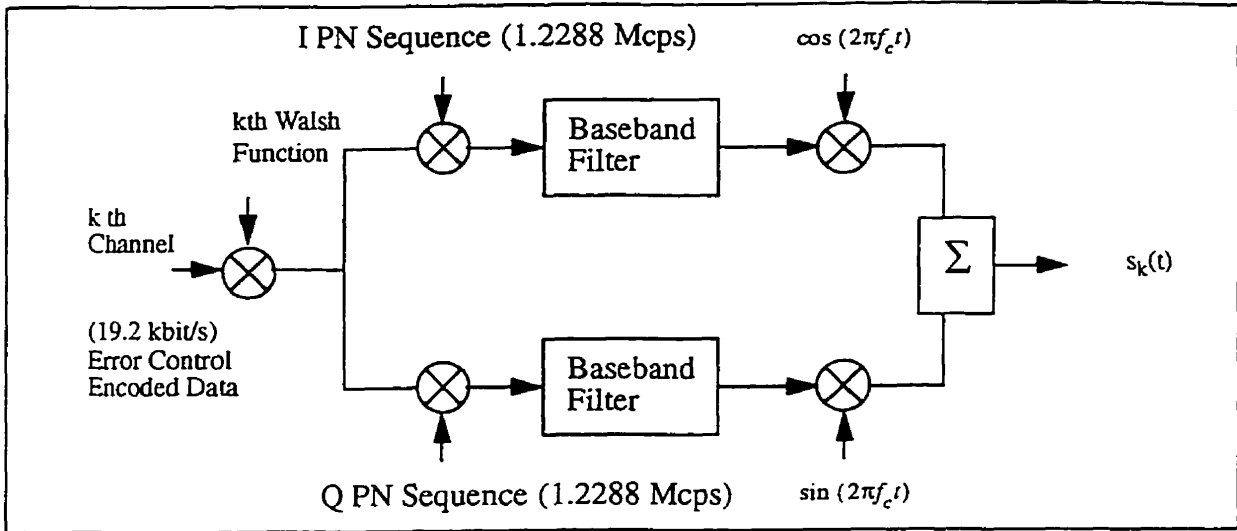
Fig 1.4 Simplified forward link transmitter structure

for users and signaling traffic. In Fig. 1.4, a simplified forward link transmitter is shown. A detailed

description of the forward link can be found in Figure 3.1.3.1-1 of the IS-95+ standard [5].

1.2.3 IS-95+ standard CDMA Reverse Link Transmitter

In the reverse link, at the transmitter of the handset, digital information is encoded by a

rate 1/3 convolutional code at a rate of 28.8 k symbols/s. It is then modulated by Walsh functions.

Walsh modulation in the reverse link is different from the modulation in the forward link. In the

reverse link, the convolutional encoded information is grouped into blocks of 6 bits. From this 6-bit

word a Walsh function is selected. In other words, each 6-bit information word is spread to 64 Walsh

chips. The Walsh chip rate is 307.2 kcps (chips per second). The Walsh spread information is then

spread by a very long PN code (period: 2^{42}-1) at a PN chip rate of 1.2288 MHz. As a result each

Walsh chip is spread by 4 PN chips. Different handsets have different time offset in the very long PN code. This provides identification and security between different handsets. In addition, due to the large period of the very long code, a large addressing space is provided.

The long PN code spread sequence is then split into two branches: the I and Q signal branches. At the I signal branch, an I-channel PN code which is the same as the one used in forward link, is used to spread the sequence. At the Q signal branch, the sequence is spread by the Q-channel PN code and then delayed by one-half of a PN chip. The I and Q-channel PN code spread sequences are filtered by a baseband filter. After the baseband filtering the I and Q signal sequences are mapped into QPSK signals. Fig. 1.5 is a simplified block diagram of the structure of the kth channel reverse link transmitter. A detailed description of the reverse link can be found in Fig. 2.1.3.1-2 of the IS-95+ standard [5].
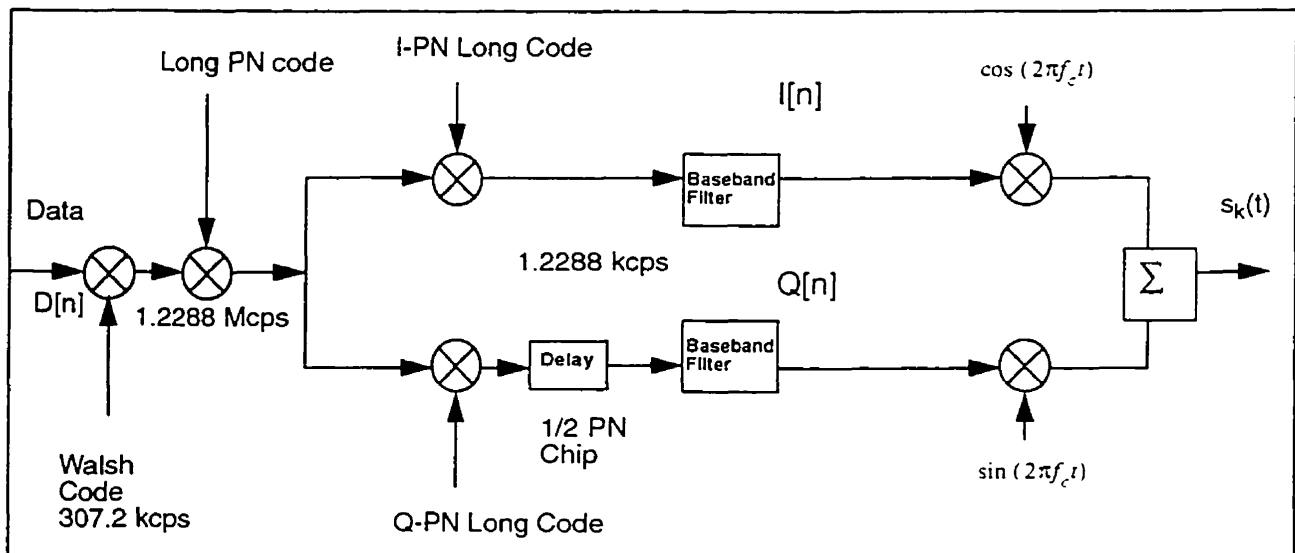
Fig. 1.5 Simplified Structure of the kth carrier channel reverse link transmitter

1.3 Overview of Per-Carrier Down-Conversion Approach
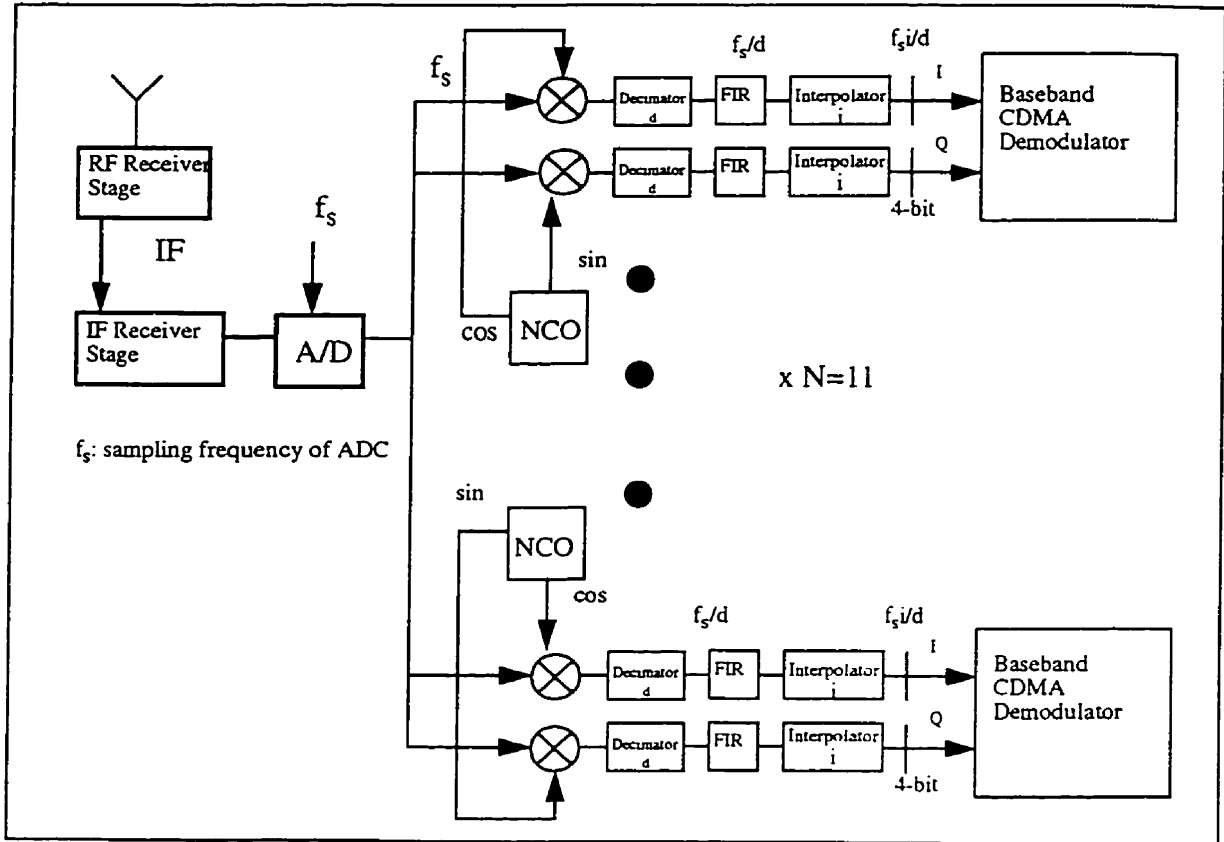
Fig. 1.6 Per-carrier down-conversion structure

The structure of the per-carrier down-conversion approach is shown in Fig. 1.6. In this approach, the CDMA signals from different carriers in the same frequency block are digitized at the IF frequency through a common ADC which samples at f_s. The relationship between f_s and f_{IF}, the center frequency of the IF, is such that f_s should be greater than or equal to two times the highest frequency component of the CDMA signals at the IF frequency, i.e. the Nyquist rate. Sampling at a rate higher than the Nyquist rate can relax the requirement on the analog bandpass filter preceding the

ADC. This is because sampling at a higher rate improves the separation between images of the spectrum of the input analog signal within the spectrum of the digitally sampled signal. These images can be attenuated via digital filtering so the analog bandpass filter design can be simplified. Moreover noise is spread over a greater frequency range by oversampling. This provides a gain in the SNR which, in turn, reduces the dynamic range requirement at the ADC. Despite the advantages of over-sampling one should also take into account that ADC speed is limited by current technology. Furthermore, the ADC sampling frequency also contributes to the system complexity since the devices immediately after the ADC have to work at the ADC's sampling frequency. As a result, the choice of f_s should be a compromise that satisfies these conflicting requirements. On the other hand, it is assumed that the baseband CDMA demodulator has an input sampling rate of $8f_{chip}$. Therefore, in order to avoid using rate change DSP to perform interpolation by a rational factor, which, in general, has high complexity, the ADC sampling frequency, f_s, should be a multiple of the chip rate.

After the ADC the selected carrier is down-shifted to baseband by multiplying the CDMA signal with in-phase and quadrature-phase oscillator signals. The frequencies of the oscillator signals are the center frequency of the selected carrier and they are generated by a direct digital synthesizer (DDS) or a numerically controlled oscillator (NCO). Each carrier in the wideband CDMA spectrum has its own down-shifting branch. After the down-shifted signal is decimated to a lower rate by a decimator, it is then processed by a carrier select FIR filter. Carrier selection at a lower rate reduces the complexity of the filter. Before the signal is fed to the baseband demodulator, it is interpolated back up to $8f_{chip}$ which is the input sampling rate for the demodulator. In addition, the CDMA signals

is rounded-off to 4-bit precision as required by the demodulator. In fact, 4-bit quantization is adequate for a DS-CDMA system assuming the usage of automatic gain control circuitry. It is found in [35] by Doi et al, that quantization of a few bits at the baseband demodulator has minimal SNR degradation in CDMA systems. Furthermore, the SNR stops improving when the number of quantization bits increases to greater than or equal to 4.

1.4 Overview of Polyphase-FFT/Transmultiplexer Approach
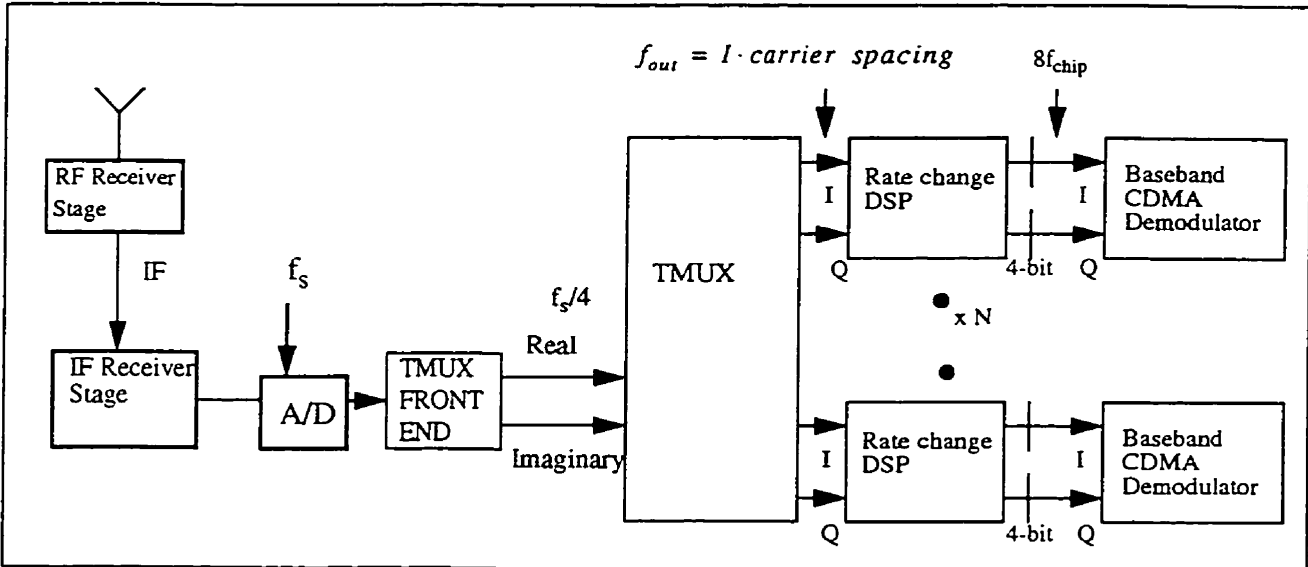
Fig. 1.7 Polyphase-FFT Transmultiplexer Structure

In this approach, the carrier demultiplexing is done by a polyphase-FFT/transmultiplexer (or in short form TMUX) system, as shown in Fig. 1.7. The IF frequency, f_{IF}, and ADC sampling frequency, f_s, should be chosen such that the Nyquist sampling criterion is satisfied. In addition, the choice of f_{IF} and f_s should allow some level of oversampling to the signals since oversampling

improves the SNR and relaxes the requirements for both the bandpass filter preceding the ADC and the ADC precision. Furthermore, if $f_s = 4f_{IF}$ then the complexity of the transmultiplexer front end is reduced. This is discussed in detail in Chapter Four. The function of the N-carrier transmultiplexer is to perform I and Q signal separation of the individual carriers digitally. After the N-carrier transmultiplexer, the N carriers are demultiplexed and translated to baseband. The output of the transmultiplexer for each carrier consists of two branches: I and Q. The sampling frequency of the output at each branch is a multiple of carrier spacing (carrier spacing is 1.25 MHz). This causes a compatibility problem with the baseband CDMA demodulators which require the input sampling rate to be an integer multiple of the chip rate, f_{chip} ($f_{chip} = 1.2288$ MHz). A rate change mechanism, which is capable of interpolating the per-carrier output of the transmultiplexer by a rational factor, has to be added to the system.

1.5 Literature Survey

The transmultiplexer approach to group demodulation was introduced by Bellanger in [8]. The transmultiplexer consists of a polyphase network (phase shifter) and a FFT. A transmultiplexer can be used as a frequency multiplexing or demultiplexing device. For the frequency multiplexing function, also called synthesis, N time domain signals are multiplexed in the frequency domain. For the frequency demultiplexing function, also called analysis, N frequency multiplexed signals are separated/demultiplexed by the transmultiplexer to become N time domain signals. In [30] Wakabayashi et al conducted an investigation on a complete hardware implementation of a 24 carrier

transmultiplexer using a digital signal processor. The transmultiplexer built was a modification of an earlier model of a transmultiplexer which employed polyphase filters and FFT. The modification was designed to reduce the word length requirement of the digital processor by reducing round-off noise. It was found that in order to comply with noise requirement by CCITT G.792, a 16 bit parallel digital signal processor is needed.

In [31], Maruta et al built two transmultiplexers using high level DSP chip sets. The transmultiplexers built are intended for frequency division multiplex (FDM)-time division multiplex (TDM) conversion of 24 and 60 carrier PCM signals. Efficient implementations of a 14-point FFT were also developed. The main difference between the transmultiplexer developed in [31] and the transmultiplexer in this thesis is that the transmultiplexer designed in [31] is intended for real single side band signals while in this thesis the transmultiplexer is designed for complex double side band signals. Furthermore, the transmultiplexer in [31] is a critically sampled filter bank. The filter banks considered in this thesis are oversampled filter banks. This issue is discussed in greater detail below.

Transmultiplexers for double side band QPSK signal carrier multiplexing were designed by Hung in [6]. Hung applied the transmultiplexer method to on-board satellite processing in communications. A time domain analysis description of the transmultiplexer was developed in his work. In addition. timing and carrier recovery was also added to the transmultiplexer system for symbol synchronization and accurate coherent demodulation. In Hung's transmultiplexer system the I and Q signal separation is performed in analog while in this thesis the received signals are digitized at the IF

frequency and I, Q separation is performed digitally. In addition, similar to the transmultiplexer designed in [31], Hung's transmultiplexer is a critically sampled filter bank.

In [6, 8,11, 30-31], it has been assumed that each carrier has passband bandwidth, 2B, smaller or equal to the carrier spacing of the FDM signal, ΔF. For a N-carrier FDM signal at a sampling rate of $N\Delta F$, the sampling rate for each of the demultiplexed carriers is ΔF. When 2B $\leq \Delta F$ the per-carrier sampling frequency at the output of the transmultiplexer can be equal to ΔF without serious aliasing. However when 2B > ΔF, sampling at ΔF for each demultiplexed carrier will cause serious distortion due to aliasing. To solve this problem Crochiere presented a detailed discussion in [9] of the modifications that have to be made to the transmultiplexer system for the case when the bandwidth of the individual carrier is greater than the FDM carrier spacing (in other words 2B>Δ F). Assume that the passband bandwidth of the carrier signal is 2B, the sampling rate for the multi-carrier FDM signal is $f_s = N\Delta F$ and $f_{carrier}$ is the sampling rate for each demultiplexed carrier. i.e. the output sampling rate of the transmultiplexer. Three cases for the design of the N-carrier transmultiplexer are discussed:

1) $$2B \leq \Delta F \qquad\qquad (1.4)$$

and

$$f_{carrier} = \Delta F \qquad\qquad (1.5)$$

This is a critically sampled filter bank and the output sampling rate for each demultiplexed carrier is equal to the carrier spacing. The other case is,

2) $$2B \geq \Delta F \qquad\qquad (1.6)$$

and

$$f_{carrier} = n\Delta F \qquad (1.7)$$

where n is an integer and n>1. This is an oversampled filter bank and the output sampling frequency for each demultiplexed carrier is equal to an integer multiple of the carrier spacing.

3) This case is similar to the second case, the carrier passband bandwidth is greater than the carrier spacing and,

$$f_{carrier} = m\Delta F \qquad (1.18)$$

where m is a rational number and m>1. The output sampling rate for each demultiplexed carrier is equal to a rational multiple of the carrier spacing of the form k/d where k and d are integers and k>d. Transmultiplexer designs according to Cases 2 and 3 are necessary when the carrier signal passband bandwidth is greater than the FDM carrier spacing. In Case 3 a new method called the weighted overlap-add structure [32] is used to design the transmultiplexer. This method is a generalization of the polyphase approach used by Cases 1 and 2 such that the polyphase carrier select filter is viewed as a "sliding time window" to the incoming signal.

In the transmultiplexer approach for the CDMA multi-carrier demodulator, the sampling rate of the per-carrier output is incommensurate with the input sampling rate of the CDMA baseband demodulator. Thus a rate conversion mechanism has to be used to interface the transmultiplexer and the demodulator. In [2], Proakis et al discuss the implementation of a second order approximation method for rate conversion by a rational factor. This method is especially useful when the acceptable quantization noise level for the approximated signal is moderate.

In [27-29], the basic theory of the CDMA cellular interface is discussed. Various factors or characteristics of the CDMA system that contribute to the high capacity of the CDMA system are also investigated in these papers. The detailed structure and specification of the CDMA cellular interface, forward link and reverse link, are discussed in [5,16,33].

A "Software Radio" architecture is proposed by Mitola in [19]. A canonical software radio architecture is developed which envisions that all the signals in a wideband spectrum share the same RF front end and the signals are digitized after RF down-conversion. He claims that with the advances made in the field of ADC and DSP techniques such an architecture is representative of the evolution of radio system technology. The ultimate goal is to conduct all radio operations, except the RF receiver stage, in the digital domain or by software. In [18], Wepman discusses the importance of ADC to the software radio architecture. Various sampling techniques and technical specification of the ADC are examined. The advantage of software radio for PCS base stations is discussed in [17] by Baines. Baines states that a software radio architecture can provide flexibility and a concentration advantage to PCS base station design. In [17] the limitations caused by the processing speed provided by current DSP relative to the high data rate demanded by a software radio system is discussed by Baines. The processing performance of various DSPs from different manufacturers are listed. Baines suggested that extensive sampling rate decimation should be employed in order to get around the "DSP bottleneck".

The design of the wideband channelizer/demultiplexer in this thesis is based on the concept of the "Software Radio". This is expected to be the direction in which advanced radio technology will evolve. This thesis gives a detailed study of the application of the "Software Radio" concept to the multi-carrier CDMA system for PCS at 1.9 GHz.

1.6 Contributions of the Thesis

The major contribution of this thesis can be summarized as follows:

1)   A per-carrier wideband DS-CDMA QPSK multi-carrier demodulator/channelizer is designed with digitization of the signal at the IF frequency. The function of the multi-carrier demodulator is to demultiplex and recover the individual carrier signals in a FDM spectrum. The resulting baseband signal is then input to a standard CDMA baseband demodulator.

2)   The time-domain description of the digital transmultiplexer by Hung [6] is extended to include the case where the per-carrier transmultiplexer output sampling frequency is an integer multiple of the carrier spacing.

3)   A DS-CDMA QPSK multi-carrier demodulator/channelizer is designed using the transmultiplexer method with digitization of the signal at IF.

4)   A rate conversion DSP system is realized using the second order approximation [2] and

        logic to implement the rate conversion DSP.

5)   Complexity estimates for the transmultiplexer and per-carrier approach for

        carrier demultiplexing are developed.

6).   Performance of the transmultiplexer multi-carrier demodulator is simulated

        and compliance with the requirements of the IS-95+ standard [5] is verified.

1.7 Presentation Outline

This thesis is divided into six chapters. Chapter One provides background including a

brief introduction to the IS-95+ CDMA standard [5], CDMA theory and the two major approaches

considered for the multi-carrier demodulator/channelizer: 1) a channelizer implemented by per-car-

rier DSP and, 2) a channelizer implemented by a transmultiplexer structure. In Chapter Two, the per-

formance requirements of the wide channelizer are derived from the specifications in the IS-95+

standard [5], rate conversion techniques and ADC precision considerations are discussed. In Chapter

Three the per-carrier channelizer is developed. In Chapter Four, the method of analytical signal gen-

eration through I and Q signal separation is developed. This is followed by a time domain analysis of

the transmultiplexer with emphasis on the case where the carrier bandwidth is greater than the carrier

spacing. Finally a rate conversion system using a 2nd order approximation DSP is developed. In

Chapter Five, the method of designing the carrier select filter that has been used in Chapters Three

and Four is presented. At the end of this chapter, different performance parameters are discussed. In

Chapter Six, conclusions and recommendations for further research are presented.

Chapter Two

Performance Requirements and System Considerations

2 Introduction

In this chapter a discussion of the performance requirements specified by the IS-95+ standard [5] and their effects on multi-carrier demodulator is presented. Since the demodulator performs its functions in the digital domain, the role of the ADC is crucial to the demodulator's operation. The interrelationship between dynamic range and quantization noise for the ADC in a DS-CDMA system is considered. As rate conversion is used extensively in the design of the demodulators, an introduction to different sampling rate conversion techniques is presented at the end of this chapter.

2.1 IS-95+ Standard CDMA System Performance Requirements

According to the IS-95+ standard [5], each I and Q CDMA signal is shaped by a baseband filter at the transmitter. The mask of the baseband filter specified by the IS-95+ standard [5] is shown in Fig. 2.1. S(f) is the frequency response of the baseband filter. The IS-95+ standard [5] has provided a set of 48 coefficients, $h[n]$, to implement this baseband filter. Fig.2.2 is the plot of the frequency response of this set of coefficients, $H(e^{jw})$. The $h[n]$ provided are for a sampling frequency of $4f_{chip} = 4.9152$ MHz. In this thesis it is assumed that the CDMA transmitter has an impulse response identical to $h[n]$.
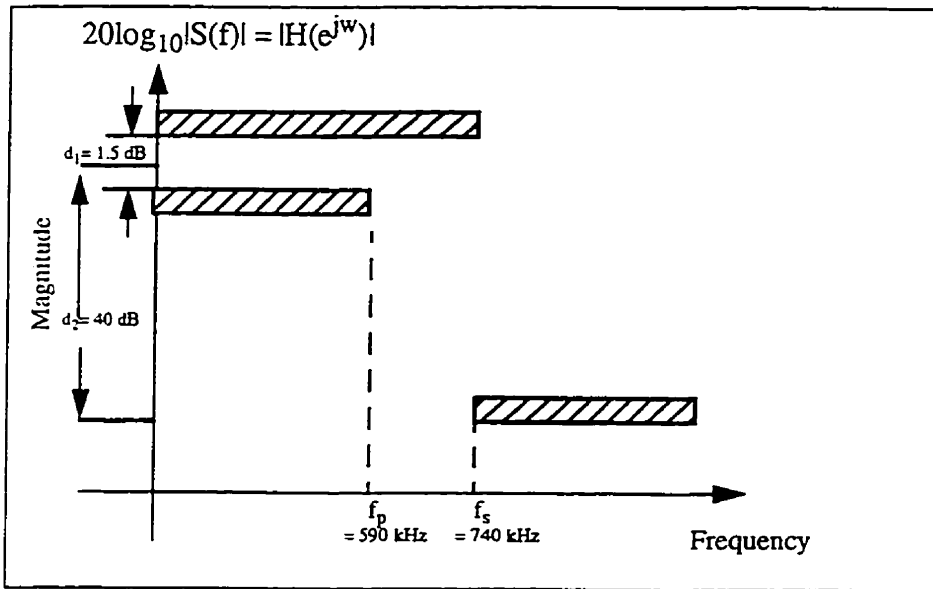
Fig. 2.1 IS-95+ standard [5] CDMA baseband filter (1.25 MHz carrier channel)
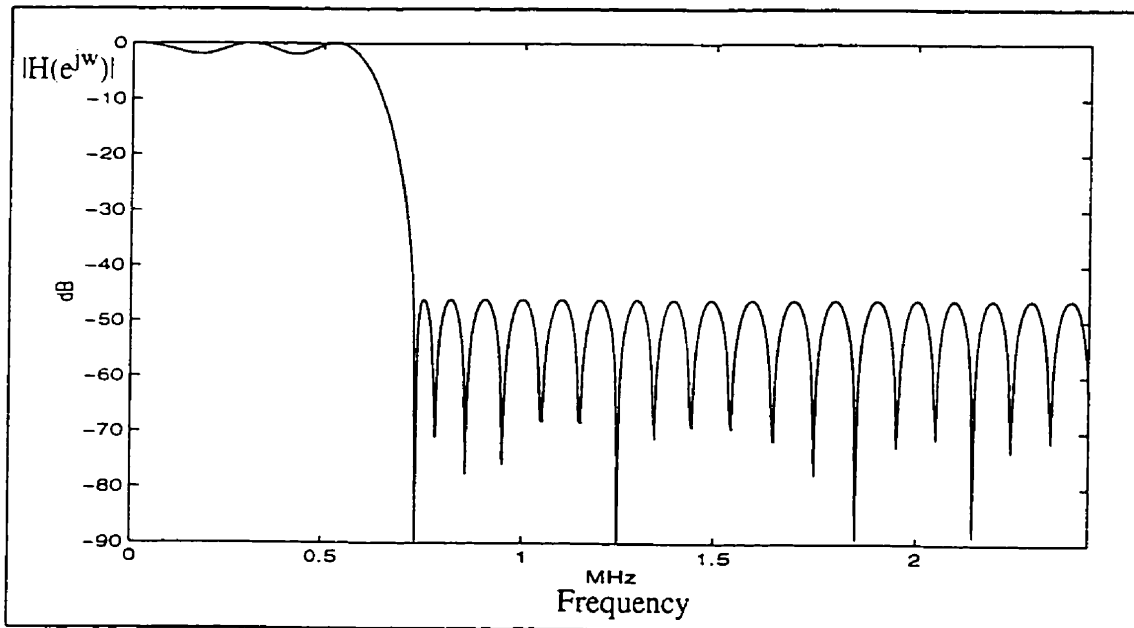
Fig.2.2 Frequency response of the IS-95+ standard baseband filter

The baseband transmitter filter specified by the IS-95+ standard [5] is a symmetric FIR filter whose phase characteristic is linear. In order to minimize intersymbol interference (ISI), the transmitter filter should be matched by a FIR filter with linear phase characteristic at the receiver.

In the Recommended Minimum Performance Requirements for Base Stations Supporting 1.8-2.0 GHz Code Division Multiple Access (CDMA) Personal Stations [16], a waveform quality factor, ρ, which measures the modulation accuracy of the transmitter is specified. ρ is measured at the receive end of the CDMA system and it is a measure of the modulation accuracy of the transmitter. The test procedure for this performance measure calls for an ideal test receiver designed to remove the ISI introduced by the transmit filter. Therefore, assuming that the transmitter has an ideal performance, ρ can be used as a measurement for the degradation to the waveform caused by an imperfect receiver, such as the demodulator developed in this thesis. By using the baseband filter specified by the IS-95+ standard [5] as the transmitter impulse response, an ideal transmitter can be assumed. In this manner, ρ can be used as a measure for the waveform quality of the receiver.

To obtain ρ, assume that $Z[n]$ is the output from a transmitter/receiver chain in which an ideal transmitter is included. Let $R_0[n]$ represent the output from an ideal transmitter/receiver filter chain with no ISI. Assuming sampling at ideal decision points, ρ is the measure of the fraction of power in $Z[n]$ that correlates with $R_0[n]$. It is a measure of the signal distortion and ISI caused by filtering in the receiver. A ρ value equal to 1 means perfect correlation and no signal power is lost due

to distortion. The formula for ρ is shown in (2.1):

$$\rho = \frac{\sum\limits_{j=1}^{N} \left| \sum\limits_{k=1}^{256} Z_{j,k} R_{0,j,k} \right|^2}{\left\{ \sum\limits_{k=1}^{256} |R_{0,j,k}|^2 \right\} \left\{ \sum\limits_{j=1}^{N} \sum\limits_{k=1}^{256} |Z_{j,k}|^2 \right\}} \tag{2.1}$$

where $Z_{j,k} = Z[256(j-1)+k]$ is the kth sample in the jth Walsh Function period, at the PN chip rate, of

the measurement interval of $Z[n]$ and $R_{0,j,k} = R_0[256(j-1)+k]$ is the corresponding sample of $R_0[n]$. It

should be noted that in the reverse link transmitter, after the Walsh spreading process, each Walsh

chip is spread by 4 PN chips. Therefore, at the PN chip rate, $f_{chip}=1.2288$ MHz, each Walsh function

period is equal to 256 PN chips.

In fact, since the sequence, $R_0[n]$, consists of terms -1 and 1, for an ideal transmitter/

receiver chain the summation over k in the numerator of the expression shown in (2.1) is equivalent

to the PN and Walsh despreading operation in the baseband CDMA demodulator in which convolu-

tion is performed over the 256 symbols of the PN/Walsh period. The terms in the denominator of the

expression in (2.1) are the normalization of the Walsh convolution result. Furthermore, the ρ value is

the correlation coefficient taken at the best synchronization/decision point. At other synchronization/

decision points the correlation coefficient will be less than the maximum ρ value. If correlation coef-

ficient values at different synchronization points are plotted, an eye shaped curve will be formed. The

highest point or the eye opening is the maximum ρ. Similar eye diagrams can be obtained if the nor-

malized summation of all the Walsh convolution results over the whole received signal sequence, at

different decision points, are plotted instead of the ρ values. As a result, the ρ value is a measure of

the maximum eye opening and a measurement of the amount of degradation the demodulator has introduced to the CDMA despreading process. Moreover, ρ is also a measure of the cross-correlation between the received signal and all possible transmitted symbols.

It is specified by [16] that a CDMA system should have a signal sensitivity such that a frame error rate (FER) of 1% or less is to be maintained in its normal operating environment. For the reverse (subscriber-to-cell-site) communications link, non-coherent reception and independent fading of all users is assumed. With dual antenna diversity, the required E_b/N_0 is 6 dB per antenna (assuming the use of a relatively powerful constraint length rate = 1/3 convolutional code) [29]. ρ and FER are related in the sense that ρ, the correlation between the received signal and the information signal, is a measure of the maximum eye opening. In the receiver there are a number of impairments, due to imperfect receiver filtering, synchronization and carrier recovery, etc. These impairments increase the E_b/N_0 required to achieve the FER objective. The design objective of the multi-carrier demodulator in this thesis is a maximum of 0.25 dB E_b/N_0 degradation due to imperfect filtering in the demodulator. This translates to a ρ value of 0.95 (since the E_b/N_0 degradation = $10\log\rho$). As a result, in order to make the CDMA system robust to ISI and to satisfy the performance specifications, an acceptable ρ value is between 0.95 and 1.

In the PCS 1.9 GHz frequency spectrum, a CDMA carrier may face interference from different sources. These interference sources can be carriers from other PCS operators, perhaps using different air interface protocols such as Time Division Multiple Access (TDMA), or existing point-to-

point or point-to-multi-point microwave systems that already use the 1.9 GHz spectrum. To obtain

acceptable performance in the presence of these degradations, system performance with a single tone

interferer is specified. Single tone desensitization is a measure of the ability to receive a CDMA sig-

nal on the assigned carrier frequency in the presence of a single tone that is offset from the center fre-

quency of the assigned carrier. In [16] it is specified that in the presence of a tone interferer, with a

frequency offset of +/- 1.25 MHz, which has a maximum strength of 90 dB above a CDMA carrier,

the SNR shall not increase by more than 3 dB to maintain a FER of less than 1.5% with a 95% confi-

dence level. In the following, we first examine the noise level in a CDMA system. In a CDMA sys-

tem, the in-band noise includes thermal noise, noise from electronic devices in the radio receiver and

quantization noise added by the ADC. The in-band noise can be calculated as follows [18]:

Noise Floor = -174 dBm + 10log(1.2288 MHz) + Noise Figure (NF)

$$= -113 \text{ dBm} + \text{NF} \qquad . \qquad (2.2)$$

The thermal noise power density of the signal at room temperature is -174 dBm/Hz [36]. At a signal

bandwidth of 1.2288 MHz, the thermal noise is -113 dBm. Noise from electronic devices and quanti-

zation in the radio can be parametrized as the system noise figure (NF). Assuming a value for the NF

is 6 dB [18], the noise floor according to (2.2) is -107 dBm. As specified by [16], at a 1% FER, the

CDMA signal should have a strength of less than -119dBm. In the spreading and despreading chain,

processing gain, G_p, is added to the CDMA signal. In (2.3) below, the processing gain given by a

direct sequence CDMA system is shown.

$$G_p = 10\log\left(\frac{B_s}{B_{info}}\right) \qquad (2.3)$$

where B_s is the bandwidth of the signal after spreading and B_{info} is the bandwidth of the original

information before spreading. This processing gain improves the SNR of the CDMA signal. In our case B_s is 1.2288 MHz which results from spreading the 9600 bit/s data by a factor of 128. Thus the processing gain is approximately 21 dB. Therefore after the despreading process, the resulting E_b/N_o is less than 9 dB. In the following we assume a CDMA receiver sensitivity of -122 dBm for a FER of 1.5 %. Thus, a tone of strength 90 dB above the CDMA signals will be equal to (-122 + 90)=-32 dBm. In order to maintain the FER of less than 1.5%, the tone that leaks through the receiver filter should be attenuated to the same level as the noise floor. In this manner, the total noise is increased by 3 dB. The SNR can then be maintained by increasing the signal power by 3 dB. As has been calculated in (2.2), the noise floor is about -107 dBm. Since the tone has a power of -32 dBm, the minimum attenuation that the receiver filter has to provide in order to attenuate the tone to the noise floor is -(107-32) dB = -75 dB. Given a margin of 10 dB for phase noise, ADC degradation and adjacent carrier selectivity, the stopband attenuation at frequency positions greater than or equal to 1.25 MHz from the CDMA carrier should be at least -85 dB. The above analysis on the minimum tone attenuation requirement is graphically illustrated in Fig. 2.3 and the corresponding calculations are tabulated in Table 2.1.

In addition to the requirements mentioned above, it is also stated in [16] that the noise bandwidth of the receiver should be less than 625 kHz. The noise bandwidth for an analog filter with an impulse response h(t) can be calculated as follows [22]:

$$B_n = \frac{\int_0^\infty |H(f)|^2 \, df}{|H_m|^2} \tag{2.4}$$

where $|H(f)|$ is the magnitude of the frequency response (gain factor) of $h(t)$ and $|H_m|$ is the maximum value of the gain factor.
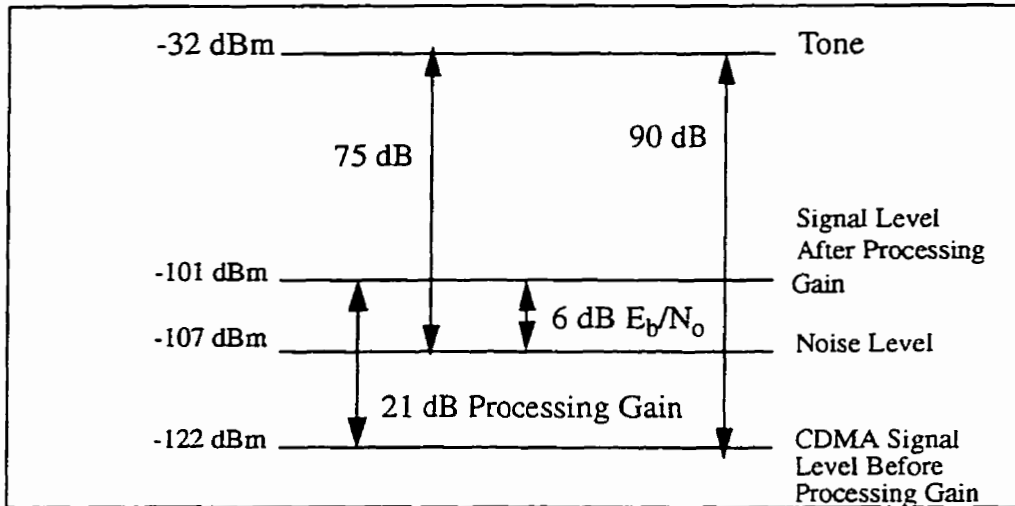
Fig. 2.3 Relationship of CDMA signal and tone level

Table 2.1: Tone attenuation requirement

Tone	90 dB above signal
Signal	-122 dBm
Tone	-32 dBm
Signal After Processing Gain	-101 dBm
Tone-noise Difference	-75 dB
margin	10 dB
Tone Attenuation needed	-85 dB

2.2 ADC Precision Considerations

By the Nyquist sampling theorem [9], the sampling rate for a baseband signal has to be at least twice the highest frequency component of a signal. Therefore the sampling frequency of the

31

ADC shown in the front end of the system in Fig.1.2 has to be at least $2(f_{IF} + \text{signal bandwidth} / 2)$.

The ADC sampling rate can be lower than the Nyquist rate for bandpass sampling [20]. However bandpass sampling for ADC is not considered in this thesis. It is possible to improve the dynamic range of an ADC by increasing the signal sampling rate. By doing so, quantization noise from the ADC is spread over a wider frequency range and the effective spurious free dynamic range (SFDR) of an ADC is increased [17]. SFDR is a measure of the ratio of signal power to the largest spurious product power. SFDR is directly related to the ADC dynamic range. The contribution to the SFDR by oversampling is

$$SFDR \; Gain_{Oversampling} = 10\log\left[\frac{Sampling \; frequency}{2 \cdot signal \; bandwidth}\right] \qquad . \qquad (2.5)$$

Due to noise and interference from other signals in a cellular environment, it is advantageous to increase the SFDR of an ADC. Increasing the signal sampling rate is one way to accomplish this increase of the SFDR.

To investigate the bit precision of the ADC used after the IF receiver stage, one should consider the acceptable noise level in the signals after sampling. As calculated in (2.2), the noise floor for the CDMA system is at -107 dBm with the assumption that the value of the NF is 6 dB. Assume that in the 6 dB NF value, 5.5 dB is allocated for noise from electronic devices excluding the ADC. The remaining 0.5 dB is due to quantization noise. The combined thermal and electronic device noise is (-113+5.5) dBm = -107.5 dBm. Define $\sigma_{Thermal \; Noise}^2$ as the power of the combined

thermal and electronics noise and $\sigma_{Quantization}^2$ as the power of quantization noise. Then

$$\sigma_{Thermal\ Noise}^2 + \sigma_{Quantization\ Noise}^2 = 10^{\frac{0.5}{10}} \sigma_{Thermal\ Noise}^2 \qquad . \qquad (2.6)$$

and

$$\sigma_{Quantization\ Noise}^2 = 0.122 \sigma_{Thermal\ Noise}^2$$

$$= -9.1 dB \ of \ \sigma_{Thermal\ Noise}^2 \qquad (2.7)$$

By (2.7) the quantization noise level is at (-107.5 - 9.1) dBm = -116.6 dBm.

As mentioned in Section 2.1, the maximum tone interferers are of strength -32 dBm. The difference between the tone and the quantization noise floor is (116.6 - 32) dB = 84.6 dB. Thus the ADC is required to provide a spurious free dynamic range (SFDR) of 84.6dB. For the case of the transmultiplexer approach to carrier demultiplexing, the half-band lowpass filter used in the transmultiplexer has a very gentle transition band roll-off and the noise bandwidth is greater than the signal bandwidth. Therefore, the gain in ADC SFDR by oversampling has to be calculated at the input of the transmultiplexer. At each of the I and Q signal branches in the receiver, see Fig. 1.7, before the transmultiplexer, the signal sampling rate is decimated to 15 MHz. By (2.5) the gain in effective ADC SFDR due to oversampling is 10.8 dB. Therefore the SFDR needed from the ADC is reduced from 84.6 dB to 73.8 dB. It is shown in [36] that the ratio of full-load sine wave power to quantizing distortion power (S/D) is:

$$\frac{S}{D} = 6n + 1.8 dB \qquad (2.8)$$

where n is the number of ADC bits. Using equation (2.8), the number of ADC bits required is 12 bits.

Given a 6 dB margin to other system impairments, 13 bits are required, as a one bit increase in resolution in the ADC corresponds to a 6 dB increase in S/D.

For the per-carrier approach, the SFDR gain due to oversampling is improved due to the fact that the digitized signal is passed through a narrow passband decimation filter. The oversampling gain can be calculated at $f_s=48f_{chip}$. By (2.5) the SFDR gain is 16.7 dB. Therefore the SFDR needed to be provided by the ADC is reduced to 67.9 dB which requires 11 bits. Adding 1 ADC bit as the margin for other system impairment and for ease of implementation, a 12-bit ADC is required.

The ADC precision calculated above is determined by the specification for single tone desensitization. The relationship between the SNR and the number of quantizing bits output by the ADC for DS-CDMA signals alone can also be calculated. Following [27] for a single cell and a single carrier system with power control,

$$\frac{E_b}{N_o} = \frac{\left(\frac{W}{R}\right)S}{(N-1)S + \sigma^2_{Thermal\ Noise} + \sigma^2_{Quantization\ Noise}} \tag{2.9}$$

where R is the user information rate, W is the bandwidth of the CDMA signal, N is the number of users sharing the same CDMA carrier and S is the signal power of a single user. In [35], it is shown that assuming that an automatic gain controller (AGC) keeps the standard deviation of the input DS-CDMA signal to one-fifth the range of an ADC, then, with a 4 bit ADC the degradation in E_b/N_o is minimal. The function of the AGC is to reduce the amplitude of the input to reduce clipping distortion.

An upper bound on the number of bits, n_{bit}, required for ADC for a multi-carrier CDMA signal with n carriers is then

$$n_{bit} = 4 + \log_2(n)$$

$$= 8 \text{ bits} \quad \text{for 11 carriers} \quad (2.10)$$

This calculation assumes (equal) power control for each carrier and mo other interference such as without single tone interference. Therefore, the ADC dynamic range required for a multi-carrier CDMA demodulator operating in the environment specified by the IS-95+ standard [5] is set by the specification for single-tone desensitization.

It should be noted that the analysis above for the required ADC bit precision is a function of the NF budgets. However the same procedure can be used to calculate the ADC bit precision for different NF budgets.

2.3 Introduction to Sampling Rate Conversion

Sampling rate conversion techniques are used extensively in the design of the multi-carrier demodulators and are applied in two main areas: 1) decimating the received signal sampling such that the digital processing of the signal is possible using current technology and to minimize system complexity and 2) interpolating the signal to the rate required by the baseband CDMA demodulator. In the following sections rate conversion techniques such as interpolation, decimation and rational factor rate conversion are discussed [9].

2.3.1 Interpolation

When the sampling rate of the signal sequence, x[n], is to be increased by an integer factor, the process is called interpolation. To do the interpolation one can pass x[n] through the structure shown in Fig. 2.4 [9]:
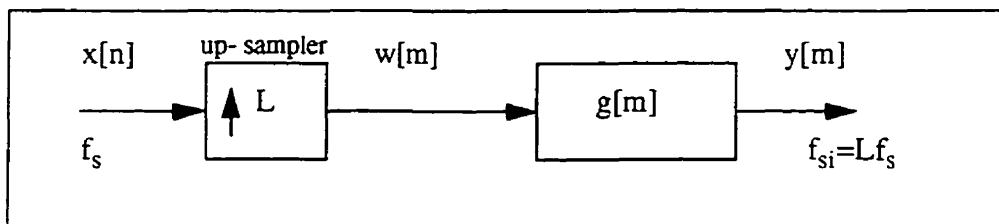
Fig. 2.4 Structure for interpolation by an integer factor L

The frequency response of x[n], $X(e^{jw})$, is shown in Fig. 2.5. By passing x[n] through the up-sampler w[m] is obtained. w[m] is a sequence at a sampling rate of $f_{si} = Lf_s$ and it is defined in (2.11):

$$w[m] = \begin{cases} x\left[\dfrac{m}{L}\right], m = 0, \pm L, \pm 2L, ... \\ 0, \qquad otherwise \end{cases} \qquad (2.11)$$

Equation (2.11) is actually a functional description of the up-sampler: a padding of L-1 zeros between every two consecutive samples of x[n]. The frequency response of w[n], $W(e^{jw})$, is shown in Fig. 2.6. From Fig. 2.6 one can see that images have been introduced at multiples of f_{si}/L or f_s. As a result a lowpass filter, g[m] with a cutoff frequency of (f_{si}/L)-B is required to remove the images introduced by the interpolation operation. $Y(e^{jw})$ is the frequency response of y[n] which is the output of the interpolation lowpass filter g[m] and it is shown in Fig. 2.7.

36
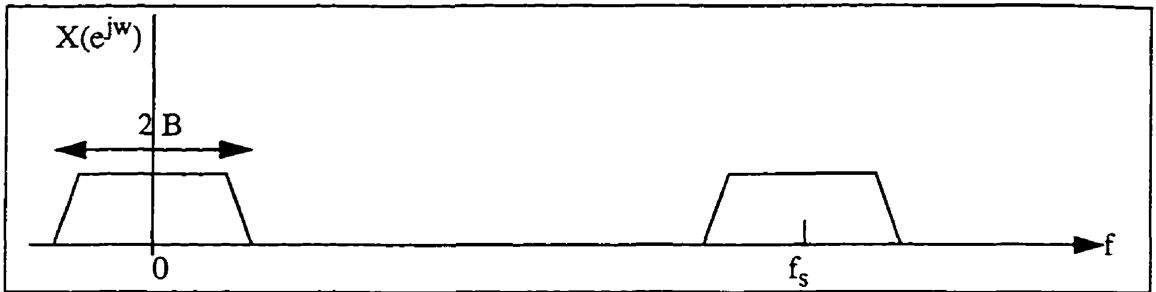
Fig. 2.5 Frequency Response of x[n]
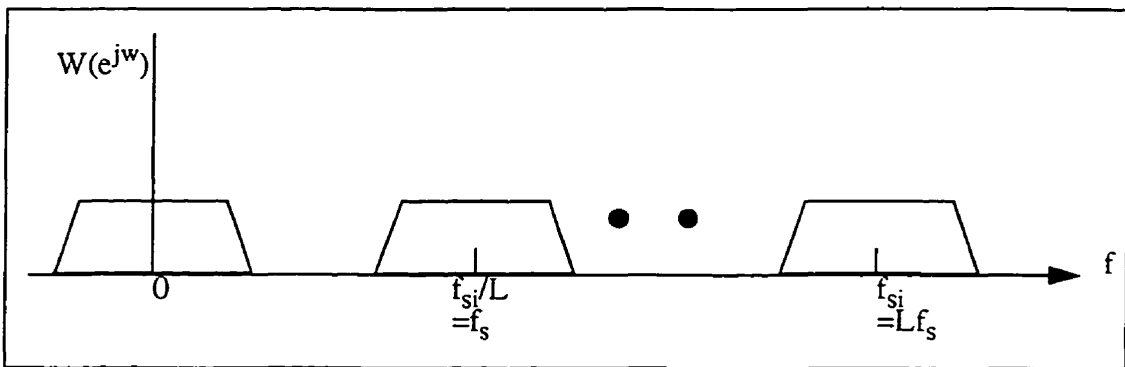
Fig. 2.6 Frequency response of w[m]
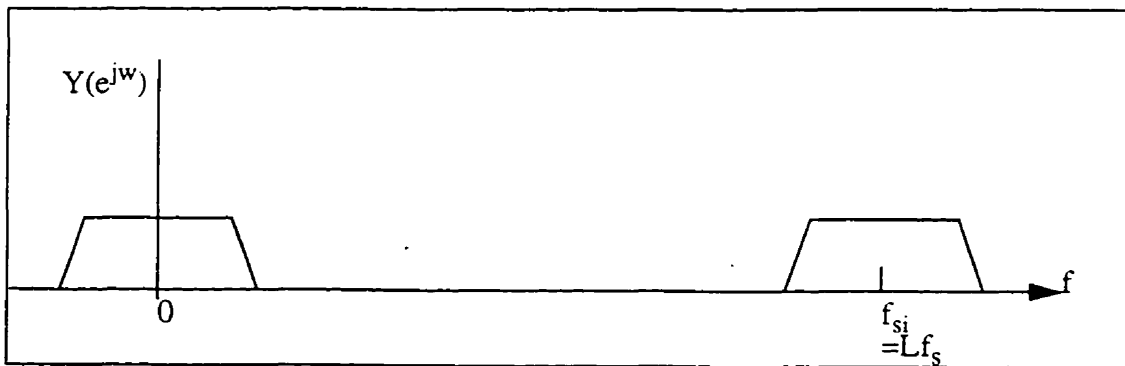
Fig. 2.7 Frequency response of y[m] at sampling rate Lf_s

The equation for interpolation by a factor of L is shown below in (2.12), (2.13) and (2.14):

$$y[m] = \sum_{k=-\infty}^{\infty} g[m-k]\,w[k] \qquad (2.12)$$

$$y[m] = \sum_{k=-\infty}^{\infty} g[m-k]\,x\left[\frac{k}{L}\right] \qquad (2.13)$$

$$y[m] = \sum_{r=-\infty}^{\infty} g[m-rL]\,x(r) \qquad (2.14)$$

where k/L is an integer. Equation (2.12) is the convolution between the zero-padded x[n], denoted w[m], and g[m]. Equations (2.13) and (2.14) show the relationship between the interpolated signal sequence y[m] and input x[n]. It should be noted that although the lowpass filter, g[m], is running at a sampling rate of Lf_s, the original input, x[n], is at a rate f_s. This is because L-1 zeros have been added between the consecutive samples of x[n].

2.3.2 Decimation

In order to reduce or decimate the sampling rate of a digitized sequence, x[n], at a sampling rate f_s by an integer factor, M, one can use the structure shown in Fig. 2.8 [9].
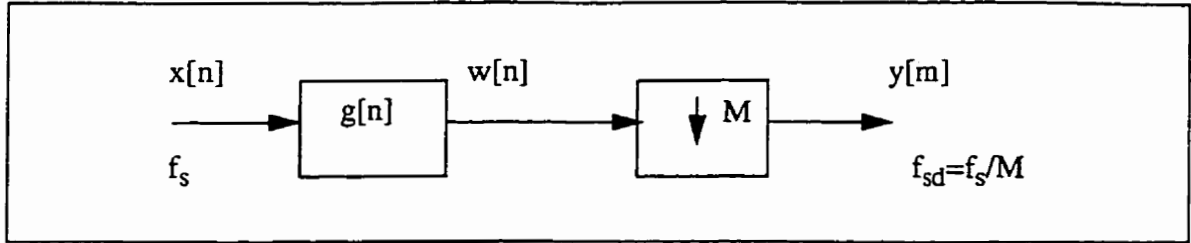
Fig. 2.8 Structure for decimation by a factor of M

The sequence, g[n], is the impulse response of a lowpass FIR filter and the second box in the diagram represents a down-sampler. In the down-sampler every Mth sample in the w[n] sequence is chosen for further signal processing. Effectively all devices to the left of the down-sampler are clocked at the rate f_s and all devices to the right of the down-sampler are clocked by $f_s/M=f_{sd}$. If we consider x[n] to be the impulse response of a lowpass signal with bandwidth 2B, and $X(e^{jw})$ to be its frequency response, then w[n] is the result of convolution between x[n] and g[n] as given in (2.15):

$$w[n] = \sum_{k=-\infty}^{\infty} g[k] x[n-k] \qquad (2.15)$$

In Fig. 2.9 and 2.10 the frequency response of x[n] and w[n] are shown respectively.
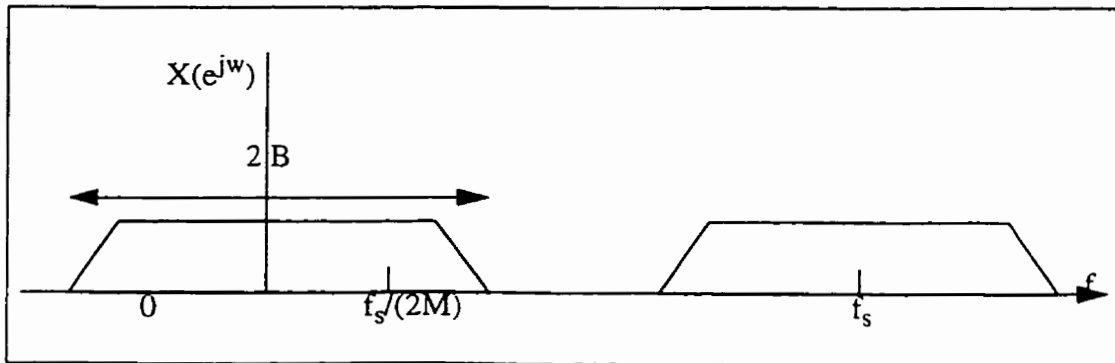
Fig. 2.9 Frequency response of x[n] at sampling rate f_s
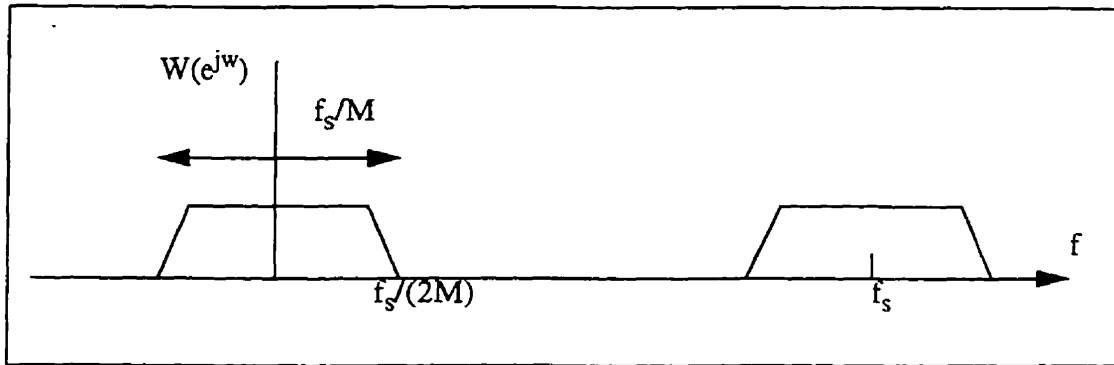
Fig. 2.10 Frequency response w[n] at sampling rate f_s
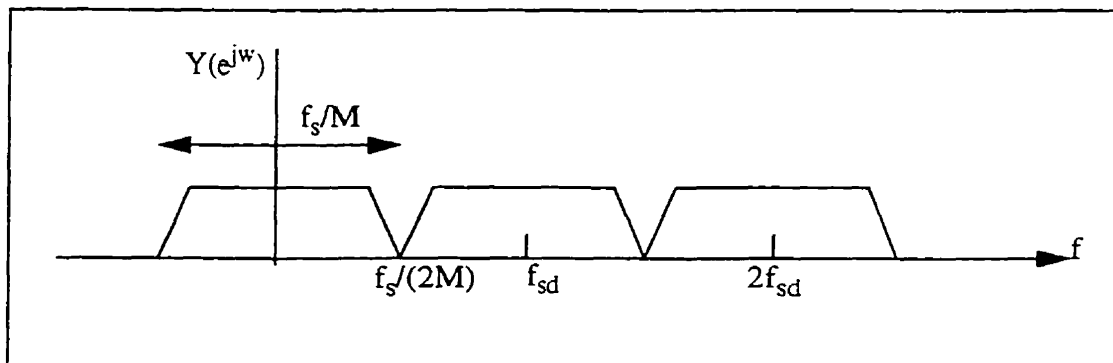
Fig. 2.11 Frequency response of y[m] at sampling rate $f_{sd}=f_s/M$

$W(e^{jw})$ is the frequency response of w[n]. In Fig. 2.10 it can be seen that $X(e^{jw})$ has been

band limited by g[n], the decimation lowpass filter. The bandwidth of $W(e^{jw})$ is f_s/M. $Y(e^{jw})$, as

shown in Fig. 2.11, is the frequency response of y[m], which is the down-sampled version of w[n]. In

the frequency domain the down-sampling process can be seen as a lateral translation of $W(e^{jw})$'s

image at f_s towards baseband. The goal of such a translation is to have $W(e^{jw})$'s image centered on

$f_{sd}=f_s/M$. If the decimation lowpass filter is omitted, the decimation process would cause serious

aliasing of the signal x[n] since the bandwidth of $X(e^{jw})$ is 2B which is bigger than f_s/M. The frequency boundaries of the down-sampled $X(e^{jw})$ would be overlapped by its image. Therefore the decimation lowpass filter with stopband at $f_s/(2M)$ is necessary to avoid aliasing caused by the decimation process. In (2.16) below, a mathematical relationship between y[m] and x[n] is shown [9]:

$$y[m] = \sum_{n=-\infty}^{\infty} g[Mm-n] x[n] \qquad (2.16)$$

It should be noted that at the down-sampler every Mth sample of w[n] is picked and all other samples are discarded. Therefore, although the decimation lowpass filter is operating at a sampling rate of f_s the effective output data rate of the filter is actually $f_s/M=f_{sd}$.

2.3.3 Rate Conversion for Rational Factor

In the previous two sections the issues of interpolation and decimation by an integer factor are discussed. If the interpolation or decimation rate is not an integer but a rational number the structures shown in the previous sections must be combined. Let the rate conversion factor be a rational number L/M, then the structure shown in Fig. 2.12 can be used to do the rational factor rate conversion [9].
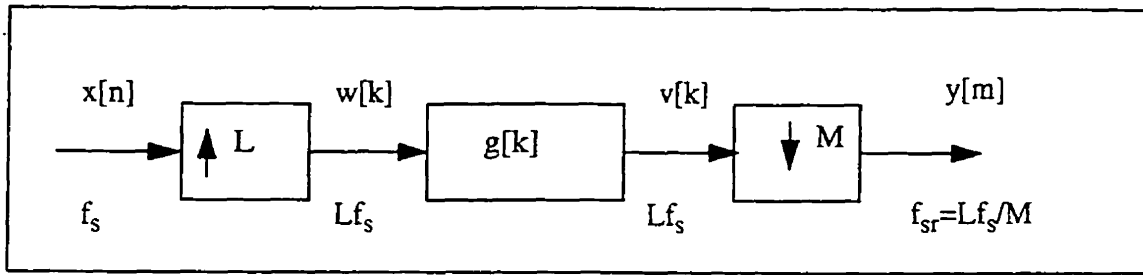
Fig. 2.12 Structure for rate conversion by a rational factor L/M

In Fig. 2.12, g[k] represents a lowpass filter used both to filter out images, introduced by the interpolation process, and avoid aliasing caused by the decimation process. The structure shown in Fig. 2.12 can be very complicated if the numerator and denominator of the rational factor are large. In this case one can use other techniques such as implementing g[k] as a polyphase filter or using 2nd or higher order linear interpolation rate conversion mechanisms. Rate conversion using 2nd order linear interpolation will be discussed in detail in Chapter Four.

Chapter Three

Per-Carrier Down-conversion Approach to Carrier Demultiplexing

3 Introduction

In this chapter the per-carrier down-conversion approach to carrier demultiplexing is discussed. The design of various components of the per-carrier system is presented. The impact of quantization error on the performance of the per-carrier demodulator is investigated. At the end of this chapter. an estimate of the system complexity of the per-carrier approach is presented.

3.1 Per-Carrier Overview
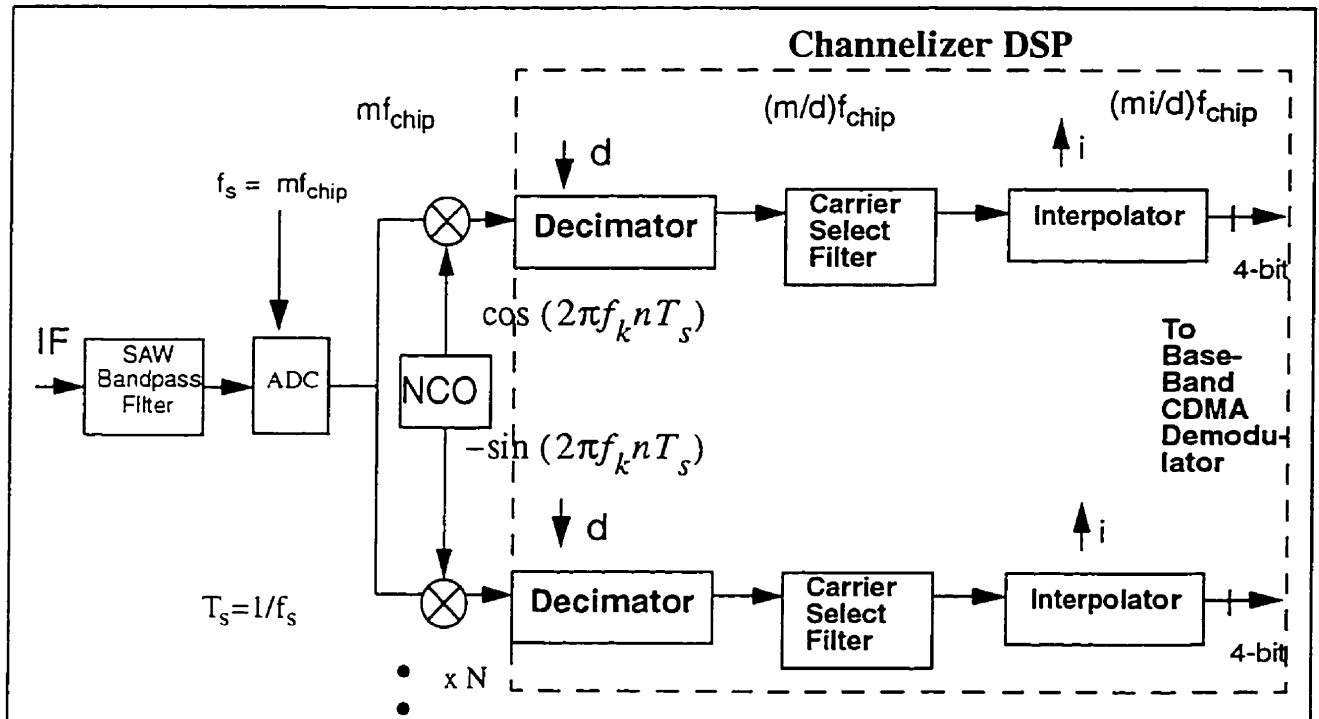
Fig 3.1 Structure of per-carrier approach for carrier demultiplexing DSP

The system block diagram shown in Fig. 3.1 represents the structure for demultiplexing one carrier from the 15 MHz CDMA spectrum using a per-carrier down-conversion approach. In order to demultiplex the N carriers multiplexed in the CDMA spectrum, there are N branches in the carrier demultiplexing DSP identical to the structure shown in Fig. 3.1. After the bandpass SAW filter, with passband bandwidth approximately equal to the CDMA signal block of interest, the CDMA signal block centered at f_{IF}, the center frequency of the IF band, is digitized by an ADC. The sampling frequency of the ADC is f_s. The carrier selected in the CDMA spectrum is down-shifted to baseband by multiplying with a sin/cos function whose oscillator frequency is tuned to the frequency of the selected carrier. The functions of the sin/cos mixers and the NCO are to perform I, in-phase, and Q, quadrature-phase, signal separation, and carrier down-conversion. After the down-conversion, the I and Q signals are processed by a channelizer DSP. Inside the DSP there is a decimator, a carrier select filter and an interpolator for each of the I and Q signal branches. At the decimator, the sampling rate of the signal is decimated by a factor of d. At the decimated sampling rate, the signal is fed into a carrier select filter at each of the I and Q signal branches. After the carrier select filter, the signal sampling rate is interpolated by a factor of i by an interpolator. The output of the channelizer is then input to the baseband CDMA demodulator.

The selection of the ADC sampling rate, f_s, and f_{IF} should provide for oversampling for the CDMA signals. The choice of f_{IF} and f_s should not only satisfy the Nyquist sampling criteria but also provide for adequate separation of the images of the analog CDMA signals so that the design of the analog circuitry preceding the ADC can be simplified. On the other hand it is possible to lower

the IF frequency to the limit that the CDMA signal approaches baseband in order to increase the over-sampling rate or alternatively to decrease the sampling rate. However, this makes the realization of the down-shifting components of the IF receiver stage more difficult. Furthermore, since the base-band CDMA demodulator requires that its input signal sampling frequency be at $8f_{chip}$, where f_{chip} =1.2288 MHz, f_s should be a multiple of the chip rate in order to avoid complicated rational factor interpolators. As a result, the frequencies, f_{IF} and f_s, are chosen to be $12f_{chip}$ and $48f_{chip}$ respectively. The f_s selection can be lowered in order to reduce system complexity. This will be discussed later in this chapter. In this way, the DSP components following the ADC can operate in a lower rate. However, in order to make a direct comparison with the transmultiplexer approach, discussed in Chapter Four, the f_{IF} and f_s are selected such that they approximate the transmultiplexer values.

It is possible to perform quadrature demodulation, i.e., I and Q signal separation, in analog and digitize the I and Q signals separately at baseband, like the approach used by Hung in [6]. However such a method requires two ADCs and introduces I, Q amplitude and phase error.

3.2 Channelizer DSP
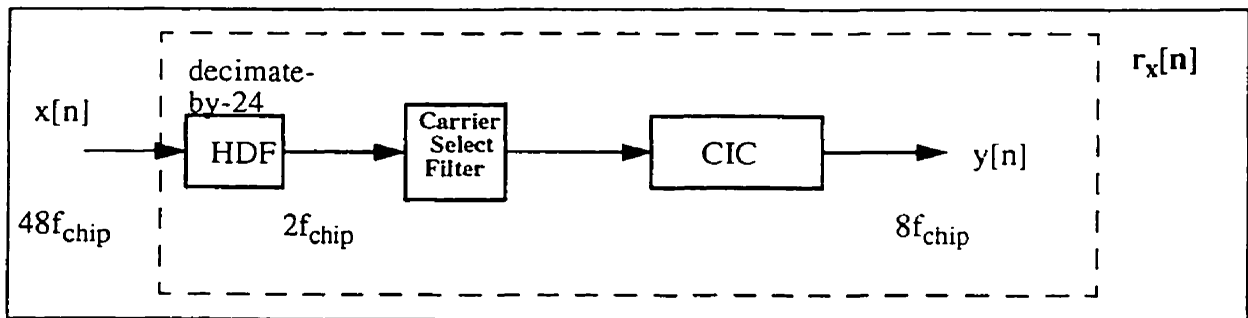
Fig. 3.2 Per-carrier channelizer DSP Structure (For 1 QPSK rail)

The per-carrier channelizer DSP shown in Fig.3.2 is implemented as a cascade of a cascaded-integrator-comb (CIC) decimator [1], a FIR filter and a CIC interpolator. The CIC decimator in this thesis is called the high decimation filter (HDF). It is a form of CIC filter which is configured as a down-sampler and a decimation filter. It is desirable to decimate the sampling frequency of the signals digitized at the IF frequency to the lowest possible rate. In this way, the number of operations that need to be performed by the per-carrier channelizer is reduced. If no decimation is done, the number of operations expressed in million instruction per second (MIPS) will be so high that the DSP will not be realizable by current technology. In addition, after the decimation process the signal sampling rate should still remain as an integer multiple of the chip rate in order to avoid using expensive rational factor rate conversion DSPs. Finally, the decimated signal sampling rate should also maintain the integrity of the signal and prevent distortion caused by aliasing during the decimation process. Based on the criteria stated above, the decimated sampling rate for the per-carrier CDMA signals is selected as $2f_{chip}$. To achieve this sampling rate reduction, a decimation rate of 24 is required at the HDF. The carrier select filter shown in Fig.3.2 is a FIR filter designed to provide carrier selection, pulse shaping and compensation for the effect of the HDF and CIC interpolator on the spectral shape of the incoming CDMA signal. In the following sections a detailed discussion of the structure for the HDF, CIC interpolator and carrier select filter design is presented.

3.2.1 High Decimation Filter (HDF)

The HDF is a cascaded-integrator-comb (CIC) decimation filter developed by Hogenauer [1]. Inside the CIC decimation filter there is an integrator section and a comb section. As shown in Fig. 3.3, there are no multiplication operations in the HDF, there are only additions. Thus no storage for filter coefficients is needed. The integrator section operates at the sampling rate f_s which is the sampling rate before decimation. In our case the sampling frequency before decimation is equal to $48f_{chip} = 58.9824$ MHz. The system function for a single integrator in z-transform notation, where $z = e^{jw}$, is

$$H_I(z) = \frac{1}{1 - z^{-1}} \tag{3.1}$$
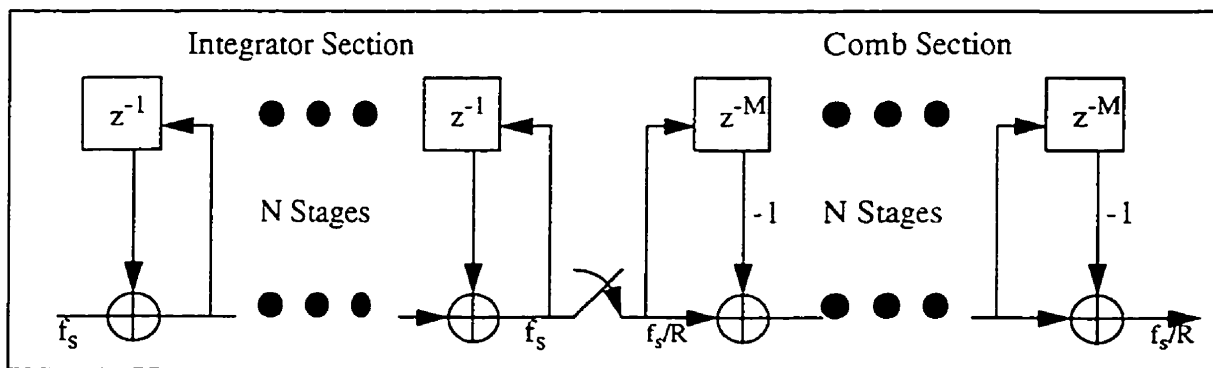
Fig. 3.3 Cascaded-Integrator-Comb decimation filter

The comb section for the CIC filter operates at f_s/R, where R is the decimation rate. In our case $f_s/R = 2f_{chip} = 2.4576$ MHz. The system function for a single comb filter is shown in (3.2):

$$H_C(z) = (1 - z^{(-RM)}) \tag{3.2}$$

where M is called the differential delay. An N stage CIC filter has an overall system function of

$$H(z) = H_I^N(z) \, H_C^N(z) = \frac{(1 - z^{-RM})^N}{(1 - z^{-1})^N} = \left[\sum_{k=0}^{RM-1} z^{-k} \right]^N \qquad (3.3)$$

It can be seen from the CIC's overall system function that it has linear phase and that it is in fact equivalent to a cascade of N FIR filters. The frequency response of the HDF filter, P(f), is [1]:

$$P(f) = \left[\frac{\sin \pi M f}{\sin \frac{\pi f}{R}} \right]^{2N} \qquad (3.4)$$

In Fig.3.4, the frequency response of a 8-stage decimate-by-24 CIC filter with $f_s = 48 f_{chip}$ as reference frequency is shown.
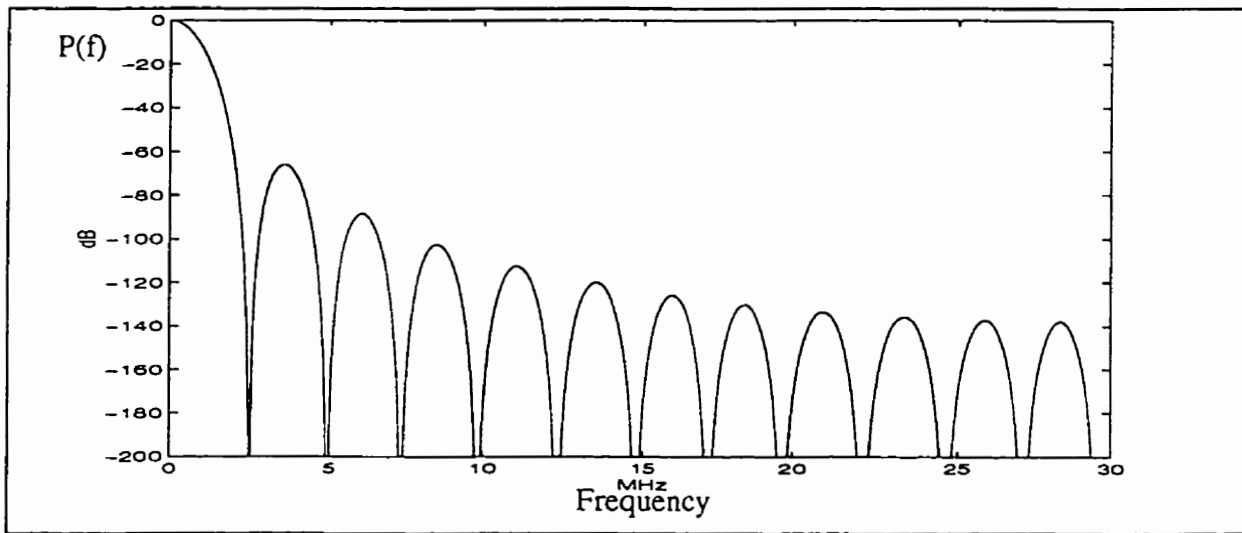
Fig. 3.4 Frequency response of HDF M=1, R=24, N=8

There are nulls at multiples of f/(RM) in the frequency response shown in Fig. 3.4. By adjusting M, the positions of the nulls, shown in Fig. 3.4, can be changed. R is the decimation rate of the HDF which is 24 in our application. In the HDF, the signals are decimated from $48 f_{chip}$ by a fac-

tor of 24 to $2f_{chip}$. In Fig. 3.5 and 3.6 the frequency responses of the HDF with its image after the decimation process are shown for M=2 and M=1 respectively. The dotted line shown in the diagrams is the image created by the decimation process. The overlapping region between the solid line and dotted line experiences distortion caused by aliasing. One of the objectives of the HDF is to make the aliasing region as small as possible. In this way the integrity of the signal can be maintained.

The differential delay, M, is chosen to be 1 for two reasons. The first reason is that the passband roll-off of a HDF with M=2 is steeper than a HDF with M=1. A steeper passband roll-off of the HDF response will make its effect on the CDMA signal more difficult to cancel out. At 625 kHz, the passband edge of the 1.25 MHz CDMA carrier, the attenuation introduced by the M=2 HDF, $H_2(e^{jw})$, is -35 dB, while for the M=1 HDF, $H_1(e^{jw})$, the attenuation at 625 kHz is only -15 dB. These results are shown in Fig. 3.5 and 3.6 respectively. The second reason, for selecting M=1, is that the memory storage requirement of a HDF for M=2 is double that of a M=1 HDF.

By measuring the difference between $H_1(e^{jw})$ and its image at a particular frequency, the SNR of the signal at that frequency is obtained. This assumes that the spectral density of the input signal is uniform across the band of interest. In Fig. 3.7, a plot of the SNR for the HDF as a function of N, the number of stages, is shown for N=4 to 8 and R=24.
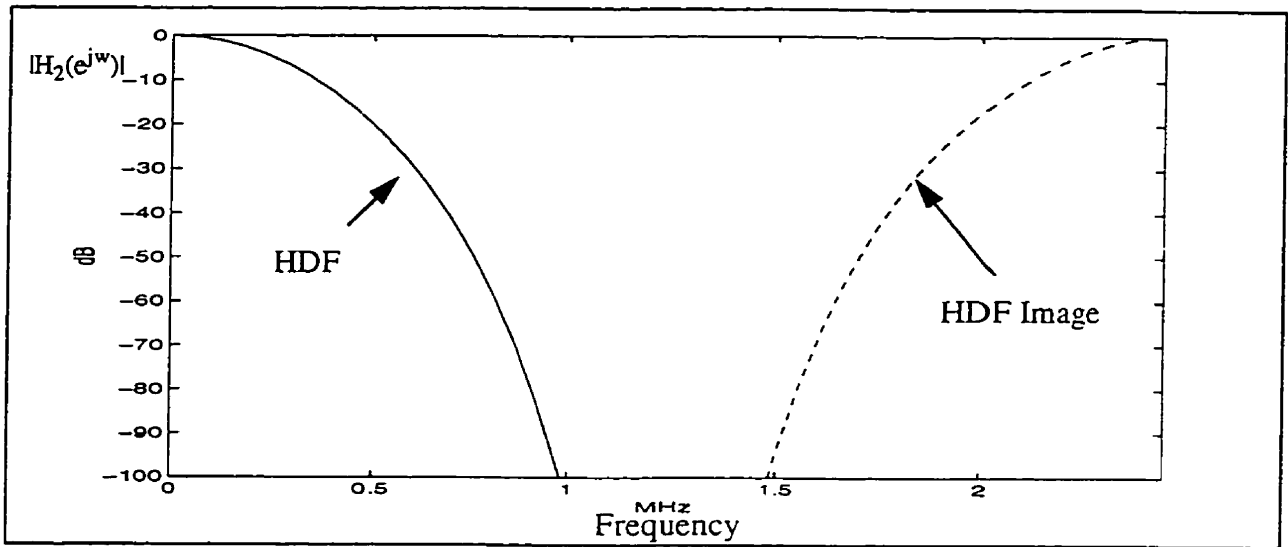
Fig.3.5 Frequency response of HDF at f_s/R: R=24,N=8, M=2
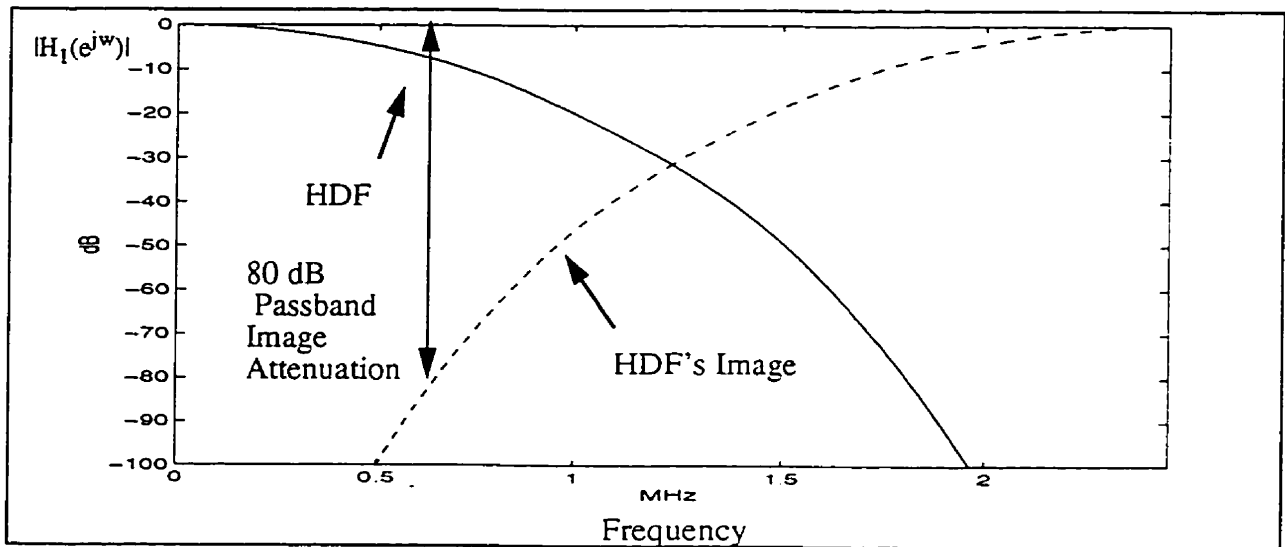
Fig 3.6 Frequency response of HDF at f_s/R: M=1, N=8, R=24
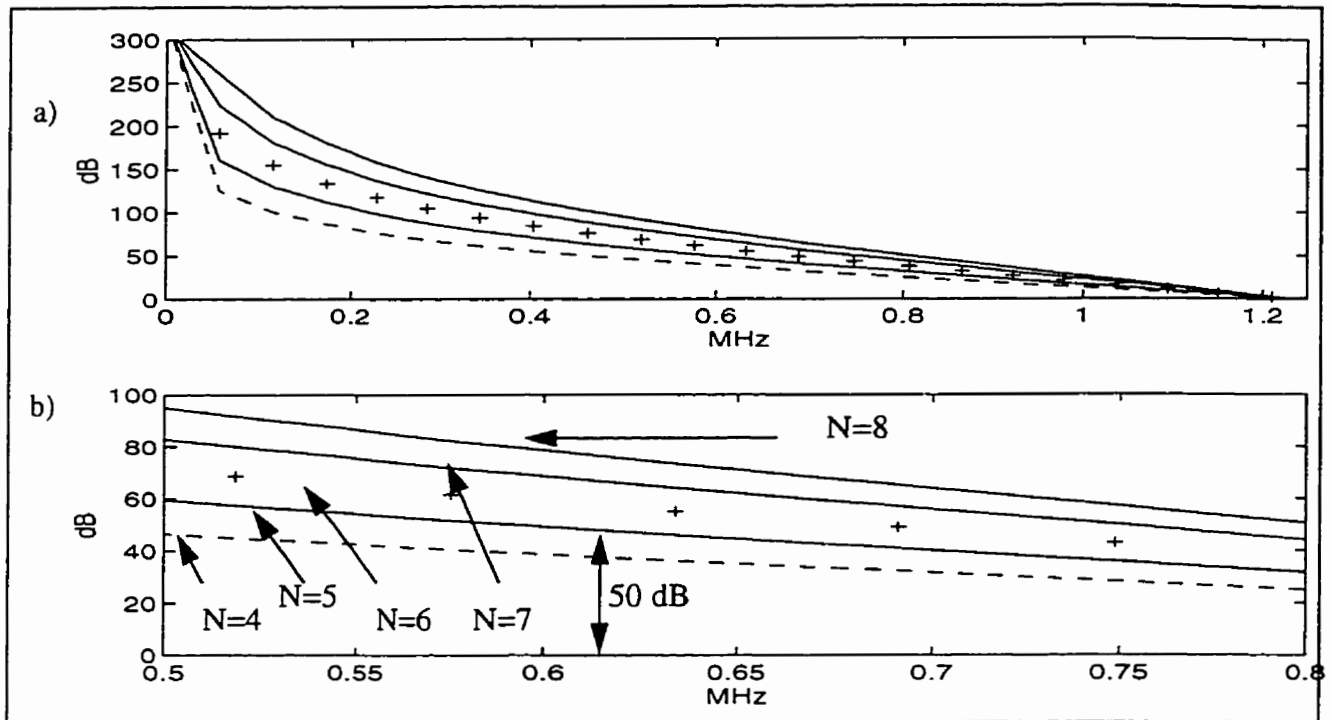
Fig 3.7 SNR vs. frequency for N=4, 5,6,7,8 with R=24 and M=1

The value of N can be used to control the amount of passband aliasing or imaging error of the HDF response after decimation. In the HDF, aliasing is inversely proportional to the number of stages. To determine the order of HDF needed, one should consider the distortion caused by the aliasing of the in-band interferers during the decimation process. The in-band interferers can be signals from sources such as the existing microwave users in the PCS spectrum or other PCS air traffic protocols, e.g. Time Division Multiple Access (TDMA) systems such as the Global System for Mobile Communications (GSM), which may share the same frequency block. Each in-band interferer is assumed to be a tone of maximum strength 90 dB above a CDMA carrier at an offset of +/- 1.25 MHz or beyond to the CDMA carrier assignment as specified by [16] (discussed in Chapter Two).

The interferers are within the 15 MHz CDMA signal spectrum, which is also inside the passband of the IF SAW bandpass filter preceding the ADC of the carrier demultiplexing DSP. These tone interferers are not attenuated at the IF receiver stage. After the decimation process, interferers at a 1.25 MHz offset to the carrier will be aliased back to a 1.25 MHz offset to the carrier. The distortion caused by the aliasing is beyond the passband, 625 kHz, of the CDMA signals. However, interferers at frequency offsets further away from the CDMA carrier will be aliased back to the passband of the CDMA carrier. Assume that such interferers have the maximum strength of 90 dB above the CDMA carrier. Taking into account the -107 dBm noise floor of the CDMA signals and a CDMA signal strength of -122 dBm, then to maintain adequate E_b/N_o a minimum of -75 dB passband image attenuation is needed from the HDF in order to attenuate the aliasing tone interferers down to the noise floor. In addition to passband image attenuation, the HDF should also provide an adequate attenuation for the images of the tone interferers introduced by carrier down-conversion. If these tone images are not attenuated sufficiently, they will alias back to the passband of the signal during the decimation process. To effectively eliminate the effect of these tone images, a 100 dB attenuation is required to provide a 10 dB margin for other system impairments. From Fig. 3.6, it is shown that an 8th order CIC decimation filter has a minimum of -80 dB passband image suppression at 625 kHz, the passband of the CDMA carrier, and more than -100 dB attenuation power at frequency offset to DC greater than 2 MHz. Therefore, it is used for the HDF. It should be noted that if in-band interferers have strength higher that 90 dB, a higher order HDF is necessary to provide adequate passband image suppression.

In addition to the distortion caused by in-band interferers, distortion can also be caused by aliasing of other CDMA carriers in the spectrum during the decimation processing. Assume that there are N users, each of power S, sharing a single CDMA carrier. For any particular user signal the internal noise confronted is from the other N-1 user signals on the same carrier with a total power of (N-1)S. For an aliasing CDMA carrier with N users as a whole, we have an aggregate power of NS. This aliasing power, NS, has to be attenuated so that it is significantly below the cochannel interference level faced by a single user's signal. Let's assume that the noise due to an adjacent carrier should be less than the noise due to a single co-channel interferer by a factor of 100, i.e the adjacent carrier attenuation is equal to $1/(100N)$ where N is the number of users in the adjacent carriers. In other words the aliasing power NS has to be attenuated by at least -38 dB assuming that there are a maximum of 64 users in the composite adjacent carrier signal. Considering the -80 dB passband image attenuation provided by the 8th order HDF, it can be concluded that the 8th order HDF provides an adequate attenuation of adjacent CDMA carriers.

The baseband signal output of the HDF is at a sampling rate of $2f_{chip}=2.4576$ MHz. This signal is then processed by the carrier select filter, discussed in the next section. After the carrier select filter, the sampling rate of the signal has to be interpolated to $8f_{chip}=9.8304$ MHz in order to feed into the baseband CDMA demodulator. This process is discussed in Section 3.2.3.

3.2.2 Carrier Select Filter
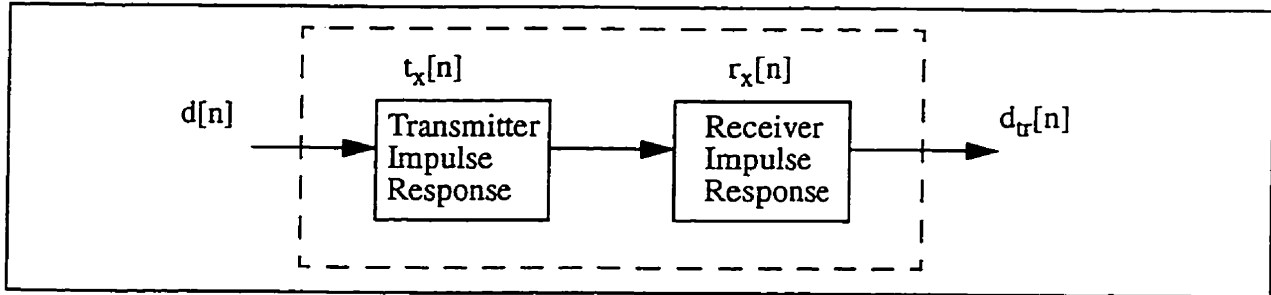
Fig. 3.8 Conceptual representation of digital transmitter and receiver chain

Assuming that there is no noise or non-linearity in the channel, and perfect carrier recovery, the transmitter/receiver chain can be represented by the structure shown in Fig. 3.8. The transmitter can be represented by its impulse response, $t_x[n]$, and the receiver filter function can be represented by its impulse response, $r_x[n]$. Let d[n] represent a sequence containing information and $d_{tr}[n]$ the corresponding output sequence of the transmitter/receiver chain. The relationship between d[n], $d_{tr}[n]$ and the transmitter/receiver chain is shown in (3.5)

$$d_{tr}[n] = d[n] \bullet t_x[n] \bullet r_x[n] \tag{3.5}$$

In the frequency domain (3.5) can be written as

$$\frac{D_{tr}(e^{jw})}{D(e^{jw})} = T_x(e^{jw}) \cdot R_x(e^{jw})$$

$$\tag{3.6}$$

$$= X(e^{jw})$$

where $D(e^{jw})$ is the frequency response for d[n], $D_{tr}(e^{jw})$ is the frequency response of $d_{tr}[n]$. $T_x(e^{jw})$ and $R_x(e^{jw})$ are the frequency response of the transmitter and receiver respectively. The product of

$T_x(e^{jw})$ and $R_x(e^{jw})$ forms the system function of the transmitter/receiver chain. In order to satisfy the Nyquist criteria for zero ISI and minimize the channel bandwidth, the system function must satisfy the following conditions [23]:

$$X(w) = \begin{cases} T & |w| \le \frac{\pi}{T} \\ 0 & |w| > \frac{\pi}{T} \end{cases} \tag{3.7}$$

where 1/T is the data rate of d[n] and X(w) is the frequency response of the transmitter/receiver chain. Raised cosine pulse shape with excess bandwidth β is a pulse shape of finite length that can satisfy the zero ISI requirement. It has a frequency characteristic as follows:

$$X(w) = \begin{cases} T & 0 \le |w| \le (1-\beta)\frac{\pi}{T} \\ \frac{T}{2}\left[1 - \sin\left[\frac{\pi}{2\beta w}\left(w - \frac{\pi}{T}\right)\right]\right] & (1-\beta)\frac{\pi}{T} \le |w| \le (1+\beta)\frac{\pi}{T} \\ 0 & |w| > (1+\beta)\frac{\pi}{T} \end{cases} \tag{3.8}$$

The condition for zero ISI is satisfied if the cascade of transmitter and receiver filters is equal to a raised cosine pulse shape. Graphically, since the passband response of a raised cosine pulse is relatively flat, the $r_x[n]$ should be designed to cancel out the passband ripple of the baseband filter shown in Fig. 2.2.

After the CDMA signals have passed through the HDF, a carrier select filter is used to filter out the out-of-band signals, which have also been down-shifted during the multiplication by the sin/cos functions, while preserving the selected carrier. In addition, the carrier select filter is also responsible for compensating for the attenuation of the signal introduced by the roll-off of the HDF

and the CIC interpolator. Besides carrier selection the carrier select filter also should be designed such that the cascade of all the components of the receiver and the transmitter approximates a raised cosine function. On the other hand, the IS-95+ standard [5] also anticipated that there may be a tone interferer of strength 90 dB above the CDMA signals at frequency greater than or equal to 1.25 MHz offset to a CDMA carrier. As a result the carrier select filter should also provide adequate attenuation to the tone interference.

$r_x[n]$ is the impulse response of the receiver system which, in the per-carrier option, consists of a HDF, a carrier select filter and a CIC interpolator. In the frequency domain, the relationship between the carrier select filter, CIC interpolator and the receiver filter is expressed in (3.9):

$$FIR(e^{jw}) = \frac{R_x(e^{jw})}{HDF(e^{jw}) \cdot CIC(e^{jw})} \qquad . \qquad (3.9)$$

where $FIR(e^{jw})$ is the frequency response of carrier select filter, $HDF(e^{jw})$ is the frequency response of the high decimation filter and $CIC(e^{jw})$ is the frequency response of the CIC interpolator. When combined with (3.6), a frequency function for the carrier select filter is obtained and it is shown in (3.10):

$$FIR(e^{jw}) = \frac{X(e^{jw})}{HDF(e^{jw}) \cdot CIC(e^{jw}) \cdot T_x(e^{jw})} \qquad . \qquad (3.10)$$

The frequency function for the carrier select filter was then used in the frequency sampling filter design method [2], discussed in Appendix A, to design the carrier select filter. Due to the nature of the frequency sampling filter design method, optimization of the transition band of the filter is

required in order to obtain satisfactory stopband attenuation. In our case, a good stopband attenuation is especially important because of the requirement for the suppression of tone interference at an offset greater than or equal to 1.25 MHz to the CDMA carrier. A 65 tap carrier select filter is designed and its frequency response, $FIR(e^{jw})$, is shown in Fig. 3.9. It has a -120 dB stopband attenuation around 1.25 MHz. The minimum attenuation at frequencies greater than 1.25 MHz is -85 dB. The passband of the filter is sloped upwards to offset the roll-off introduced by the HDF and CIC interpolator. The carrier select filter is designed at a sampling frequency of $4f_{chip}$. Since the HDF has already decimated the signal from $48f_{chip}$ to $2f_{chip}$, the carrier select filter has to be decimated by 2 in order to operate on this signal. The decimated version of the carrier select filter has 33 taps. In Fig. 3.10, the frequency response of the cascade of the HDF and the carrier select filter at $f_s = 2f_{chip}$, $HF(e^{jw})$, is shown. The upward slope in the passband has been evened out slightly due to the roll-off of the HDF. In other words, the roll-off of the HDF is cancelled. The remaining upward slope in the passband is to cancel out the roll-off introduced by the CIC interpolator.

The functions of the carrier select filter are: (i) to compensate for the passband ripple introduced by the baseband transmitter filter, (ii) to provide good stopband attenuation for a single tone interferer and (iii) to offset the passband degradation caused by different elements in the receiver. The FIR filter that satisfies such a complicated specification can be designed by the frequency sampling filter design method [2]. This follows as for this method, a filter can be designed to have the desired frequency response specified at a set of equally spaced frequencies. Other methods of FIR filter design are felt not to be directly applicable to meet the criteria needed for the carrier

select filter.
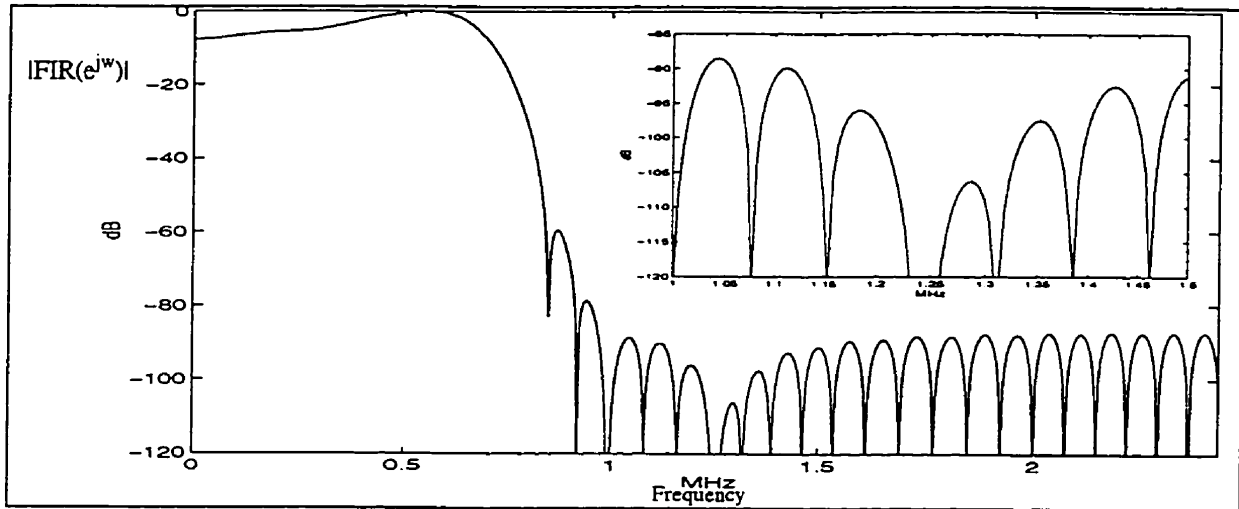
Fig. 3.9 Frequency response of 65 tap carrier select filter at $f_s=4f_{chip}$
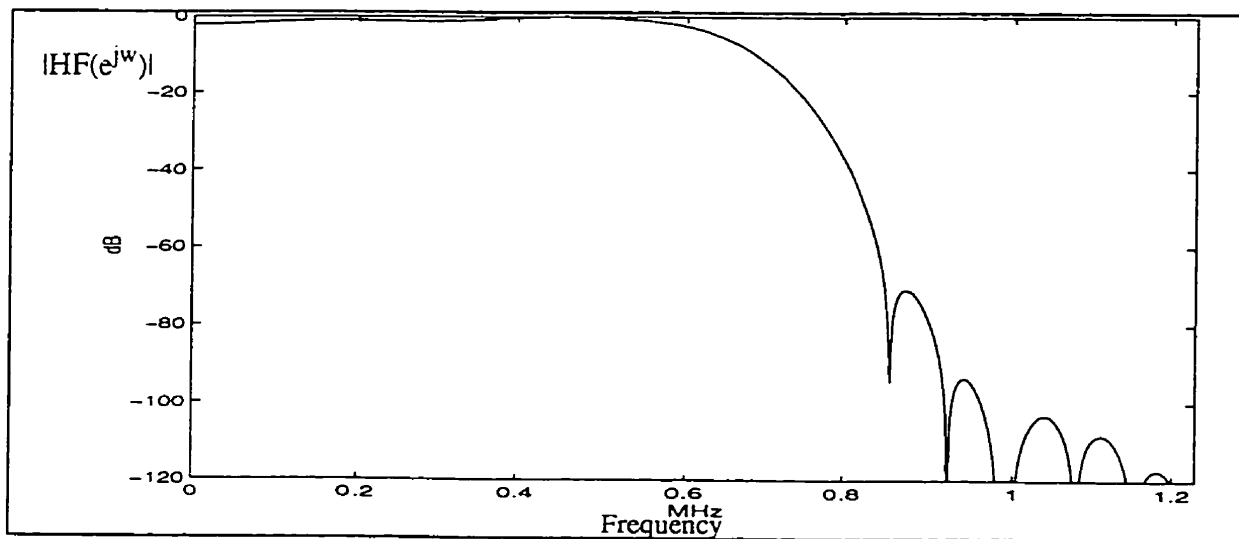
Fig. 3.10 Frequency response of cascade of HDF and carrier select at $f_s=2f_{chip}$

58

3.2.3 CIC interpolator

As suggested by Hogenauer [1], the CIC can be a decimator or an interpolator. In Fig. 3.14 the structure of the CIC interpolator is shown.
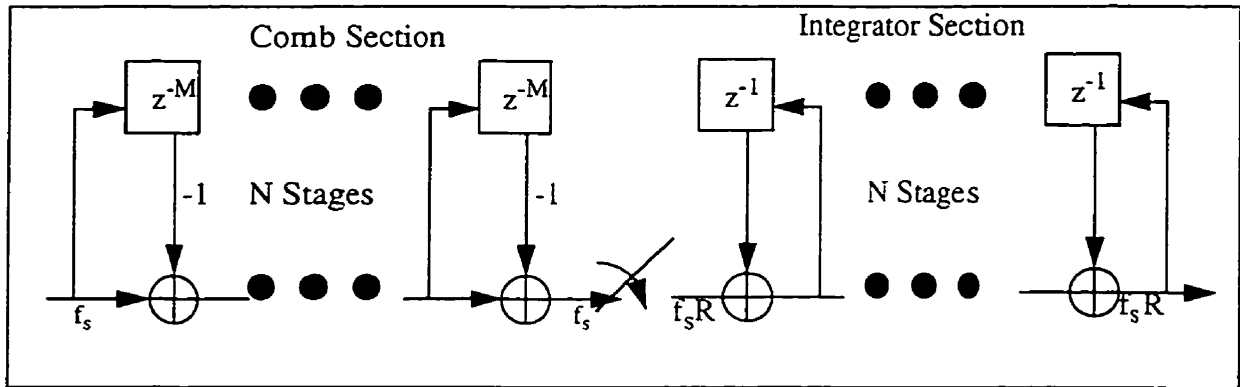
Fig. 3.11 Structure of the N-stage CIC interpolator

The structure shown in Fig. 3.11 is the exact opposite to the one shown in Fig. 3.3, the N-stage decimator. The comb section operates at the lower sampling frequency, f_s, and the integrator section operates at the higher or interpolated frequency, f_sR. Similar to the case of the N-stage CIC decimator, no multiplication is needed for the interpolator. In fact, this is the main attraction of the CIC interpolator. The output of the carrier select filter is at $2f_{chip}$. The CIC interpolator up-samples the signal by a factor of 4 to $8f_{chip}$ or 8 samples per CDMA chip. Optimization in the passband of the carrier select filter has been performed so that the distortion caused by the roll-off in the passband of the CIC is minimized. The slope of the passband roll-off of the CIC interpolator is proportional to the number of stages. The number of stages for the integrators and comb filters in the CIC interpolator is

chosen so that the output of the channelizer DSP has a ρ value, defined in equation (2.1), greater than 0.95 and a good image attenuation, while the complexity of the channelizer DSP is to be minimized. In fact, these requirements are in opposition to each other in terms of the CIC interpolator order. To minimize the complexity of the channelizer DSP, the complexity of the carrier select filter and the CIC interpolator have to be reduced. To maintain a good image attenuation, a CIC interpolator of higher order is desired. However the usage of high order CIC interpolator also requires a longer carrier select filter. This is because the roll-off introduced by a high order CIC filter is steeper. The degradation to the passband is more severe and more difficult to cancel. A longer carrier select filter has to be used to cancel out the effect of the CIC interpolator while an acceptable ρ is maintained. In addition, it is not desirable to distort the signal's passband too much as the carrier select filter cannot restore the distortion completely. Therefore, a low order CIC interpolator is preferred in terms of reducing system complexity and maintaining signal quality. However, the image attenuation of such a low order CIC is also relatively weaker. A compromise that satisfies these conflicting requirements was found and it is a N=3, M=1 and R=4 CIC interpolator. Its frequency response, $CIC(e^{jw})$, of the CIC interpolator is shown in Fig. 3.12. The frequency response at the output of the CIC interpolator, $HFC(e^{jw})$, is shown in Fig. 3.13.
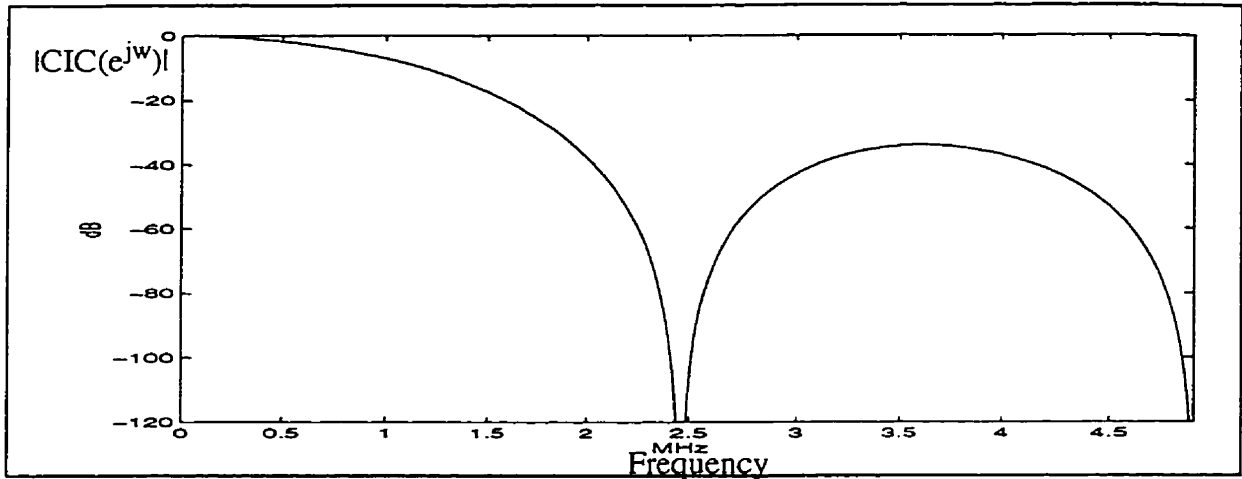
Fig. 3.12 Frequency response of the CIC interpolator N=3, R=4, M=1
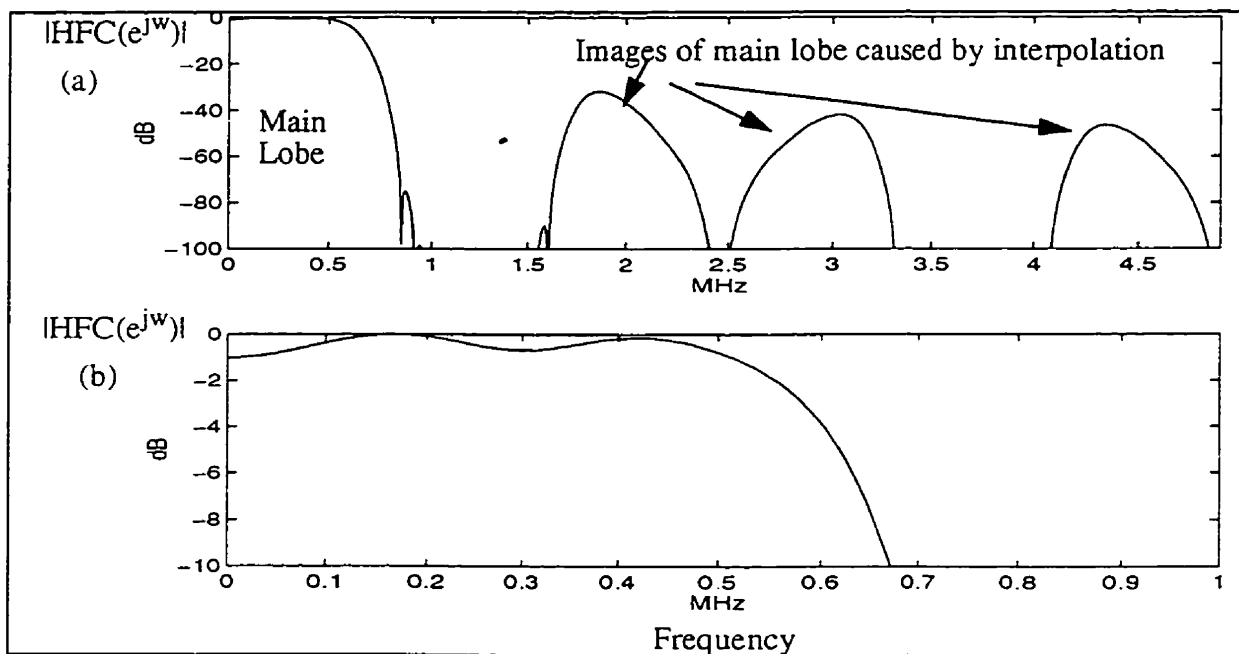
Fig. 3.13a and b Frequency response at the output of the CIC interpolator

It should be noted that the frequency response shown in Fig. 3.13 is not the system function of the channelizer DSP. The side lobes shown in Fig. 3.13 are the images introduced by the 4 times interpolation. In fact the response at frequencies that are smaller than 1.2288 MHz represents

the system function of the channelizer. In case there is a tone interferer at frequency position beyond 1.2288 MHz, the system function has more than -100 dB attenuation power in this region. Moreover, the noise bandwidth for the receiver filtering chain was calculated as 520 kHz which is within the limit allowed by the specification given in Section 2.1. The combination of filters, transmitter and receiver, results in a ρ value, as defined in (2.1), of 0.990 when a random sequence, which represents the PN chip sequence, is input to the transmitter/receiver chain. Due to the weak stopband attenuation of the 3rd order CIC interpolator, images caused by interpolation are only suppressed by -33 dB. However, considering that the input to the baseband CDMA demodulator is quantized to 4 bits, and oversampled to $8f_{chip}$, only approximately 33 dB SNR is needed. This point will be discussed further in Section 4.4. Therefore, it is concluded that a -33 dB noise floor is acceptable. It will be shown in Chapter Five that these -33dB side lobes have the same correlation with the data sequence as does white noise. Therefore, it is fair to say that the side lobes responses are uncorrelated with the information signal represented in the main lobe and their effect on system performance is equivalent to white noise. Furthermore, the side lobes will "disappear" under the quantization noise introduced by the 4-bit quantization by the baseband CDMA demodulator. This point will be shown in Section 5.6. However if a better stopband and ρ value are desired, a higher order CIC interpolator or other multistage interpolation filters should be used.

3.3 Complexity Estimate

The following sections report on the estimates of the complexity for various components

of the per-carrier channelizer DSPs. These estimates include the complexity of 1) the Sin/Cos numerical controlled oscillator(NCO); 2) the HDF and CIC interpolator; and 3) the carrier select filter. The complexity estimate is an operation count in which all operations performed by the DSPs are assumed to be of equal weight. The operations included in the complexity estimate are (i) addition, (ii) multiplication, (iii) table look-up and (iv) multiply-accumulate. As a result, the complexity estimate of the DSPs will be different according to the technology used to implement these different kinds of operations.

3.3.1 Complexity Estimate for Sin/Cos NCO

In the per-carrier down-conversion approach, the sin/cos functions, whose frequencies are tuned to the selected carrier, are generated by a NCO. For an IF frequency centered at $12f_{chip}=$ 14.7456 MHz, the maximum carrier frequency for a CDMA carrier is 20.9956 MHz. The NCO can only generate frequencies within the Nyquist limit which is half of the clock rate [12]. Therefore the minimum clock rate of the NCO is 41.9912 MHz.

In the IS-95+ standard [5], it is required that the frequency be accurate to about +/- 5×10^{-8} of the frequency assignment. Taking into account that the frequency assignment is about 1.9 GHz, the frequency tolerance is about 100 Hz. For a NCO with f_{ck}, the clock frequency, and N-bit phase

accumulator, the output frequency, f_{out}, is obtained as follows [12]:

$$f_{out} = \frac{\Delta\phi \cdot f_{ck}}{2^N} \qquad (3.11)$$

where $\Delta\phi$ is the phase increment per clock cycle. In our case, when the clock frequency is

58.9824MHz, it is found that a 20-bit phase accumulator can give a 56.25 Hz frequency resolution.

This satisfies the 100 Hz frequency precision requirement specified by the IS-95+ standard [5].

Each time the phase accumulator is incremented, the corresponding amplitude of the sine

wave is derived from a look-up table. In most modern NCO implementations only one quarter of the

sine function is stored in memory. Assuming that the address bus of the look up table has 8 bits, there

are 256 entries in the look up table. If each entry consists of a 2 byte word, the total memory/ROM

storage requirement for a NCO is 512 bytes.

There are 4 operations performed per input: 1) 2 multiplications at the mixer for the sine

and cosine functions; 2) 1 phase accumulator addition; and 3) 1 table look-up under the assumption

that 1 table look up operation is adequate for both the sine and cosine quadrature components. In our

case, the data rate at each branch of the channelizer is about $48f_{chip} = 58.98$ MHz. As a result the

complexity of the NCO mixer is 236 millions operations per-carrier per (I+Q) branches. Among the

236 million operation, 59 million operations are table look-ups, 59 million operations are additions

and the remaining 108 million operations are multiplications. It should be noted that the sampling

frequency of the ADC can be decreased in order to reduce the NCO complexity. It is chosen as

$48f_{chip}$ in order to directly compare this method with the transmultiplexer approach to carrier demul-

tiplexing discussed in Chapter Four.

3.3.2 Complexity Estimate for the HDF and CIC interpolator

The HDF has a very simple and uniform structure. There are no multiplications in the HDF. As a result the HDF only involves additions. When N=8, inside the integrator section there are 8 integrators operating at $48f_{chip}$=59.9824 MHz. Similarly there are 8 comb filters in the comb section that are running at $2f_{chip}$ = 2.46 MHz. A tabulation of the number of additions is given below where M represents 1 million.

In each integrator: $48f_{chip}$ = 58.98 M additions

In the integrator section:

$$58.98 \text{ MHz} \cdot 8 = 471.8 \text{ M additions}$$

In each comb filter: $2f_{chip}$ = 2.46 M additions

In the comb section:

$$2.46 \text{ MHz} \cdot 8 = 19.7 \text{ M additions}$$

Total complexity per-carrier per (I+Q) branches is 983 M additions.

Total complexity of the HDF for 11 carriers per (I+Q) branches is 10813 M additions

Although the complexity appears to be large, it should be noted that the operation count in the HDF is not of the same nature as with other FIR operation counts since the arithmetic operations

involve only additions and no multiplications. In addition, the CIC structure consists of regular integrator and comb filter unit with simple connections which facilitates VLSI implementation.

The complexity of the third order CIC interpolator can be calculated as given below. The 3 comb sections operate at the input data rate which is $2f_{chip}$. The 3 integrator sections operate at the interpolated rate which is $8f_{chip}$. A tabulation of the number of additions is given below:

In each comb filter: $2f_{chip} = 2.46$ M additions

In the comb section:

$$2.46 \text{ MHz} \cdot 3 = 7.4 \text{ M additions}$$

In each integrator: $8f_{chip} = 9.83$ M additions

In the integrator section:

$$9.83 \text{ MHz} \cdot 3 = 29.5 \text{ M additions}$$

Total complexity per-carrier per (I+Q) branches is 73.8 M additions.

Total complexity CIC interpolator for 11 carrier per (I+Q) branches is 811.8 M additions

3.3.3 Complexity Estimate for the Carrier Select Filter

The carrier select filter has 33 taps and it operates at $2f_{chip} = 2.4576$ MHz. All the arithmetic operations of a FIR filter are in the forms of multiplications and additions. In most modern DSPs, an addition and a multiplication operation can be implemented by one operation which is called a multiply-accumulate (MAC)operation [37]. Thus the FIR complexity per carrier per (I+Q)

branches is

$$2.46 \text{ MHz} \cdot 33 \cdot 2 = 162.4 \text{ M multiply-accumulate (MAC) operations}$$

For the whole system with 11 carriers the FIR filter complexity per (I+Q) branches is about 1786.4 M multiply-accumulate operations.

3.3.4 Total Complexity Estimate for the Per-Carrier Approach Channelizer

The total complexity of the per-carrier approach is summarized in Table 3.1.

Table 3.1: Complexity of per-carrier channelizer

NCO additions per-carrier (I+Q)	59 M operations
NCO multiplications per-carriers (I+Q)	118 M multiplications
NCO Table Look-up per-carrier (I+Q)	59 M additions
HDF per-carrier (I+Q)	983 M additions
Carrier Select Filter per-carrier (I+Q)	162.4 M multiply-accumulate operations
CIC Interpolator per-carrier (I+Q)	73.8 M additions
Total per-carrier Table Look up(I+Q)	**59 M operations**
Total per-carrier Additions (I+Q)	**1115.8 M additions**
Total per-carrier Multiply-accumulate (I+Q)	**162.4 M multiply-accumulate operations**
Total per-carrier multiplications	**118 M multiplications**
Total operations per 11 carriers (I+Q)	**16007.2 M operations**

As discussed earlier the number of operations can be reduced by decreasing the sampling

frequency of the ADC. The number of operations, N_{op}, per 11 carriers, as a function of the sampling frequency, f_s, is

$$N_{op} = 11 \cdot [(4+2N_{HDF})f_s + 2N_{HDF} \cdot 2.46 + 236.2] \text{ M operations} \qquad (3.12)$$

where N_{HDF} is the order of the HDF. The constants in (3.12) come from the carrier select filter and the CIC interpolator. These two components always operate at the same rate regardless of the ADC sampling rate. For example, assuming $N=8$, if $f_s = 32f_{chip}$, then $N_{op} = 11682$ M operations. There is a reduction of 27 % in the number of operations relative to $f_s = 48fchip$.

3.4 Quantization

The analysis in the preceding sections assumes that the DSP components in the channelizer DSP effectively have infinite arithmetic precision and storage register width. In a real application this is seldom the case. In the following sections the distortion effect due to the finite word length of the DSP components in the channelizer are discussed.

3.4.1 FIR Filter Quantization

The analysis in the preceding sections of this chapter assumes that the carrier select filter coefficients effectively have infinite word length. However in practical implementation, a digital filter can only have finite coefficient length. Truncation of filter coefficients will induce noise and distortion to the magnitude of the filter's frequency response. It has no effect on the phase characteristic

of the filter [2]. There are two sources of quantization noise (1) noise from finite filter coefficient word lengths and (2) noise from finite precision arithmetic in the FIR filters. For a FIR filter with L coefficients, each output of the filter is obtained by the operation expressed in (3.13).

$$y[k] = \sum_{l=0}^{L} a[l] \cdot x[k-l] \qquad (3.13)$$

where y[k] is the kth filter output, a[l] is the lth filter coefficient and x[m] is the signal sample input to the filter. If each filter coefficient is represented by m bits and each signal sample is represented by n bits, each of the multiplications shown in the summation of (3.13) requires m+n bits to store the product. The first source of quantization error comes from the limited word lengths for the filter coefficients, a[l]. The accumulator in which the summation in (3.13) is performed requires $n+m+\log_2 L$ bits to represent the sum of product denoted in (3.13). If the sum is truncated, a flat quantization noise is added to the whole frequency band represented by the FIR filter. This is the second source of quantization error. Truncating the accumulator output won't affect the stopband attenuation of the filter since quantization noise is added indiscriminately to both the passband and stopband of the filter. The relative power difference between the passband and stopband still remains the same. As a result, for the carrier select filter, its tone suppression function will not be affected by the quantization noise due to finite precision arithmetic.

The criteria that governs the width of the filter coefficients word length for the carrier select filter is its stopband attenuation at and beyond 1.25 MHz. The major effect of quantization of the filter coefficients is to introduce noise which in turn raises the "noise floor" into the filter's fre-

quency response in the stopband. Assume that the addition of one filter coefficient bit improves this "noise floor" by 6 dB. Recall from Section 2.1 that a -85 dB stopband attenuation is needed at 1.25 MHz and beyond. Therefore at least 85/6 bit or approximately 14 bit precision is needed. Through simulations using MATLAB software tools [13], it was found that the stopband of the carrier select filter can be maintained to be around -85 dB for 16-bit quantization. The ρ value obtained for the channelizer system when the coefficients of the carrier select filter alone are quantized is 0.990. The frequency response of the 16-bit quantized carrier select filter, $Q(e^{jw})$ is shown in Fig. 3.14.
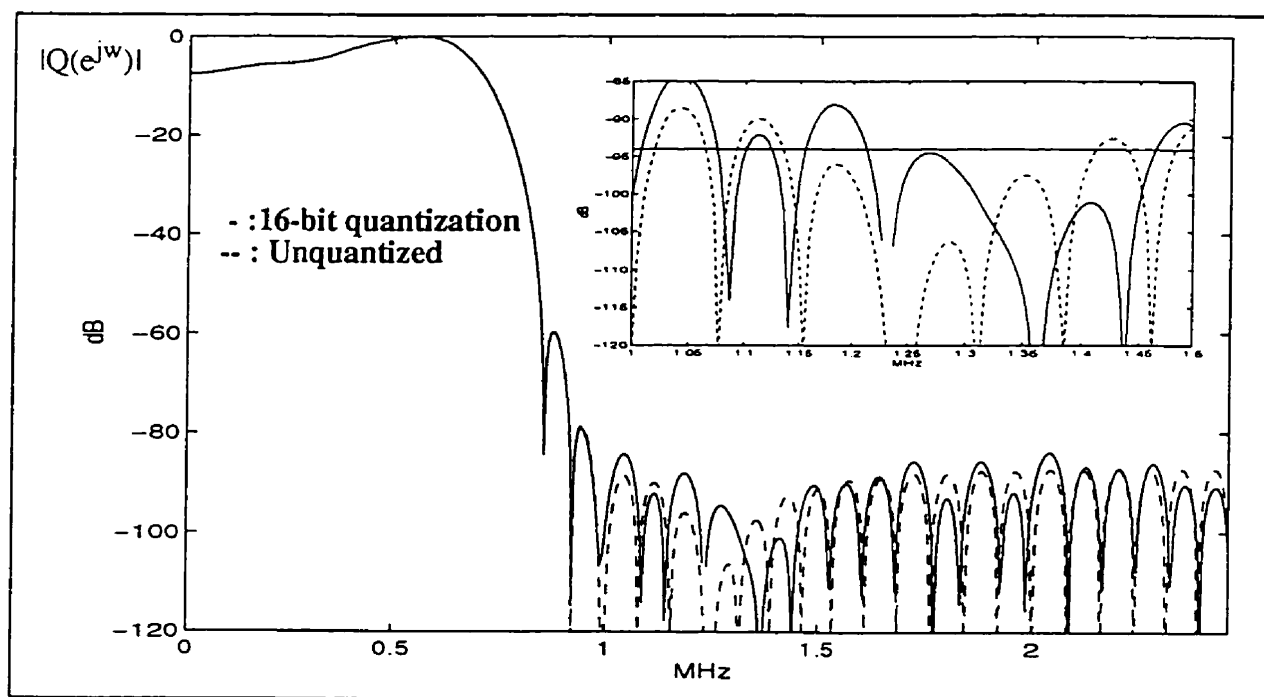
Fig. 3.14 Frequency response of FIR 16-bit quantization $f_s=4f_{chip}$

3.4.2 CIC Filter Quantization

In the channelizer DSP there are other quantization noise sources in addition to the carrier

71

select filter such as the HDF and the CIC interpolator. Since the HDF and CIC interpolator have an identical structure their quantization noise analysis is similar. The main source for quantization noise is the limited accumulator width. For the HDF, it is stated in [9] that the maximum accumulator size in bits can be calculated as follows:

$$B_{max} = \lceil N\log_2 RM + B_{in} - 1 \rceil \qquad (3.14)$$

where B_{in} ,the number of bits input to the HDF is the resolution of the ADC, N is the order of the HDF, R is the decimation rate, $\lceil x \rceil$ equals to the smallest integer that is greater than or equal to x and M is the differential delay. In our case, it is assumed that $B_{in}=12$, R=24, M=1 and using (3.14) B_{max} is calculated as 48 bits. B_{max} is the upper bound of the accumulator register width of each filter stage of the HDF [1]. Truncation, that is discarding the least significant bits, can be used at each filter stage to reduce the widths of the registers of the HDF. Using the method suggested by [1], the resulting register widths from the first integrator stage to the 8th comb filter stage are: 48, 47, 43, 41, 38, 37, 36, 36, 34, 33, 29, 28, 26, 25, 24,18. The output of the HDF is further truncated to 16-bit. The frequency response of the quantized/truncated 8th order HDF, with reference to the higher sampling frequency, is shown in Fig. 3.15. It can be seen on the diagram that truncation has slightly distorted the stopband of the HDF response. As discussed in previous sections the HDF is designed to provide adequate image suppression, -100 dB, in order to attenuate images introduced by carrier down-conversion. By quantizing according to the scheme stated above. the noise floor of the HDF is about - 100 dB which satisfies the design objective of the HDF.

For the case of the CIC interpolator, the accumulator width increases stage by stage [1].

Assume the input to the CIC interpolator is 16 bits. Through MATLAB ™[13] simulations it is found that unlike the HDF, the distortion is not limited to the side lobes, but also distorts the main lobe of the frequency response of the CIC. This distortion at the main lobe would degrade p to a point where it no longer meets the specification stated in Chapter Two. The combination of 16,16,16, 26,28 and 30-bit registers, with the first number corresponding to the first comb filter stage, and the last number corresponding to the last integrator stage, results in negligible distortion to the passband. The frequency response of the quantized CIC interpolator, $CICq(e^{jw})$ is shown in Fig. 3.16. The dotted line is the frequency response of the unquantized CIC interpolator.

The p value obtained by quantizing the HDF, carrier select filter and the CIC interpolator is 0.989. This is very close to the unquantized p value, 0.990. The 0.001 (0.1 %) difference from quantization noise is insignificant. The frequency response of the cascade of the transmitter baseband filter and the quantized channelizer DSP is shown in Fig. 3.17. The dotted line in the diagram represents the unquantized composite response. As can be seen from the graph, the quantized and unquantized responses are in excellent agreement which results in a good p value.
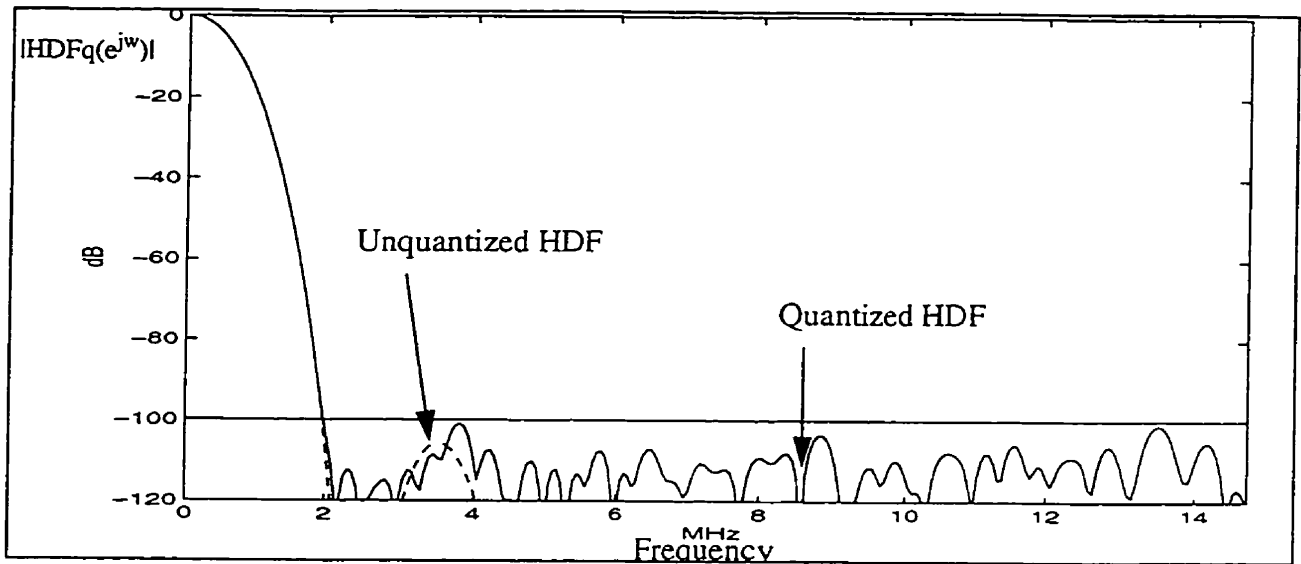
Fig. 3.15 Frequency response of quantized HDF
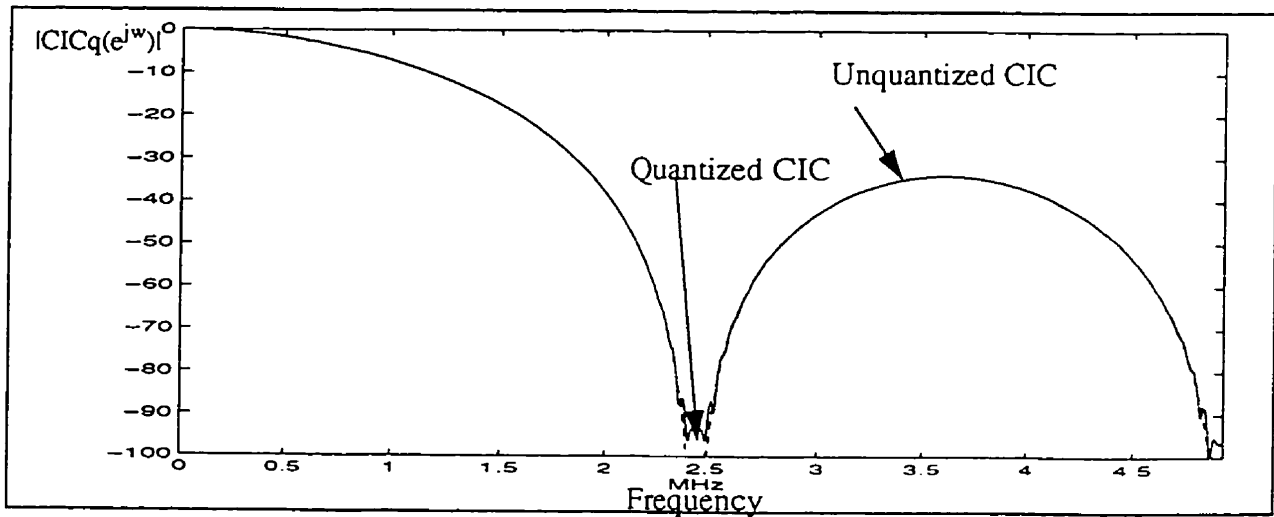
Fig. 3.16 Frequency response of quantized CIC interpolator

74
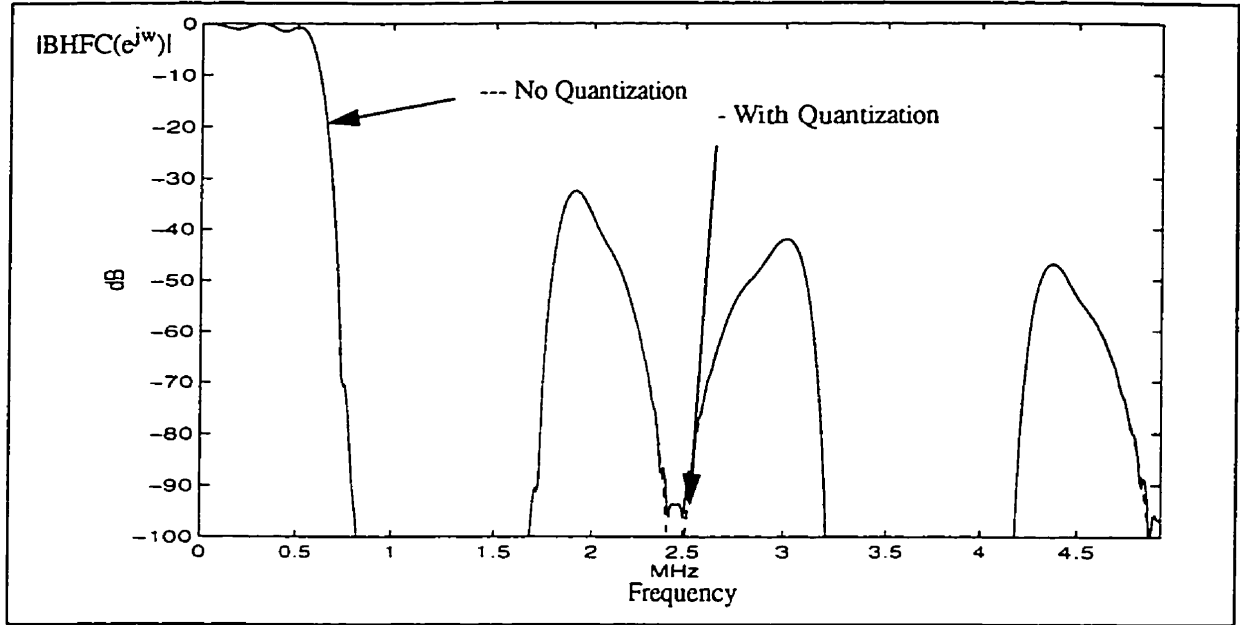
Fig. 3.17 Frequency response of cascaded of baseband filter and quantized channelizer DSP

3.5 Conclusion

In this chapter a per-carrier channelizer was developed. In this approach N independent channelizer DSPs are needed to demultiplex the N different carriers in the CDMA spectrum. After the signals are digitized at IF, with a sampling rate of f_s, each carrier is down-shifted by a NCO tuned to its center frequency. The sampling rate is then lowered by an eighth order high decimation filter (HDF) to $2f_{chip}$. This allows the carrier select filter to run at a lower rate which translates to a lower complexity. Besides sampling rate decimation, the HDF also attenuates the out-of-band signals. A 33 tap carrier select filter running at $2f_{chip}$ is used to perform carrier shaping, tone suppression and

HDF/CIC compensation to reduce ISI. It should be noted that ISI has not been completely removed. To further reduce the ISI and provide good stopband attenuation requires an increase in the number of coefficients of the carrier select filter. This would increase the complexity of the system. On the other hand, the sub-optimum filter with respect to ISI satisfies the performance requirements set in Section 2.1. Since the baseband CDMA demodulation requires $8f_{chip}$ sampling rate, the output from the carrier select filter at $2f_{chip}$ has to be interpolated by a 3rd order CIC interpolator. When cascaded with the ideal transmitter baseband filter as specified by the IS-95+ standard [5], the ρ value in equation (2.1) is calculated as 0.990, which meets the system performance objective.

It is found that at least 16 bits are required for storing the coefficients of the carrier select filter. This is mainly due to the fact that a low noise floor has to be maintained so that there is a 85 dB stopband attenuation for suppression of tone interferers at frequencies greater than 1.25 MHz. When the quantization noise from the HDF and CIC interpolator is taken into account, the ρ value is about 0.989.

The complexity of the per-carrier approach is 1455.2 M operations per-carrier. The NCO and HDF account for a big proportion in this complexity estimate. However it should be noted that the HDF only involves addition operations which are "simpler" operations than multiplications. In fact, if the sampling frequency of the ADC is lowered, the NCOs and the HDFs can operate at a lower frequency which results in a lower system complexity while the complexities for the carrier select filter and the CIC interpolator remain constant regardless of the ADC sampling rate. For example, if the

ADC sampling frequency is lowered to $32f_{chip} = 39.3216$ MHz, there will be a 27 % reduction in total system operations count. The regular structure of the HDF also simplifies VLSI implementation. The advantage of the per-carrier approach is its low start up cost. When there are one or two carriers occupying the spectrum, a cellular operator can simply use the corresponding number of per-carrier channelizers. Furthermore, the cost of the per-carrier approach is incremental. The operator adds per-carrier channelizers as the number of carriers occupying the spectrum increases. In fact, if the spectrum is not solely occupied by CDMA carriers, the per-carrier channelizer approach is a very efficient and flexible approach. Carriers for the different cellular interfaces have different channel characteristic such as channel bandwidth and signal strength. The per-carrier approach can adapt to these different carrier types by changing the parameters of the individual per-carrier channelizer. This flexibility is difficult to achieve with a transmultiplexer. Typically, a transmultiplexer channelizer has to operate in an environment where all carriers in the spectrum belong to the same air interface protocol or have similar spectral characteristics. It is difficult to modify the transmultiplexer for an individual carrier.

Chapter Four

Polyphase-FFT/Transmultiplexer Approach to Carrier Demultiplexing

4 Introduction

In this chapter the polyphase-FFT/transmultiplexer approach to carrier demultiplexing is presented. The design of various components of the transmultiplexer system is discussed. The operation of the transmultiplexer is also investigated. At the end of the chapter, estimates of the complexity of the transmultiplexer system are presented.

4.1 Polyphase-FFT/Transmultiplexer System Overview

The polyphase-FFT or transmultiplexer system for demultiplexing CDMA signals consists of four main components: 1) an ADC, 2) a pair of sin/cos mixers and lowpass filters, 3) a transmultiplexer, and 4) a rate change mechanism. The detailed structure of the transmultiplexer system is shown in Fig. 4.1. In this approach to carrier demultiplexing, CDMA signals are digitized at the IF frequency by an ADC after the bandpass SAW filter, with passband bandwidth approximately equal to the CDMA signal block of interest. The digitized signals are down-shifted and decimated by the transmultiplexer front end. At the N-carrier transmultiplexer, the carriers that have been frequency multiplexed in the CDMA spectrum are demultiplexed and down-shifted to baseband. Each of the demultiplexed carriers at the outputs of the transmultiplexer are then input to a rate change mechanism in order to interpolate the signal according to the requirements specified by the baseband CDMA demodulator. At the baseband CDMA demodulator, signals from the rate change mechanism are decorrelated.
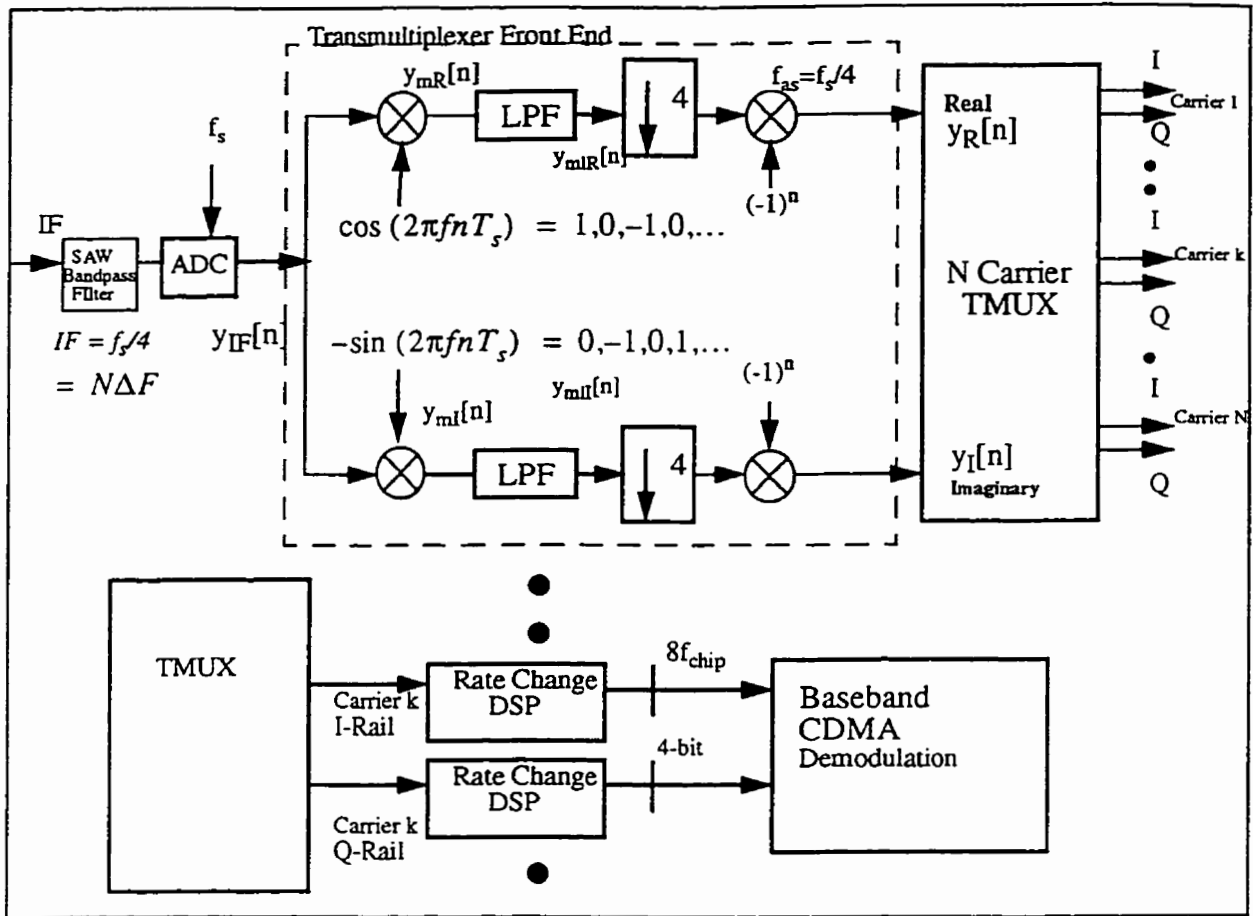
Fig. 4.1 Polyphase-FFT system structure

It has been shown in [9] that the sampling frequency of the signal input to the TMUX should be equal to $mN\Delta F$ where N is the number of carriers to be demultiplexed, m is an integer and ΔF is the carrier spacing. In our case m is chosen to be one and $\Delta F = 1.25$ MHz. The sin/cos mixers and lowpass filters of the transmultiplexer system are designed for I and Q signal separation. At the output of the transmultiplexer, the sampling rate for each of the demultiplexed carriers, the per-carrier output sampling frequency, is $N\Delta F/S$ where S is an integer from 1 to N. Due to the fact that the baseband lowpass filter specified by the IS-95+ standard [5] has a stopband greater than one-half the CDMA carrier spacing, a S value less than the N value is necessary to avoid distortion caused by aliasing. A possible choice for the per-carrier output sampling fre-

quency of the transmultiplexer is $2\Delta F = 2.5$ MHz. This is incompatible with the baseband CDMA demodulator, which requires an input at a sampling frequency that is a multiple of the chip rate, $8f_{chip}=8(1.2288$ MHz$)=9.8304$ MHz. Since this frequency is not an integer multiple of 1.25 MHz, a rate change system has to be used in order to interpolate the signal at the output of the transmultiplexer by a rational factor.

The choice of f_{IF}, the center frequency of the IF band, and the ADC sampling frequency, f_s, should ensure that the Nyquist sampling criterion is satisfied. Moreover, f_s should be chosen such that it is four times the f_{IF}. This reduces the complexity of the DSP stages following the ADC as discussed in Section 4.2.2. Furthermore, the selection of the f_{IF} and f_s pair should also enable some level of oversampling of the digitized IF signals. Oversampling provides more margin for separating the CDMA signal and its image at the given sampling frequency. These images can be attenuated by digital filters and thus the design for the analog SAW bandpass filter can be simplified. To satisfy the requirements stated above the f_{IF} and f_s are chosen as 15 MHz and 60 MHz respectively.

In the transmultiplexer system developed by Hung in [6], I and Q signal separation is done in analog and the signals are digitized at baseband. In the structure shown in Fig. 4.1. the signals are digitized at the IF frequency by an ADC. Thus, I and Q signal separation are performed digitally. This follows the "software radio" concept proposed by Mitola in [19]. In addition, by sampling the I and Q signals through the same ADC and separating them digitally afterwards, the I and Q signal sampling points are synchronous. Thus there will be no timing offset between the I and Q signals. Furthermore, analog I and Q signal separation requires two

ADCs while sampling before I and Q separation requires only one ADC. By using one ADC and IF sampling there is no I, Q amplitude imbalance or phase error. Besides these differences, the transmultiplexer developed in [6] is a critically sampled filter bank in which the sampling frequency of the spectrum of multiplexed carrier signals, $N\Delta F$, is decimated by a factor equal to the number of carriers in the spectrum. The total number of samples in the per-carrier signals is equal to the total number of samples in the signal input to the transmultiplexer. The per-carrier output sampling rate of the critically sampled transmultiplexer is equal to the carrier spacing. In our case, if the transmultiplexer is critically sampled, its per-carrier output sampling rate is $\Delta F = 1.25$ MHz which is smaller than two times the stopband of the signal specified by the IS-95+ standard [5]. The CDMA per-carrier output of the critically sampled transmultiplexer is distorted by aliasing. Modifications have been made to the transmultiplexer so that the per-carrier output has a higher sampling rate.

Recall from Fig. 1.2 that the PCS carrier allocation plan has 11 carriers and a guard band at each end of the 15 MHz spectrum. In order to provide better aliasing protection from interfering signals in the adjacent frequency bands and a more efficient implementation of the FFT. N is set to 12 rather than 11. Since there are only 11 carriers, one of the N per-carrier outputs of the N-point FFT in the transmultiplexer contains no data and will be discarded.

4.2 Transmultiplexer Front End

The transmultiplexer front end is designed for I and Q signal separation for the digitized QPSK-CDMA signals. The output of the transmultiplexer front end is a complex analytic

signal [2, 9]. The mechanism of the transmultiplexer front end processing is discussed in the following sections.

4.2.1 QPSK I and Q Signal Separation

The digitized IF QPSK-CDMA signals can be represented as:

$$y_{IF}[n] = \sum_{k=0}^{N-1} Q_k[n]$$

(4.1)

$$= \sum_{k=0}^{N-1} [i_k[n] \cos(((w_{IF} + w_k)nT_s)) + q_k[n] \sin(((w_{IF} + w_k)nT_s))]$$

where w_{IF} is the IF center frequency, w_k is the offset from the kth carrier to w_{IF}. $Q_k[n]$ is the kth digitized QPSK-CDMA carrier, $i_k[n]$ and $q_k[n]$ are $Q_k[n]$'s in-phase and quadrature-phase components, respectively.

Let us consider the signal at the kth carrier when it is multiplied by $\cos(w_{IF} nT_s)$ where $T_s = 1/f_s$.

$$\begin{aligned}
Q_k[n] \cos(w_{IF}nT_s) &= i_k[n] \cos((w_{IF} + w_k)nT_s) \cos(w_{IF}nT_s) \\
&\quad + q_k[n] \sin((w_{IF} + w_k)nT_s) \cos(w_{IF}nT_s) \\
&= \frac{i_k[n]}{2} [\cos(w_k nT_s) + \cos((2w_{IF} + w_k)nT_s)] \\
&\quad + \frac{q_k[n]}{2} [\sin(w_k nT_s) + \sin((2w_{IF} + w_k)nT_s)]
\end{aligned}$$

(4.2)

After the lowpass filter, it is assumed that all signal components at 2w$_{IF}$ are filtered away and Q$_{kR}$

[n] is produced where

$$Q_{kR}[n] = \frac{i_k[n]}{2}\cos(w_k nT_s) + \frac{q_k[n]}{2}\sin(w_k nT_s) \qquad . \qquad (4.3)$$

Similarly,

$$Q_k[n](-\sin(w_{IF}nT_s)) = \frac{i_k[n]}{2}[\sin(w_k nT_s) + \sin((2w_{IF} + w_k)nT_s)]$$

$$-\frac{q_k[n]}{2}[\cos(w_k nT_s) + \cos((2w_{IF} + w_k)nT_s)] \qquad (4.4)$$

Now after the lowpass filter, Q$_{kI}$[n] is produced where

$$Q_{kI}[n] = \frac{i_k[n]}{2}\sin(w_k nT_s) - \frac{q_k[n]}{2}\cos(w_k nT_s) \qquad . \qquad (4.5)$$

When considering Q$_{kR}$[n] as the real part and Q$_{kI}$[n] as the imaginary part of a signal, for the kth

QPSK carrier, we have

$$Q_{kR}[n] + jQ_{kI}[n] = \frac{1}{2}(i_k[n] - jq_k[n])(\cos(w_k nT_s) + j\sin(w_k nT_s))$$

$$= \frac{1}{2}(i_k[n] - jq_k[n])e^{jw_k nT_s} \qquad . \qquad (4.6)$$

Therefore, when taking account all N carriers:

$$y[n] = \frac{1}{2}\sum_{k=0}^{N-1}(i_k[n] - jq_k[n])e^{jw_k nT_s} = y_R[n] + jy_I[n] \qquad (4.7)$$

where:

$$y_R[n] = \frac{1}{2}\sum_{k=0}^{N-1}i_k[n]e^{jw_k nT_s} \quad \text{and} \quad y_I[n] = \frac{1}{2}\sum_{k=0}^{N-1}(-q_k[n])e^{jw_k nT_s} \qquad (4.8)$$

The expression in (4.8) is called a complex analytic signal [9] for y$_{IF}$[n]. In Fig. 4.2 the opera-

tions performed by the transmultiplexer front end are illustrated in a graphical format.
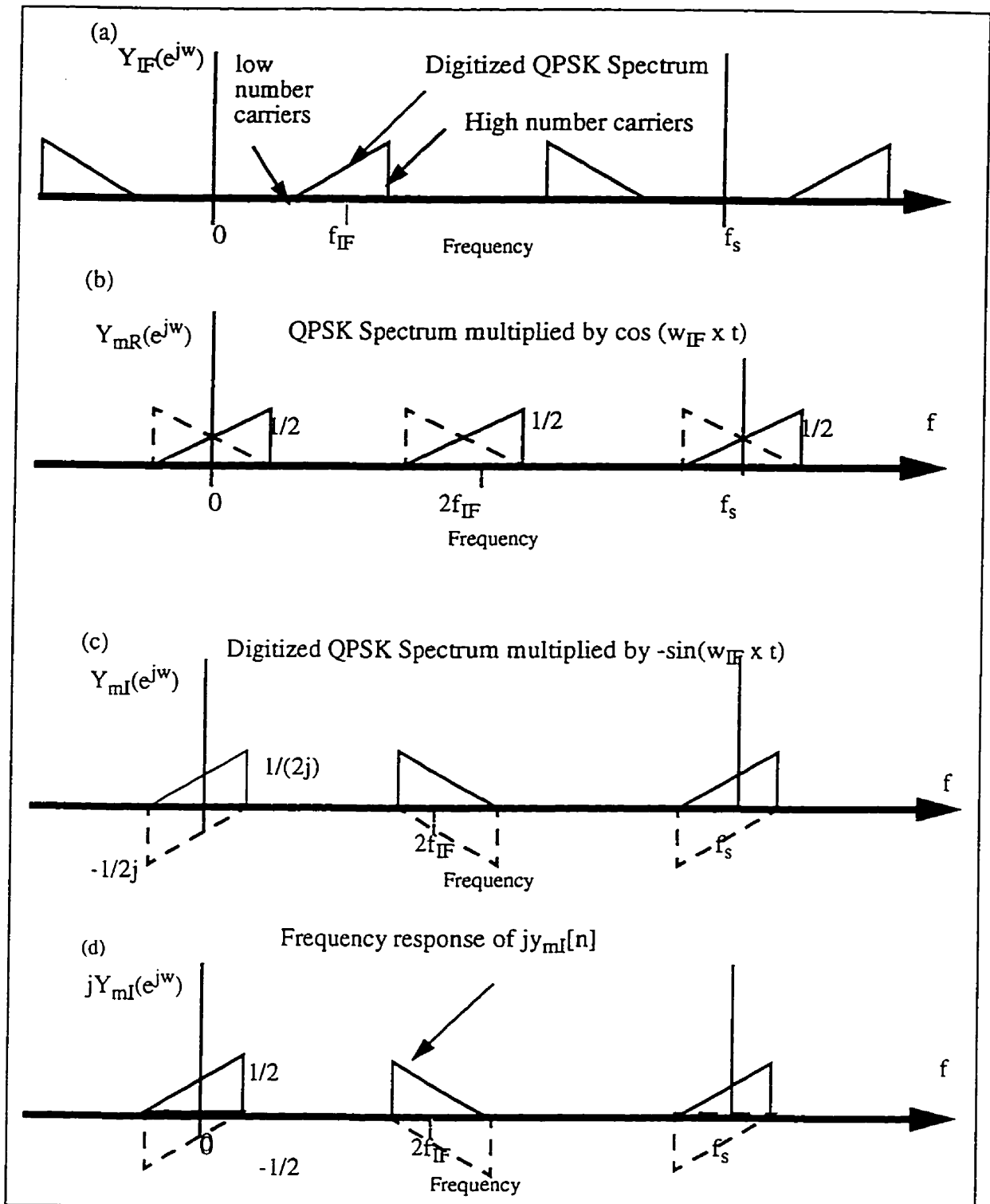
Fig. 4.2 a,b,c,d QPSK separation of the transmultiplexer front end
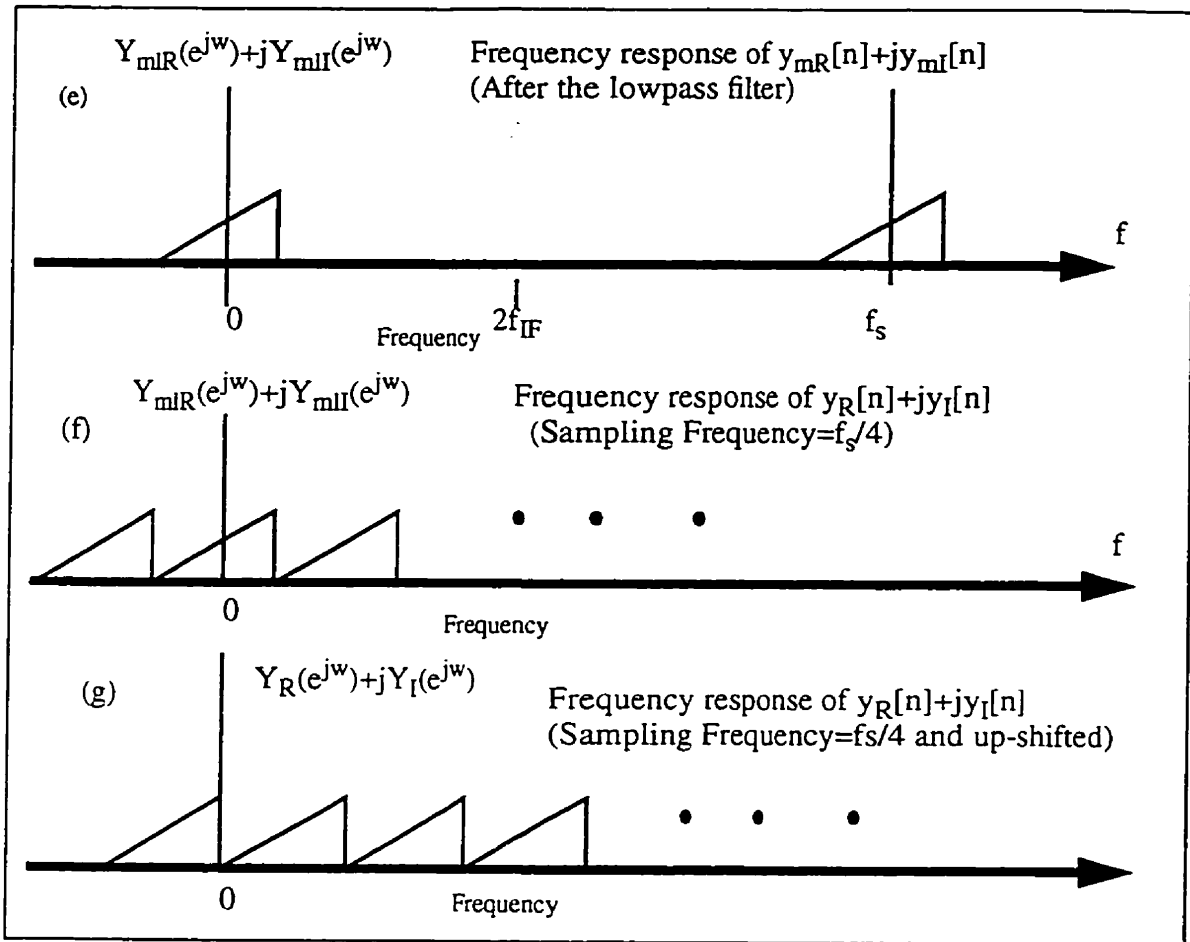
Fig. 4.2 e,f and g Digitized QPSK signal spectrum

Multiplications by sin/cos are represented by bi-directional translations:

$$\cos(wt) = \frac{e^{jwt} + e^{-jwt}}{2} \tag{4.9}$$

and

$$-\sin(wt) = \frac{-e^{jwt} + e^{-jwt}}{2j} \tag{4.10}$$

Each sin/cos function contains an up-shift and down-shift component. In Fig. 4.2a, the digitized QPSK signal is shown. The frequency block containing the group of N multiplexed QPSK carrier

signals is graphically represented by a triangle. Recall from Fig. 1.2, the carrier allocation plan, there are 11 carriers and two guard bands in the spectrum starting from the left-most guard band and Carrier #1 at the lower tip of the triangle to Carrier #11, and the right-most guard band at the other end of the triangle. By multiplying $y_{IF}[n]$ with cos(wt) (Fig. 4.2b), the down-shifted $y_{IF}(e^{jw})$ (solid triangles) is overlapped by its up-shifted version (dotted triangles). All versions are scaled by a factor of 1/2. Similarly in $-y_{IF}[n]$sin(wt) (Fig. 4.2c) its down-shifted version is overlapped by its up-shifted version. The down-shifted versions are scaled by a factor of 1/(2j) and the up-shifted version is scaled by a factor of $-1/(2j)$. $y_{IF}[n]$sin(wt) is treated as the imaginary part of the complex signal. In Fig. 4.2d the frequency response of the $jy_{IF}[n]$sin(wt) is shown. By comparing Fig. 4.2c and d, one can see that the j factor in $jy_{IF}[n]$sin(wt) has cancelled out the j factor in $y_{IF}[n]$sin(wt). Passing $y_{IF}[n]$cos(wt) and $y_{IF}[n]$sin(wt) through lowpass filter eliminates the signal at $2f_{IF}$. In $y_{IF}[n]$cos(wt)+$jy_{IF}[n]$sin(wt), all the up-shifted versions have the same amplitude but opposite sign. Therefore they cancel each other as shown in Fig. 4.2e. What remains is the right-most portion of the CDMA spectrum at baseband and a laterally flipped version of the left-most spectrum at the sampling frequency. Since there is no signal in the spectrum between these two signals, the sampling rate can be decimated by a factor of 4 without any further filtering as indicated in Fig. 4.4f. The signals are up-shifted by $f_{IF}/2$ so that the leftmost guard band appear at the baseband. The frequency response of the up-shifted signals are shown in Fig. 4.2g.

4.2.2 Hardware Saving in Sin/Cos Mixer

The sin/cos mixers in the transmultiplexer front end output digitized sinusoidal signals at f_{IF} which is the center frequency of the IF band. The digitized sinusoidal wave is sampled at $f_s = 4f_{IF}$. Since f_{IF} is a quarter of the sampling frequency, f_s, $T_s = 1/f_s = 1/(4f_{IF})$ and

$$\sin(2\pi f_{IF} t) = \sin(2\pi f_{IF} nT_s)$$

$$= \sin(\pi n/2)$$

$$= 0, 1, 0, -1..........$$

and thus the digital sine function only has the values -1, 0, 1. Similarly,

$$\cos(2\pi f_{IF} t) = 1, 0, -1, 0......$$

and thus the digital cosine function only has the values -1, 0, 1.

The sine and cosine mixers are reduced to the sequence 1,0, -1,0 with a period of 4 symbols. Therefore the necessity of using a NCO to generate digital sine and cosine functions is eliminated. It should be noted that the analysis above is a general result for quadrature modulation and is often used in modem design.

4.2.3 Lowpass Filtering

To eliminate the images introduced by the sin and cos mixers in the transmultiplexer front end, a lowpass filter is required in each of the two branches of the transmultiplexer front end. There is an advantage in down-shifting the CDMA signal by $f_{IF} = 15$ MHz from the IF frequency. It can be seen from Fig. 4.2b,c that there is a space of 15 MHz between the right-most band edge

87

of the down-shifted CDMA signals and the left-most band edge of its image centered at $2f_{IF}$. The lowpass filter that is needed to eliminate the image signals can have a wide transition bandwidth of 15 MHz. In Fig. 4.3, the frequency mask for the lowpass filter is shown. This relaxed specification results in fewer taps in the FIR filter implementation for the lowpass filter and thus lower complexity. The lowpass filter is designed to attenuate the image at $2f_{IF}$ introduced by frequency down-shifting. If there are in-band or out-of-band tone interferers in the CDMA spectrum, their images are also going to appear in the frequency band centered at $2f_{IF}$. In order to eliminate the images of the tone interferers, the lowpass filter has to provide at least a 90 dB stopband attenuation of the image at $2f_{IF}$ based on the assumption that the in-band and out-of-band tone interferers have a maximum strength of 90 dB above the CDMA carrier signals. Considering other impairments added by the receiver system, a 10 dB margin is included. Therefore the minimum stopband requirement of the lowpass filter is -100 dB. In this way the distortion caused by the tone interferer image is minimized.
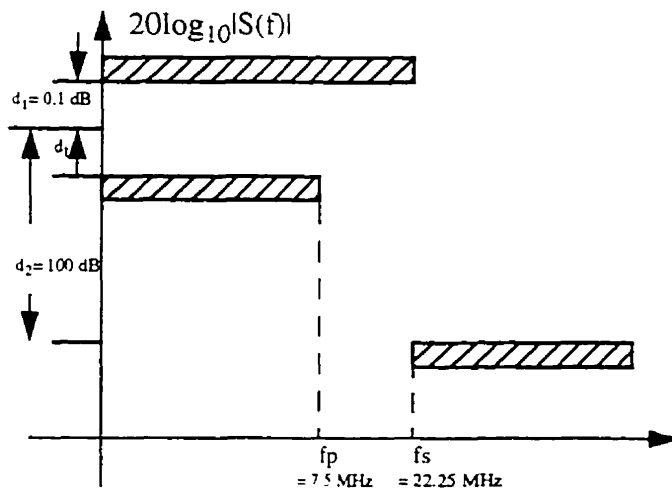
Fig 4.3 Lowpass filter mask
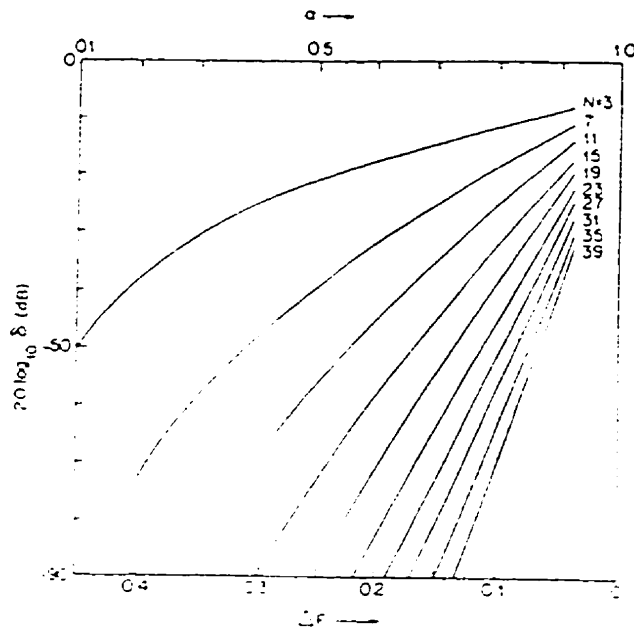
Fig. 4.4 Design relation of half-band FIR filters [9]

The lowpass filter can be designed as half-band FIR filter. A half-band lowpass filter has the following characteristics [4]:

$$r_s = r_p \qquad (4.11)$$

and

$$f_{stop} = \frac{f_s}{2} - f_p \qquad (4.12)$$

where r_s represents the stopband ripple. r_p represents the passband ripple. f_{stop} represents the stop-band of the filter . f_s represents the sampling frequency and f_p is the passband of the filter. The half-band lowpass filters are filters with all the even taps equal to zero and the 3 dB bandwidth equal to $0.25f_s$ .where f_s is the operating frequency of the filters [4]. Since close to half of the coefficients are zeros. the half-band filter is a very good candidate to implement the lowpass filter

used in the transmultiplexer front end where system complexity is to be minimized. The curves shown in Fig. 4.4 represent the design relations for the half-band FIR filters from [9]. The symbol, α, is equal to the passband bandwidth divided by $f_s/4$. In our case α is equal to 0.5. The stopband requirement for the half-band lowpass filter used in the transmultiplexer front end is -100 dB. From the diagram in Fig. 4.4, it is found that a 23 tap half-band filter is adequate. Of the 23 filter coefficients, 10 are zero.

The following observation can be made when the signal at the in-phase signal branch passes through the lowpass filter. At the in-phase signal branch the digital CDMA signals centered at f_{IF} is mixed with a $\cos(2\pi f_{IF} nT_s) = 1, 0, -1, 0....$ sequence. Consider, $y[n]$, the sequence input to the cosine mixer of the form:

$$..., y_{10}, y_9, y_8, y_7 y_6, y_5, y_4, y_3, y_2, y_1, y_0, y_{-1} y_{-2}, \cdots$$

After it passed through the cosine mixer, it is changed to $y_c[n]$:

$$..., -y_{10}, 0, y_8, 0, -y_6, 0, y_4, 0, -y_2, 0, y_0, 0, -y_{-2} \cdots$$

Suppose the half-band lowpass filter at the transmultiplexer front end, $h[n]$, has the following coefficients:

$$...0, h_3, 0, h_2, 0, h_1, h_0, h_1, 0, h_2, 0, h_3, 0...$$

Also, suppose at $t=kT_s$, where k is a constant, $h[n]$ is aligned with the $y_c[n]$ sequence in the following pattern:

$-y_{10}$	0	y_8	0	$-y_6$	0	y_4	0	$-y_2$	0	y_0	0	$-y_{-2}$
0	h_5	0	h_4	0	h_3	0	h_2	0	h_1	h_0	h_1	0

Then the result of the convolution is $y_0 h_0$. At $t=(k+4)T_s$, after the decimate-by-4 process, we

have

$-y_{10}$	0	y_8	0	$-y_6$	0	y_4	0	$-y_2$	0	y_0	0	$-y_{-2}$
0	h_3	0	h_2	0	h_1	h_0	h_1	0	h_2	0	h_3	0

and the result of the convolution is $h_0 y_4$. At $t=(k+8)T_s$:

$-y_{10}$	0	y_8	0	$-y_6$	0	y_4	0	$-y_2$	0	y_0	0	$-y_{-2}$
0	h_1	h_0	h_1	0	h_2	0	h_3	0	h_4	0	h_5	0

and the result of the convolution is $y_8 h_0$. Provided that $h[n]$ is normalized by its maximum coefficient, $h[0]$, subsampling the output of the convolution above by a factor of 4 results in a sequence which is exactly the same as the sequence, $y[n]$, decimated by a factor of 4. Therefore the half-band lowpass filter actually has no effect on the sequence, $y[n]$. As a result the mixer and the lowpass filter at the in-phase signal branch can be dropped. The same saving is not possible in the quadrature-phase signal branch. The quadrature-phase signal sequence at the quadrature-phase signal branch mixer is: $0,-1,0,1....$ Suppose that the sequence input to the sine mixer is the same as the one in the cosine mixer. Let the sequence at the output of the sine mixer be equal to $y_s[n]$ and it has the form:

$$...0, -y_9, 0, y_7, 0. -y_5, 0, y_3, 0, -y_1, 0, y_{-1}, 0...$$

Using the same $h[n]$, at $t=kT_s$ $h[n]$ and $y_s[n]$ are aligned as follows:

0	$-y_9$	0	y_7	0	$-y_5$	0	y_3	0	$-y_1$	0	y_{-1}	0
0	h_5	0	h_4	0	h_3	0	h_2	0	h_1	h_0	h_1	0

and the result of the convolution is $-h_1 y_1 + h_1 y_{-1}.....$. At $t=(k+4)T_s$, after the decimation by a fac-

0	$-y_9$	0	y_7	0	$-y_5$	0	y_3	0	$-y_1$	0	y_{-1}	0
0	h_3	0	h_2	0	h_1	h_0	h_1	0	h_2	0	h_3	0

and the result of the convolution is $-h_1y_5+h_1y_3$...... At $t=(k+8)T_s$, we have

0	$-y_9$	0	y_7	0	$-y_5$	0	y_3	0	$-y_1$	0	y_{-1}	0
0	h_1	h_0	h_1	0	h_2	0	h_3	0	h_4	0	h_5	0

and the result of the convolution is $-h_1y_9+h_1y_7+...$ The sequence, $y_s[n]$, is actually equal to a dec-imate-by-2 version of the sequence, $y[n]$, when the sign changes are ignored. In fact, from the analysis above, the sign changes in the sequence can be implemented by a modified half-band lowpass filter whose alternate coefficients are negative. In addition, one can see that h_0 is always multiplied with a zero sample points therefore it can be eliminated. As a result, the quadrature-phase signal branch can be implemented by decimating the sequence, $y[n]$, by a factor of 2, then pass it through a modified lowpass half-band filter. The output of the filter is further decimated by a factor of 2. By decimating $y[n]$ by a factor of 2 before it enters the modified half-band filter, the number of storage registers for sample points in the filter is reduced. This is because the stor-age registers corresponding to the zero coefficients of the filter no longer have to store anything. The modified half-band lowpass filter can be derived from the 23 taps half-band filter chosen ear-lier. In the modified half-band filter, the alternate coefficients are negative. Therefore half of the coefficients are positive and other half are negative. It should be noted that while the mixer and the lowpass half-band filter at the in-phase signal branch is not required, it should be replaced by a delay equal to the time it takes for the sequence at the quadrature-phase signal branch to pass through the modified half-band lowpass filter. The saving of the half-band lowpass filter is only

possible if the cosine sequence equals to 1, 0, -1, 0.... is used with a half-band lowpass filter followed by a decimation by a factor of 4, 8, 12.... . The feasibility of this arrangement has been confirmed by a simulation in MATLAB ™ [13].

4.2.3.1 ADC Quantization Noise in the Transmultiplexer Front End

The quantization noise of the ADC is uniformly distributed from 0 to 30 MHz. After the IF signal is block down-converted to baseband the nominal bandwidth of the I and Q branches is 7.5 MHz. If the I and Q branches are lowpass filtered with a nominal bandwidth of 7.5 MHz, then the quantization noise in each branch is reduced by $10\log(30/7.5) = 6.02$ dB and the total quantization noise is also reduced by 6.02 dB since

$$\sigma_{Total}^2 = \sigma_I^2 + \sigma_Q^2 \qquad (4.13)$$

where σ_{Total}^2, σ_I^2, σ_Q^2 are the total quantization noise power, quantization noise power for I and Q signal branches respectively.

Note however that for a half-band filter, the nominal noise bandwidth is $f_s/4$. Therefore the total quantization noise is reduced by $10\log(30/15) = 3.02$ dB. The use of a half-band filter simplifies the complexity of the transmultiplexer front end but results in a quantization noise bandwidth penalty of about 3 dB. In the case of the per-carrier approach, the HDF is a filter with a very narrow noise bandwidth. The nominal quantization noise after filtering is equal to the bandwidth of the carrier signal. The quantization noise reduction is much better, approximately 3 dB, in this situation.

4.3 Transmultiplexer Analysis

To understand the mechanism of the transmultiplexer, let us consider the analysis filter

bank structure [2] shown in Fig. 4.5.
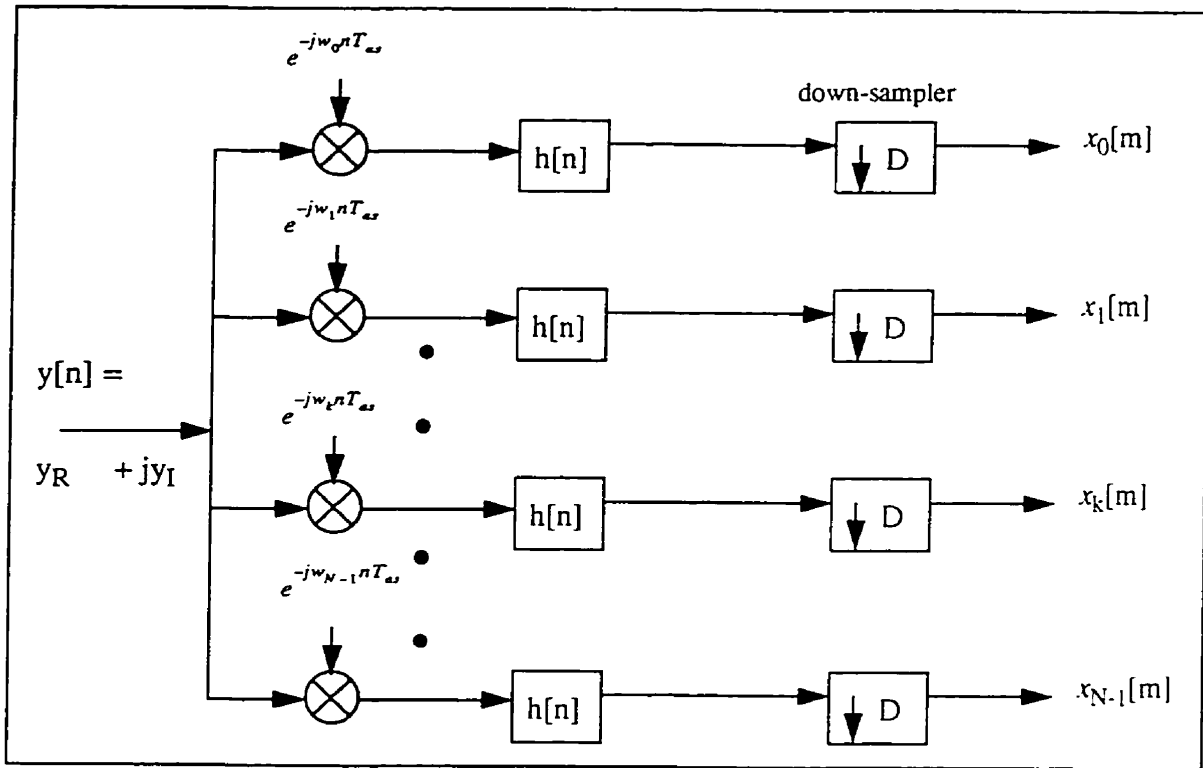
Fig. 4.5 Analysis filter bank

The analysis filter bank shown in Fig. 4.5 is functionally equivalent to a transmulti-

plexer [2]. $y[n]$ is an analytical signal containing N carrier signals from 0 to $N\Delta F$. The sampling

frequency of $y[n]$ is $N\Delta F$ (in our case $\Delta F = 1.25$ MHz). The real part of $y[n]$ is the output of the

in-phase signal branch of the transmultiplexer front end and the imaginary part of $y[n]$ is the out-

put of the quadrature-phase signal branch of the transmultiplexer front end. In the analysis bank,

the $y[n]$ sequence is split into N parallel branches. In the kth branch, the kth carrier is down-

shifted to baseband by multiplying by a $e^{-jw_k nT_{as}}$ factor where $w_k = 2\pi k \Delta F$ and $1/T_{as}$ is the sampling frequency of y[n], which is equal to $N\Delta F$. h[n] represents a baseband filter operating at $N\Delta F$ which acts as a carrier select and shaping filter. It picks out the kth carrier from the down-shifted spectrum. The output of the baseband filter, at the kth branch, is at a sampling rate of $N\Delta F$. It can be decimated to a lower rate through a decimator to form $x_k[m]$. At the kth branch of the analysis filter bank:

$$x_k[m] = \sum_{n=-\infty}^{\infty} y[n] h[mD-n] e^{-jw_k nT_{as}} \tag{4.14}$$

We can use the periodic property of $e^{-jw_k nT_{as}}$ to simplify equation (4.14). When n is equal to a multiple of N (i.e. n=rN where r is an integer), $e^{-jw_k rNT_{as}}$ is equal to 1. For D=N, let n=rN+i where r is an integer from 0 to N-1 and

$$e^{-jw_k nT_{as}} = e^{-j2\pi k \frac{n}{N}}$$

$$= e^{-j2\pi kr} e^{-j2\pi k \frac{i}{N}} \tag{4.15}$$

$$= e^{-j2\pi k \frac{i}{N}}$$

since $e^{-j2\pi kr} = 1$. Therefore, for D=N, (4.14) can be rewritten as,

$$x_k[m] = \sum_{i=0}^{N-1} \sum_{r=-\infty}^{\infty} y[rN+i] h[mN-rN-i] e^{-j2\pi k \frac{i}{N}} \tag{4.16}$$

Define

$$y_i[r] = y[rN+i] \quad \text{and} \quad h_i[m] = h[mN-i] \tag{4.17}$$

95

Then

$$x_k[m] = \sum_{i=0}^{N-1} \sum_{r=-\infty}^{\infty} y_i[r]h_i[m-r]e^{-j2\pi k\frac{i}{N}}$$

(4.18)

$$= \sum_{i=0}^{N-1} y_i[m] \bullet h_i[m] e^{-\left(\frac{j2\pi ik}{N}\right)}$$

where $\bullet$ denotes a convolution operation.

The expression shown in (4.18) resembles a N-point FFT which has the following form:

$$A_k = \frac{1}{N} \sum_{i=0}^{N-1} B_i e^{-\left(\frac{j2\pi ik}{N}\right)}$$

(4.19)

where A_k equals $x_k[m]$ and B_i equals the convolution of $y_i[m]$ and $h_i[m]$. $y_i[m]$ can be obtained by decimating $y[n]$ by a factor of N with an offset of i through a commutator with N terminals and $h_i[m]$ can be obtained by decimating $h[n]$ by a factor of N with an offset of -i. Equation (4.18) shows that the decimated-by-N version of $y[n]$ with an offset i is convolved with the decimated-by-N version of $h[n]$ with an offset -i. This combination of $h_i[m]$ and $y_i[m]$ requires the commutator to rotate in a clockwise manner[2]. The set of $h_i[m]$ represents a polyphase filter bank [9]. Each $h_i[m]$ is one of the N subfilters of the polyphase network. It should be noted that the $y_i[m]$ sequence is a complex analytic signal. It can be filtered by $h_i[m]$ by passing the real part and the imaginary part of $y_i[m]$ separately into two identical subfilters since the coefficients of $h_i[m]$ are real. As a result two polyphase networks with identical subfilters are needed. One of them accepts input from the in-phase signal branch of the transmultiplexer front end and outputs a fil-

96

tered real signal to the FFT processor. The other identical polyphase network accepts input from the quadrature-phase branch of the transmultiplexer front end and outputs a filtered imaginary signal to the FFT. This is equivalent to the transmultiplexer described by Hung in [6].

As mentioned in Chapter Two, at the transmitter each carrier's CDMA signal is shaped by a lowpass filter with parameters specified by the IS-95+ standard [5]. The stopband of the lowpass filter is 740 kHz, see Fig. 2.1. This is greater than one-half the carrier spacing of 625 kHz. Suppose that, as shown in Fig. 4.5, the output of h[n] is decimated by a factor D=N. The sampling frequency of x_k [m] is ΔF which is 1.25 MHz. The sampling frequency is smaller than the Nyquist sampling frequency for the CDMA carrier signal(1.48 MHz). Serious distortion will result according to this scheme. In order to minimize distortion caused by aliasing between the per-carrier output signal and its image, the output sampling frequency has to be increased. By setting the output sampling frequency to $2\Delta F$ the problem of aliasing is solved. In this way the stopband of the per-carrier signal at baseband is separated by about 1.02 MHz from its image for a sampling frequency of 2.5 MHz.

According to the analysis filter bank structure shown in Fig. 4.5, x_k[m] can be decimated by D=N/I=M so that x_k[m] is at a sampling rate of $I\Delta F$ where I is an integer. For D=N/I, let

$n = rN + i$ and using (4.15), we have

$$x_k[m] = \sum_{i=0}^{N-1} \sum_{r=-\infty}^{\infty} y[rN+i]\, h[mM-rN-i]\, e^{-j2\pi k \frac{i}{N}}$$

$$\qquad\qquad (4.20)$$

$$= \sum_{i=0}^{N-1} \sum_{r=-\infty}^{\infty} y[rN+i]\, h[(m-rI)M-i]\, e^{-j2\pi k \frac{i}{N}}$$

Again define

$$y_i[r] = y[rN+i] \qquad\qquad (4.21)$$

but now define

$$h_i[m] = h[mM-i] \qquad\qquad (4.22)$$

Then equation (4.20) can be rewritten as

$$x_k[m] = \sum_{i=0}^{N-1} \sum_{r=-\infty}^{\infty} y_i[r]\, h_i[m-rI]\, e^{-j2\pi k \frac{i}{N}} \qquad\qquad (4.23)$$

Recalling the equation for an interpolation filter from (2.12), one sees that the expression in the summation over r in (4.23) defines an interpolator with interpolation factor I [9]. The structure shown in Fig. 4.6 is the realization of such a transmultiplexer. This structure can be used for the case when the per-carrier output sampling rate, f_{out}, is an integer multiple of the carrier spacing, i.e., $f_{out} = I\Delta F$.

The sequence, $y_i[r]$, in Fig. 4.6, represents a signal with a sampling rate of f_{as}/N. In the subfilter branch $y_i[r]$ is interpolated by a factor of I and processed by a subfilter which also functions as a interpolation filter with a sampling rate of $f_{as}/M = I\Delta F$. $h_i[m]$ is a decimated-by-M, where $M = N/I$, version of $h[n]$ with an offset of $-i$ where i can take on any value from 0 to N-1.

98

However there are only M possible values of i in a decimated by M version of h[n]. As a result, the $h_i[m]$ are an extended set of filters and they are related within the set. In this configuration the output sampling rate of the transmultiplexer, f_{out}, must be an integer multiple of the carrier spacing.
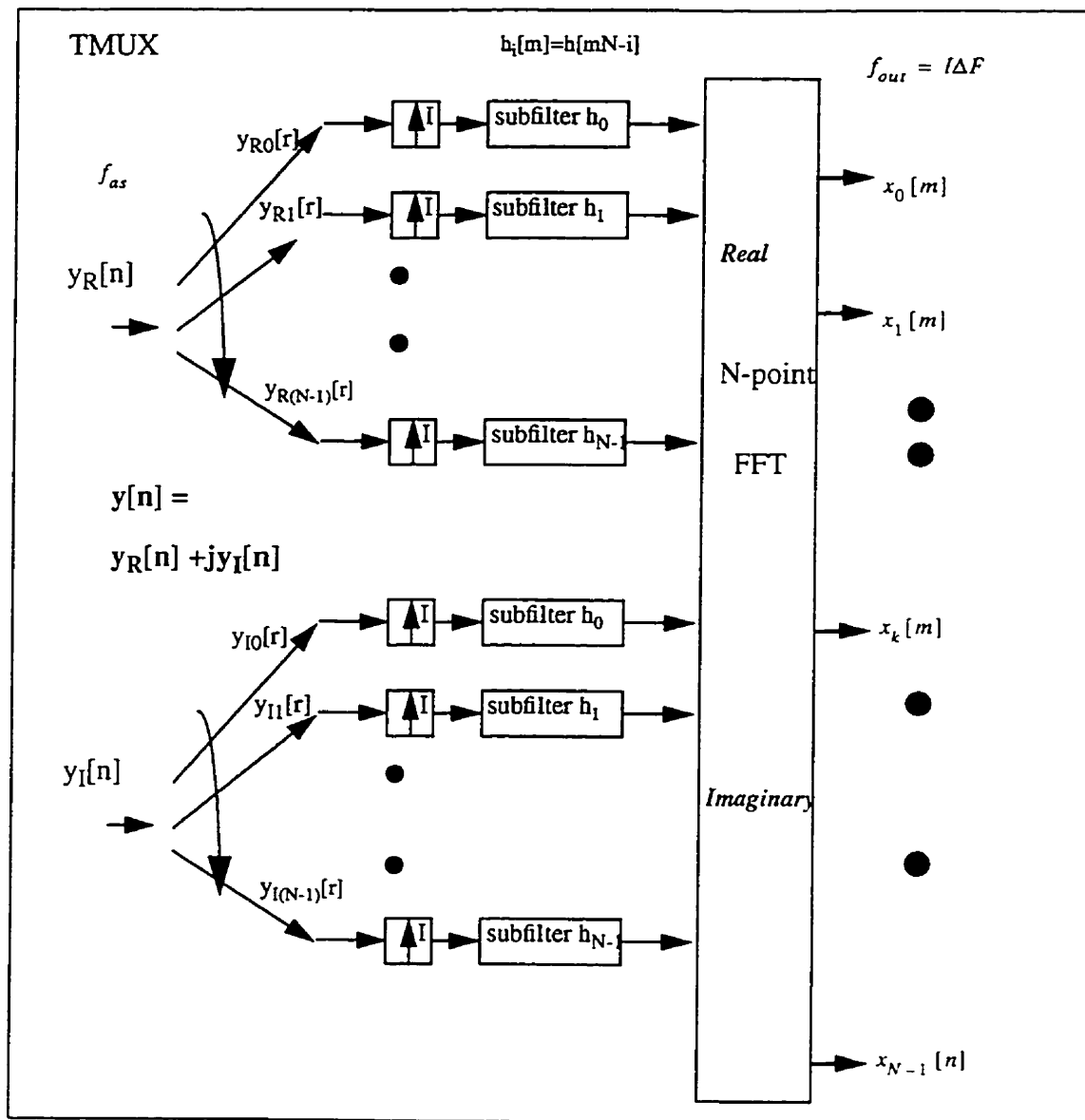
Fig. 4.6 Transmultiplexer structure when $f_{out} = I\Delta F$

4.3.1 Alternative Implementation of a Transmultiplexer-Weighted Overlap-Add Method

When the output sampling rate of the FFT for each of the demultiplexed carriers is required to be equal to $f_{out} = d\Delta F$ where d, the oversampling ratio, is a rational number, the weighted overlap-add structure for implementing the transmultiplexer can be used [9]. In the weighted overlap-add structure h[n] is acting like a sliding analysis window which selects and weights a short-time segment of the signal y[n]. To convert our point of reference from a fixed time frame to that of the sliding time frame which is centered at the origin of the analysis window formed by h[n], let D=M=N/I and r=n-mM. Then equation (4.14) can be rewritten as

$$x_k[m] = \sum_{r=-\infty}^{\infty} h[-r] y[r+mM] e^{-j2\pi k \frac{(r+mM)}{N}}$$

(4.24)

$$= e^{-j2\pi k \frac{mM}{N}} \sum_{r=-\infty}^{\infty} h[-r] y[r+mM] e^{-j2\pi k \frac{r}{N}}$$

Let

$$g_m[r] = h[-r] y[r+mM]$$

(4.25)

If $g_m[r]$ is subdivided into blocks of N samples, and $u_m[r]$ is defined as

$$u_m[r] = \sum_{l=-\infty}^{\infty} g_m[r+lN]$$

(4.26)

$$= \sum_{l=-\infty}^{\infty} h[-r-lN] y[r+lN+mM]$$

where r = 0 to N-1.

Then

$$x_k[m] = e^{-j2\pi km\frac{M}{N}}\left(\sum_{r=0}^{N-1} u_m[r]\, e^{-j2\pi k\frac{r}{N}}\right)$$ (4.27)

The expression shown in (4.27) is of the form of a FFT. The weighted overlap-add transmulti-plexer can be implemented by a set of shift registers, a filter bank and a FFT[9]. In the weighted overlap-add transmultiplexer, input data, y[n], are shifted into an N_h-sample shift register in blocks of M samples, where N_h is the number of taps of h[n], the analysis window filter. The data in the shift register are weighted with the time reversed window, h[-r], to produce the N_h-sample short-time sequence, $g_m[r]$. This sequence is then divided into blocks of N samples, starting at r=0, which are time-aliased according to equation (4.26) to form $u_m[r]$. The N-point FFT of the $u_m[r]$ is then computed followed by multiplication by a $e^{-j2\pi kmM/N}$ factor to form $x_k[m]$. Fig. 4.7 described an alternative structure that can be used when $f_{out}=I\Delta F$ where I is an integer. Each sub-filter of the filter bank, $h_i[m]$, can be obtained by inserting I-1 zeros between each consecutive sample of the decimated-by-N version of h[n] with an offset -i, where i can be an integer from 0 to N-1. The sliding widow effect is achieved by feeding y[n], the input to the transmultiplexer, into a set of N symbols shift registers with the capability of shifting one symbol per $1/f_{as}$. There are N branches connected to the N symbol at the shift registers as there are N terms in the summation of (4.27). At the end of the ith branch is a subfilter, $h_i[m]$. Data stored at the register just noted is latched to each subfilter every N/I samples. Due to the fact that y[n] is a complex sequence, one set of registers and a polyphase filter bank is needed for each of the two components of the com-plex signal.

In this thesis, the transmultiplexer designed by the method illustrated in Fig. 4.7 is implemented, with M=N/I where I = 2 in our case, and its performance in a CDMA environment is tested in Chapter 5. The filter, h[n], is the impulse response of a carrier select filter operating at f_s=15 MHz. The design of this filter is discussed in Chapter Five. It has 192 taps and is designed to provide good carrier selection and ISI performance.

For a transmultiplexer designed by the weighted overlap-add structure, the sampling rate of the transmultiplexer per-carrier output, f_{out}, can be controlled by adjusting the size of the sample block, M, that is shifted into the N_h-sample shift register. In general

$$f_{out} = \frac{f_{as}}{S} \qquad (4.28)$$

where f_{as} is the sampling rate of the input to the transmultiplexer and S is an integer which takes any value from 1 to $f_{as}/\Delta F$. The case when the sampling rate for each of the demultiplexed carrier is equal to $I\Delta F$, where I is an integer, i.e., like the structure shown in Fig. 4.7, is a special case of the weighted overlap-add transmultiplexer where $S = f_{as}/(I\Delta F)$.
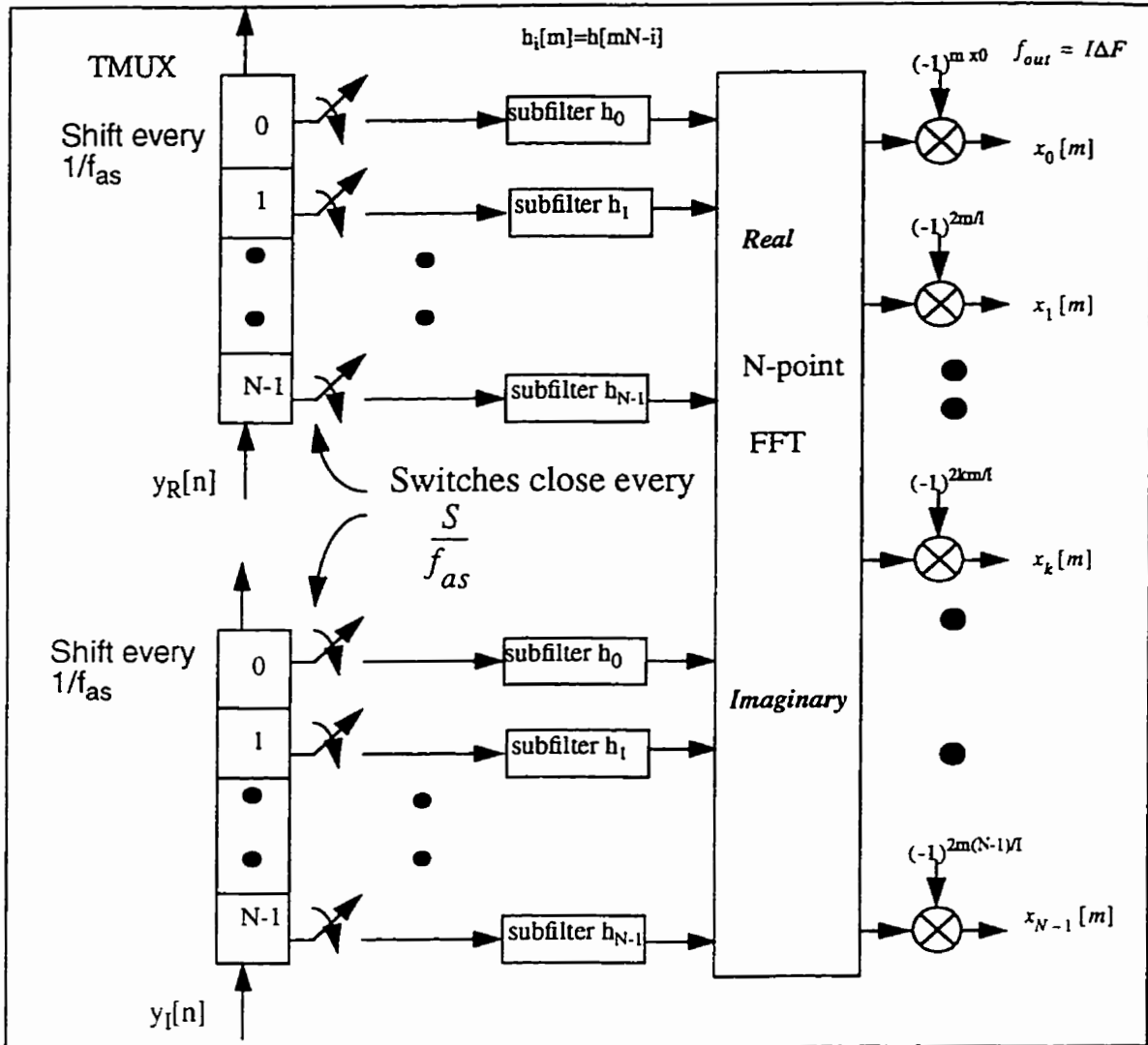
Fig. 4.7 Structure of the Transmultiplexer for per-carrier sampling rate equals to $I\Delta F$

4.3.2 FFT Implementation

There are 11 CDMA carriers with spacing 1.25 MHz each and 2 guard bands of 625 kHz each in the 15 MHz CDMA spectrum. A natural and straight forward choice is to use a 11-point FFT for implementation of the transmultiplexer, but this does not allow for guard bands.

Although a FFT algorithm exists [38] for an 11-point FFT, it will be shown later in Section 4.3.3 that such a choice results in too much interference from aliasing. In addition, a 11-point FFT changes the sampling rate to 13.75 MHz and places very tight constraints on filters. When a 12-point FFT is used the two 625 kHz guard bands can be combined together as an "unused" carrier. After the transmultiplexer front end, the guard bands are at the boundary of the 15 MHz complex analytic signal. There are efficient ways to implement a 12-point FFT. The 12-point FFT can be implemented by three 4-point FFTs and four 3-point FFTs [20], as shown in Fig. 4.8 and 4.9 respectively.

The complex operations of a N-point FFT can be expressed as [2]:

$$X[k] = \sum_{n=0}^{N-1} x[n] e^{-j\frac{2\pi kn}{N}} = X_R[k] + jX_I[k] \qquad (4.29)$$

where x[n] is a complex sequence which is equal to $x_R[n]+jx_I[n]$, X[k] is the result of the FFT operation, $X_R[k]$ is the real part of X[k] and $X_I[k]$ is the imaginary part of X[k]. In terms of real operations on $x_R[n]$ and $x_I[n]$, $X_R[k]$ is given by [2]

$$X_R[k] = \sum_{n=0}^{N-1} \left[x_R[n] \cos\frac{2\pi kn}{N} + x_I[n] \sin\frac{2\pi kn}{N} \right] \qquad (4.30)$$

and $X_I[k]$ is given by [2]

$$X_I[k] = -\sum_{n=0}^{N-1} \left[x_R[n] \sin\frac{2\pi kn}{N} - x_I[n] \cos\frac{2\pi kn}{N} \right] . \qquad (4.31)$$

The number of real multiplications is equal to 4 times the number of complex multiplications. A more detailed look into the 4-point FFT reveals that

$$\cos\frac{2\pi kn}{4} = \cos\frac{kn\pi}{2} = 1, 0, -1, 0 \qquad (4.32)$$

for n=0, 1,2, 3 .... respectively.

$$\sin\frac{2\pi kn}{4} = \sin\frac{kn\pi}{2} = 0, 1, 0, -1 \qquad . \qquad (4.33)$$

for n=0, 1, 2, 3.... respectively. Thus, the operations performed by the 4-point FFT include multiplication by a +/- j factor, complex addition and sign inversion. The multiplication by a +/- j factor operation can be implemented by interchanging the real and imaginary part of the input signal sequence to the FFT[20]. As a result, and as shown in Fig. 4.8 [20], there are no complex multiplies in the 4-point FFT.
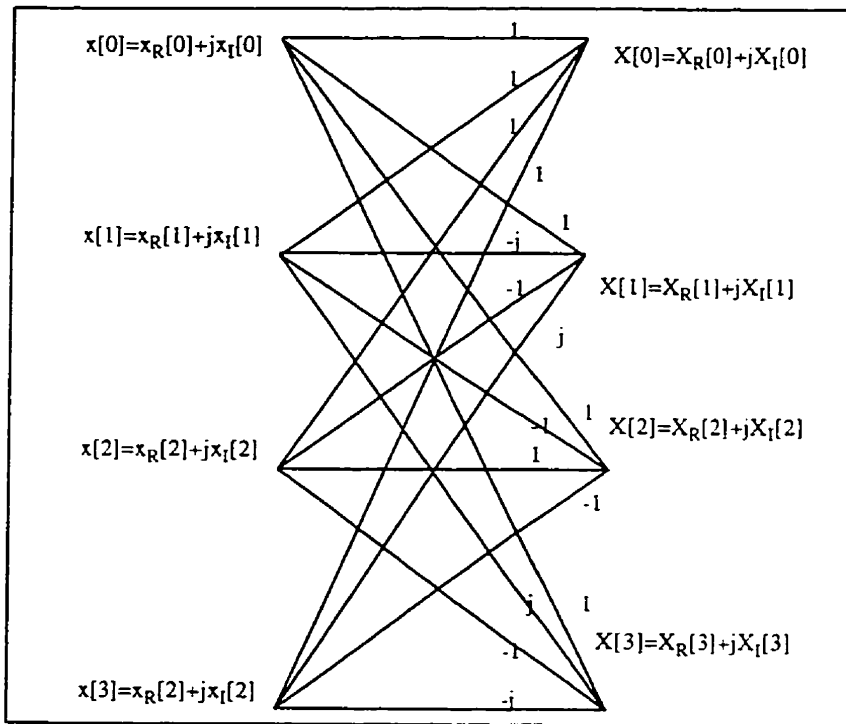
Fig. 4.8 Efficient implementation of 4-point FFT(4-point butterfly)

The 4-point butterfly, shown in Fig. 4.8, is a realization of the 4-point FFT. The sequence, x[n], shown to the left of the 4-point butterfly is a complex signal with real part, $x_R[n]$, and imaginary part, $x_I[n]$. The symbol on each branch of the butterfly represents a multiplication performed on the signal and consists only of sign inversion or multiplication by a +/- j factor. At

the end of the group of four attaching branches, a summation of four terms is constructed which is equivalent to 3 complex additions. There are a total of 12 complex additions for the 4-point butterfly. Considering one real addition per real part and one real addition per imaginary part, 12 complex additions are equivalent to 24 real additions. There are 4 real and imaginary part interchanges, i.e., for the multiplication by a +/-j factor, and 4 sign inversions.
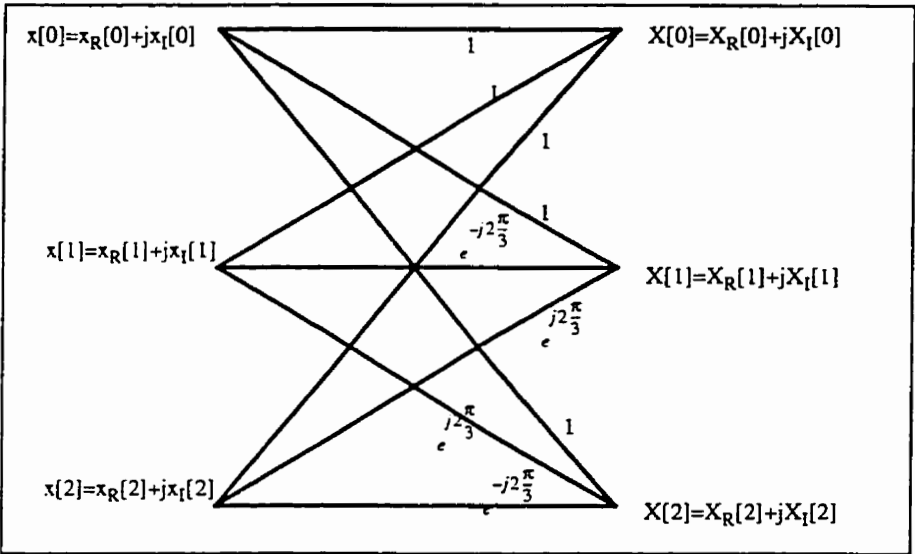
Fig. 4.9 Efficient implementation of 3-point FFT

An efficient implementation of a 3-point FFT is shown in Fig. 4.9. Similar to the 4-point butterfly shown in Fig. 4.8, the symbol on each branch represents a multiplication operation performed on x[k]. In Fig. 4.9 it can be seen that each 3-point FFT has 4 complex multiplications equivalent to 16 real multiplications. Considering 1 real addition per real and imaginary part of the signal there are 8 real additions accompanying the 4 complex multiplications. There are also 6 complex additions in each 3-point FFT which are equivalent to 12 real additions. The total number of arithmetic operations for a 3-point FFT is 16 real multiplications and 20 real additions.
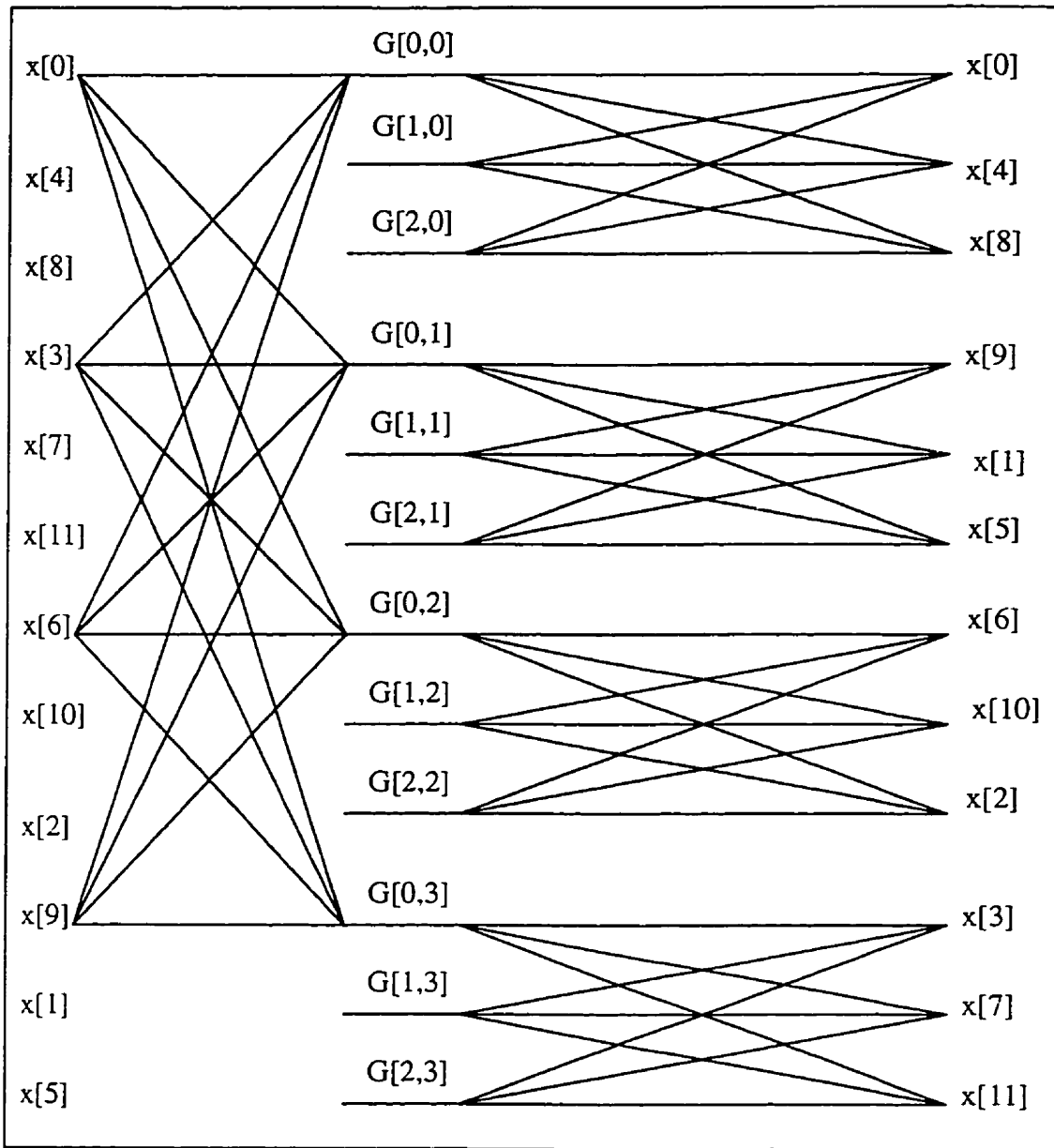
Fig. 4.10 Efficient implementation of 12-point FFT

In Fig. 4.10, one-third of the efficient implementation of the 12-point FFT is shown. There are a total of 64 real multiplications, 152 real additions, 12 real and imaginary part interchange and 12 sign inversions in the whole FFT process.

4.3.3 IF Filter Consideration
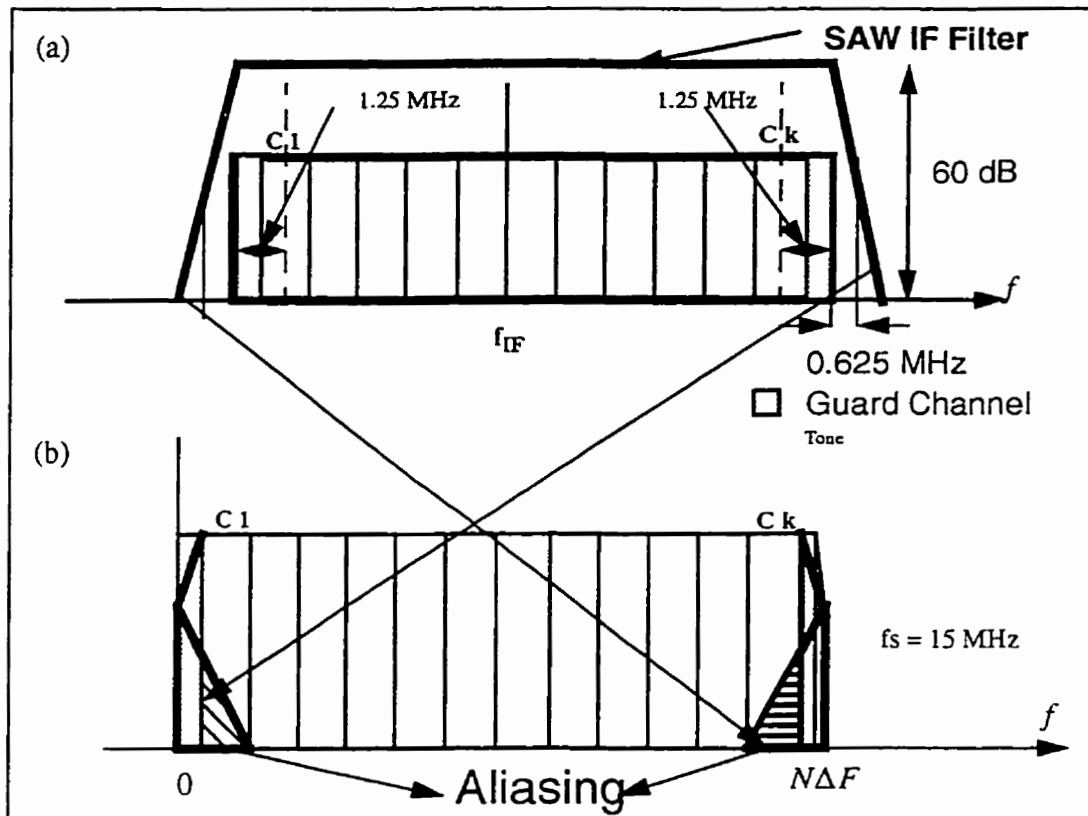
Fig. 4.11a and b CDMA spectrum at IF and baseband

In most modern radio architectures, a SAW IF bandpass filter is used to filter out the out of band signals at the IF frequency. When the digitized IF CDMA signals are down-shifted to the baseband and decimated by a factor of 4, the input signals attenuated by the skirts of the SAW filter will alias back into the guard band at each end of the spectrum as shown in Fig. 4.11b. The leakage from the roll-off of the SAW filter beyond 625 kHz from the guard band band edge(or 1.875 MHz from the first or last carrier) will alias to either the first carrier and the last carrier depending on which end of the spectrum the roll-off is from. If the attenuation provided by the SAW filter at 625 kHz from the guard band band edge is not satisfactory, aliasing may signifi-

cantly degrade carriers at the boundaries of the CDMA spectrum. In this case it is necessary to increase the number of unused carriers so that the distance between the first and last carrier at the baseband analytic signal is larger. This reduces the aliasing error due to the roll-off of the SAW. filter. If a 13-point FFT is used, one more subfilter is needed for the polyphase network and the sampling frequency is increased. Other than this, there is no significant impact on the overall system complexity. A 14-point FFT could also be used for the same purpose.

4.4 Rate Change Mechanism

The output sampling rate of the TMUX is $2\Delta F = 2.5$ MHz. The input signal sampling rate to the baseband CDMA demodulator is required to be $8f_{chip} = 9.8304$ MHz. Obviously a rate change system which can perform rational factor interpolation is needed to change the signal sampling rate from 2.5 MHz to 9.8304 MHz. Fig. 4.12 shows a block diagram of the rate change mechanism. In order to reduce complexity, the rate change system is implemented as a cascade of a 3rd order CIC interpolation filter and a second order approximation mechanism. The signal sequence is interpolated to 10 MHz before the 2nd order approximation is carried out.
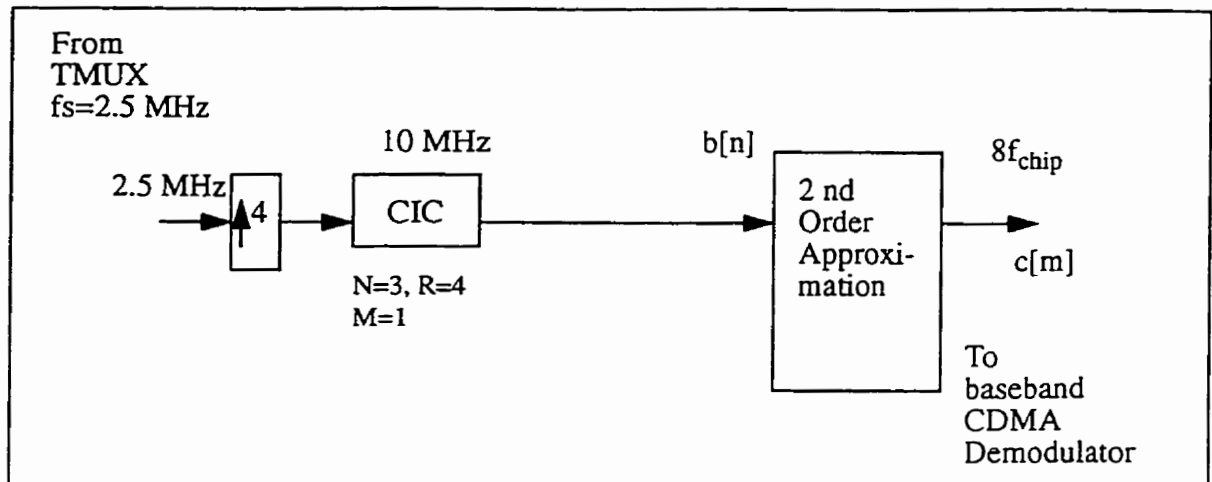
Fig. 4.12 Structure of the rate change mechanism

4.4.1 Second Order Approximation

The signal resolution required at the input of the baseband CDMA demodulator is 4 bits per QPSK signal branch. Therefore the maximum SNR required is about 24 dB assuming 6 dB SNR per bit. In addition, since the input sampling rate is $8f_{chip}$, the in-band SNR is improved by $10\log(8f_{chip}/1.25 \text{ MHz}) = 9$ dB. Therefore the maximum SNR due to quantization noise is about 33 dB. Typically, an automatic gain control circuit will keep the standard deviation of the CDMA signal to one-quarter or less the range of the ADC. As a result, the design objective for the 2nd order approximation system is to provide a signal-to-distortion ratio (SDR) of at least 33 dB, which is less than or equal to 12 dB below the quantization noise.

In the second order approximation, two adjacent samples at 10 MHz are used to compute (i.e. interpolate) the desired signal at the sampling rate of $8f_{chip}$ [2]. This point is illustrated in Fig. 4.13.

110
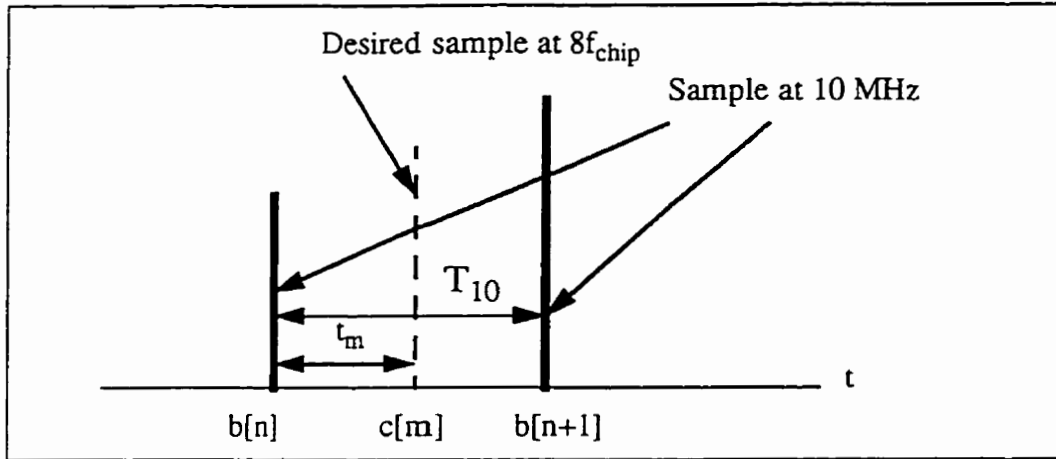
Fig. 4.13 Second order approximation

Assume that c[m] is the desired signal at $8f_{chip}$ and it lags b[n], a sample of the signal sequence at 10 MHz, by a time interval of length, t_m. These quantities are illustrated in Fig. 4.13. Let the time interval between b[n] and b[n+1] be T_{10} and let $u = t_m / T_{10}$. The desired signal c[m] can be found by the linear interpolation of b[n] and b[n+1] [2]:

$$c[m] = (1-u) b[n] + ub[n+1] \qquad 0 \le u \le 1 \qquad \cdot \qquad (4.34)$$

The calculation of t_m is a major operation in the second order approximation. Once t_m is found, u and (1-u) are calculated. Then to obtain the desired sample at $8f_{chip}$ requires two multiplications and one addition. Let T_{8fc} be equal to the period of the $8f_{chip}$ clock and T_{10} be equal the period of the 10 MHz clock. Using the concept illustrated in Fig. 2.12 for rational factor interpolation, in order to convert the sampling frequency of a signal from 10 MHz to 8fchip, the signal has to be interpolated by a factor of 3072 and then decimated by a factor of 3125. There is no common factor between 3072 and 3125 and therefore the interpolation and decimation factors are

both the minimum possible values. In terms of sampling interval,

$$T_{8fc} = \frac{3125}{3072}T_{10} \qquad (4.35)$$

Therefore

$$T_{8fc} - T_{10} = \frac{53}{3072}T_{10} \qquad (4.36)$$

Then:

$$t_m = [53m]_{modulo\,3072} \cdot \frac{T_{10}}{3072} \qquad (4.37)$$

and

$$u = \frac{[53m]_{modulo\,3072}}{3072} \qquad (4.38)$$

Define:

$$u_i = [53m]_{modulo\,3072} \qquad (4.39)$$

Using the formula in (4.39), a circuit designed to calculate u_i is shown in block diagram form in Fig. 4.14.
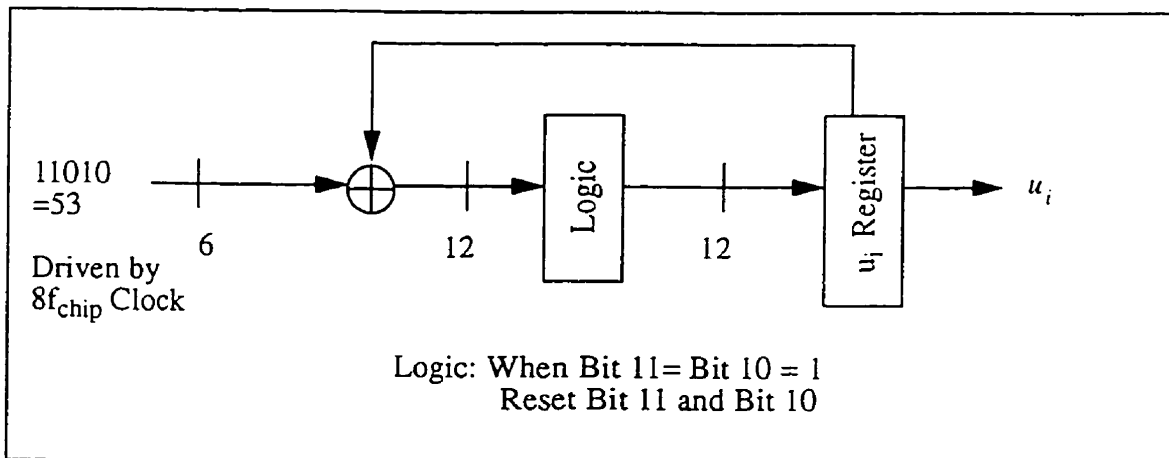

Fig. 4.14 Circuit for u_i calculation

To explain the operation of this circuit let the input to the circuit be a 6-bit fixed value

equal to 53 (a decimal number). It is clocked to the circuit every T_{8fc} seconds and added to the previous u_i value. Therefore u_i is incremented at the c[m] sample time. In order for the circuit to work, the $8f_{chip}$ clock should lag the 10 MHz clock by T_{10} since it takes two b[n] samples to calculate/interpolate one c[m] sample. There are 12 bits in the u_i registers in Fig. 4.14. The logic block in the circuit implements the modulo operation by resetting bit 11 and bit 10 of the u_i registers when they are both equal to 1. This is because $2^{11} + 2^{10} = 3072$. The two most recent b[n] samples are stored in a set of shift registers. The shift registers operate at a frequency equal to 10 MHz. Whenever u_i is incremented, c[m] is obtained by linear interpolating the two most recent b[n] samples stored in the shift registers. The outputs of the u_i registers are split into two paths: one for the circuit's output and the other is fed back to the accumulator.
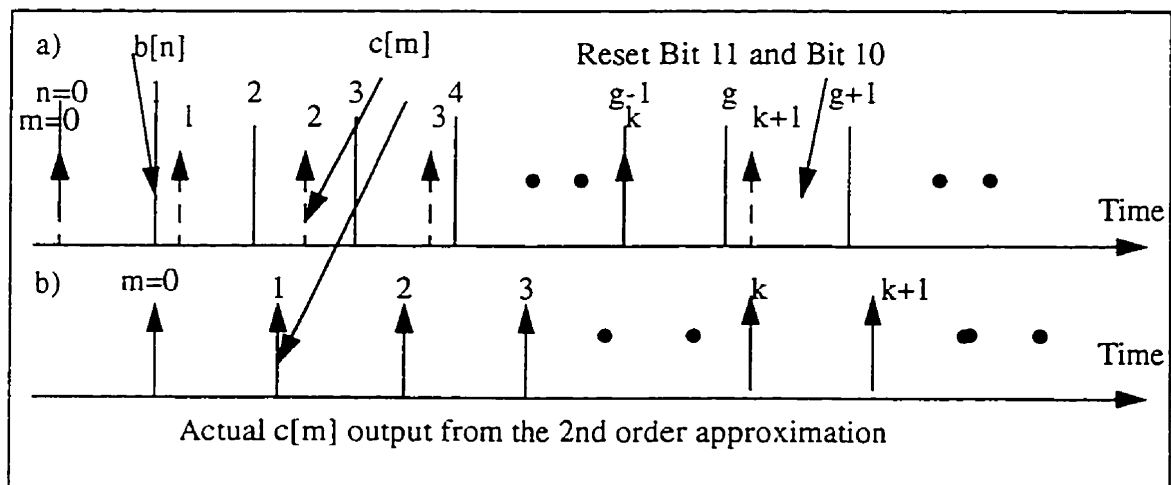
Fig. 4.15 Graphical representation of the operation of the 2nd order approximation

Fig. 4.15 is a graphical representation of the operations of the 2nd order approximation. The dotted arrows at Part a of the diagram represent the theoretical positions of the c[m] sequence relative to the b[n] sequence. At n=0, both b[n] and c[m] are aligned. Since both sequences have a different sampling frequency, their sampling points diverge when n>0 and m>0.

113

In general, since the sampling frequency of the c[m] sequence is smaller than the sampling frequency of the b[n] sequence, c[m] sampling points lag the b[n] sampling points. The arrows shown in Part b of Fig. 4.15 represent the actual output of the 2nd order approximation. There is a T_{10} delay in the actual c[m] output. This is because the interpolation process requires two b[n] sample points to calculate one c[m] sample. At m=1, u_i is incremented and c[1] is obtained by interpolating b[1] and b[2]. At m=s, u_i is incremented and c[s] is obtained by interpolating the two most recent b[n] values stored in the shift registers in Fig. 4.14. At m=k+1, the bit 10 and bit 11 are reset due to the modulo operation in the u_i generation circuit. The most recent b[n] samples stored in the register are b[g+1] and b[g]. Therefore c[k+1] is obtained by interpolating b[g+1] and b[g].

The second order approximation requires the signal sequence to be interpolated by a factor of I before the operation described in (4.34) is carried out. The relationship between I and the SDR[2] is

$$I = \frac{2f_p}{fs}\pi \sqrt[4]{\frac{10^{\frac{SDR}{10}}}{80}} \qquad (4.40)$$

where f_p is the passband bandwidth of the signal and f_s is the reference sampling frequency of the signal. When I is set to one which means that no interpolation is done to the sequence at the original sampling rate, f_s=10 MHz, a SDR of 35 dB is obtained. By providing a SDR of 35 dB, the 33 dB SDR requirement given in Section 4.4.1 is met.

For better ISI performance and better image suppression a pair of two stage interpolation filters IFIR1 and IFIR2 with improved stopband attenuation relative to the CIC can be used to

interpolate the signal from 2.5 MHz to 10 MHz. The two stage interpolation filters, IFIR1 and IFIR2, have to meet the masks shown in Fig. 4.16 and 4.17 respectively. The passband of both masks is equal to the bandwidth of one composite CDMA carrier. After the first interpolation stage, the sampling frequency is increased to 5 MHz. An image is introduced at 2.5 MHz and its boundary closest to baseband is at 1.875 MHz. To eliminate the image term the stopband of the interpolation filter, IFIR1, should be at 1.875 MHz. Similarly, after the second interpolation stage to a sampling frequency of 10 MHz, an image is introduced at 5 MHz. Therefore the stopband of the mask for IFIR2 is set at (5 - 0.675) = 4.375 MHz. As mentioned before the baseband CDMA demodulator requires a SNR of at least 33 dB. The noise floor of the input to the demodulator is to be -33 dB. To provide such performance the interpolation filters must provide image suppression of at least -33 dB. To provide a margin for other system impairments. a margin of 27 dB is added to the stopbands of the filters. As a result both filter masks have stopband attenuation of -60 dB. The filters specified by the mask can be implemented by an 11 tap and 7 tap half-band filter designed by Goodman[4]. The Goodman filters are notable for their simplicity and can be implemented as a succession of shifts and adds. Multiplications are not required in the implementation.
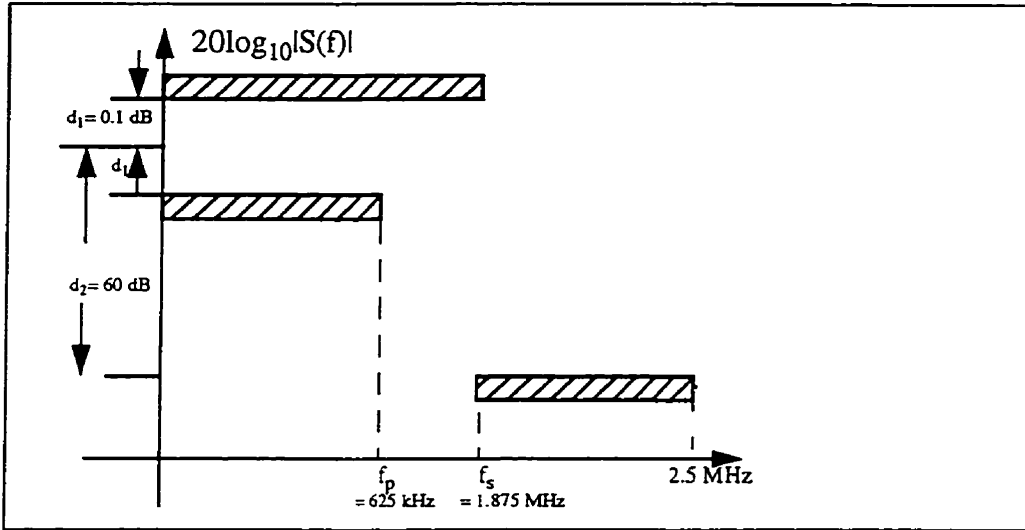
Fig. 4.16 Filter mask for IFIR1
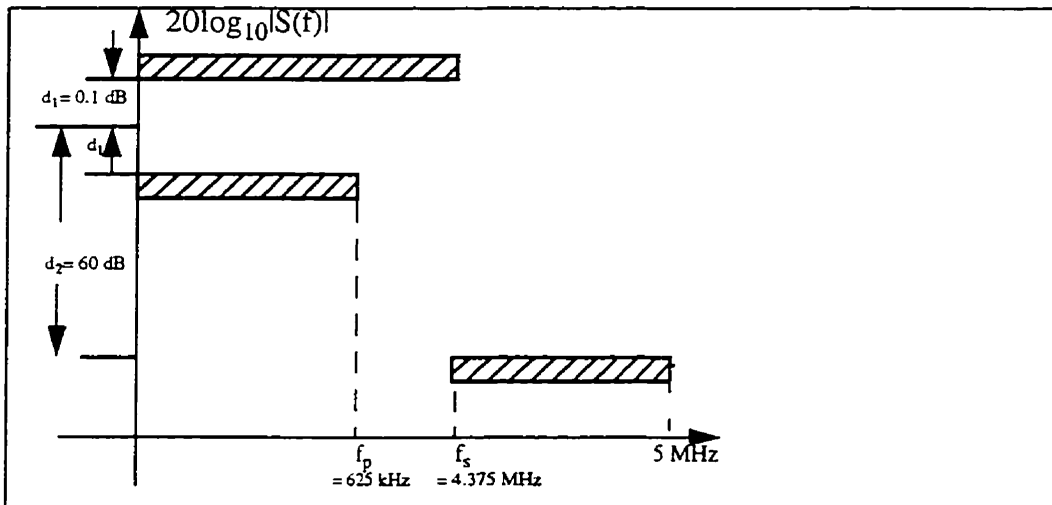
Fig. 4.17 Filter mask for IFIR2

4.5 System Complexity Estimate

The main components of the polyphase-FFT system are: 1) a 60 MHz ADC, 2) a pair of sin/cos mixers and a lowpass filter, 3) a pair of polyphase networks, 4) a N-point complex FFT and 5) a rate change system.

4.5.1 Complexity Estimate for the Transmultiplexer Front End

The transmultiplexer front end, as shown in Fig. 4.1, includes a pair of sin/cos mixers, lowpass filters and sign inverters. However, as explained earlier, due to the nature of the cosine sequence the cosine mixer and the lowpass filter at the QPSK in-phase signal branch can be saved. A delay is to be added to the in-phase signal branch so that the signal from the sine and cosine branch have the same timing. In addition, the sine mixer can be eliminated and the low-pass filter at the quadrature-phase signal branch is implemented by a 12 taps modified half-band filter derived from the 23 tap half-band lowpass filter chosen earlier. The complexity of the low-pass filter per (I+Q) branches per 11 carriers, in an effective data rate of 15 MHz, is

$$12 \cdot 15 \text{ MHz} = 180 \text{ M multiply-accumulate (MAC) operations}$$

with the assumption that a DSP can execute a multiply-accumulate (MAC) as a single operation [37]. The sign inverters in the transmultiplexer are not absolutely necessary. Their function is only to shift the CDMA carrier block so that the guard band is at DC. It has no impact to the performance of the transmultiplexer system. As a result, in order to reduce complexity, the sign inverters are eliminated.

117

4.5.2 Complexity Estimate for the Polyphase Network

The polyphase network consists of two identical polyphase filters. There are 12 subfilters in each of the polyphase filter. The complexity of the polyphase network per (I+Q) branches per 11 carriers is

$$192 \text{ tap} \cdot 2.5 \text{ MHz} \cdot 2 = 960 \text{ M multiply-accumulate (MAC) operations}$$

4.5.3 Complexity Estimate for the FFT

As mentioned in 4.3.2, the 12 point FFT can be implemented by three 4-point FFTs and four 3-point FFTs. It requires 12 real, imaginary interchange and 12 sign inversions. 64 real multiplications and 152 real additions.The complexity of the FFT is

$$64 \cdot 2.5 \text{ MHz} = 160 \text{ M real multiplications}$$

$$152 \cdot 2.5 \text{ MHz} = 380 \text{ M real additions}$$

$$12 \cdot 2.5 \text{ MHz} = 30 \text{ M operations}$$

$$12 \cdot 2.5 \text{ MHz} = 30 \text{ M operations}$$

The total complexity per (I+Q) branches per 11 carriers is 540 M multiply and addition operations and 60 operations for real and imaginary interchange and sign inversion. However, it should be noted that some of the real additions performed in the 3-point FFT can be combined with the multiply operations and become multiply-accumulate (MAC) operations.

At the output of the FFT for each of the demultiplexed carriers of odd carrier numbering, there is a sign change operating at the rate of 2.5 MHz and its complexity is

$$2 \cdot 6 \cdot 2.5 \text{ MHz} = 30 \text{ M operations}$$

4.5.4 Complexity Estimate for the Rate Change Mechanism

The rate change mechanism consists of a 3rd order CIC interpolation filter and a 2nd order approximation. The CIC interpolator has complexity per-carrier per (I+Q) branches as shown below:

Comb filter stage:

$$2.5 \text{ MHz} \cdot 3 \cdot 2 = 15 \text{ M additions}$$

Integrator stage:

$$10 \text{ MHz} \cdot 3 \cdot 2 = 60 \text{ M additions}$$

Total complexity per (I+Q) branches per-carrier: 75 M additions

Total complexity per (I+Q) branches per 11 carriers: 825 M additions

To improve the ρ value two Goodman half-band filters, IFIR1 and IFIR2, can be used. IFIR1 has 7 non-zero coefficients and IFIR2 has 5 non-zero coefficients. Therefore the complexity per (I+Q) branches per carriers is

$$2 \cdot (7 \cdot 2.5 \text{ MHz} + 5 \cdot 5 \text{ MHz}) = 85 \text{ M multiply-accumulate (MAC) operations}$$

Total complexity per 11 carrier per (I+Q) branches is 935 M multiply-accumulate (MAC) operations. Since the 2-stage option has higher complexity, only the CIC option is considered. The second order interpolation is carried out at $8f_{chip}$ and this procedure requires two multiplications and one addition. Moreover one addition is performed in order to obtain u_i and one addition to otbain $1 - u_i$. It should be noted that these two additions can be shared by all the

119

11 carriers in the CDMA spectrum. The complexity of the 2nd order approximation per (I+Q) branches per 11 carriers is

$$2 \cdot (8 \cdot 1.2288 \, \text{MHz} \cdot 3 \cdot 11 \,) + 1.2288 \, \text{MHz} \cdot 8 \cdot 2 = 669 \, \text{M multiply addition operations}$$

The total complexity for the rate change mechanism is:

$$825 + 669 = 1494 \, \text{M multiply-accumulate (MAC) operations}$$

4.5.5 Total System Complexity Estimate

The total system complexity per (I+Q) branches per 11 carriers is 3535 M multiply accumulate operations. A detailed description of the operation required is presented in Table 4.1.

Table 4.1 Comparison of complexity of transmultiplexer and per-carrier implemented channelizer (per 11 carriers per I+Q)

	Transmultiplexer (M operations)	Per-Carrier (M operations)
LPF	180 (multiply-accumulate)	
FFT	600 (multiply and addition)	·
FFT(sign inverters)	30(operations)	
NCOs		2596 (operation)
HDF		10813 (addition)
Polyphase Filter	960(multiply-accumulate)	
Carrier Select Filters		1786(multiply-accumulate)
3rd Order CIC Interpolator	825 (addition)	812 (additions)
2nd Order Rate Change	669(multiply and addition)	
Total	3264	16007

4.6 Comparison of Polyphase-FFT and Per-Carrier Approach

Table 4.1 presents a comparison of the complexity of the polyphase-FFT/transmulti-plexer and the per-carrier approach. From the table one can see that the polyphase-FFT approach has close to a factor of 5 advantage in terms of the total complexity compared to the per-carrier approach. This is for a complexity measure that involves a count of all opeartions performed by the demodulator. However, it should be noted that the comparisons made in the table are not exact. The reason is that not all the operations between the two approaches are of equivalent complexity. In particular, the operation count for the CIC/HDF in the per-carrier approach has to be distinguished from the rest of the table since the HDF involves only additions. No multiplication is required. Additions are less expensive to implement in VLSI (requires fewer gates) than multiplications.

Taking account of the differences in operation type, it can be concluded that the low complexity of the polyphase-FFT approach over the per-carrier approach is because the former approach has replaced the operation intensive NCOs and HDFs with FFT and LPF operations. The digital down conversion operation of the per-carrier approach needs 11 dedicated NCOs. In addition, the large ROM storage requirement of the NCOs adds complexity. In the polyphase-FFT system, because of the relationship between the sampling rate and the IF frequency, an NCO is not required.

In terms of carrier selection, the polyphase filter has a complexity about half of the carrier select filter in the per-carrier approach. The CIC interpolators following the carrier selec-

tion used in both the polyphase-FFT and per-carrier approach are actually the same. The difference in operation count is due to the minor difference in data rate. In the polyphase-FFT approach the data rate is a multiple of 1.25 MHz while in the per-carrier approach the data rate is multiple of the chip rate = 1.2288 MHz.

It should be noted that although the polyphase-FFT approach has an advantage over the per-carrier approach in terms of system complexity for a fully deployed system with 11 carriers, the polyphase-FFT approach incurs a high start-up cost. In the polyphase-FFT system only the cost of the CIC interpolators and the 2nd order approximation unit is incremental. In other words, no matter how many CDMA carriers are present in the spectrum, a cellular operator has to absorb the cost of installing the front end, the polyphase filter and the FFT, except sign inverters. which adds up to a total of 1740 M operations. For each carrier an incremental cost due to the rate change unit is approximately 139 M operations. As a result the complexity of the polyphase-FFT is:

1740 M operations + 139 n M operations

where n is the number of carriers and n > 0.

In the case of the per-carrier approach, all the parts in the system are incremental per-carrier. Its complexity is:

1455 n M operations

where again n is the number of carriers.

Fig. 4.18 shows a comparison between the two approaches. It can be seen that the

cross over point between the two approaches is at 2 carriers which means that the advantage or economy of the polyphase-FFT approach comes when there are more than 2 carriers in the spectrum.

It should be noted that the ADC sampling frequency of the per-carrier approach can be lowered in order to reduce system complexity. The high ADC sampling frequency is chosen in order to compare complexity directly with the polyphase-FFT approach. However, even if the sampling frequency of the per-carrier approach is reduced to f_s=32fchip= 39.3216 MHz the cross-over point is still at 2 carriers. This result shows that the polyphase-FFT approach is more efficient as the traffic increases in CDMA PCS systems and multiple carriers are deployed.
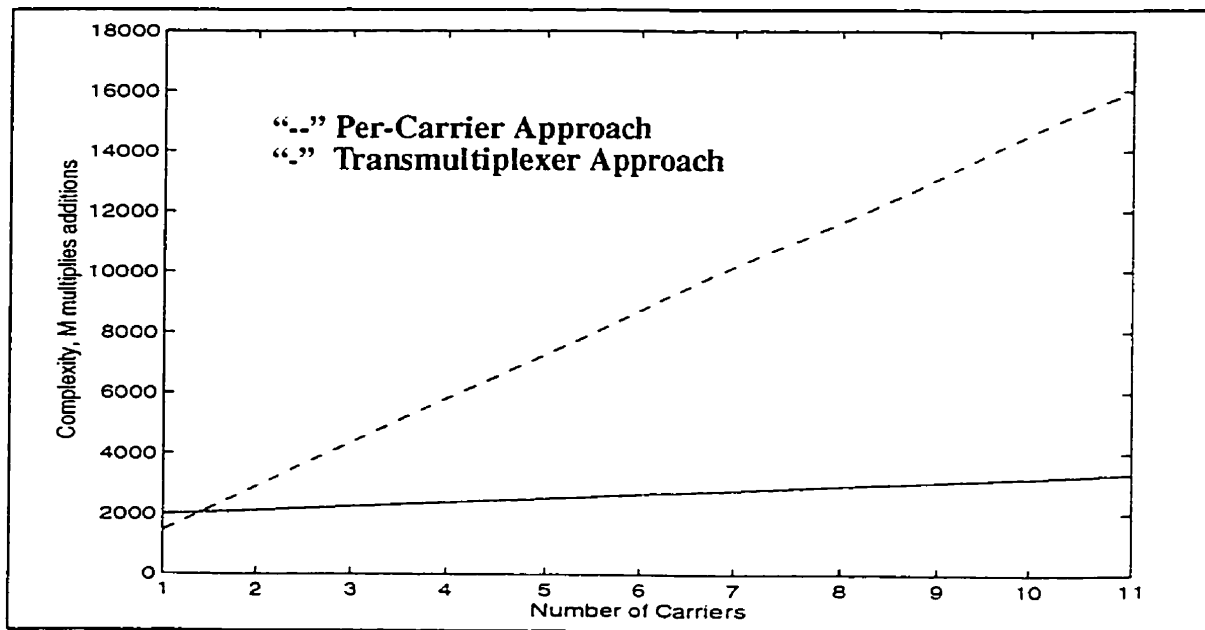

Fig. 4.18 Complexity comparison between transmultiplexer and per-carrier approach to carrier demultiplexing

Chapter Five

Receiver Filter Design and System Performance Verification

5 Chapter Overview

In this chapter, the design method for the polyphase carrier select filter is presented. In order to verify that the transmultiplexer channelizer designed in Chapter Four satisfies the performance requirements given in Section 2.1, various system tests are conducted. The simulation model and the testing results are discussed in the second part of this chapter.

5.1 Receiver Filter Design

As mentioned in Section 3.2.2 the cascade of the transmitter baseband filter, $t_x[n]$, and the receiver filter, $r_x[n]$, should approximate a pulse shape which satisfies the Nyquist criteria for no ISI. Due to the infinite length of such a pulse shape, it is not physically realizable[2]. However, one can use an approximation to a raised cosine pulse which has a limited length to satisfy the criteria for no ISI. By graphically overlapping the frequency response of the ideal transmitter filter given by the IS-95+ standard [5] with a root raised cosine pulse having an excess band-width, β, it was found, by visual inspection, that a root raised cosine with 15 % excess bandwidth, $R_{\text{rrc}}(e^{jw})$, provides a good match to the transmitter filter. This comparison is in terms of the transition band and passband bandwidth, and ignores the fact that the passband ripples positions are not aligned. This observation is shown in Fig. 5.1. Assuming that both the transmitter filter and the receiver filter are root raised cosine filters with 15 % excess bandwidth then the cascade of the

two filters will be a raised cosine response with 15 % excess bandwidth, $r_{rc}[n]$. The frequency response of the raised cosine pulse is $R_{rc}(e^{jw})$. A raised cosine pulse shape with 15 % excess bandwidth can be used as a design target for the cascade of $t_x[n]$ and $r_x[n]$. Using (5.1) below, a frequency mask for the receiver filter function can be obtained as

$$R_x\left(e^{jw}\right) = \frac{R_{rc}\left(e^{jw}\right)}{T_x\left(e^{jw}\right)} \qquad (5.1)$$

where $R_x(e^{jw})$ is the frequency response of $r_x[n]$ and $T_x(e^{jw})$ is the frequency response of $t_x[n]$.
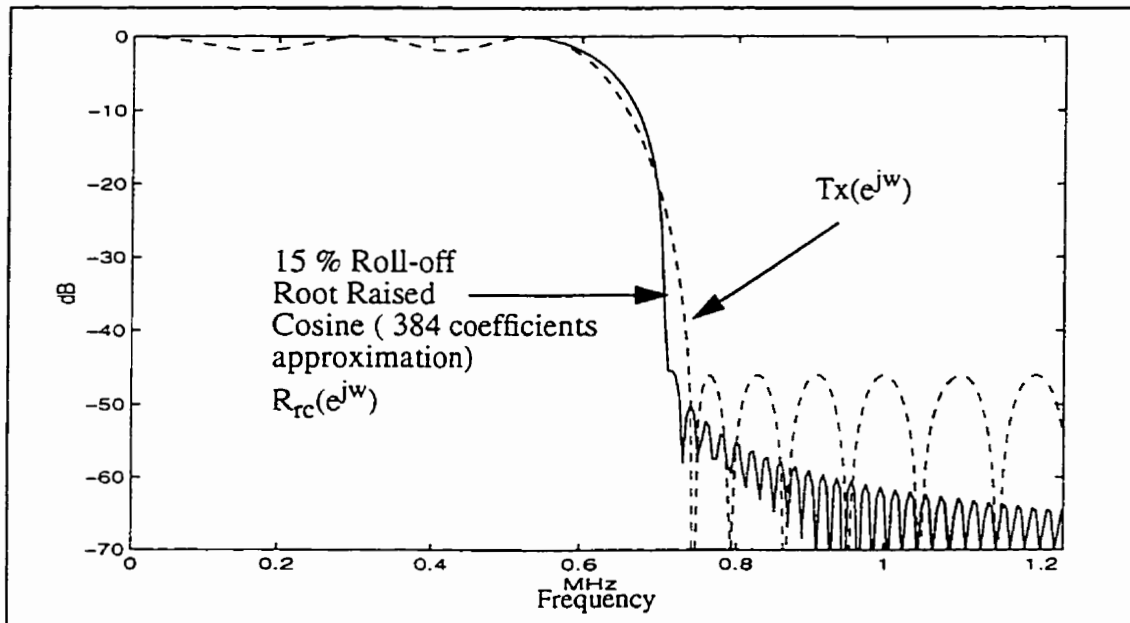
Fig. 5.1 Frequency response of Tx[n] and a 15% root raised cosine pulse with 15 % excess bandwidth

5.1.1 Carrier Select Filter Design for the Transmultiplexer System

In the transmultiplexer approach, the receiver filter function consists of a low pass filter, a polyphase carrier select filter and a CIC interpolator. The effect of the low pass filter on the receiver filter function is ignored due to its relatively flat and large passband. Thus, in the time

125

domain, the receiver function is considered as a cascade of the polyphase carrier select filter and the CIC interpolator. Their relationship in the frequency domain is given in (5.2),

$$R_x\left(e^{jw}\right) = R_p\left(e^{jw}\right) \cdot CIC\left(e^{jw}\right)$$ (5.2)

where $R_p(e^{jw})$ is the frequency response of the polyphase carrier filter and $CIC(e^{jw})$ is the frequency response of the CIC interpolator. Combining (5.1) and (5.2), the relationship between the baseband filter, carrier select filter and the CIC interpolation is given in the frequency domain in (5.3) as,

$$R_p\left(e^{jw}\right) = \frac{R_{rc}\left(e^{jw}\right)}{T_x\left(e^{jw}\right)CIC\left(e^{jw}\right)}$$ (5.3)

The frequency domain relation shown in (5.3) can be used to calculate the desired frequency response for the polyphase carrier select filter using the frequency sampling filter design method. In this frequency response the passband degradation due to the roll-off of the CIC interpolator has already been compensated. The two frequency sampling filter design methods, represented by α = 0 and α =0.5, are discussed in detail in Appendix A. The frequency sampling filter design method with $\alpha = 0.5$ was used in conjunction with a Kaiser window function for the design of the polyphase carrier select filter in order to obtain a stopband attenuation characteristic which satisfies the requirements given in Section 2.1. In addition, the transition band of the filter designed was widened in order to achieve a better stopband attenuation. Using the methods discussed above, a 192 tap FIR filter was designed. The frequency response of the filter is illustrated in Fig. 5.2. The carrier select filter designed has a stopband attenuation of -90 dB at 1.25 MHz and beyond. The passband of the carrier select filter is slightly curved upward in order to compensate for the roll-off of the CIC interpolator. The noise bandwidth for the receiver filter function, $R_x(e^{jw})$, is 520 kHz. In terms of stopband attenuation and noise bandwidth, the carrier select filter

126

and its corresponding receiver filter function satisfy the requirements specified in Section 2.1. In Fig. 5.2 the frequency response of the carrier select filter without compensation for the CIC interpolator is shown in order to emphasize the upward curved passband of the carrier select filter.
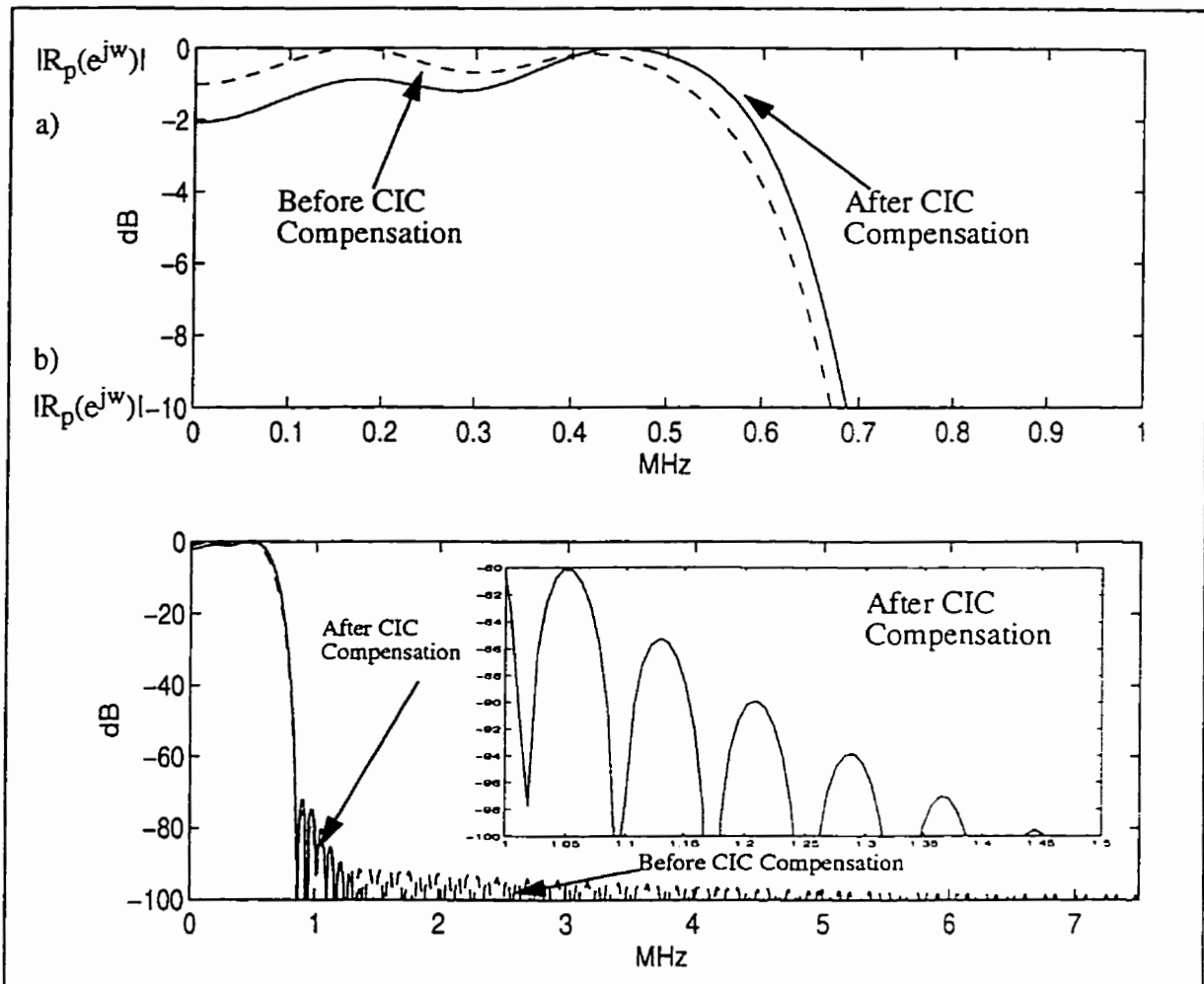

Fig. 5.2 Frequency response of the carrier select filter $f_s = 15$ MHz

The ρ value of the transmultiplexer channelizer system using the carrier select filter designed in this section will be discussed later in this chapter.

5.2 TMUX Testing System Setup

To investigate the performance of the transmultiplexer channelizer against the performance requirements derived in Section 2.1, a simulation model for the CDMA transmitter and receiver system was developed according to the architecture specified by the IS-95+ standard [5]. The block diagram for the simulation model is shown in Fig. 5.3. In the model, the $i_k[n]$ and $q_k[n]$ sequences are the data sequence for the in-phase signal branch and the quadrature-phase signal branch respectively, of the kth CDMA carrier transmitter. The baseband filter at the transmitter is the 48 tap FIR filter specified by the IS-95+ standard [5]. After baseband filtering, the $i_k[n]$ and $q_k[n]$ sequences are modulated to the frequency position of the kth carrier in the IF band in the QPSK modulation format. The different QPSK modulated carriers are summed together to form a channel signal. In this simulation model no non-linearity or noise is added to the signal by the channel. At the receiver for the model, the signal sequence consisting of n carriers, where n is equal to the number of QPSK CDMA carriers in the channel, is fed into the transmultiplexer channelizer for carrier demultiplexing. The $i_{ek}[m]$ and $q_{ek}[m]$ sequences are the estimated values of the $i_k[n]$ and $q_k[n]$ data sequences at the output of the transmultiplexer channelizer. The simulation model illustrated in Fig. 5.3 is the model for all the system performance verifications performed in this thesis.

Since the simulation is for a discrete-time model, it is desirable to have the transmitted signal sequence have a common reference sampling rate with the ADC in the receiver model. Since the baseband filter operates at $4f_{chip}$, an interpolator, which is capable of handling interpolation by a rational factor, is used to interpolate to 60 MHz, the sampling frequency of the ADC
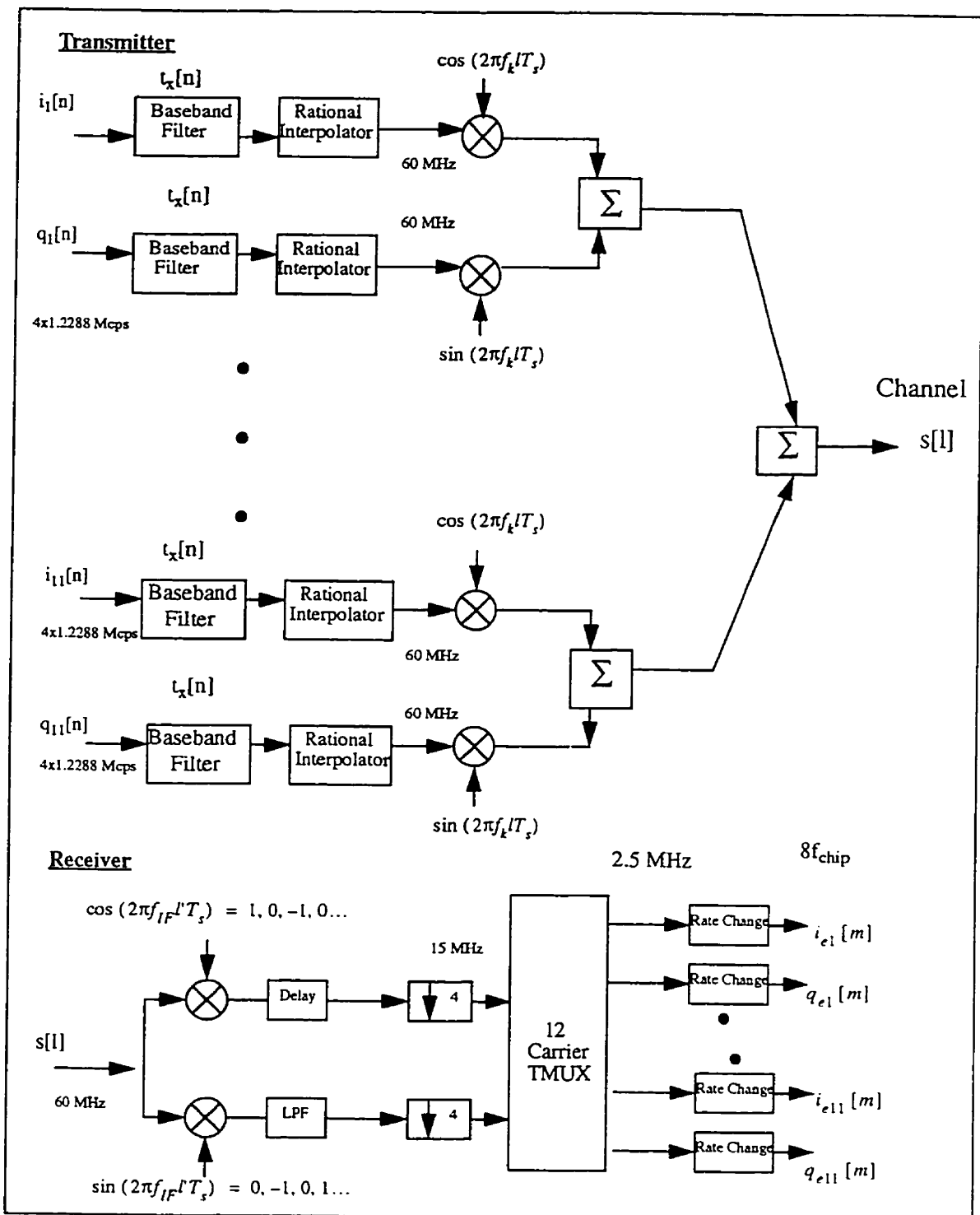
of the receiver.

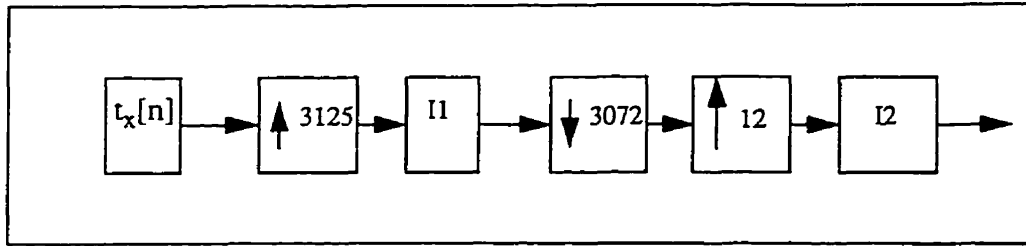Fig. 5.3 Transmitter/ receiver simulation model

Fig. 5.4 Setup of rational interpolator

In Fig. 5.4, the block diagram of the rational interpolator is shown. The QPSK modulation was interpolated to a sampling frequency of 60 MHz. In this way, no further rate conversion is necessary in order to convert the sampling rate of the transmitted signal sequence to the ADC sampling rate. By the interpolator shown in Fig. 5.4, a perfect rational interpolation is made. $t_x[n]$ is the impulse response of the transmitter filter given by the IS-95+ standard [5]. I1 and I2 are the interpolation filters used to eliminate the image introduced by the interpolation procedure. In practice, the signal is interpolated by 3125 through a cascade of 5 interpolate-by-5 operations since a one-time interpolation of 3125 would make the interpolation filter exceedingly long, complex and hard to design [2].

5.3 Per-Carrier FFT Output Response

Fig. 1.2 is used as a reference for carrier numbering; the center frequency of carrier n is 1.25n+7.5 MHz, where n can be an integer from 1 to 11. In Fig. 5.5, $S(e^{jw})$, the frequency response of a carrier at 16.25 MHz, the position of the 7th carrier, with a sampling rate of 60 MHz, is shown. The center of the IF band, f_{IF}, is 15 MHz. The carrier signal is generated by modulating the impulse response of the baseband filter of the I and Q signal branches at a sampling frequency of 60 MHz with a carrier at 16.25 MHz.

130

In the transmultiplexer front end, the signal is down-shifted and converted to an analytical signal. In Fig. 5.6, $S_A(e^{jw})$, the frequency response of the analytical signal of the single carrier at the position of the 7th carrier (8.75 MHz) is shown. This analytical signal is then the input to the TMUX and Fig. 5.7 shows the I and Q signal outputs of the FFT for the 7th carrier, $FFT_{7I}(e^{jw})$ and $FFT_{7Q}(e^{jw})$ respectively. It is shown in the diagram that the I and Q signals are perfectly aligned with each other. Since the I and Q signals at the outputs of the FFT are the same, from this point on, only the I signal is discussed and it represents both the I and Q signal responses. As shown in Fig. 5.7, the attenuation around 1.25 MHz is about -140 dB. This is the sum of the attenuations from the -50 dB stopband of the transmitter filter and the -90 dB stopband of the polyphase carrier select filter. The upward slope is due to the compensation for the CIC interpolator, which has been built into the polyphase carrier select filter.
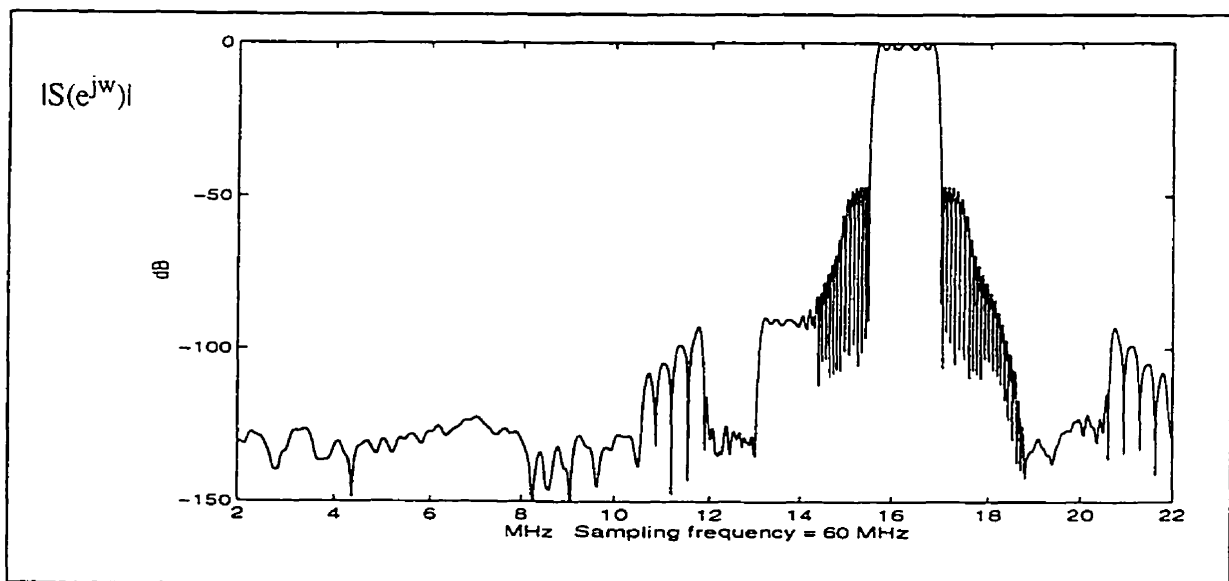

Fig. 5.5 Frequency response of a single carrier at 16.25 MHz (the 7th carrier)
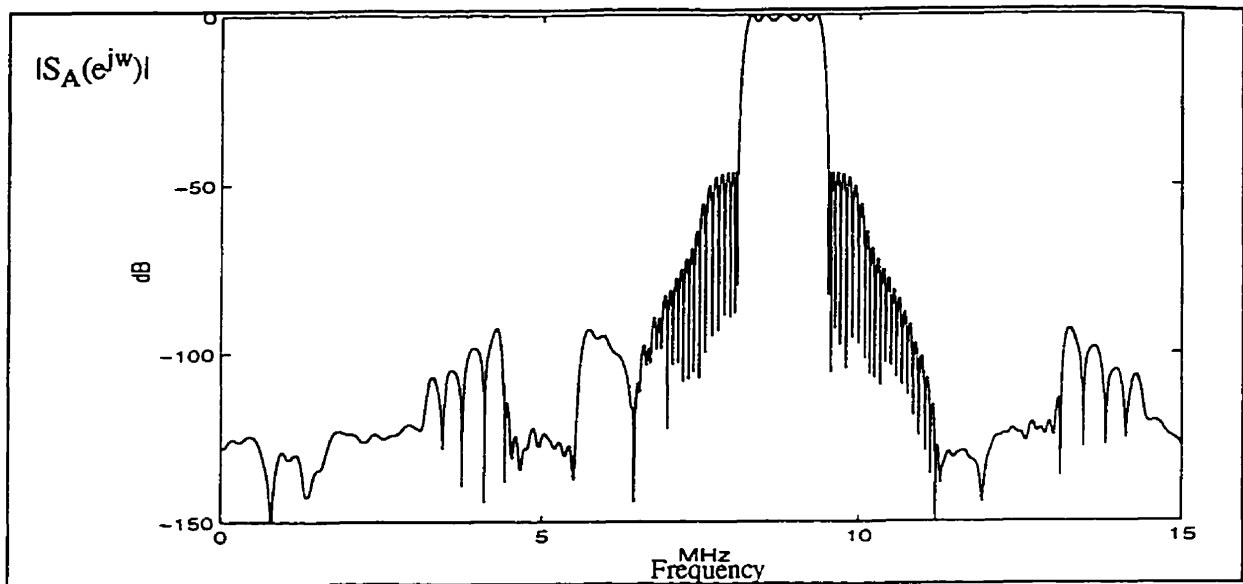
Fig. 5.6 Frequency response of the analytical signal of one carrier at the position of the 7th carrier
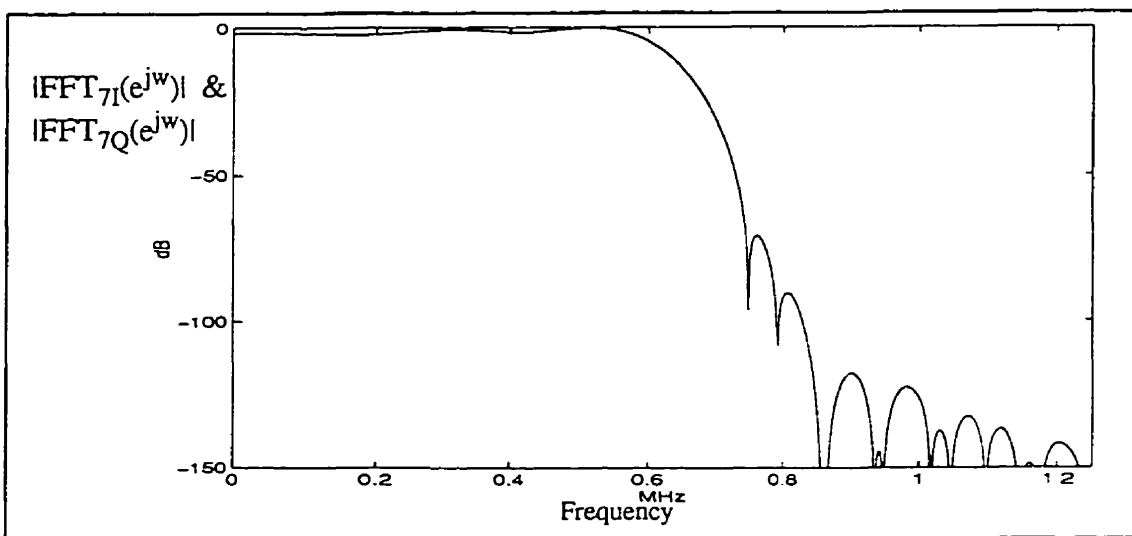
Fig. 5.7 Frequency response of the FFT output for the 7th carrier (I,Q)

The I and Q signal output of the FFT for the 7th carrier at a sampling rate of 2.5 MHz is then fed into the rate change mechanism, which consists of a third order CIC and a second order linear approximation. In Fig. 5.8a, the impulse response of the 7th carrier's signal at a sampling rate of 10 MHz before the second order linear approximation, $d_{e10}[n]$, is shown. Its impulse

132

response after the second order approximation, $d_{e8fc}[m]$, is shown in Fig. 5.8b. The output shown in Fig. 5.8b has a sampling rate of $8f_{chip} = 9.8304$ MHz.

In Fig. 5.9 the frequency response of the output of the rate change mechanism, $D_{e8fc}(e^{jw})$, and the frequency response of the signal at 10 MHz before the 2nd order approximation (dotted line), $D_{e10}(e^{jw})$, is shown. Fig. 5.9 shows that the 2nd order interpolation has increased the noise floor of the signal. Other than adding this impairment to the signal, the passband of the output from the 2nd order approximation agrees very well with the original signal at a sampling rate of 10 MHz. The -33 dB side lobes shown in Fig. 5.9 are due to the gentle image
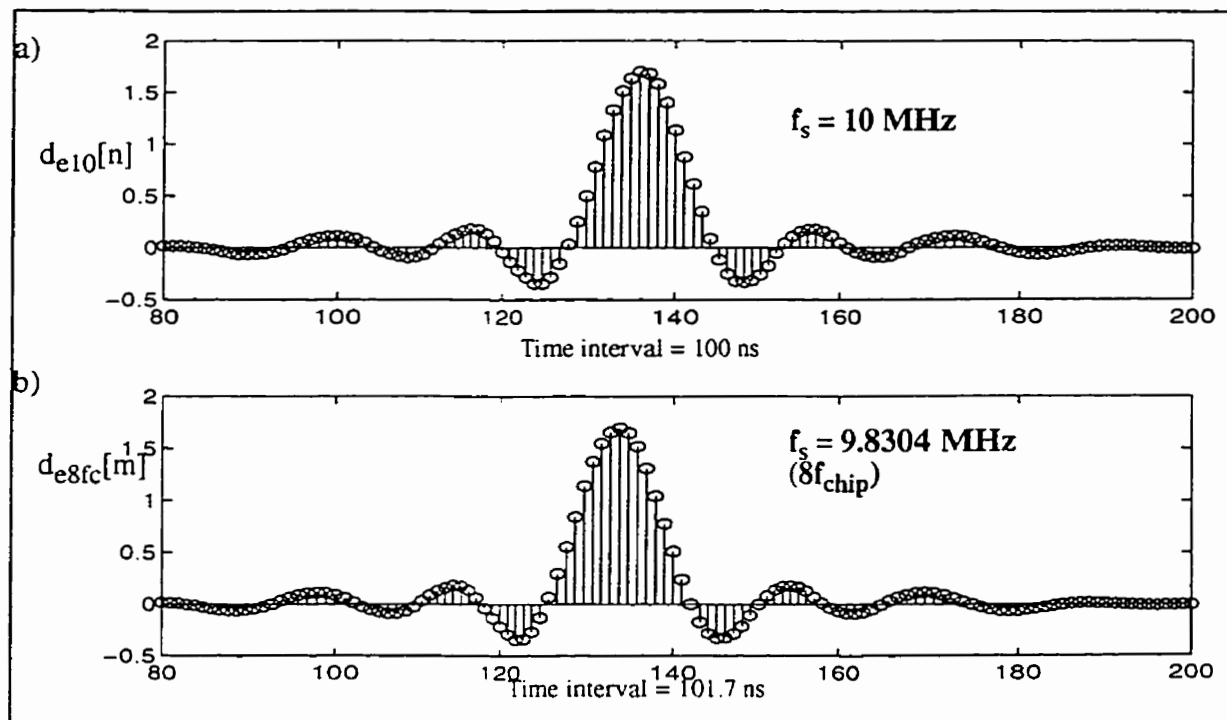

Fig. 5.8a,b The 7th carrier's impulse response before and after the 2nd order approximation

attenuation of the CIC interpolator to the images introduced by the interpolation process. The

magnitude of these side lobes is the same as in the per-carrier approach. The signal contained in these side lobes has the same correlation to the information signal contained in the main lobe as white noise. This is discussed further in Section 5.6. Note, however that an interferer at a frequency position about 2 MHz offset from the carrier will be attenuated by at least 90 dB, the stop-band attenuation of the polyphase carrier select filter.
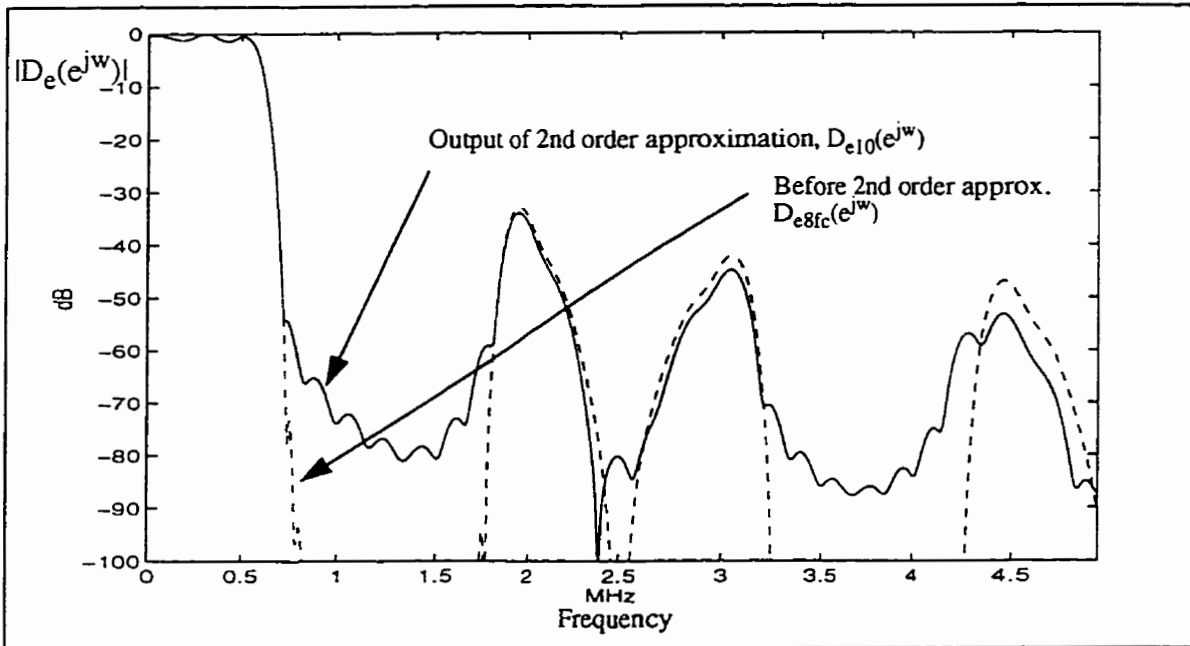
Fig. 5.9 Frequency response at the output of rate change mechanism

5.4 Signal-to-Aliasing Ratio (SAR)

In the TMUX, the analytical signal is decimated by a factor of 6 from 15 MHz to 2.5 MHz and filtered by the polyphase carrier select filter. Assume that there is only one carrier in the CDMA spectrum. During the decimation process the signal in the carrier is distorted by aliasing from its own image. The amount of distortion is determined from the shape and the stopband attenuation of the polyphase carrier select filter. The signal-to-aliasing ratio (SAR) is a measure

134

of the ratio of the signal power to the distortion caused by aliasing. In Fig. 5.10 the frequency

response of the polyphase carrier select filter, $R_p(e^{jw})$, is shown with its image (the dotted line)

centered at $f_s = 2.5$ MHz sampling rate. Portions of the $R_p(e^{jw})$ spectrum are overlapped or

aliased by its image. However, the level of distortion, as noted on the diagram, is approximately -

105 dB. Therefore, from Fig. 5.10, it can be concluded that the SAR value of the transmultiplexer

is -105 dB.
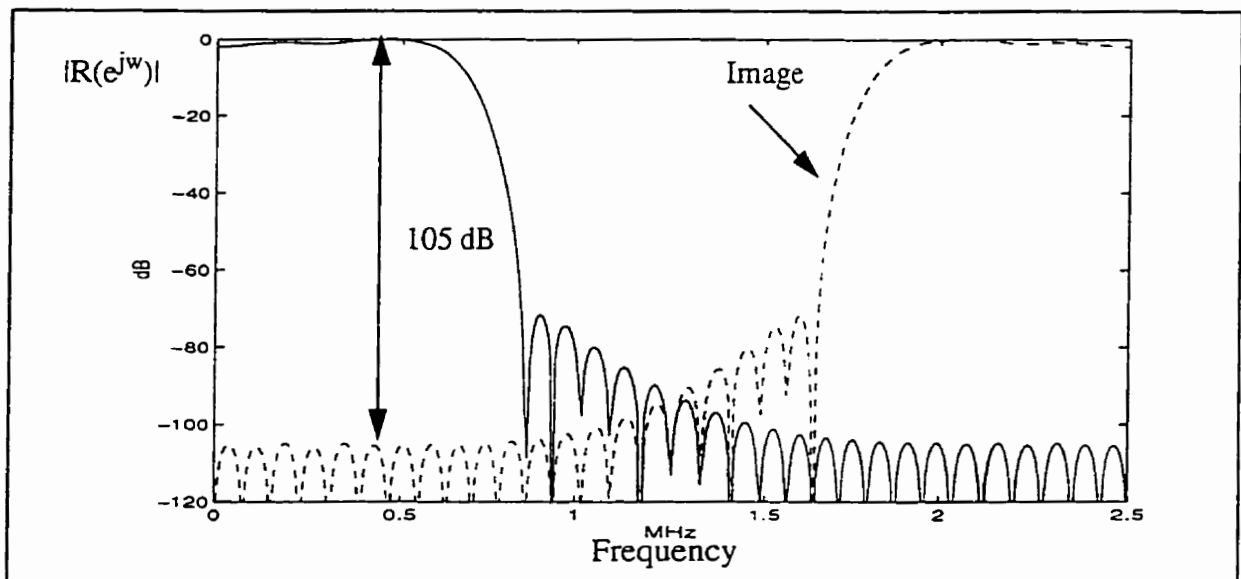
Fig. 5.10 Frequency response of carrier select filter at 2.5 MHz sampling rate

5.5 Signal-to-Crosstalk Ratio (SCR)

As shown in Fig. 2.2, the stopband of the transmitter baseband filter is at 740 kHz

which is greater than one-half of the 1.25 MHz carrier spacing, 625 kHz. Therefore, when there is

more than one carrier in the CDMA spectrum, crosstalk, due to overlap of the adjacent carrier is

expected. The crosstalk caused by an adjacent carrier is shown in Fig. 5.11. In the diagram the

frequency responses of two transmitter baseband filters, $T_x(e^{jw})$, 1.25 MHz apart are shown. The region where the two frequency responses overlap each other is the crosstalk region. The signal-to-crosstalk ratio (SCR) is a measure of the ratio of the signal power to crosstalk noise. To examine the SCR value the following experiments were done. For a spectrum width of 15 MHz, only one carrier is taken to form the transmultiplexer receiver input and the carrier number is 7. The signal power at the per-carrier FFT output, corresponding to the 7th carrier, is calculated. Then, the same 15 MHz spectrum occupied by ten carriers, i.e., all carriers except the 7th carrier, is used as an input to the TMUX. The analytical signal at the transmultiplexer output, $S_A(e^{jw})$, is shown in Fig. 5.12. At about 8.75 MHz, the position of the 7th carrier in the analytical signal, there is a null. The difference in magnitude between the other carriers and the bottom of the null is about 50 dB. This shows that no signal is occupying the position of the 7th carrier. Therefore the power appearing at the 7th carrier's FFT per-carrier output is purely noise due to crosstalk. In Fig. 5.13, the frequency response of the output of the FFT for the 7th carrier, $FFT_7(e^{jw})$, is shown.
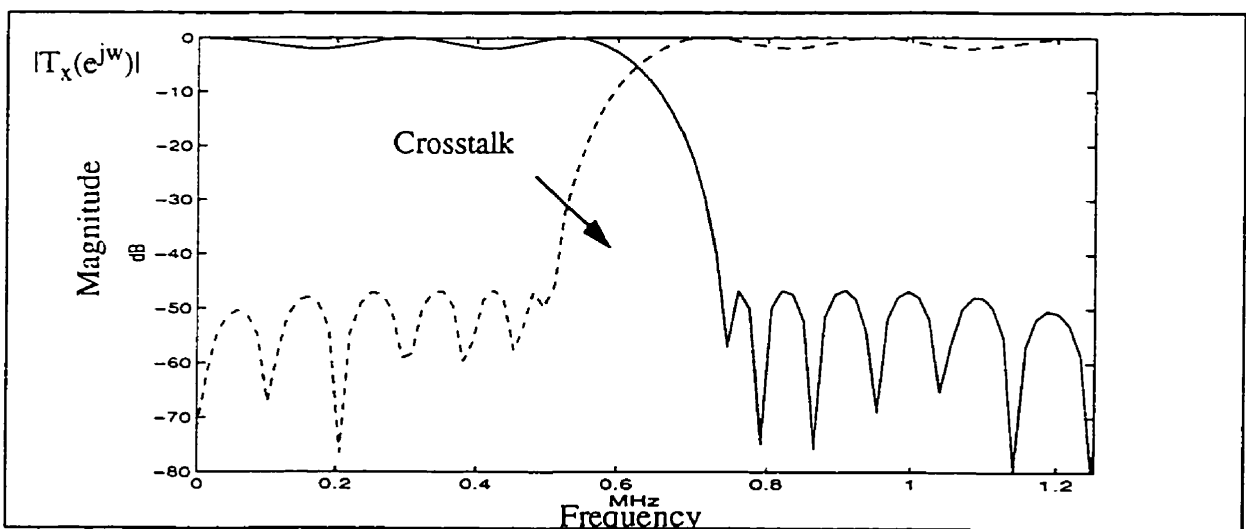
Fig. 5.11 Frequency response of two adjacent carriers
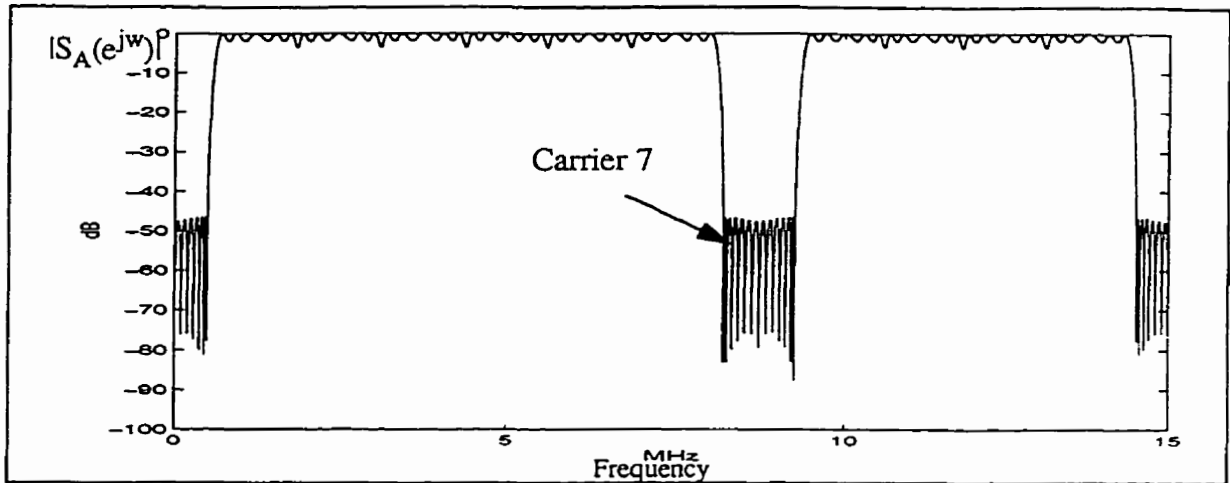
Fig. 5.12 Analytical signal of 10 carriers in front of TMUX
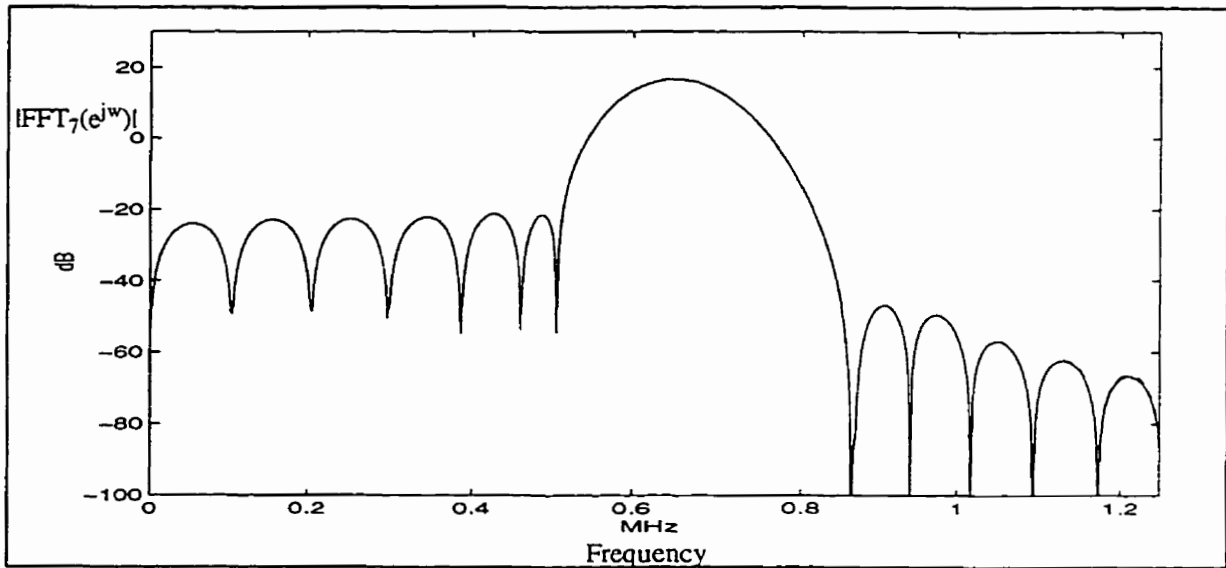
Fig 5.13 Crosstalk at the position of the 7th carrier

By comparing Figs. 5.11 and 5.13, it is found that the shape of the crosstalk is. as expected, greatest in the overlapping region between the two adjacent carriers. Furthermore. the crosstalk's main lobe is centered at 625 kHz, which is also the cross-over point between the two adjacent carriers. After calculating the power of the signal in the FFT output for the 7th carrier without crosstalk, and the power of noise caused by crosstalk, the SCR value was found to be 14.7

dB. The SCR value was higher for a boundary carrier, that is, the first and the 11th carrier. The SCR value was 17.7 dB for the boundary carrier. This is due to the fact that the carrier at the boundary of the CDMA spectrum has crosstalk from the adjacent carrier on only one side. However, for other carriers the source of crosstalk is from adjacent carriers on both sides. As a result there is a 3 dB difference in SCR values for these two cases.

Similar calculations have been done for the carrier signals at the output of the rate change mechanism. It is found that for non-boundary carrier positions, the SCR value was found to be 16.7 dB and for boundary carrier, it was found to be 19.7 dB. The enhancement to the SCR value is due to the attenuation introduced by the 3rd order CIC interpolator in the rate change mechanism. Recall from Fig. 3.15, at 625 kHz the CIC filter has an attenuation of about 2 dB.

Simulations have been carried out such that the transmit filter and the receive filter are replaced with ideal root raised cosine filters with 15 % excess bandwidth. It is found the SCR value is 14 dB for the case of a boundary carrier where crosstalk only comes from an adjacent carrier on one side. The transmultiplexer, with a SCR value at the input to the baseband CDMA demodulator of 19.7 dB, has a better performance than an ideal root raise cosine filter in terms of crosstalk attenuation.

In fact, as suggested earlier, the distortion due to crosstalk is caused by the relationship between the carrier bandwidth and the carrier spacing of the CDMA system specified by the IS-95+ standard [5]. With the stopband frequency of the baseband filter, which shapes the carrier

signal at the transmitter, greater than one-half the carrier spacing, it is certain that spectrum overlap will occur. Therefore, the crosstalk noise is a characteristic of the CDMA system and is not caused by the polyphase carrier select filter in the transmultiplexer system. However, the polyphase carrier select filter can, to some extent, reduce the crosstalk by a having a sharper transition band. Nonetheless, a sharper transition band also means that a longer filter is needed. This, in turn, would increases the system complexity. As will be shown below, this is unnecessary.

Let's investigate the impact of crosstalk noise on the SNR of the CDMA signals. Assume that there are N users occupying a CDMA carrier and, in particular, that there are N users in each of the carriers adjacent to the carrier. Ignoring thermal noise and other noise sources, the noise power faced by a user's signal in a carrier is given in (5.4),

$$noise_{total} = (N-1)S + noise_{crosstalk} \qquad (5.4)$$

where S is the signal power of one user. We have made the assumption that every user has the same signal power due to perfect power control and that the $noise_{crosstalk}$ is the noise power due to crosstalk. Since there are N carriers in each of the adjacent carriers, the crosstalk noise power is:

$$noise_{crosstalk} = N\frac{S}{x} \qquad (5.5)$$

where 1/x is the crosstalk attenuation provided by the transmultiplexer system. The 1/x value varies depending on the relative position of the carrier in the CDMA spectrum. The SNR of a user signal can be calculated as follows :

$$SNR = \frac{S}{(N-1)S + N\frac{S}{x}} = \frac{1}{(N-1) + \frac{N}{x}} \qquad . \qquad (5.6)$$

Judging from (5.6) the impact on the SNR of the attenuated crosstalk noise relative to increasing

the number of co-channel users by one is lower by a factor of N/x. For a typical CDMA system

with N=32 [27] and the SCR equal to 16.7 dB, the SNR degradation caused by crosstalk is 0.68

the SNR degradation caused by adding one more in-band user. These results show that the

impairment caused by adjacent carrier interference, or crosstalk, is minor.

5.6 Simulations with Real Random Data in the Transmitter/TMUX Chain

In this section of the thesis, a random sequence, $x_k[n]$, is input to the simulation model

of the transmitter/receiver chain shown in Fig. 5.3. The sequence, $x_k[n]$, is a random sequence

which simulates the PN spread sequence on the reverse link specified by the IS-95+ standard [5].

Each symbol of the random sequence represents a chip. Unlike the reverse link transmitter archi-

tecture, which uses a Q-PN spread sequence with a half PN chip delay at the Q signal branch, and

a I-PN spread sequence at the I signal branch, only one random sequence, $x_k[n]$, is to simulate the

I and Q-PN spread chips. This is due to the fact that in this simulation only the QPSK signal per-

formance of the transmultiplexer channelizer is investigated, so the offset QPSK feature and the

modulation of the I and Q signals with two different PN sequences, which are related to the

CDMA despreading processes, specified by the IS-95+ standard [5] in the transmitter is simpli-

fied. These two features will be included in the simulations discussed in Section 5.7.

The ADC of the transmultiplexer receiver samples the IF signal at a rate of 60 MHz.

In our simulation, the sampling rate of the output of the transmitter is required to be at 60 MHz.

Since 60 MHz is not an integer multiple of f_{chip}=1.2288 MHz, the basic unit of the transmitter

sampling rate, an interpolator, which is capable of handling interpolation by a rational factor, has to be used to interpolate the random sequence to a sampling frequency of 60 MHz. Ideally, the exact interpolation method described in Fig. 5.4 could be used. However, the memory required to perform this interpolation is beyond the available computing resource. It should be noted that the exact interpolation method is viable for the simulation tests carried out in the preceding sections due to the fact that only the relatively short sequence corresponding to the baseband transmitter filter is interpolated. For a long random sequence, a less memory intensive interpolation method, the 2nd order approximation method described in Chapter Four, is used. The structure of the transmitter with the 2nd order approximation is shown in Fig. 5.14.
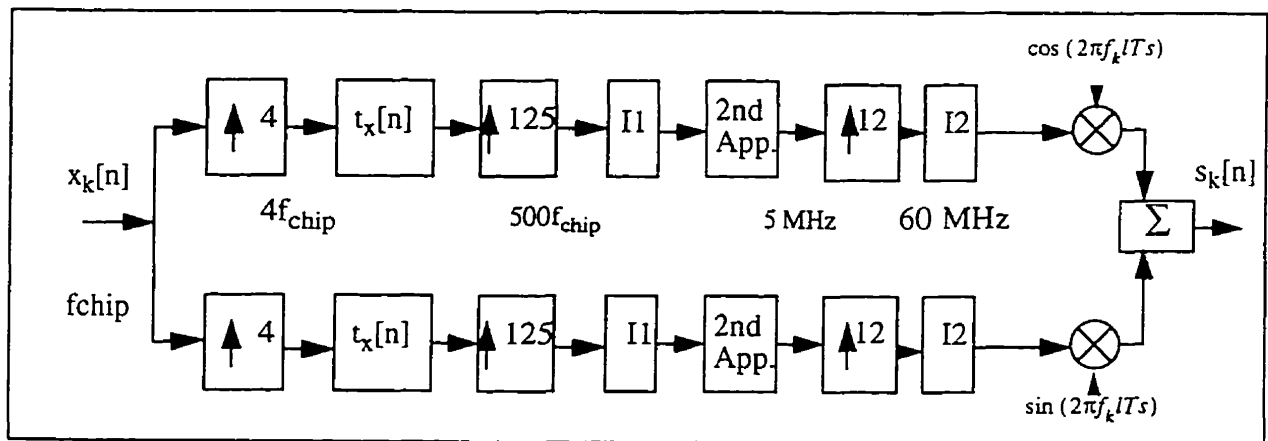

Fig. 5.14 Structure of CDMA transmitter for data simulation

In Fig. 5.14, $x_k[n]$ is the random sequence for the kth carrier at a sampling rate of $f_{chip}=1.2288$ MHz. The up-sampler adds 3 zeros between every 2 consecutive samples of $x_k[n]$ to interpolate the sampling rate to $4f_{chip}$. $t_x[n]$ is the baseband lowpass filter specified by the IS-95+ standard [5]. After the random sequences at the I and Q signal branches have been bandlimited by $t_x[n]$ they are interpolated by a factor of 125. The interpolation is implemented by a three-stage interpolator with interpolation by a factor of 5 at each stage. Using equation (4.40), it is

141

found that the 2nd order linear approximation can provide about 107 dB SDR by interpolating the signal by a factor of 125. Since the 2nd order approximation is not ideal, additional quantization noise is added to the signals and the result of simulation is expected to be slightly worse than the ideal ones. After the 2nd order approximation, the sampling frequencies of the I and Q signal sequences are interpolated to 5 MHz and they are further interpolated to 60 MHz. Finally, the I and Q signal sequences are modulated to the frequency position of the 6th carrier. The frequency response of the 6th carrier's signal, $S_6(e^{jw})$, in front of the TMUX front end is shown in Fig. 5.15. The signal is centered at 15 MHz. The frequency response of modulated signal of the 6th carrier at the output of the rate change mechanism, $D_{e6}(e^{jw})$, is shown in Fig. 5.16. For the same reason as in Fig. 5.9, the side lobes shown in Fig. 5.16 are due to the gentle stopband attenuation by the third order CIC interpolator of the images caused by interpolation. The ρ value is found to be 0.988. This ρ value is lower than the one obtained in the per-carrier approach which is 0.990. This is due to the quantization noise added by the 2nd order approximation employed both in the transmitter and the receiver of the simulation model.

Besides modulating the baseband filtered $x_k[n]$ to the position of the 6th carrier. it is also modulated to the frequency position of the 11th carrier which is centered at 21.25 MHz. After the transmultiplexer front end, the transmultiplexer operation and the rate change mechanism, the ρ value for the 11th carrier modulated signal is found to be 0.988. It is the same as the ρ value obtained for the signal at the 6th carrier frequency.
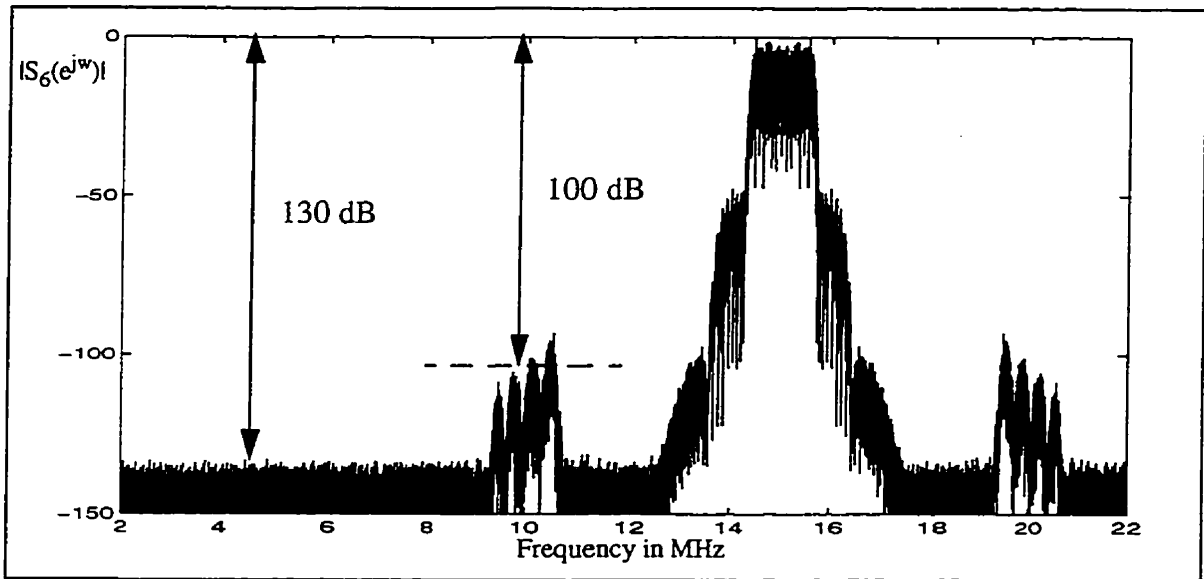
Fig. 5.15 Frequency response of $s_6[n]$, modulated signal of the 6th carrier at $f_s = 60$ MHz
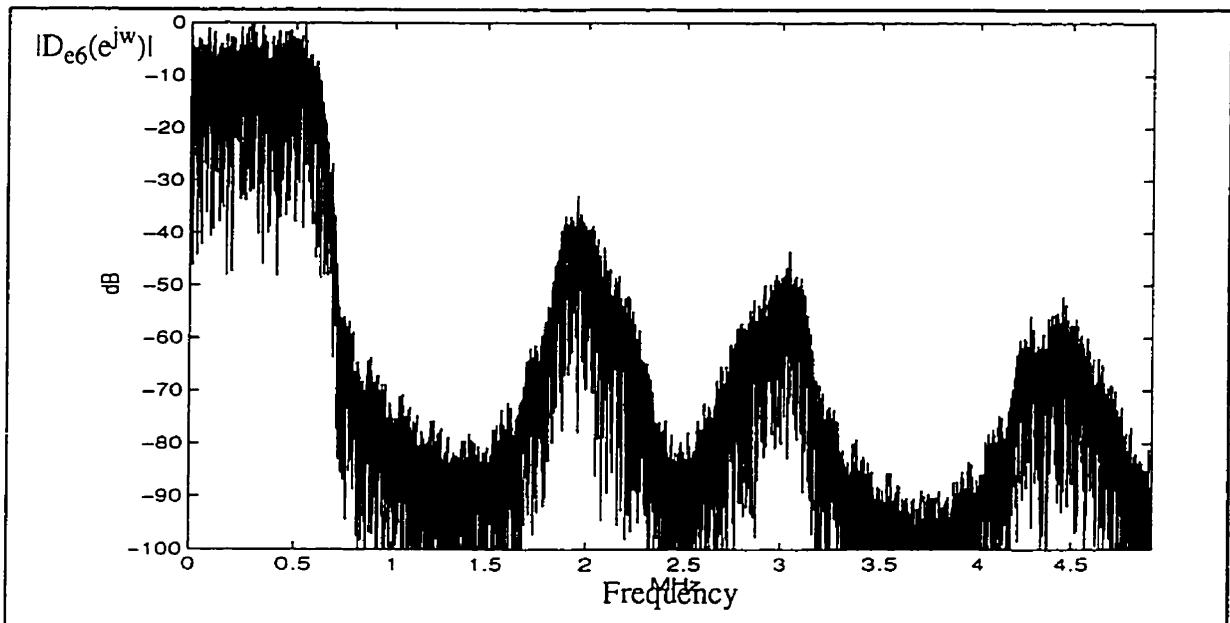

Fig. 5.16 Frequency response of the modulated signal of the 6th carrier at the output of the rate change mechanism
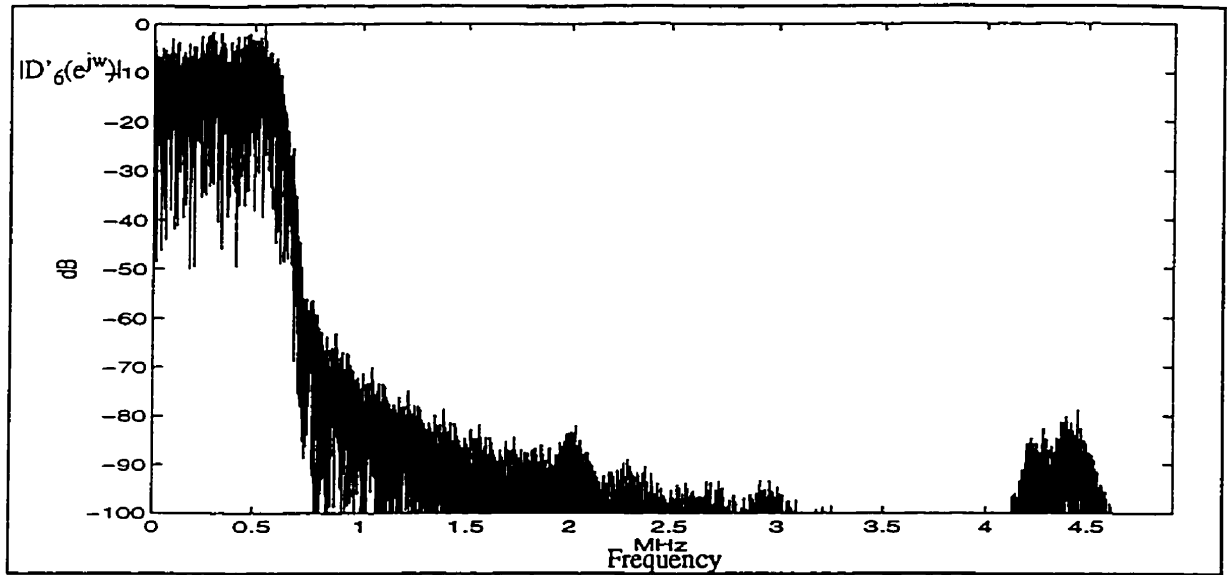
Fig. 5. 17 Frequency response of the modulated signal of the 6th carrier at the output of Goodman half-band filter implemented rate change mechanism

As suggested in Section 4.4.1 the side lobes shown in Fig. 5.16 can be eliminated by using interpolation filters with better stopband attenuation, such as the Goodman half-band filters. A simulation has been carried out with a 19 tap and a 11 tap Goodman half-band filter as the two-stage interpolation filters used in the rate change mechanism. The Goodman half-band filters used in this simulation have better performance than the filters suggested in Section 4.4.1. The best ρ value is obtained when the side lobes are completely eliminated. The frequency response of the modulated signal of carrier 6 at the output of the rate change mechanism, $D_{e6}(e^{jw})$, when Goodman half-band filters are used, is shown in Fig. 5.17. In the diagram it can be seen that the side lobe has been lowered to -70 dB. The ρ value is enhanced to 0.991. In terms of the ρ value, the Goodman half-band filters have better performance than the CIC interpolator. In other words, the side lobes introduced by the CIC interpolator degrade the ρ value slightly. Simulations have been carried out such that the output of the rate change mechanism is high pass filtered and, thus, only the side lobes remain. The sequence corresponding to the side lobes is compared with the

data sequence which is the input to the transmitter receiver chain. It is found that the correlation between these two sequences is zero, i.e. the same as the correlation between a Gaussian noise sequence and the data sequence. Therefore, it can be concluded that the information contained in the side lobes has the same correlation to the input to the transmitter/receiver chain as Gaussian noise. Although the Goodman half-band filters have better performance in terms of the ρ value, this advantage disappears after the input to the baseband demodulator is quantized to 4 bits. The frequency response of the 4-bit quantized output of the CIC interpolator rate change mechanism, $D_{e6q}(e^{jw})$, is shown in Fig.5.18. It can be seen that the noise floor has been elevated by the 4-bit quantization noise to a level such that the side lobes are masked. Thus, the degrading effect of the side lobes to the signal is negligible after the 4-bit quantization.
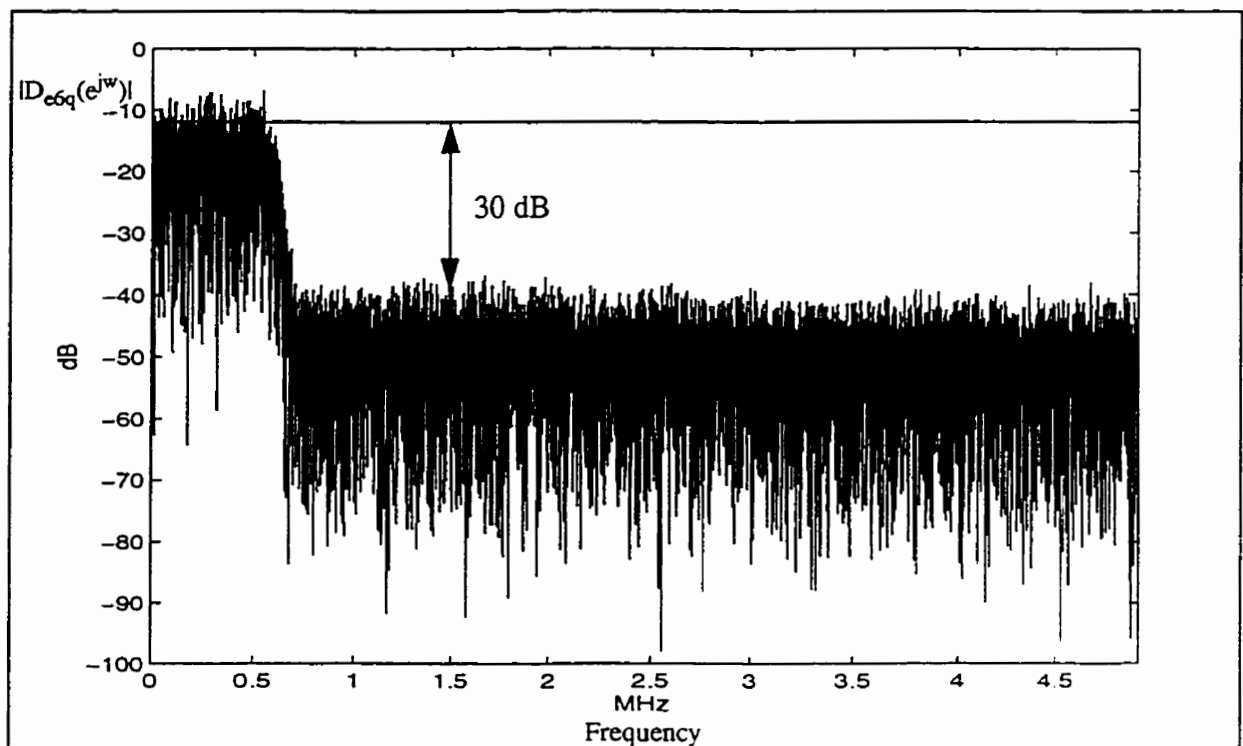

Fig. 5.18 Frequency response of the modulated signal of the 6th carrier after the 4-bit quantization at the baseband CDMA demodulator

5.6.1 QPSK Eye Diagram

The eye pattern shown in an eye diagram is the synchronized superposition of all possible signals of interest that constitute the output from the receiver viewed within a particular signaling interval [23 - 25]. For a binary system, such as each of the QPSK branches of the transmultiplexer receiver, the eye pattern resembles the shape of a human eye. In this thesis the eye pattern for each QPSK signal branch is called the QPSK eye pattern. The interior region of the eye pattern is called the eye opening. The middle or "zero" of the eye opening is the threshold for a binary system. The width of the eye opening tells one the time interval over which the received signal can be sampled without error from ISI for a system without noise. If the vertical distances between the middle of the eye in either the positive or negative direction are decreasing then the eye is closing and the likelihood that a small noise will cause an error when the sampling error in the received signal is increased. Therefore the eye opening of a signal can indicate the quality of the receiver chain and thus the performance of the receiver. The ideal eye opening with no ISI is 100%.

Eye diagrams have been plotted for signal sequences output from the rate change mechanism when the modulated signals for the 6th and 11th carrier are used as input to the transmultiplexer receiver system. The eye diagrams are shown in Fig. 5.19 and Fig. 5.20 for Carrier 6 and 11 respectively. The QPSK eye openings for the 6th and the 11th carrier are both found to be 80.5%. Recall from Section 5.6, Carrier 6 and 11 modulated signals also have identical ρ values. Since both the QPSK eye opening and the ρ values are indicators for ISI performance it can be concluded that carrier positions at the center of the 15 MHz CDMA spectrum have approx-
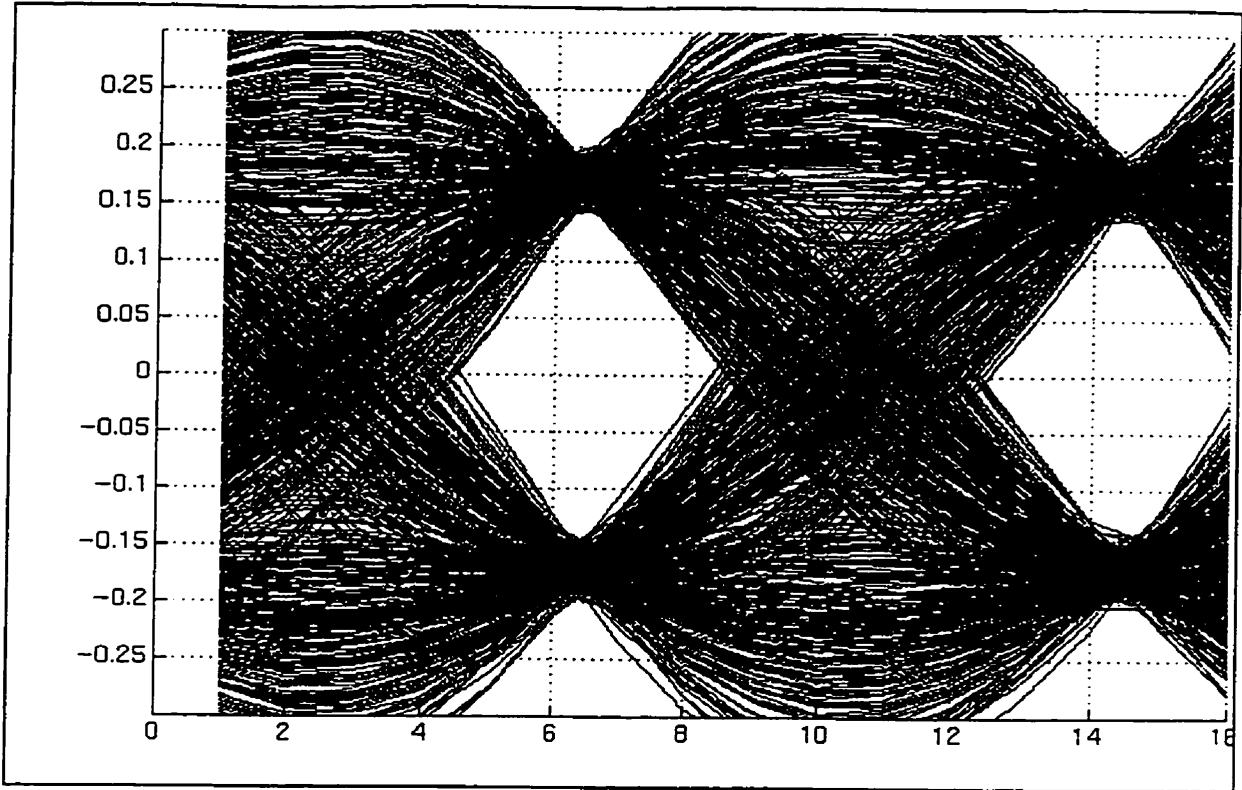
i

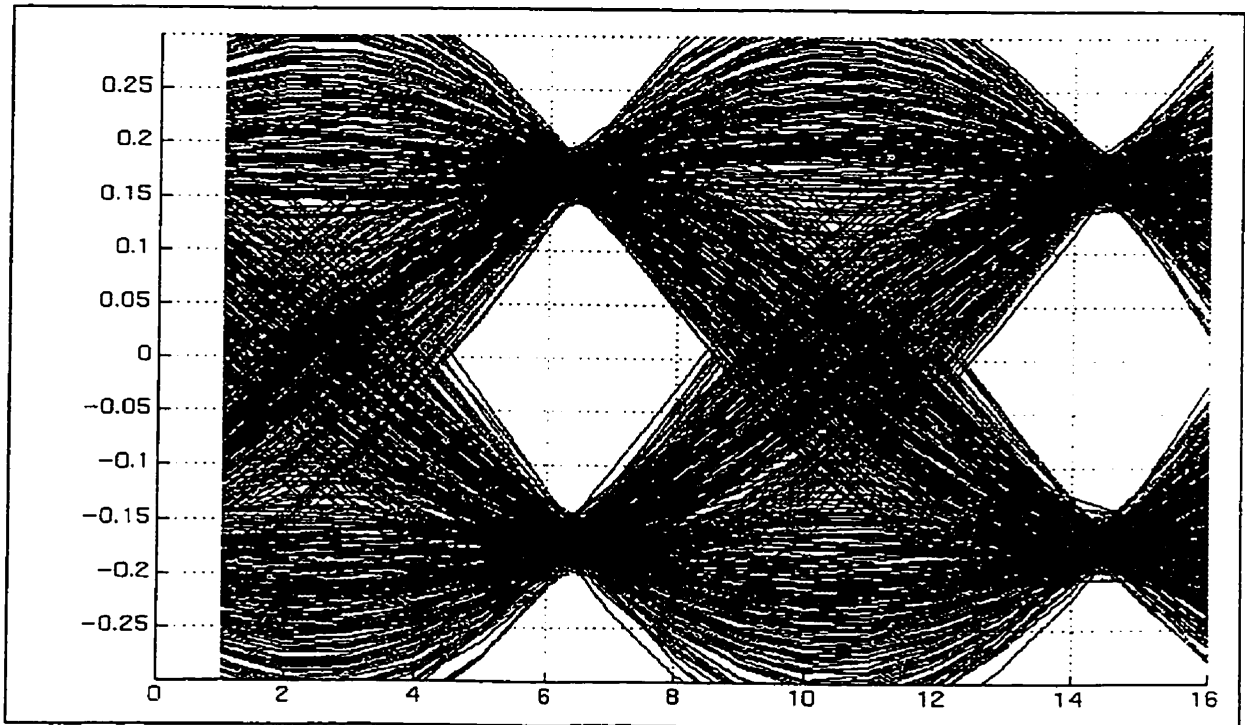Fig. 5.19 QPSK Eye diagram of the modulated signal of the 6th carrier

Fig. 5.20 QPSK Eye Diagram of the modulated signal of the 11th carrier

+ the same ISI performance as a carrier at the boundary of the spectrum.

It should be noted that the QPSK eye diagrams for the QPSK CDMA signals shown are not a realistic performance indicator of the transmultiplexer in CDMA applications. As calculated in Section 2.1, normally, the CDMA signal is -15 dB below the noise floor for at a E_b/N_0 value of 6 dB. In this situation the eye for the QPSK signal will be closed. In other words, the eyes for the QPSK signals in a CDMA system are expected to be closed under normal operating conditions. The CDMA despreading process will "open" the eye. Therefore, a better indicator of the performance of the receiver channelizer is the ρ value specified by the IS-95+ standard [5] and the plot of Walsh convolution results after the PN and Walsh despreading processes in the baseband CDMA demodulator. These are discussed in Section 5.7. Nonetheless, the eye diagrams for the QPSK signal are an indication of the transmultiplexer channelizer's performance for tone interference suppression.

5.6.2 Tone Interferers Suppression

It is specified in [16] that in the presence of a tone interferer of maximum strength 90 dB above the CDMA signal at an offset greater than or equal to +/- 1.25 MHz to the CDMA frequency assignment, the CDMA system should be able to maintain a FER of less than 1.5% without increasing the signal power by more than 3 dB. Simulations have been carried out in order to investigate the performance of the transmultiplexer receiver in the presence of such a tone interferer. A 90 dB tone has been added to the transmitted signal before it enters the transmultiplexer

front end. Two simulations have been conducted: 1) a tone is placed at 16.25 MHz with the presence of a modulated signal of Carrier 6 centered at 15 MHz; 2) a tone is placed at 22.5 MHz with the presence of a modulated signal of Carrier 11 centered at 21.25 MHz. In Fig. 5.21, the frequency response of modulated signal of the 11th carrier, $S_{11}(e^{jw})$, with the 90 dB tone is shown. After the modulated signal of the 11th carrier has been processed by the transmultiplexer, it is fed into the rate change mechanism. The frequency response of the output of the rate change mechanism for the 11th carrier, $D_{e11}(e^{jw})$, is shown in Fig. 5.22. In the transmultiplexer, the tone interferer is attenuated by the polyphase carrier select filter to approximately the same level as the signal. In the rate change mechanism, the residue of the tone is further attenuated to -35 dB by the CIC interpolator. Similar simulations have been conducted for modulated signal of the 6th carrier. The ρ values for Carrier 6 and 11 are obtained and they are both equal to 0.988. This is the same as the ρ values obtained for Carrier 6 and 11's signal when there is no tone. QPSK eye diagrams are also obtained for Carrier 6 and 11's signal and the eye openings for both carriers are equal to 80.5% which is the same as the QPSK eye openings when there is no tone. The QPSK eye diagrams for Carrier 11 and Carrier 6, with tone interference suppressed, are shown in Fig. 5.23 and 5.24 respectively. Based on these simulation results, it can be concluded that, in terms of FER and ISI performance, the effects of tone interference on carriers in the CDMA spectrum have been minimized.
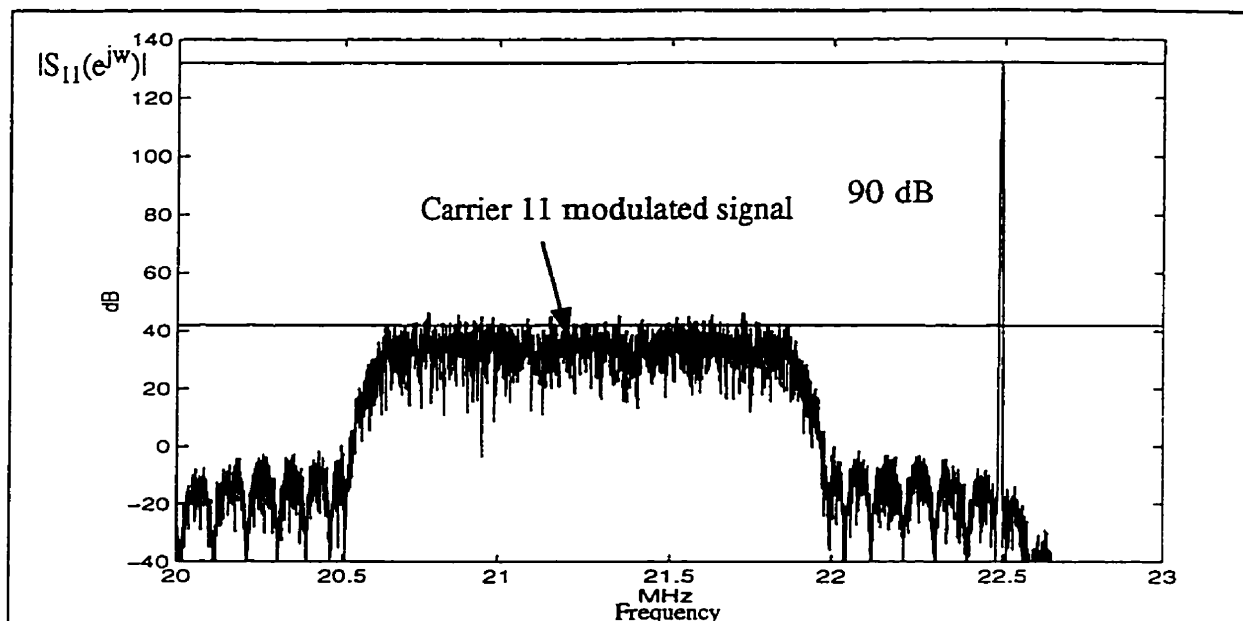
.

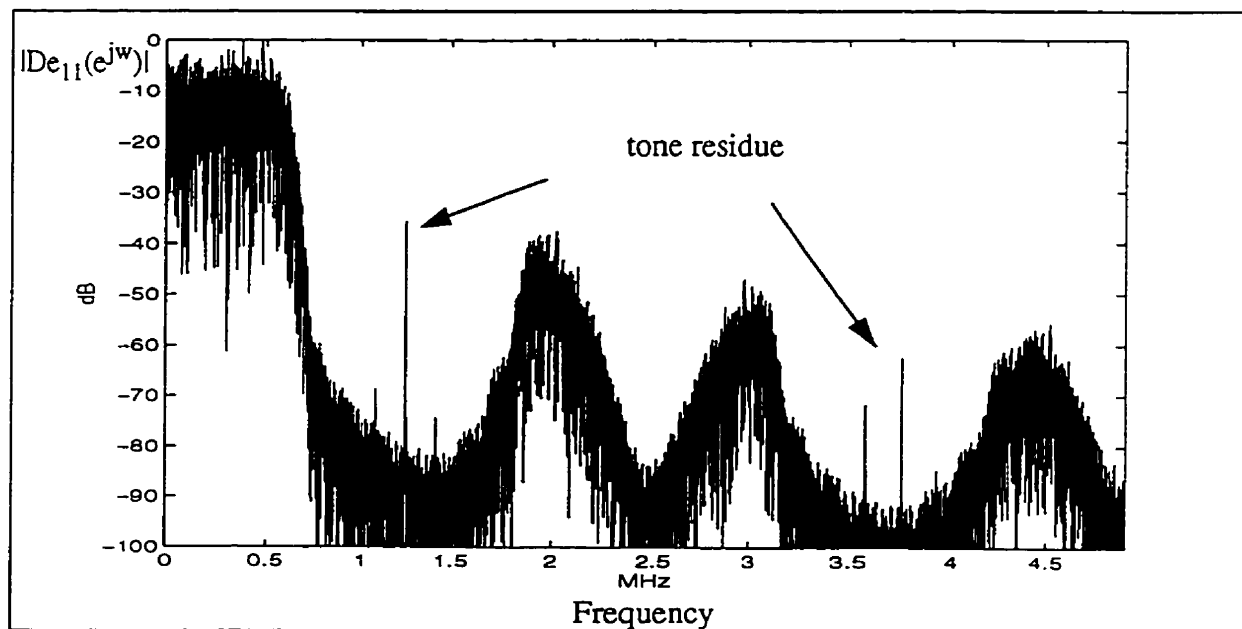Fig. 5.21 Carrier 11 with 90 dB tone before TMUX front end

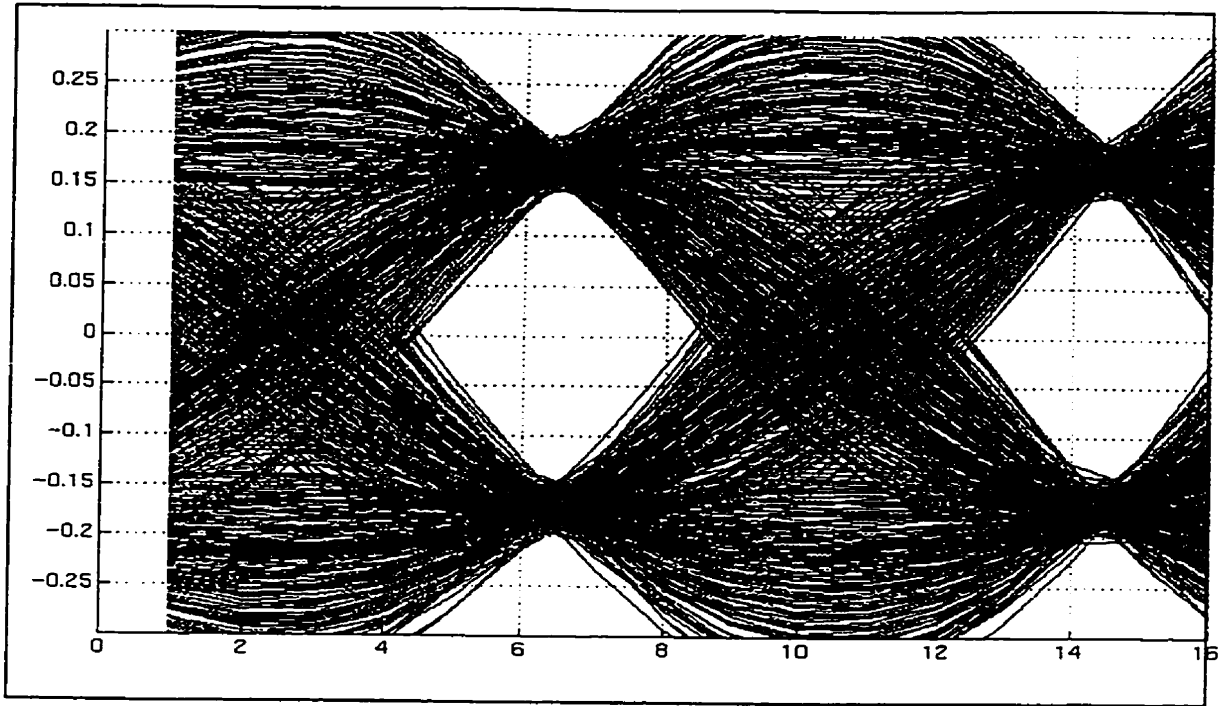Fig. 5.22 Output from Rate Change Mechanism with 90 dB tone

Fig. 5.23 QPSK Eye diagram for the modulated signal of the 11th carrier with 90 dB tone
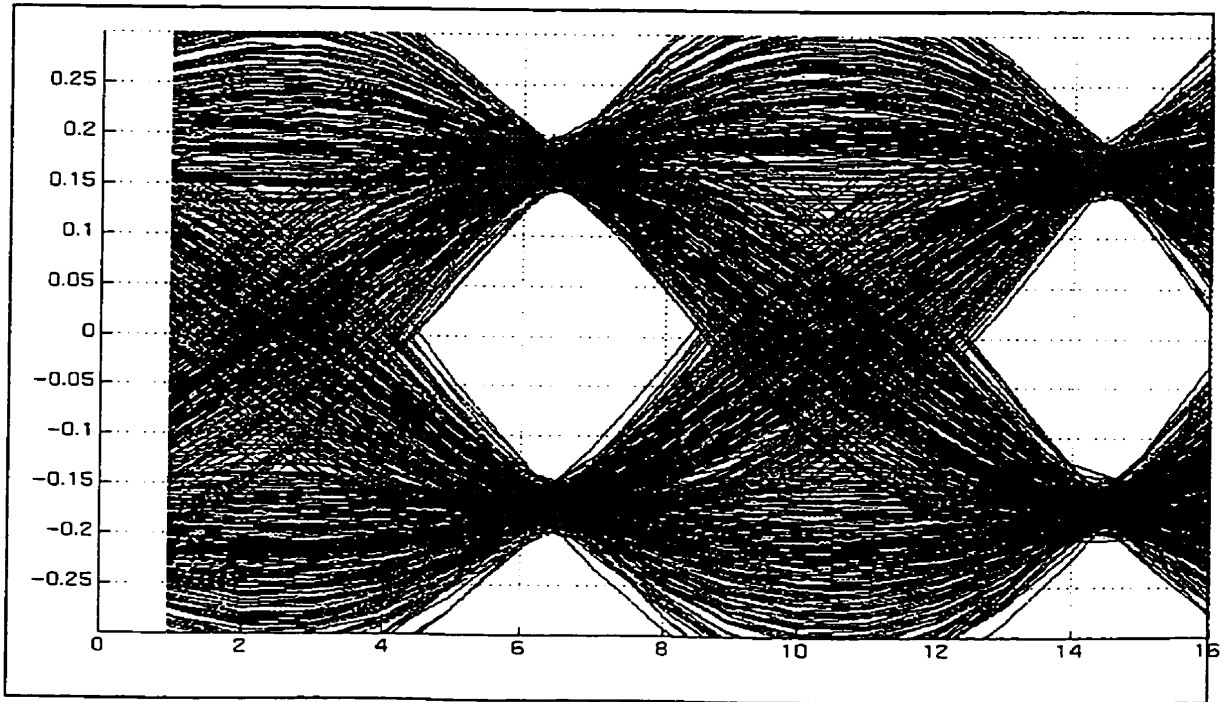

Fig. 5.24 QPSK Eye diagram for the modulated signal of the 6th carrier with 90 dB tone

5.6.3 Quantization Noise to the Transmultiplexer Demodulator

In all the previous test cases it has been assumed that the FIR filters used in the trans-multiplexer system and the FFT effectively have infinite word length and arithmetic precision. However, in practical application, this is seldom the case. Similar to the analysis performed in Chapter Three, the coefficient word length of the FIR filters used in the transmultiplexer system are determined by examining the desired stopband attenuation required of the filters. For the case of the lowpass filter used in the transmultiplexer front end, -100 dB attenuation is required. Assuming 1 bit corresponds to approximately 6 dB dynamic range, 18 bits are needed to meet this goal. In the case of the polyphase carrier select filter, -85 dB stopband attenuation is expected. Therefore at least 14 bits are needed for the filter coefficient word length. 16 bits are used in the following simulations.

In all the previous test cases, direct computation of the FFT is assumed. Using the linear noise model suggested in [20], quantization error is added to the FFT because of the finite precision complex multiplications of the input, $x[n]$, by the complex exponential factor, W_N^{kn}. As shown in Fig. 5.25, the quantization noise is modeled as white noise and it is added to the FFT system after each complex multiplication. $e[n,k]$ is the complex error introduced by rounding off the product $x[n]W_N^{kn}$. $E[k]$ is the summation of all such quantization errors. Since there are four real multiplications for each complex multiplication, there are 4 quantization error sources for each complex multiplication. In the simulation each real multiplication is quantized. It is found that to reproduce the performance of the transmultiplexer when no quantization effect is included, each real FFT multiplication must be quantized to 16 bits. The CIC interpolator used in

the rate change mechanism can use the register truncating scheme described in Section 3.4.2 to minimize the impact of the quantization noise due to finite arithmetic precision.
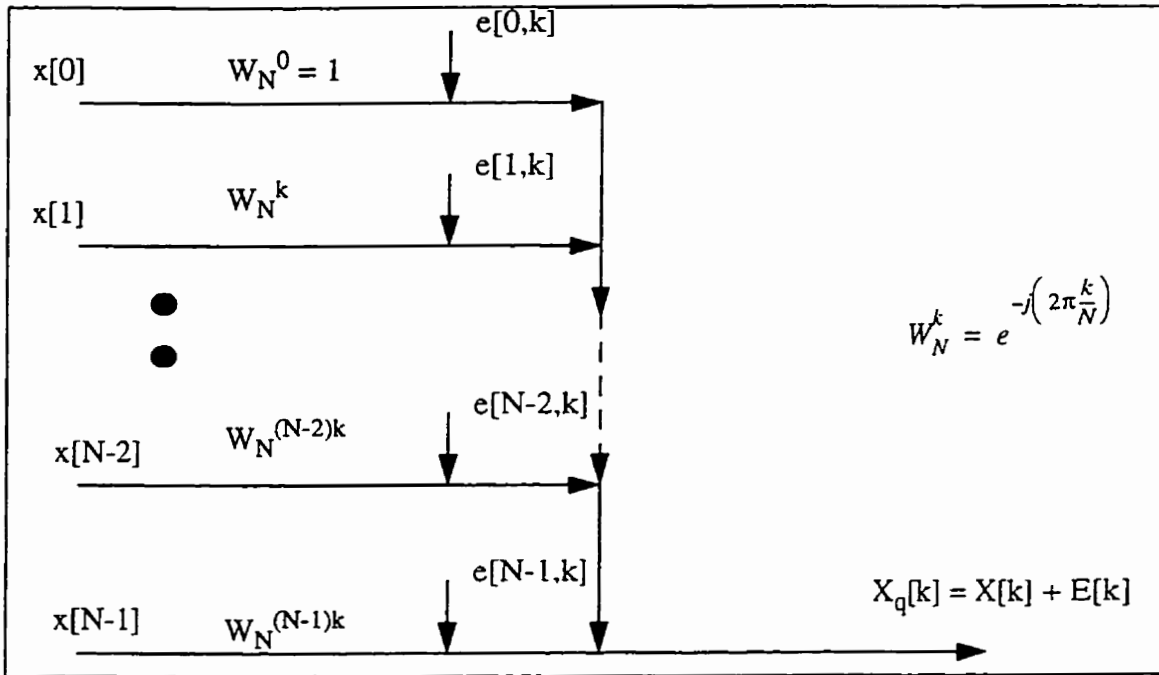

Fig. 5.25 Linear noise model for quantization of direct form FFT computation

Simulations similar to the ones described in Section 5.6 have been conducted with the effect of the quantization errors taken into account. Signals from Carrier 6 and 11 are input to the quantized transmultiplexer with and without a tone interferer. It is found that without the tone the ρ values and QPSK eye openings for the signal from both carriers are the same as for the unquantized case. However, when a tone interferer is present, the ρ values for both carrier signals are degraded slightly to 0.987 and the QPSK eye openings are degraded to 80%. The degradation in ISI performance, as shown by the ρ value and the QPSK eye opening through quantization is expected since the major effect of quantization error is to raise the noise floor. Performance can be improved by increasing the word length in the transmultiplexer system. However, this will also increase the cost and complexity of the DSP system used to implement the transmultiplexer/

channelizer system. Nonetheless, this is unnecessary because the effect on the PN/Walsh despreading process and FER due to the quantization noise is negligible as will be seen in the next sections.

5.7 A Simple DS-CDMA Spreading and Despreading Model

A simple DS-CDMA spreading and despreading model was designed in order to investigate the impact of the performance of the transmultiplexer channelizer to the CDMA baseband demodulation processes and the effect of tone interference. The structure of the transmitter is shown in Fig. 5.26. The transmitter model shown is based on the reverse link architecture specified by the IS-95+ standard [5]. However, the model does not include the long PN code modulation after the Walsh modulation. This has no impact on the analysis as the purpose of the long PN code is to distinguish different users within the same carrier while in this simulation only one user per-carrier is assumed. The random data sequence, d[n], is to simulate convolutional encoded
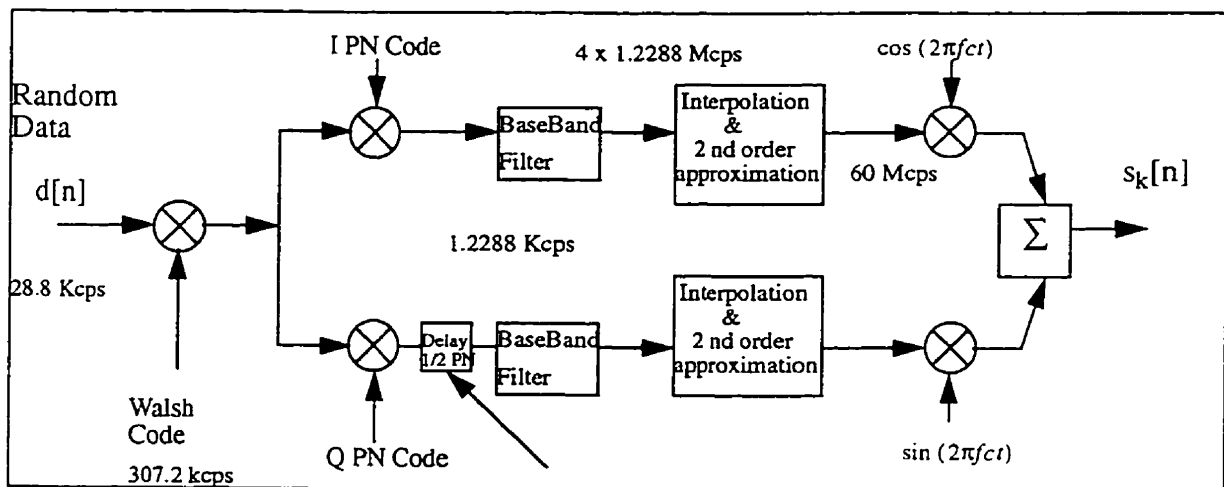
Fig. 5.26 Transmitter structure for spreading model

information at a rate of 28.8 kcps. It should be noted that each Walsh chip consists of either a 1 or -1. The mapping of the Walsh chips follows the industry practice. Every 6 symbols of the data sequence, d[n], are mapped to or spread by a Walsh symbol of 64 chips. Each Walsh chip is further spread by 4 I/Q-PN chips. Note, the I and Q-PN sequences are two different sequences with the same period. As a result, the symbol rate after the I/Q-PN spread is 1.2288 Mcps (chips per second). There is a delay of 1/2 PN chip before the Q-PN spread sequence is baseband filtered while the I-PN code spread sequence is baseband filtered directly. The I and Q baseband filtered signal sequences are interpolated and modulated by sine and cosine functions tuned to a specific carrier frequency. The combination of the delay and QPSK modulation is called offset QPSK modulation [34]. At the receiver end, after the transmultiplexer channelizer, the CDMA signal is demodulated by the structure shown in Fig. 5.27. In this model, non-coherent demodulation is used as specified by the reverse link structure of the IS-95+ standard [5]. At the receiver, the output of the transmultiplexer-rate conversion system is at a sampling rate of $8f_{chip}$. Since the Q signal has been delayed by 1/2 PN chip at the transmitter, the I signal at the output of the receiver is delayed by the same interval to offset the delay at the transmitter. Perfect synchronization is assumed. After decimating by a factor of 8, the sequences at the I and Q signal branches are despread by the I and Q-PN codes. According to a non-coherent demodulation scheme, the I and Q signal branches are split into 4 branches as shown in Fig. 5.27. After despreading by the PN codes, the sequences are at a frequency of 307.2 kcps. Groups of 64 symbols at each branch are further despread by Walsh functions. The sequence from branch d in Fig. 5.27 is subtracted from the sequence at branch a and i_o is formed. Also from this figure, the sequence from branch b is added to branch c and q_o is formed. i_o and q_o are then passed through an envelope detector. The Walsh function which has the highest matched filter output for the group of 64 received signal

symbols is chosen as the detected sequence. The sequence of the 6 symbols corresponding to the chosen Walsh function is the estimate of the data sequence sent by the transmitter, $d_{es}[n]$.
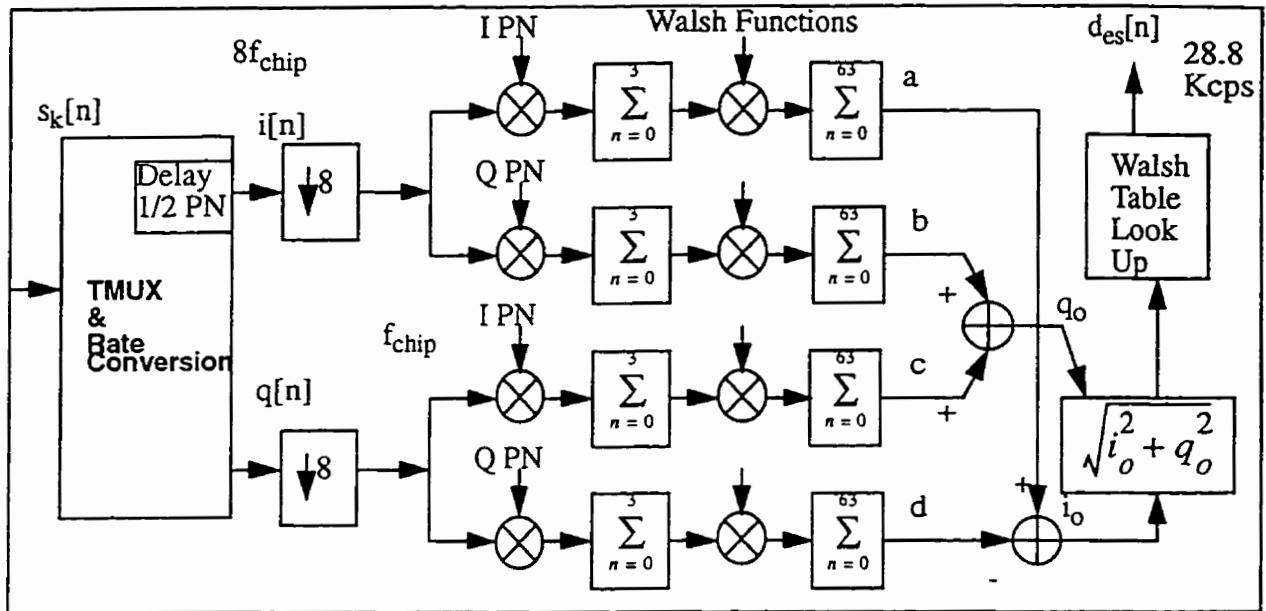
Fig. 5.27 Receiver structure for despreading

To understand the operation described above and depicted in Fig. 5.27 denote the I and Q signal output from the transmultiplexer system to be i[n] and q[n] respectively. Together they form a complex sequence $r[n] = i[n] + j \, q[n]$. Also assume that $i_{pw}[n]$ and $q_{pw}[n]$ are the combined sequence of the I, Q-PN codes and Walsh symbols, which form a complex sequence $s[n] = i_{pw}[n] + jq_{pw}[n]$. Non-coherent CDMA demodulation can be represented as given in (5.7).

$$r[n] \cdot s[n]$$

$$= (i[n] + jq[n]) \, (i_{pw}[n] + jq_{pw}[n]) \qquad (5.7)$$

$$= (i[n] \, i_{pw}[n] - q[n] \, q_{pw}[n]) + j(i[n] \, q_{pw}[n] + q[n] \, i_{pw}[n])$$

$$= i_o[n] + jq_o[n]$$

By using an envelope detector, the magnitude of the envelope of the complex product sequence described in (5.7) can be found. This is depicted as the input to the "Walsh table look up" box in Fig. 5.27.

Simulations have been carried out with the length of d[n] equal to 300 symbols. These 300 symbols simulate 300 convolutionally encoded symbols. Since the coding aspect of the CDMA system described by the IS-95+ standard [5] is not within the scope of this thesis, the 300 symbols are represented by random numbers. 50 Walsh symbols are generated after the Walsh spreading process. The sequence of the Walsh symbols generated by the Walsh spreading process at the transmitter is referred to as the "reference" sequence. The I and Q-PN spread sequences are modulated to 21.25 MHz, the frequency of Carrier 11. We assume there is no noise in the channel between the transmitter and receiver. At the receiver, the signal sequence is processed by the transmultiplexer channelizer. It should be noted that quantization errors have been included in the operations of the channelizer. The output of the channelizer is despread by the PN codes of the same offset and the same sequence of Walsh symbols (the "reference" sequence) which have been used to spread the data sequence, d[n], at the transmitter. Each Walsh symbol consists of 64

Walsh chips. The Walsh despreading process is given in (5.8):

$$c_{j,g} = \sum_{k=1}^{64} w_{j,k} s_{j,k,g} \qquad (5.8)$$

where $w_{j,k} = w[64(j-1)+k]$ is the kth Walsh chip within the jth Walsh period of the "reference" Walsh sequence, $s_{j,k,g} = s[32(64(j-1)+k)+g]$ is the kth PN despread received symbol at the jth Walsh period with an offset of g, the sampling offset in the $8f_{chip}$ received signal sequence, and $c_{j,g}$ is the convolution result of the jth Walsh period at an offset g. Fig. 5.28 is the result of the convolution, $c_{j,g}$, between the Walsh symbols in the "reference" sequence and the received data, which has already been PN despread, with and without the presence of a 90 dB tone at 22.5 MHz. In Fig. 5.28a, the "o" symbols are the convolution results when there is no tone. In Fig. 5.28b, the "+" symbols are the convolution results when there is a single tone interferer 90 dB above the CDMA signal and offset from the carrier by 1.25 MHz. The height of each "o" or "+" symbol is the result of convolution between a group of 64 PN despread symbols and a group of 64 Walsh chips (a Walsh symbol) from the "reference" Walsh sequence. Different columns of "o" or "+", that is, different g, represent different sampling offsets, in one-eighth of a PN chip interval, in the $8f_{chip}$ sequence at the output of the transmultiplexer rate change system. The highest point, g=G, represents the optimum synchronization/decision point. The diagram formed has a shape that is similar to an eye diagram. Comparing the relative positions of the "o' and "+" symbol, it is found that they overlap each other. This shows that the PN and Walsh despreading processes have not been affected by the tone interferer.

In fact, the locus of points formed by despreading the received signal sequence by the "reference" PN and Walsh sequence has a direct relationship with the ρ values specified in Sec-

tion 2.1. Recalling the equation for the ρ calculation shown in (2.1), each of the summation over 256 terms, at PN chip rate (4 times Walsh chip rate), denoted in the numerator of the expression is equivalent to a convolution between a 64-chip Walsh symbol and a group of symbols of the PN despread received signal sequence, at the Walsh chip rate. In the Walsh eye diagram, Fig. 5.28a, the convolution result is represented by the "o" symbol To obtain the ρ value from the Walsh convolution results, $c_{j,g}$ shown in Fig. 5.28a, one must normalize them according to the expression shown in (5.9) below:

$$\rho_d[g] \;=\; \frac{\displaystyle\sum_{j}^{N} |c_{j,g}|^2}{\left\{\displaystyle\sum_{k=1}^{64} |w_{j,k}|^2\right\}\left\{\displaystyle\sum_{j=1}^{N}\sum_{k=1}^{64} |s_{j,k,g}|^2\right\}} \tag{5.9}$$

where $\rho_d[g]$ is the ρ value obtained from the convolution results at an offset g in the received signal sequence, N is the length of the "reference" Walsh sequence in units of Walsh symbols and $s_{j,k,g}$ is the kth PN despread received symbol at the jth Walsh period with an offset g. Equation (5.9) is actually the same as the equation for ρ shown in (2.1). It should be noted that the summation period in (2.1) is 256 PN chips while the summation period in (5.9) is equal to the Walsh period, that is, 64 Walsh chips. The difference is due to fact that in (5.9), the received signal sequence is despread and decimate-by-4 by the PN chip sequence and then further despread by the Walsh functions at one-quarter the PN chip rate while in (2.1), the received signal is despread by the PN and Walsh functions at the PN chip rate. R[n], the ideal sequence from the transmitter/ receiver chain output for no ISI, is equivalent to $w_{j,k}[n]$ and Z[n], the output sequence of the imperfect transmitter/receiver chain, which has been degraded by ISI, is equivalent to $s_{j,k,g}[n]$. When applying equation (5.9) to calculate the convolution between the PN despread signal sequence and the Walsh symbols from the "reference" Walsh sequence at the optimum sampling

time, that is, g=G, and without tone interferer, a ρ_d [G] value of 0.988 is obtained. This is the

maximum ρ_d value and, recall that ρ is the correlation coefficient taken at the best synchroniza-

tion/decision point, ρ_d [G] = ρ . The best sampling time occurs when the locus of points of the

convolution results are the highest, g=G, in Fig. 5.28a. The ρ_d[G] value obtained was within

the specification given in Section 2.1. Using the same argument as for ρ, a ρ_d [G] value of

0.988 corresponds to a 0.05 dB E_b/N_o degradation due to eye closure. The same value for ρ_d [G]

(0.988) was obtained in the presence of a 90 dB interfering tone.

Simulations have been carried out such that each group of 64 PN despread chips is

despread by all 64 Walsh symbols. The results of the convolution between each group of 64 PN

despread symbols in the transmitted data sequence and each of the 64 Walsh functions with and

without the tone interferer, $c_{j,g}$, are shown in Fig. 5.29 . In Fig. 5.29a, a "o" is the convolution

result between a group of 64 PN despread symbols and the Walsh symbol in the "reference"

sequence of Walsh symbols, and the "x" symbol is the convolution result between a group of 64

PN despread symbols and one of the 63 Walsh symbols which does not belong to the "reference"

Walsh sequence when there is no interfering tone. In Fig. 5.29b, the "*" and the "+" correspond

to the symbols "o" and "+" respectively when a 90 dB tone is present. The convolution results

between the Walsh symbols, which do not belong to the "reference" Walsh sequence, and the PN

despread signal symbols are noise to the Walsh despreading process. It is noise in the sense that if

the convolution results between a non-"reference" Walsh symbol and the received signal

sequence is greater than the convolution result between the "reference" Walsh symbol and the

received sequence then the non-"reference" Walsh symbol is selected as the best estimate for the

received sequence. In this manner an error is made. It can be seen from the diagram that every
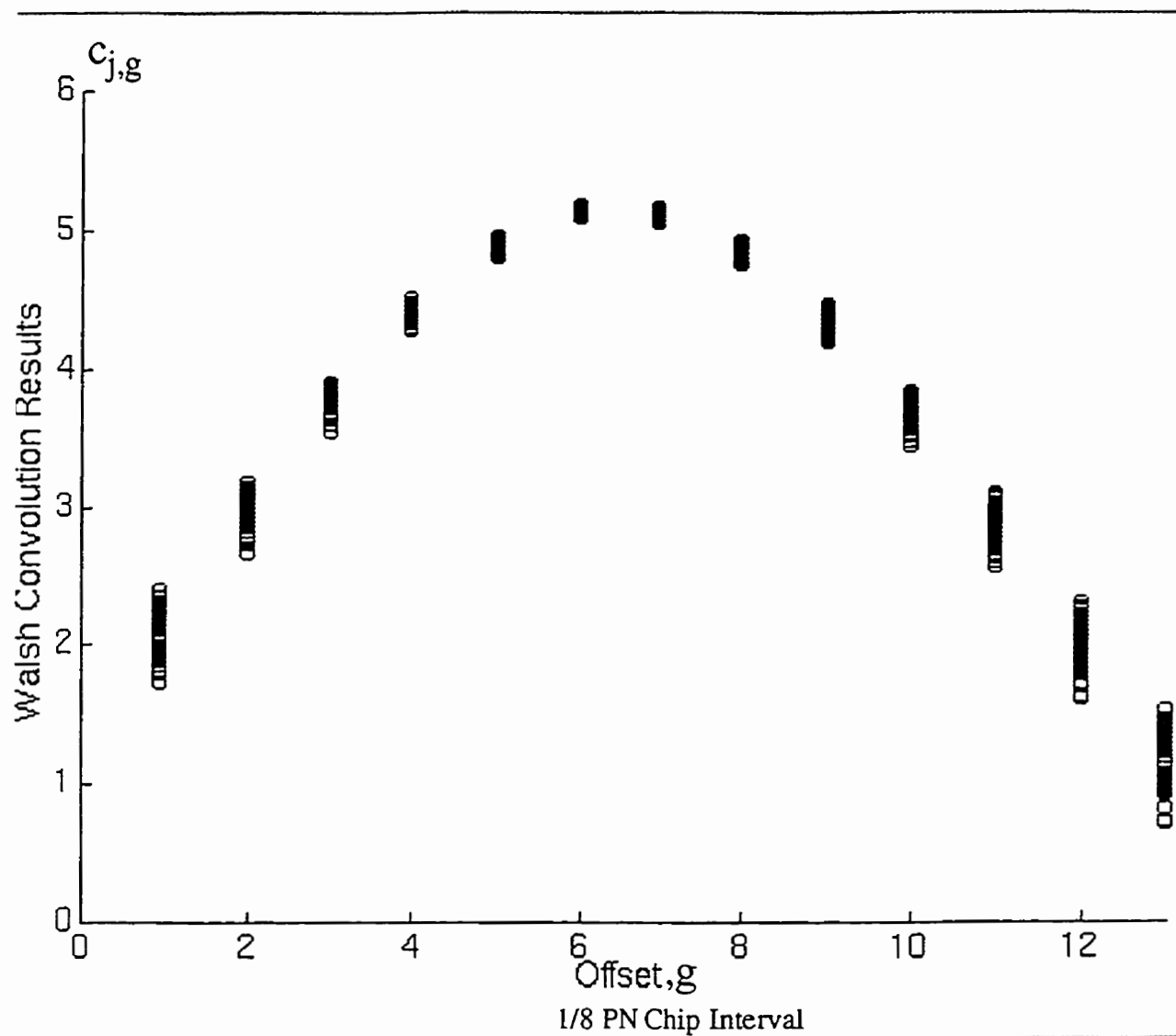
160

Fig. 5.28 a Eye diagram of Walsh despreading process(no tone)
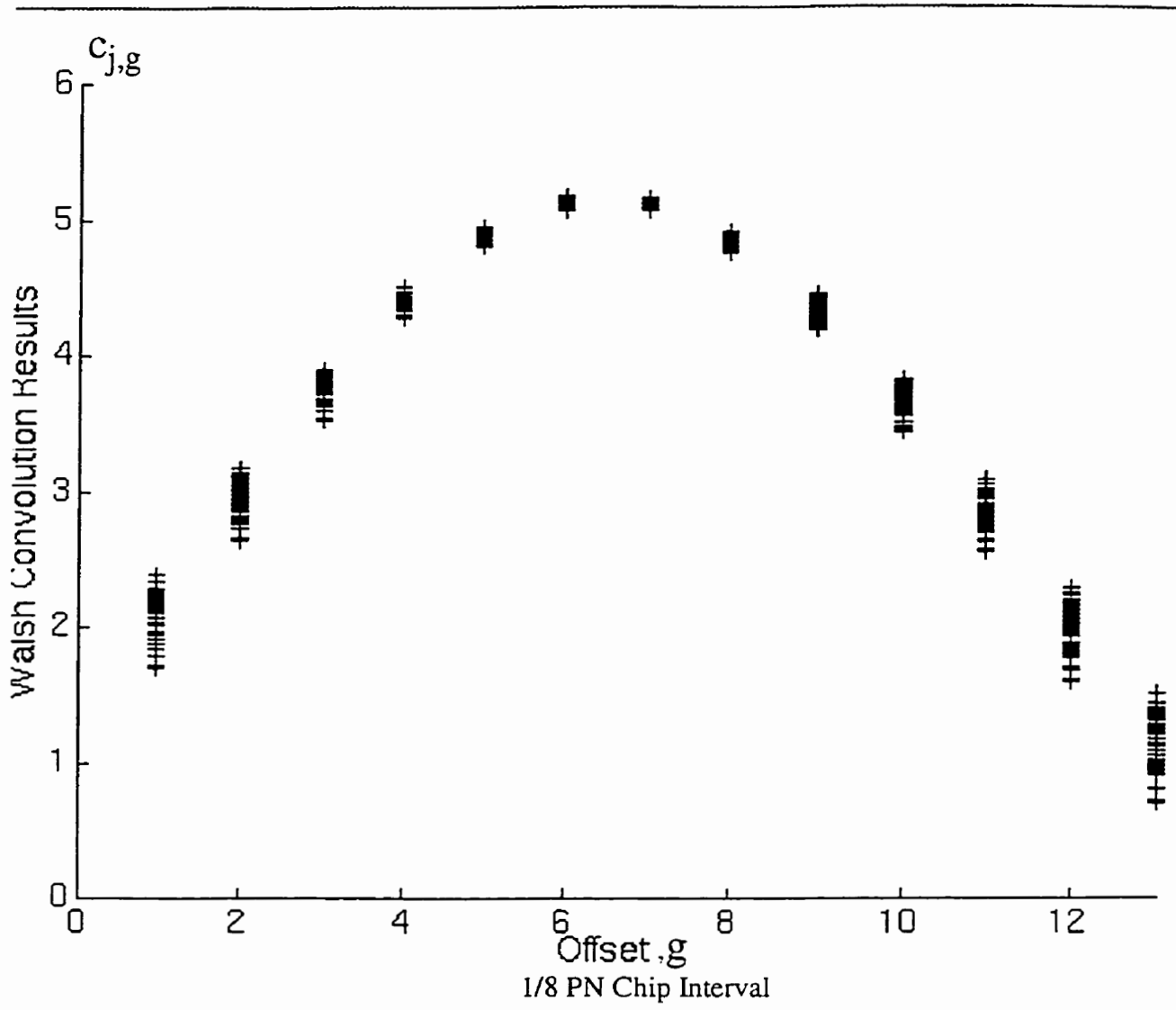
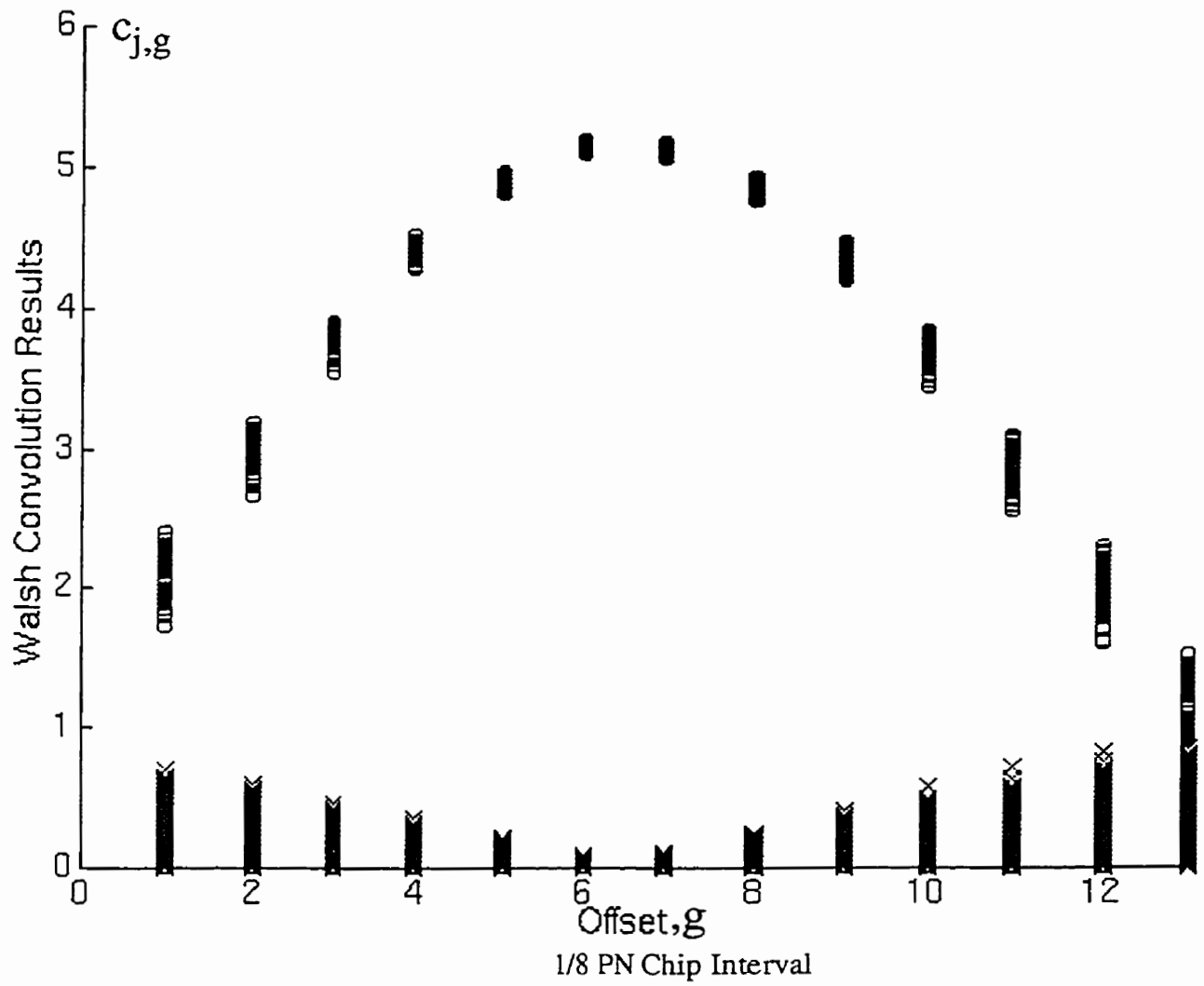Fig. 5.28 b Eye diagram of Walsh despreading process (90 dB tone)

Fig. 5.29a Eye diagram of Walsh despreading process (no tone)
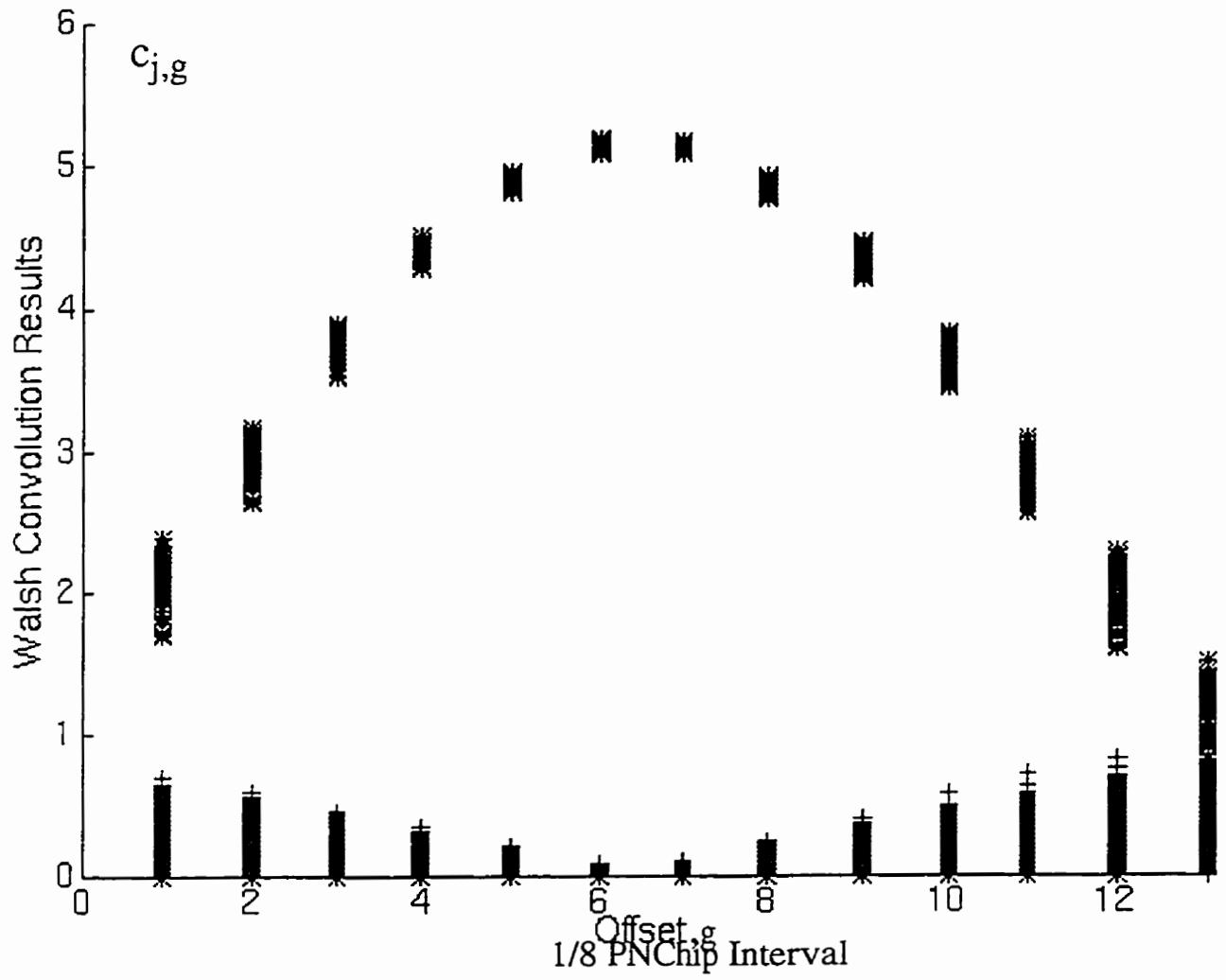"o" reference Walsh sequence, "x" other Walsh sequences

Fig. 5.29b Eye diagram of Walsh despreading process (90 dB tone)
"*" reference Walsh sequence, "+" other Walsh sequences

"o" symbol is overlapped by a "*" symbol and every "+" symbol is overlapped by a "x" symbol. The results of the Walsh despreading operation remain the same regardless of the presence of the tone. Moreover, the Walsh despreading process noise is essentially unchanged by the tone interferer.

The results obtained above show that the degradation due to a tone interferer at the boundary of the CDMA spectrum, on the PN and Walsh code despreading of the carrier signal has been minimized. Similar simulations in which the modulated signal of the 6th carrier was used with a tone interferer is placed at 1.25 MHz offset were carried out. The results of the simulations, in terms of the ρ value and the loci of the Walsh convolution results, are the same as the case when a modulated signal of 11th carrier was used. Therefore it can be concluded that the effect on the CDMA PN and Walsh despreading process due to a tone interferer inside or at the boundary of the CDMA spectrum have been minimized and is independent of carrier signal location.

5.7.1 Tone Suppression in the Presence of Noise

In this section Gaussian noise will be added to the transmitted signal before it enters the receiver as illustrated in Fig. 5.30. Using equations (1.1) and (1.2), the in-band SNR before despreading is

$$SNR = \frac{E_b}{N_o} - G_p \tag{5.10}$$

where G_p is the processing gain. The SNR before spreading is -15 dB assuming a E_b/N_o ratio of 6 dB [29].

It should be noted that the Gaussian noise added to the signal that is input to the transmitter receiver chain is bandlimited. This is because the additive noise has been bandlimited by the SAW bandpass filter in the IF receiver stage preceding the ADC. Assuming that the SAW filter has a perfect passband and stopband characteristic of rectangular shape with 15 MHz band-
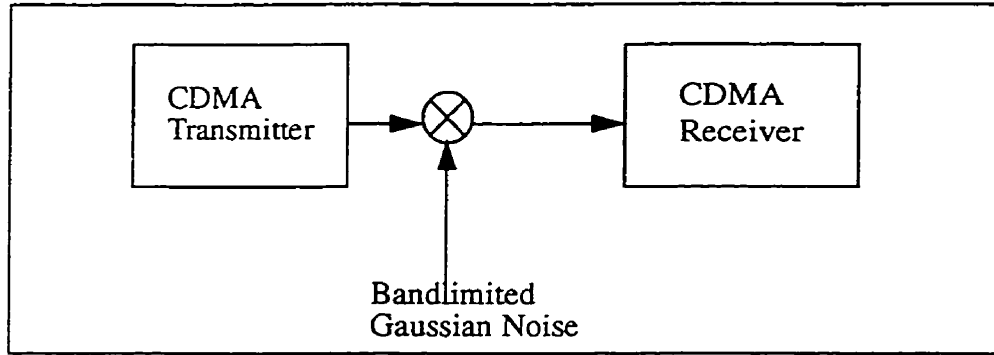

Fig. 5.30 Noise model for CDMA transmitter receiver chain

width, a 15 MHz bandlimited Gaussian noise signal centered at f_{IF}=15 MHz will represent the noise added to the CDMA signal. By the central limit theorem [36], Gaussian noise can be approximated by a sum of a large number of sinusoidal waves of different frequencies having uniform random phases:

$$g_{BP}[m] = \sum_{k=1}^{N} A_k \cos(2\pi f_k m T_k + \theta_k)$$

(5.11)

where A_k is the amplitude of the kth sinusoidal wave, N is the number of sinusoidal waves used to approximate the bandlimited Gaussian noise signal, f_k is the frequency of the kth sinusoidal wave, and θ_k is the phase of the kth sinusoidal wave. The amplitudes of all N sinusoidal waves are set to be constant [36] while θ_k is a random phase variable with an uniform distribution from $-\pi$ to π. The frequencies of all the sinusoidal waves are equally spaced in the frequency spectrum. By set-

ting the frequency of the k=1 sinusoidal wave equal to 7.5 MHz and the frequency of the k=N

sinusoidal wave equals to 22.5 MHz, an approximation of a bandpass Gaussian noise signal is

obtained. It is stated in [36] that the higher the value of N is the better the summation of the sinu-

soidal waves approximates bandlimited Gaussian noise. As a result, N=10,000 cosine waves of

random phase are summed in order to generate bandlimited Gaussian noise. MATLAB™ software

tools [13] were used to conduct the simulation. The N value is several orders more than required.

The simulated bandpass Gaussian noise power spectral density, $|G_{BP}(e^{jw})|^2$, is shown in Fig. 5.31.
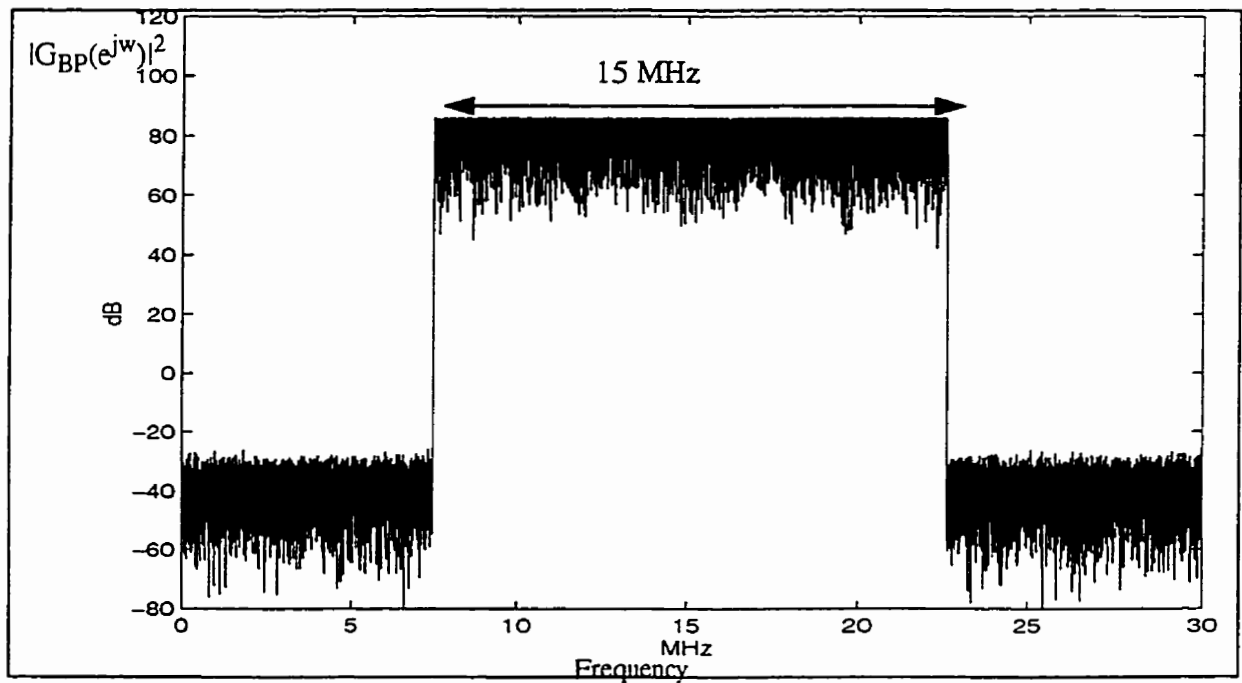

Fig. 5.31 Bandlimited Gaussian noise generated by summation of cosine functions

Simulations have been conducted using the set up described in Section 5.8 and a noise

corresponding to a E_b/N_o of 6 dB added to the CDMA signal. Walsh eye diagrams for the Walsh

despread signal are plotted in Fig. 5.32 and 5.33. With the addition of noise, a Walsh eye diagram

for the convolution results, $c_{j,g}$, between the received signals of Carrier 11 and the "reference" Walsh symbols is plotted in Fig. 5.32a . Fig. 5.32b shows similar results with the addition of a tone interferer at 22.5 MHz and noise. Due to the addition of the noise the "eye openings" are reduced. The ρ value found from the Walsh convolution is 0.015. However, It can be seen that in the eye diagrams the locus of the "reference" Walsh despread results in the presence of tone interferers is the same as the locus of the "reference" Walsh despread results when there is no tone interferer.

With the addition of noise, a Walsh eye diagram for the convolution results between the received signals of Carrier 11 and all 64 Walsh symbols is plotted in Fig. 5.33a . Fig. 5.33b replots the results for a tone interferer at 22.5 MHz and noise. The locus of the non-"reference" Walsh convolution results, noise to the Walsh despreading process, when there is no tone is the same as the locus of the non-"reference" Walsh convolution results when there is a tone, see Fig. 5.33. The legends in Fig. 5.32 and 5.33 are the same as the legends of in Fig. 5.28 and 5.29. Similar results were obtained with a modulated signal at the 6th carrier instead of the 11th carrier. Together with the results obtained in the last section, it can be concluded that the transmultiplexer successfully recovers the CDMA signals and meets the performance objectives defined for the IS-95+ standard [5].
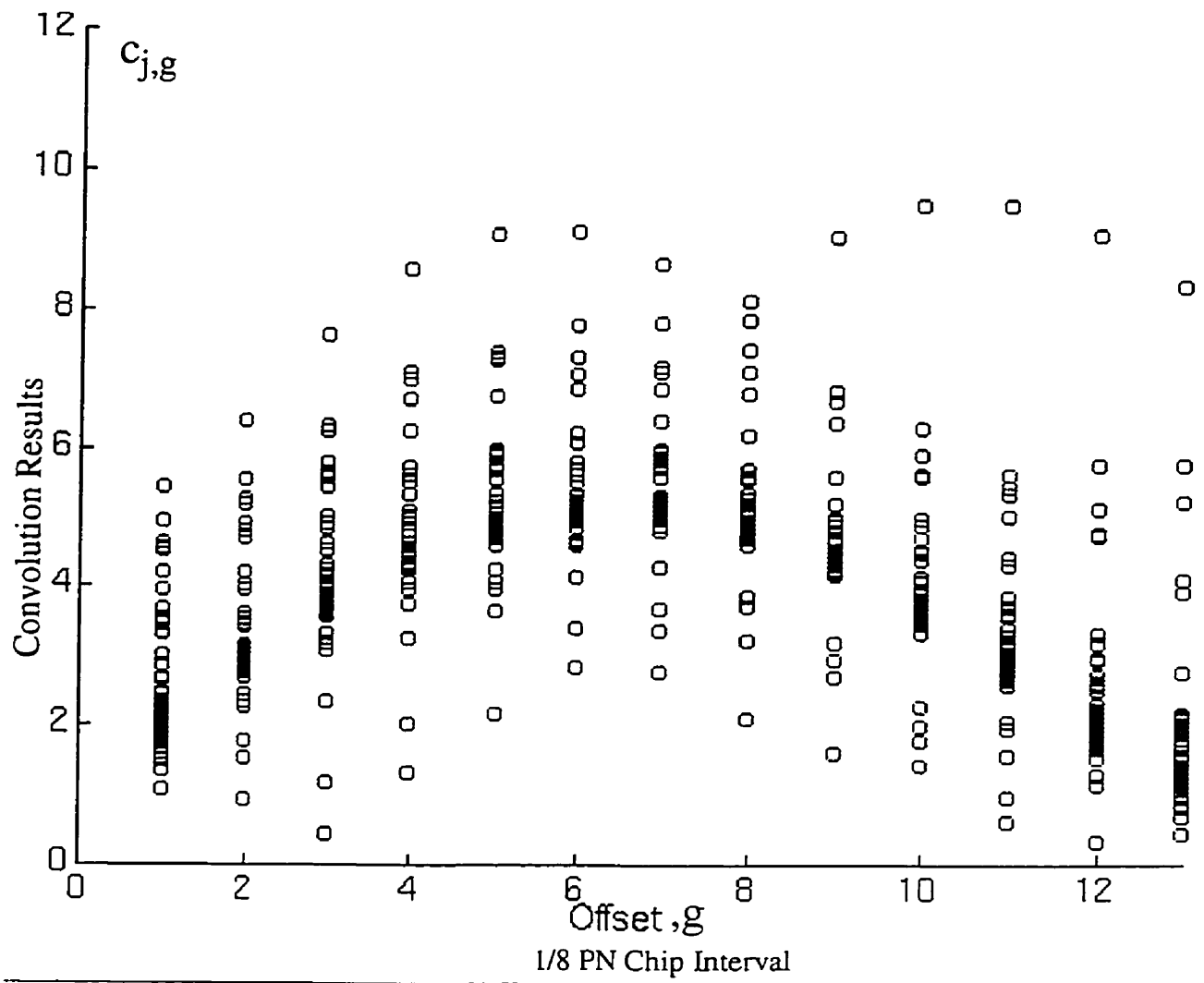
Fig. 5.32 a Eye diagram of Walsh decode (noise, $E_b/N_o = 6$ dB)
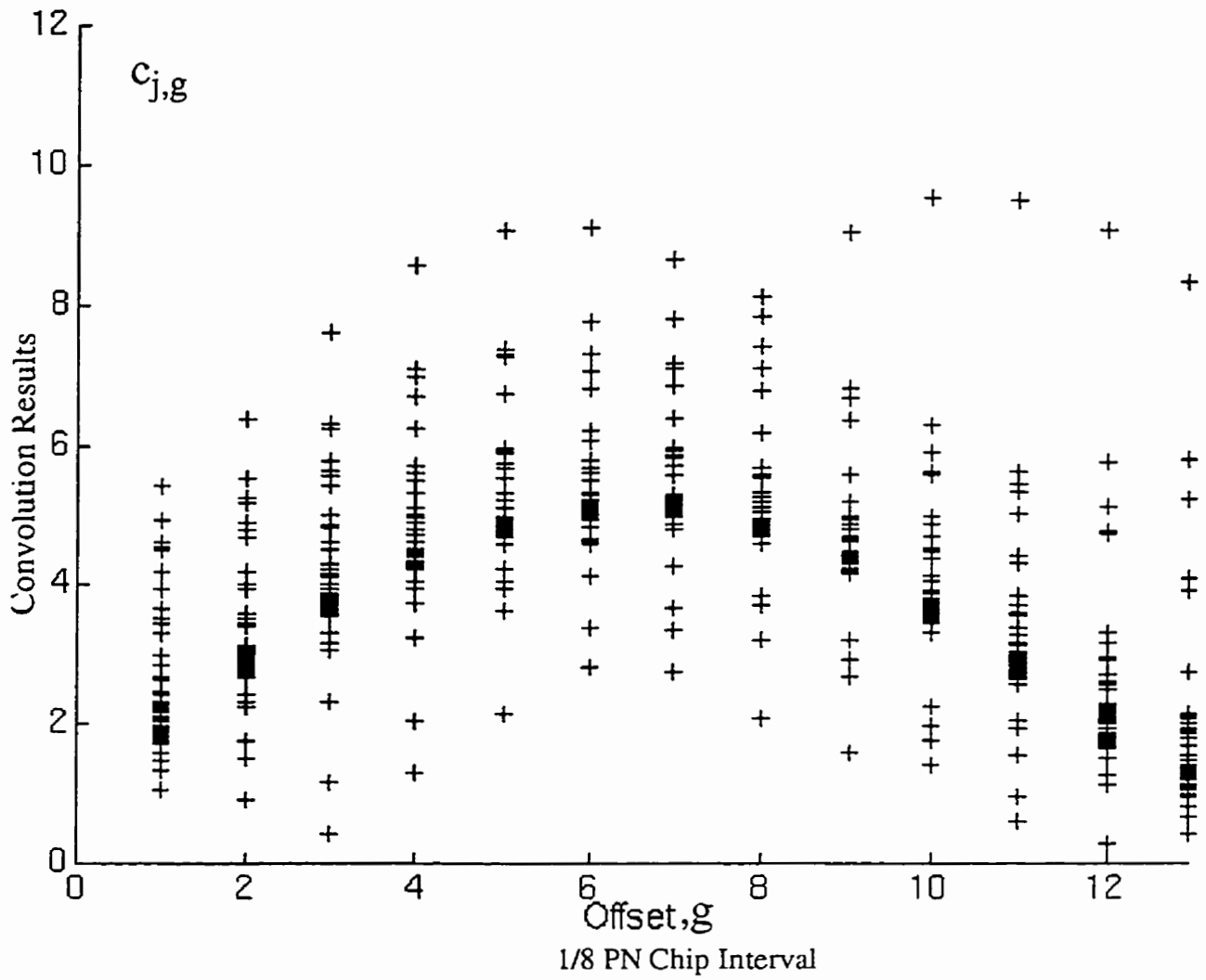
Fig. 5.32 b Eye diagram of Walsh despreading process (90 dB tone and noise, E_b/N_o = 6 dB)
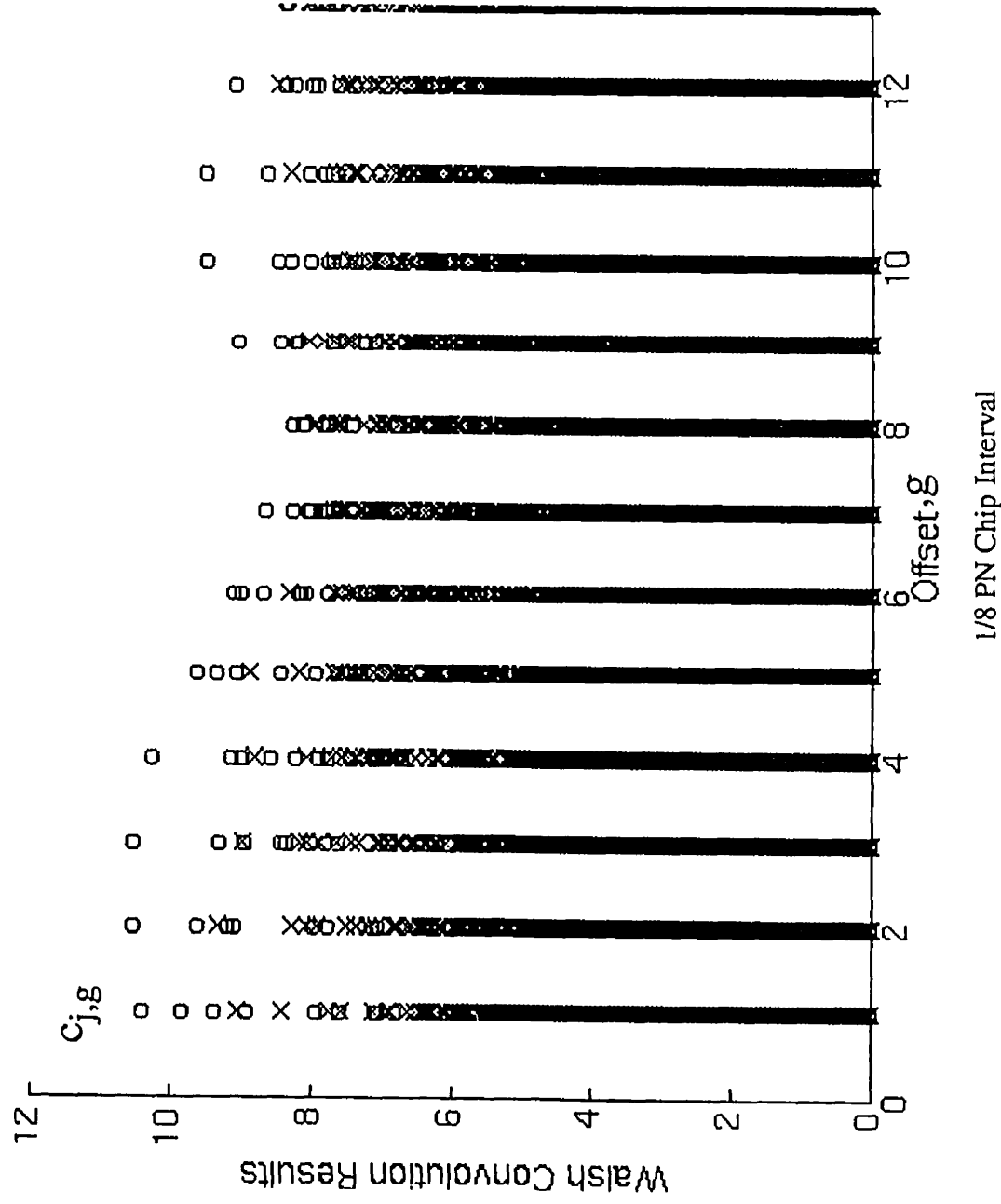
Fig. 5.33a Eye diagram of Walsh despreading process (tone and noise. $E_b/N_o = 6$ dB)
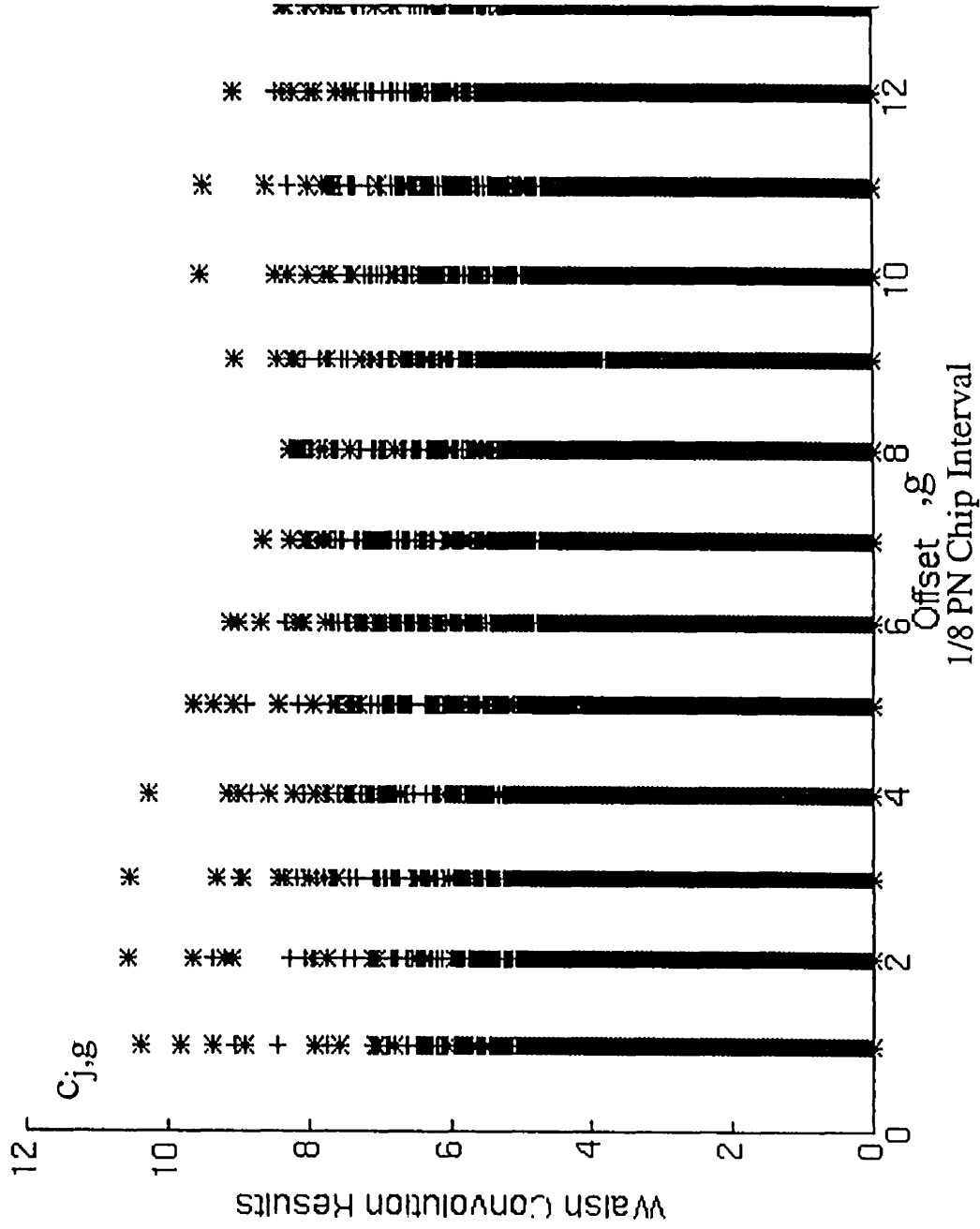"o" reference Walsh sequence, "x" other Walsh sequences

Fig. 5.33b Eye diagram of Walsh despreading process (tone and noise, $E_b/N_o = 6$ dB) "*" reference Walsh sequence, "+" other Walsh sequences

172

5.8 TMUX Performance Summary

Table 5.1 summarizes the performance of the transmultiplexer channelizer.

Table 5.1 Performance of transmultiplexer implemented channelizer

Polyphase Channel Select Filter	Performance Parameters
Number of Coefficients	192
Stopband Attenuation greater or equal to 1.25 MHz	-90 dB
TMUX:	
Noise Bandwidth (Receiver System Function)	520 kHz
ρ	.988
SAR	105 dB
SCR	16.7 dB (non-boundary carrier) 19.7 dB (boundary carrier)
QPSK Eye Opening	80.5 %
Tone (90 dB):	
ρ	.987
QPSK Eye Opening	80 %
After PN/Walsh Despread	
ρ	0.988
ρ with Tone Interferer	0.988
ρ with E_b/N_o Noise Added	0.015

5.9 Conclusion

In this chapter a polyphase carrier select lowpass FIR filter for the transmultiplexer wideband channelizer was designed. The filter was designed using the frequency sampling filter design method. It has a minimum of -90 dB stopband attenuation at frequencies greater than or equal to 1.25 MHz relative to DC. This satisfies the -85 dB minimum stopband attenuation specification given in Section 2.1. The receiver filter chain of the transmultiplexer system has a noise bandwidth of 520 kHz which is within the noise bandwidth requirement given in Section 2.1.

The SAR value, which is a measure of distortion caused by aliasing from the decimation operation of the transmultiplexer, was found to be -105 dB which results in virtually no distortion to the received signal. The SCR value which is a measure of distortion caused by adjacent carriers, i.e. crosstalk noise, for the transmultiplexer was determined. SCR values for carriers at the boundaries of the CDMA spectrum are different from the SCR values for the other carriers. This is because there is only one carrier beside the boundary carrier while there are two carriers adjacent to a non-boundary carrier. As a result, there is a 3 dB difference in SCR values between the two cases. The SCR value for a non-boundary carrier following the rate change mechanism is 16.7 dB. This crosstalk noise is due to the relationship between baseband filter stopband and carrier spacing specified by the IS-95+ standard [5]. In a typical CDMA system (with a capacity of 32 users) the SCR provided by the transmultiplexer has a SNR degradation effect smaller than the impact of adding a single co-channel user.

The ρ value, see equation (2.1), has been obtained for the transmultiplexer system. It

is found that the ρ value, 0.988, satisfies the requirements given in Section 2.1, and is independent of the carrier. Eye diagrams have been plotted for the QPSK signals output from the transmultiplexer. The ρ value and the QPSK eye opening for a carrier are essentially unchanged by a single tone interferer and quantization noise due to the finite word length of the implementation. This shows that in terms of ISI, the interference effect of a tone interferer to the QPSK carrier signal has been minimized. The ρ values satisfy the performance requirement.

To examine the impact of the transmultiplexer channelizer on the PN and Walsh despreading processes in the baseband CDMA demodulation, a simple DS-CDMA spreading and despreading model was developed. The locus of the convolution results between the PN/Walsh codes and the received signal was plotted. This plot forms an "eye" diagram. There is a direct relationship between the Walsh convolution and ρ value. The value of ρ was obtained using the locus of points at the highest point of the eye and was found to be 0.988. The E_b/N_o degradation associating with this ρ value is 0.05 dB which satisfies the performance requirement. An "eye" diagram was plotted when a tone at a 1.25 MHz offset to a carrier is added. It was found that the two eye diagrams have the same locus of points. This shows that the presence of a tone interferer has not affected the PN and Walsh despreading process. Thus, its effect on the CDMA demodulation process has been minimized. Furthermore, similar tests have been performed in the presence of noise corresponding to a E_b/N_o of 6 dB. A single tone interferer does not affect the results. The transmultiplexer successfully recovers the CDMA signals of the individual carriers and meet the performance objective defined for the IS-95+ standard [5].

Chapter Six

Conclusions

6.1 Conclusions

1. An extension was made to the time domain analysis of the transmultiplexer by Hung [6] to the case where the sampling frequency for each of the per-carrier transmultiplexer outputs is a multiple of the carrier spacing. This enables the transmultiplexer concept to be used in the DS-CDMA air interface protocol specified by the IS-95+ standard [5]. The approach in [6] was also extended to include a digital IF section to take advantage of the advance in DSP.

2. It is determined by complexity estimation that a wideband demodulator based on the transmultiplexer implementation has a 5-to-1 complexity advantage over the per-carrier wideband demodulator. This is for a complexity measure that involves a count of all operations performed by the demodulator. It should be noted that this advantage is only possible when there are a large number of carriers using the same air interface protocol and occupying the wideband spectrum. If the wideband spectrum is only occupied by a few carriers, or different protocols are used on these carriers, the per-carrier wideband demodulator offers a more efficient and flexible solution.

3. A simple DS-CDMA spreading and despreading model has been designed in order to verify that the degradation to the CDMA PN/Walsh despreading processes caused by the transmultiplexer channelizer system satisfies the performance requirements given in the IS-95+

standard [5]. The ρ value obtained by the Walsh convolution eye diagram is 0.988 which corresponds to a 0.05 dB E_b/N_0 degradation. The E_b/N_0 degradation caused by the transmultiplexer is well below the 0.25 dB limit, given in the IS-95+ standard [5]. In addition the noise bandwidth of the transmultiplexer filter chain is 520 kHz which satisfies the 625 kHz limit given in the IS-95+ Standard [5].

      4) The required in-band tone interferences suppression performance of the transmultiplexer implementation of a wideband CDMA demodulator has been verified. Both the QPSK and Walsh convolution eye pattern confirm that the effect of a tone interferer, at +/-1.25 MHz offset to a CDMA carrier assignment, has been minimized. In addition. the computed Walsh eye pattern under an additive Gaussian noise, corresponding to an E_b/N_0 of 6 dB. has confirmed that the effect of a tone interferer to the PN/Walsh despreading processes has been minimized.

6.2 Suggestions for Further Study

      1. In this study. the results were obtained through idealized MATLAB™ simulations [13]. Many of the impairments and non-linearities of actual components were ignored. The results would be more realistic if the wideband demodulator designs were implemented by DSP processors or dedicated ASICs and tested in real-time in the laboratory or in the field. The wideband demodulator should be integrated with a complete chain of CDMA transmitter/demodulators specified by the IS-95+ standard [5] so that the impact on the CDMA system performance can be found.

2. The effect of fading and all other channel impairments in a mobile communication environment should also be included as the wideband demodulators are designed for such applications.

References

[1]   E. Hogenauer, *"An Economical Class of Digital Filters for Decimation and Interpolation"*, IEEE Transaction on Acoustic, Speech, and Signal Processing, Vol. ASSP-29, No.3, pp 155-162,April 1981.

[2]   J. Proakis and D. Manolakis, *Digital Signal Processing - Principles, Algorithms, and Applications*, Second Edition, Macmillan, 1992.

[3]   J. F. Kaiser, *"Nonrecursive Digital Filter Design Using the Io - Sinh Window Function"*, Proc IEEE Int. Symp. Circuit Syst., pp. 20-23, April 1974.

[4]   D. Goodman, *"Nine Digital Filters for Decimation and Interpolation"*, IEEE Transaction on Acoustic, Speech, and Signal Processing, Vol. ASSP-25, No.2, pp121-126, April, 1977.

[5]   *IS-95+ CDMA Standard - Personal Station- Base Station Compatibility Requirements for 1.8 to 2.0 GHz Code Division Multiple Access (CDMA) Personal Communications Systems.* Published Version, ANSIJ-STD-008, March 24, 1995.

[6]   K. Hung, *"Design and Test of a Regenerative Satellite Transmultiplexer"*,Master of Science Thesis, Queen's University, Kingston, Ontario, Canada, May, 1993.

[7]   M. Bellanger, *"Digital Filtering by Polyphase Network: Application to Sample-Rate Alteration and Filter Banks"*, IEEE Transactions on Acoustics, Speech, and Signal Processing, Vol. ASSP-24, No.2, pp 109-114, April 1976.

[8]   M. Bellanger and J. Daguet,*"TDM-FDM Transmultiplexer: Digital Polyphase and FFT"*, IEEE Transactions on Communications, Vol COM-22, No.9, pp 1199-1205, September 1974.

[9]   R. Crochiere and L. Rabiner, *Multirate Digital Signal Processing*, Pentice Hall, 1983.

[10]   W. Press, B. Flannery, S. Teukolsky, W. Vetterling, *Numerical Recipes in C: The Art of Scientific Computing*, Cambridge University Press, New York, 1990

[11]   M. Bellanger, *"On Computational Complexity in Digital Transmultiplexer Filters"*, IEEE *Transactions on Communications*, Vol. COM-30, No7., pp 1461-1465, July 1982.

[12]   G. Edwards, *The DDS Handbook*, Third Edition, Standford Telecommunications, August, 1992.

[13]   T. Krauss, L. Shure, J. Little, *Signal Processing Toolbox-For Use with MATLAB*, The Math Works Inc., November, 1993.

[14] N. Sollenberger and J. Chuang, *"Low-Overhead Symbol Timing and Carrier Recovery for TDMA Portable Radio Systems"*, Bell Communication research

[15] J. Saw, T. Cameron, M. Suthers, *"Impact of SAW Technology on the System Performance of High Capacity Digital Microwave Radio"*, IEEE 1993 Ultrasonics Symposium, pp 59-65, 1993.

[16] *Recommended Minimum Performance Requirements for Base Stations Supporting 1.8 2.0 GHz Code Division Multiple Access(CDMA) Personal Stations*, PN-3383

[17] R. Baines, *"The DSP Bottleneck"*, IEEE Communications Magazine, pp 46-54, May, 1995.

[18] J. Wepman, *"Analog-to-Digital Converters and Their Applications in Radio Receivers"*, IEEE Communications Magazine, pp 39-45, May, 1995

[19] J. Mitola, *"The Software Radio Architecture"*, IEEE Communications Magazine, pp 26-38, May, 1995.

[20] A. Oppenheim and R. Schafer, *Discrete-Time Signal Processing*, Prentice Hall, 1989

[21] R. Dixon, *Spread Spectrum System* , Wiley-Interscience, 1984

[22] J. Bendat and A. Piersol, *Random Data: Analysis and Measurement Procedures*, Wiley-Interscience, 1971.

[23] J. Proakis, *Digital Communications*, 2nd Edition, MeGrew-Hill Computer Science Series, 1989.

[24] M. Jeruchim, P. Balaban, K. Shanmugan, *Simulation of Communication System*, Plenum Press, 1992

[25] S. Haykin, *Communication Systems*, Wiley, 1994

[26] R. Gitlin, J. Hayes, S. Weinatein, *Data Communication Principles, Plenum Press*, 1992

[27] K. Gilhousen, I. Jacobs, R. Padovani, A. Viterbi, L. Weaver and C. Wheatley," *On the Capacity of a Cellular CDMA System"*, IEEE Transactions on Vehicular Technology, Special Issue on Digital Cellular, November 1990.

[28] W. Lee, *"Overview of Cellular CDMA"*, IEEE Transactions on Vehicular Technology, May, 1991.

[29] I. Jacobs,"*A proposal for the Application of Code Division Multiple Access to Digital Cordless Telecommunications as a 'Canadian Common Radio Interface Standard"*, Qualcomm Inc Document, December 7, 1990.

[30] K. Wakabayashi, T. Aoyama, K. Murano, F. Amano, "*TDM-FDM Transmultiplexer Using a Digital Signal Processor*", IEEE Transactions on Communications, Vol. COM-30, No. 7, pp 1552-1559, July 1992.

[31] R. Maruta, A. Kanemasa, H. Sakaguchi, M. Hibino, K. Nakayama,"*24- and 120 Channel Transmultiplexers Built with New Digital Signal Processing LSI's*", IEEE Transactions on Communications, Vol. COM-30, No. 7, pp1528-1539 July 1992.

[32] R. Crochiere, "*A Weighted Overlap-Add Method of Fourier Analysis/Synthesis*", IEEE Transactions on Acoustic Speech Signal Processing, Vol. ASSP-28, No.1, pg. 99-102, February, 1980.

[33] *Recommended Minimum Performance Standards for Base Station supporting Dual Mode Wide Band Spread Spectrum Cellular Mobile Stations*, Official Ballot Version, PN-3120(IS-97), February 18, 1994.

[34] R. Peterson, R. Ziemer, D. Borth, *Introduction to Spread Spectrum Communications*, Prentice Hall, 1995.

[35] N. Doi, T. Yano, N. Kobayashi," *DS/CDMA prototype system transmitting low bit-rate voice and high bit-rate ISDN signals*", IEEE Document, 1994.

[36] Members of the Technical Staff, Bell Telephone Laboratories, *Transmission Systems for Communications*, Bell Telephone Laboratories, Incorporate, Fifth Edition, 1982.

[37] J. Lane and G. Hillman, *Motorola Digital Signal Processors - Implementing IIF/FIR* Filters with Motorola's DSP56000/DSP56001, Motorola, 1993.

[38] C.M. Rader, " Discrete Fourier Transforms When the Number of Data Samples is Prime", Proc. IEEE, Vol 56, pp 1107-1108, June 1968.

Appendix A

Frequency Sampling FIR Filter Design Method

The frequency sampling filter design method is in fact an inverse FFT to the frequency mask. However, the number of points in a conventional inverse FFT dictates its accuracy. The frequency sampling method is a special inverse FFT in which good accuracy is achieved with a low number of filter coefficients. There are two types of frequency sampling method: one for $\alpha = 0$ and one for $\alpha=0.5$. For $\alpha = 0$, the frequency mask input to the frequency sampling design method is sampled at intervals of f_s/M where M is the length of the filter and f_s is the sampling frequency. For $\alpha = 0.5$, the frequency mask input to the frequency sampling design method is sampled at intervals of f_s/M with an offset of α.

Consider the case of the design of a symmetric FIR filter with the $\alpha=0$ frequency sampling method. $H[2\pi k/M]$ is the discrete frequency mask for the filter and M is the length of the filter. Now define

$$G[k] = (-1)^k H\left[\frac{2\pi k}{M}\right] \qquad G[k] = -G[M-k] \qquad (A.1)$$

Then h[n], the FIR filter designed by the frequency sampling method is

$$h[n] = \frac{1}{m}\left\{ G[0] + 2 \sum_{k=1}^{U} G[k] \cos 2\pi \frac{k}{M}\left(n + \frac{1}{2}\right)\right\} \qquad (A.2)$$

where

$$U = \begin{cases} \dfrac{M-1}{2} & M \ odd \\[3mm] \dfrac{M}{2}-1 & M \ even \end{cases} \qquad\qquad . \qquad (A.3)$$

For the $\alpha=0.5$ frequency sampling method, G[k] can be defined as follows:

$$G\left[k+\frac{1}{2}\right] = (-1)^k H\left[\frac{2\pi}{M}\left(k+\frac{1}{2}\right)\right] \quad \text{and} \quad G\left[k+\frac{1}{2}\right] = G\left[M-k-\frac{1}{2}\right] \qquad (A.4)$$

The FIR filter impulse response, h[n], designed by the frequency sampling method is

$$h[n] = \frac{2}{M}\sum_{k=0}^{U} G\left[k+\frac{1}{2}\right]\sin\frac{2\pi}{M}\left(k+\frac{1}{2}\right)\left(n+\frac{1}{2}\right) \qquad (A.5)$$

To obtain better stopband attenuation and keep the same number of filter coefficients one can use a window function such as the Kaiser window[2-3] defined below:

$$\frac{I_o\left[\beta\sqrt{\left(\dfrac{M-1}{2}\right)^2 - \left(n-\dfrac{M-1}{2}\right)^2}\right]}{I_o\left[\beta\left(\dfrac{M-1}{2}\right)\right]} \qquad (A.6)$$

where $I_0[x]$ is the modified zeroth-order Bessel function and β is a constant that specifies a frequency response trade-off between the peak height of the sidelobe ripples and the width of energy of the main lobe[3]. The Kaiser window function can be used together with the $\alpha = 0.5$ frequency sampling filter design procedure in order to improve stopband attenuation. In general, $\alpha = 0.5$ gives better stopband performance than $\alpha = 0[2]$. By widening or adjusting the transition band of the frequency mask input to the frequency sampling filter design method, a further improvement

of stopband performance can be achieved.

IMAGE EVALUATION
TEST TARGET (QA-3)

1.0
1.1
1.25
1.4
1.6
1.8
2.0
2.2
2.5
2.8
3.2
3.6
4.0

150mm

6"
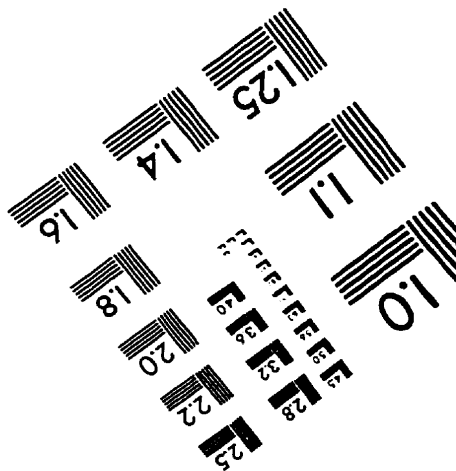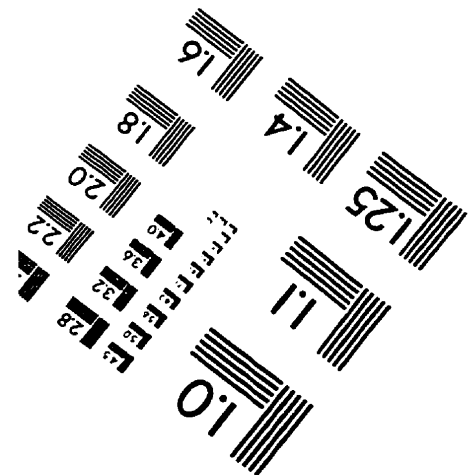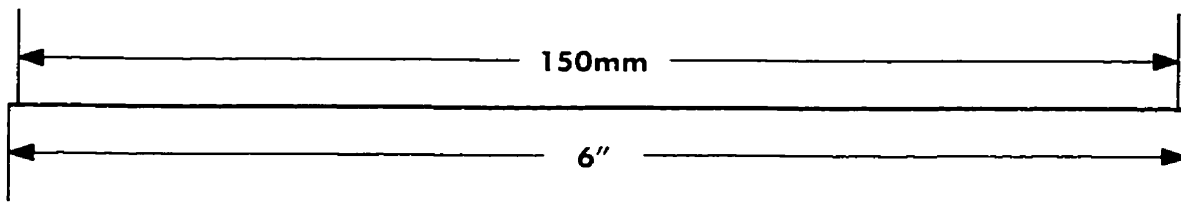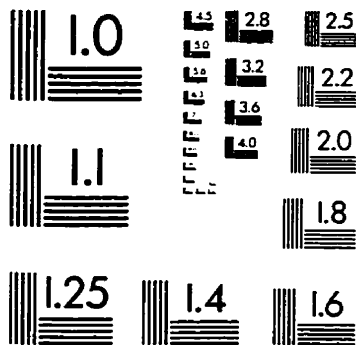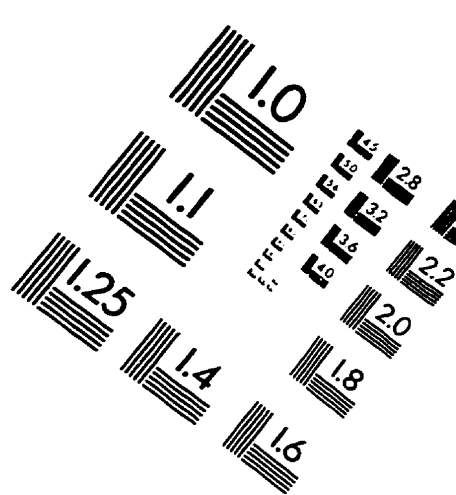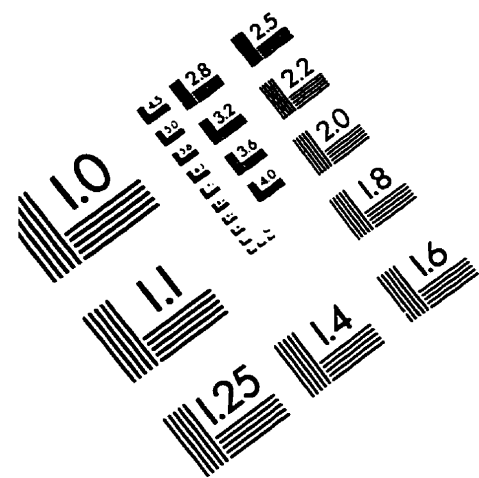
APPLIED IMAGE . Inc
1653 East Main Street
Rochester, NY 14609 USA
Phone: 716/482-0300
Fax: 716/288-5989